10-1-1993

NOVEL TECHNIQUES FOR THE DETECTION AND ESTIMATION OF THREE-WAVE COUPLING WITH APPLICATION TO HUMAN BRAIN WAVES

David Lee Sherman
Purdue University School of Electrical Engineering

Michael D. Zoltowski
Purdue University School of Electrical Engineering

NOVEL TECHNIQUES FOR THE DETECTION AND ESTIMATION OF THREE-WAVE COUPLING WITH APPLICATION TO HUMAN BRAIN WAVES

DAVID LEE SHERMAN
MICHAEL D. ZOLTOWSKI

TR-EE 93-33
OCTOBER 1993

SCHOOL OF ELECTRICAL ENGINEERING
PURDUE UNIVERSITY
WEST LAFAYETTE, INDIANA 47907-1285

NOVEL TECHNIQUES FOR THE DETECTION AND ESTIMATION OF THREE-WAVE COUPLING WITH APPLICATION TO HUMAN BRAIN WAVES

by

David Lee Sherman and

Michael D. Zoltowski

1285 Electrical Engineering Building

Purdue University

West Lafayette, IN 47907-1285

ABSTRACT

Composite linear and quadratic systems produce three-wave coupling when stimulated by random-phase input sinusoids. Due to the non-linearity of the system the output frequencies are arithmetically related to the input. Using third order cumulant statistics and their associated bispectrum, techniques are devised based on phase-insensitive matrix structures for detection and frequency estimation of coupling frequencies. The separation of the third order cumulant series into symmetric and skew-symmetric portions allows us to exploit their characteristic eigendecompositions for frequency estimation. After symmetrization, biphases can be easily extracted as coefficients of the cumulant sequence. Using a generalized eigenvector representation, we can relate symmetric and skew-symmetric bases by a subspace rotation algorithm. Biphases can be estimated directly from generalized eigenvalues of the matrix pencil formed by symmetric and skew-symmetric matrices. The dimensionality of our matrices can be reduced through the use of cumulant projections which yield a slice of the bispectrum. The Radon transform procedure is related to bispectral processing through an isotropic radial slice Volterra filter. The compact third order Kronecker product matrix formulation and algorithms for coupling frequency estimation can also be converted for use in biphase estimation. Simulations showing the performance of the above procedures are also presented for both synthetic and biomedical time series. These include the detection and estimation of specific frequencies exhibiting non-linearities in electroencephalographic(EEG) data.

Table Page

Appendix
Table

LIST OF FIGURES

Figure Page

Figure Page

Figure Page

Figure Page

Figure Page

Appendix
Figure Page

CHAPTER 1
INTRODUCTION

"The question of linearity of a system is dependent on the level of hierarchy considered." †

1.1 Natural and Man-Made Occurrences of Three-Wave Coupling

Three-wave coupling occurs in a composite linear and quadratic system. Two random phase input sinusoids become phase-locked to a third sinusoid which is generated in a non-linear system. In three wave coupling or other kinds of wave-wave interactions, energy is transferred from one or more sinusoids to sum and difference sinusoids whose frequencies and phases are arithmetically related to the input frequencies and phases. Examples of three-wave coupling in both natural and man-made systems abound. Several case studies follow below.

For many systems such as plasma in a fusion reactor's (tokamak) edge or shoaling ocean waves, harmonic generation is referred to as turbulence [1-3]. To describe the changes in the dynamic frequency content of many physical systems, we can rely on the interpretation by Dr. Edward J. Powers, Jr. of the University of Texas at Austin. Refemng to fluids and plasma under certain conditions he relates, "In such media, departures from thermodynamic equilibrium...can act as a source of energy for various unstable modes or waves. Initially the unstable modes grow in a linear fashion, then, at sufficiently large amplitudes, begin to non-linearly interact. As a result of this interaction, energy is transferred from the most unstable modes to new sum and difference frequencies, waves or modes. For this reason, non-linear wave interactions constitute an important mechanism whereby energy is redistributed from the most

† P. Nunez, *The Electric Fields of the Brain*, Oxford. New *York*, 1981, p. 301

unstable modes to damped waves. This process is often called energy cascading. The final result of the energy cascading process is turbulence which is manifested by fluctuations of the relevant physical parameters in both space and time." [4].

System physiologists model neural systems, especially sensory transducers, which are responsible for energy conversion. Sound and light, as well as other stimuli impinge upon appropriate receptors and are converted into electrical energy that can be interpreted by higher centers in our nervous systems. Input and output energy spectra cannot be related by a simple linear system model that furnishes gain and phase shift alteration. A monochromatic light input to a visual receptor yields output at the input frequency plus a double frequency term. This is illustrated in Fig. 1.1 below where the output of a cell from the retina contains both single and phase-locked double frequency terms [5].

In man-made sensory systems such as radar, the backscatter from certain materials such as semi-conductors with non-linear I-V characteristics has new frequency components as well [3]. The synthesis of sum-and-difference frequency components in the backscatter is explained by a non-linear radar cross-section. Both the received and transmitted signal spectra are related by coupled linear and quadratic transfer functions inherent in their respective cross-sections and antenna gain characteristics. Walton and Jouny discuss and demonstrate the use of methods for multipath and multiple reflections off of objects from radar [6]. Due to multiple reflections an object may appear to be further away from a radar, because of longer time delays before being received. However, multiple reflections are simply phase-locked and delayed versions of the primary reflection. It is desirable to have methods to discriminate multiple from simple reflections.

An off-shore tethered oil platform is impacted by the sea waves. The input, sea wave, and the surge response of the platform can best be modeled by linear and quadratic coupled system responses. Quadratic wave drift and linear wave excitation schemes provide the best 'fit' between input and output models based on coherence studies [4].

Other cases of wave-wave interactions appear in optical systems. Optical scientists experiment with solitons. These are "light pulses so stable they do not spread in an optical fiber even after thousands of kilometers..." [7]. Optical fibers have to be selected so that the trade-offs between dispersion and non-linearity are balanced. Modeling the action of the optical fiber on the soliton requires the use of a scheme to capture phase shift and harmonic generation together.

As a final example, consider the electroencephalogram (EEG). The generation of the EEG is not well understood. As an unobtrusive measurement of brain function,

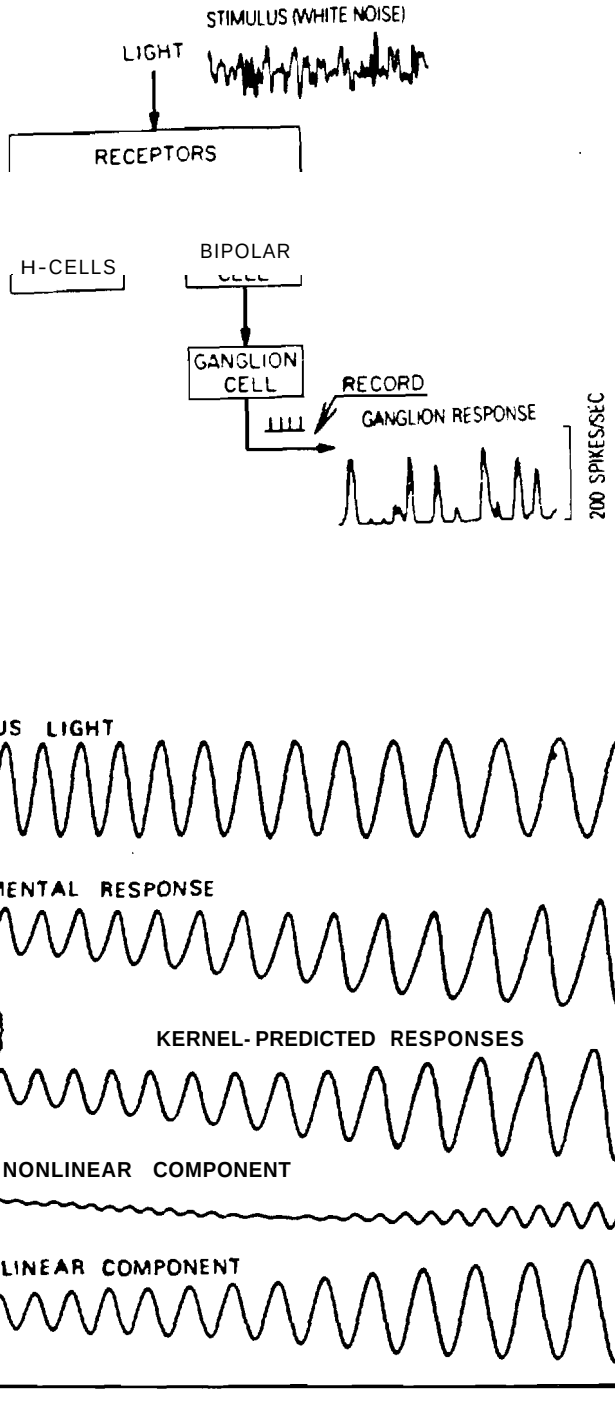

Figure 1.1 **Linear and Nonlinear Output from Retinal Horizontal Cell from Sinusoidal Input [5]**

the mechanism of EEG generation is not a primary concern to neurologists. Instead the EEG problem is a pattern recognition problem to aid neurologists in their diagnosis of patients. The quiescent brain is often characterized by large alpha wave content in the region between 8-13 Hz. Often alpha is defined as a complex wave with coupling with other frequencies at sub- and supra-harmonic levels. Alpha is not a pure sinusoid by any stretch of the imagination. Some individuals show more coupling to other harmonics than others. In the active brain when alpha blocking or desynchronization occurs, the coupling among frequencies is lost. Though coupling is lost and the alpha wave disappears, some harmonic energy persists. Through experimentation it is desirable to discern why some individuals exhibit coupling and other do not. Sensitive measures to correlate EEG and arousal state are sought. Development of measures to analyze coupling and the shape of the coupled waveforms is challenging because of the non-stationary character of the EEG.

The measurement and detection of three-wave coupling is the problem confronted in this dissertation. Sometimes the detection of three-wave coupling is a preliminary step along the way to non-linear system identification. Often, sinusoids are used as a probe stimulus to detect non-linearities in a system. More often than not, the presence of non-linearities helps us to differentiate states of a system.

Higher order spectra and correlations such as the bispectrum and the third order cumulant provide information about three wave coupling. The cross-bispectrum provides information about quadratic interactions between input and output sequences. The auto-bispectrum shows phase locking among components within a single time series. Both preserve phase and can aid in the signal reconstruction problem when no phase information is available from ordinary second order power spectra and autocorrelation. The higher order spectra are also immune to additive Gaussian noise. Often, non-Gaussian signals are immersed in Gaussian noise so that the signal detection by way of the bispectrum avoids performance deterioration by contaminating noise. In addition non-Gaussian random processes require correlation information beyond the second order for a completely adequate description of their statistics.

In this thesis several high performance methods for detection of quadratic phase coupling among sinusoids immersed in additive Gaussian and non-Gaussian noise are designed. These methods work directly with the third order cumulant sequence. They furnish information about coupling frequencies and the relative phase shift among constituent sinusoids. These phase shifts relate directly to waveform dispersion and generate shape information.

These methods are then applied to the EEG or brain wave time: series recorded from the scalps of human subjects. A key goal in this research is to use these

algorithms with real or naturally occurring data. The EEG is often considered to be strictly Gaussian with limited nonlinearities or frequency couplings. As the third order cumulant sequence is insensitive to Gaussian noise, the algorithms should easily detect the presence of coupled sinusoids and estimate the coupling frequencies.

1.2 Three-Wave Coupling, the Bispectrum and System Theory

Higher order spectra have a role in the description of systems generating non-linear output from random input data. Consider a linear time-invariant (LTI), $H_L(\omega)$, with pure random phase sinusoidal input,

$$x(n) = \sum_m A_m \exp[\, j(\omega_m n + \phi_m)] \tag{1.1}$$

where ω_m are individual frequencies with their associated amplitudes A_m and phases ϕ_m. We may assume that the phases are randomly distributed over the interval $[0, 2\pi]$. Then the output of this system, $y_L(n)$ is merely a phase shifted, amplified version of the input signal. Specifically there are no interactions among the individual frequency components upon output

$$y_L(n) = \sum_m H_L(\omega_m) A_m \exp[\, j(\omega_m n + \phi_m)] \tag{1.2}$$

$$y_L(n) = \sum_m B_m \exp[\, j(\omega_m i + \phi_m + \theta_m)] \tag{1.3}$$

where $\theta_m = \arg\{ H_L(\omega) \} + \phi_m$ and $B_m = |H_L(\omega_m)| A_m$. Though the phases and amplitudes have been altered upon output, the phase characteristic still possesses a random character. Individual phase terms do not enter into any deterministic relation with one another. So in the linear case the spectral powers at two different frequencies are independent of one another.

On the other hand if the same collection of random phase sinusoids is passed through a higher order system, such as a quadratic system, no longer do the phases retain a totally random character as in Fig. 1.2. In this figure the higher order system function, $H_Q(\omega_1, \omega_2)$, otherwise known as the 2nd order Volterra frequency domain kernel, imposes a specified structure among the sinusoids. Here the subscript " Q signifies quadratic. The quadratic system portion of the coupled system output, $y_Q(n)$ is:

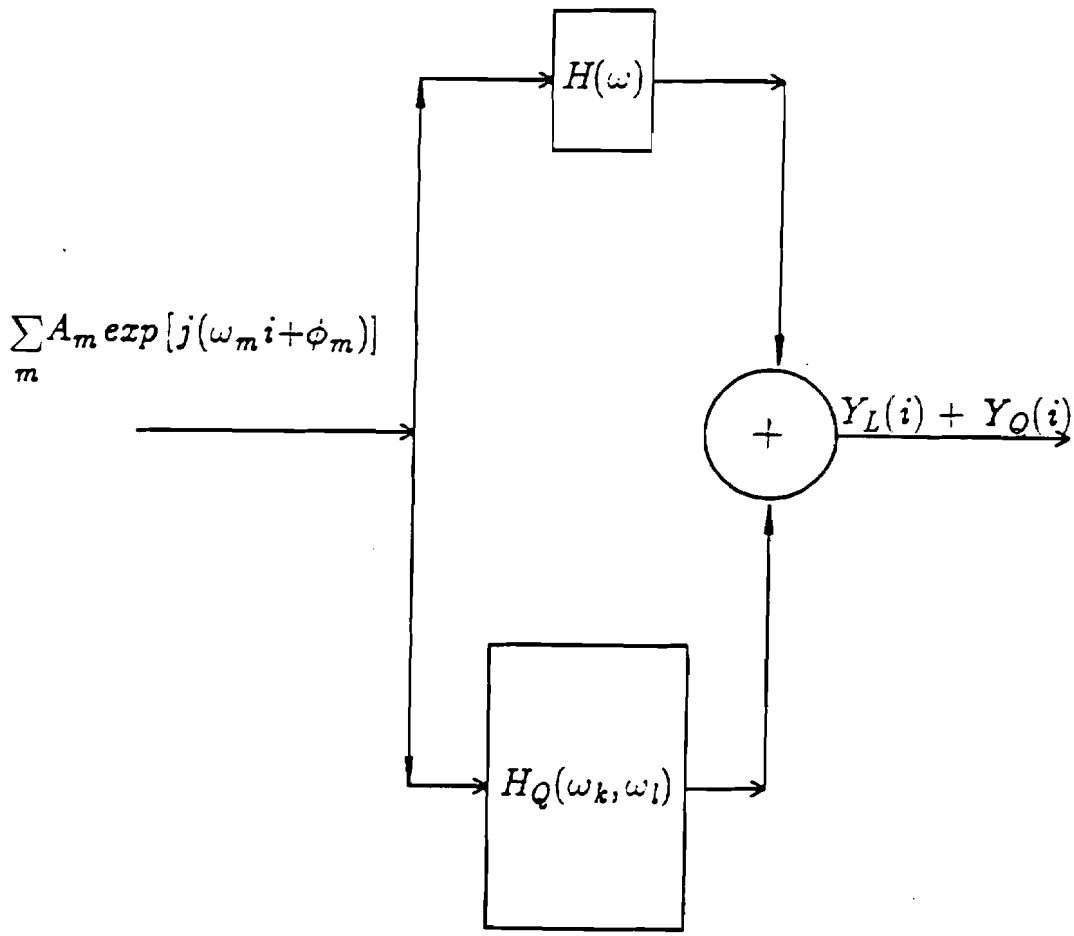

Figure **1.2** **Coupled linear and quadratic system functions and their output time series**

$$y_Q(n) = \sum_m \Big(\sum_k \sum_l H_Q(\omega_k, \omega_l) A_k \exp[\, j(\omega_k n + \phi_k)] \, A_l \exp[\, j(\omega_l n + \phi_l)] \Big). \quad (1.4)$$

At this point we note that contributions to each frequency value ω_m depend on the strength of quadratic system function at each frequency pair (k, 1) such that $k + 1 = m$. Frequency components sum together to create new components at new frequencies through the interactive effect. New frequency terms synthesized from this action are called the coupled frequencies. For higher order Volterra frequency terms strength of the couplings are among three, four, etc. frequency components. The output can be written in the form

$$y_Q(i) = \sum_m \Big(\sum_k \sum_l Q_{kl} A_k A_l \exp[j((\omega_k + \omega_l)n + \phi_k + \phi_l + \gamma_{kl})] \Big). \quad (1.5)$$

The coefficient, Q_{kl}, is the quadratic amplitude coefficient and determines strength of the generated harmonics [5, 8] and

$$Q_{kl} = |H_Q(k,l)| \quad \gamma_{kl} = \arg\{ H_Q(k,l)\} \quad (1.6)$$

In the three wave coupling scenario, we need to consider that the linear and quadratic systems are coupled together. Examining how phase coupled harmonic generation occurs, suppose two sinusoids

$$x(n) = A_k \cos(\omega_k + \alpha_k) + A_l \cos(\omega_l + \alpha_l) \quad (1.7)$$

are input to this coupled linear/quadratic system. To exhibit three wave or quadratic phase coupling for real signals, the output of a system with linear and 2nd order nonlinear kernels, y(n), has three sinusoids,

$$y(n) = B_k \cos(\omega_k + \theta_k) + B_l \cos(\omega_l + \theta_l) + B_m \cos(\omega_m + \theta_m) \quad (1.8)$$

The first two sinusoids represent the linear system output. The third sinusoid is newly generated from the quadratic system function at a single frequency pair combination. Once again amplitude is determined by the amplitude of the system kernel $H_Q(k,l)$, i.e. $B_m = \frac{1}{2}|H_Q(k,l)|A_k A_l$. The frequency and phase of the quadratic or synthesized frequency component is related to the input sinusoids' frequencies and phases in the following manner when three wave coupling occurs:

$$\omega_m = \omega_k + \omega_l \quad (1.9)$$

$$\theta_m = \alpha_k + \alpha_l - \gamma_{kl}. \quad (1.10)$$

Here γ_{kl} is a constant linear offset which may be zero. Though the linear system output has random phases (the first two sinusoids), there is a third sinusoid present in the output whose phase is a result of a quadratic interaction between the first two. Here

we have a case of three wave coupling. Frequencies and phases are said to be related in an arithmetic fashion so that the third sinusoid's arguments may be the difference of the first two as well as their sum. As a result of the non-linear response the phases become coupled and there is a deterministic relationship among phase components. The cubic kernel determines the intensity of the coupling among four frequencies, for example.

The detection of the phase coupling in the output time series cannot achieved using the power spectrum as this statistic is insensitive to phase relationships among sinusoids. Another quantity known as the bispectrum is able to detect coupling. The bispectrum $B_{yyy}(\omega_1, \omega_2)$, a two dimensional function of frequency, exhibits a peak in its region of support at the point (ω_1, ω_2) when there is phase coupling among the members of the corresponding frequency triad. The bispectrum is the 2-D Fourier transform of the third order autocorrelation or cumulant of the time series, $R(k,l)$,

$$B_{yyy}(\omega_1, \omega_2) = \sum_{k=-\infty}^{\infty} \sum_{l=-\infty}^{\infty} R(k,l) \exp\{-j(\omega_1 k + \omega_2 l)\} . \qquad (1.11)$$

For a real-valued zero mean stationary time series, the third order cumulant is defined by the expectation of a doubly time lagged triple product,

$$R(k,l) = E\{y(n)y(n+k)y(n+l)\}. \qquad (1.12)$$

As in the case of the power spectral density there is a frequency domain definition of the bispectrum [2, 9].

$$B_{yyy}(\omega_1, \omega_2) = E\{Y(\omega_1)\, Y(\omega_2)\, Y^*(\omega_1+\omega_2)\} \qquad (1.13)$$

where

$$Y(\omega) = \sum_{n=-\infty}^{\infty} y(n) \exp(-j\omega n). \qquad (1.14)$$

This is implemented by means of Fourier transforming segments of a time series, forming all triple products for each segment and then averaging across all segments as discussed in chapter 2. This averaged triple product is called the biperiodogram. Note that the frequency decomposition of the third moment of a zero mean random process is exhibited by the bispectrum.

Contrast the bispectrum with the definition of the power spectrum, $P(\omega)$. This is defined as the Fourier transform of the autocorrelation function, $R(k)$ or

$$P(\omega) = \sum_{m=-\infty}^{\infty} R(m)\exp(-j\omega m). \tag{1.15}$$

For a stationary time series, $y(t)$, $R(m)$ is the expectation over time of the second order lagged product, i.e. $E\{y(t)y(t+m)\}$ where $y(t)$ has zero mean. An alternate definition of the power spectrum is the following

$$P(\omega) = E\{Y(\omega)Y^*(\omega)\} \tag{1.16}$$

where $Y(\omega)$ represents the Fourier transform of the time series in question. The power spectrum is said to express the frequency diversity in the second order moment of a time series, i.e. $E\{y^2(t)\}$.

Unlike the power spectrum, the bispectrum is a complex valued quantity and has a phase term. Kim, Beall et al. define the biphase as sum of the constituent phases,

$$\gamma(\omega_1,\omega_2) = \phi(\omega_1) + \phi(\omega_2) - \phi(\omega_3) \tag{1.17}$$

when $\omega_3 = \omega_1 + \omega_2$ [2]. This relationship is the same as the relative phase offset of the output sinusoids from the coupled linear and quadratic system. The quadratic phase coupling phenomenon discussed above where the biphase is zero is the most cited case in the literature. If $\phi(\omega_3)$ is coupled to the other two random phase frequency components such that there is always a constant offset, either negative or positive, between the sum $\phi(\omega_1) + \phi(\omega_2)$ and $\phi(\omega_3)$, then we say that there is a non-zero biphase. An example of a system with non-zero biphase is the squarer with delay T, i.e. $y(n) = x^2(n-T)$. When this occurs, the quadratic kernel has the following representation, $H_Q(\omega_k,\omega_l) = \exp[-j(\omega_k + \omega_l)]$ [13]. When no such phase shift occurs, then we have a simple squarer, $y(n) = x^2(n)$ with $H_Q(\omega_k,\omega_l) = 1$.

We note that the frequency decomposition of the third moment for a zero mean random process is exhibited by the bispectrum. So summing across the entire bispectral domain gives us the third order moment, $E\{x^3(n)\}$, of a random process. This is analogous to the summed power spectrum revealing total power. By default when we refer to the bispectrum, we mean the autobispectrum, $B(\omega_1,\omega_2) \equiv B_{yyy}(\omega_1,\omega_2)$ as above. A critical quantity involved in ascertaining the degree of coupling between input and output time series is the cross-bispectrum, $B_{xxy}(\omega_1,\omega_2)$. This entity is defined as $B_{xxy}(\omega_1,\omega_2)=E\{X(\omega_1)X(\omega_2)Y^*(\omega_1+\omega_2)\}$. Details about the relevance of the cross-bispectrum appear later in this manuscript under consideration for system identification.

Another quantity called the squared bicoherence, $bic^2(\omega_1,\omega_2)$ or simply the bicoherence is the normalized bispectral measurement. The bispectral magnitude is normalized by the power spectral values at the respective frequency triad,

$(\omega_1, \omega_2, \omega_3)$.

$$bic^2(\omega_1, \omega_2) = \frac{|B(\omega_1, \omega_2)|^2}{P(\omega_1)\, P(\omega_2) P(\omega_3)} \tag{1.18}$$

At this point it is worthwhile to examine another important property of the third order cumulant and the bispectrum: the immunity of these measures to additive Gaussian noise. This property can be best examined by focusing on the definition of the cumulant a little more closely.

1.3 Properties of Higher Order Cumulants

Considering a random variable (r.v.) x with characteristic function, $\phi_x(\omega)$, if all the moments up to order k exist, then the k-th order cumulant, γ_k^x, also exists and is defined as the k-th order coefficient in the Taylor series expansion of $\phi_x(\omega)$:

$$\ln\phi_x(w) \equiv \ln E\{e^{j\omega x}\} = \sum_{k=0}^{\infty} \gamma_k^x \frac{(j\omega)^k}{k!} \tag{1.19}$$

Note if we have a Gaussian r.v. with mean μ and variance, σ^2, then

$$\phi_x(\omega) = e^{-j\omega\mu - \sigma^2 \frac{\omega^2}{2}}. \tag{1.20}$$

We note that after taking logarithms and comparing with the equations above, it is clearly seen that the Gaussian distribution has all cumulants equal to zero for $k > 2$.

We may expand the expression Taylor series for the cumulants about zero [21], for a collection of random variables for the kth-dimensional case, $\mathbf{x}$ is a k-dimensional vector. Then for all orders up to and including the nth order, we have

$$\ln\phi_x(\omega) = \sum_{\nu_1 + \cdots + \nu_k \le n} \frac{j^{\nu_1 + \cdots + \nu_k}}{\nu_1! \cdots \nu_k} c_{\bar{x}}^{(\nu_1, \cdots, \nu_k)} \omega_1^{\nu_1} \cdots \omega_k^{\nu_k} \tag{1.21}$$

where $c_{\bar{x}}^{(\nu_1, \cdots, \nu_k)}$ denotes the cumulants of the random variables, $x^{\nu_1}, \ldots, x_k^{\nu_k}$.

Typically in random process theory we only examine the case where each random variable is held to a power of unity, i.e. $\nu_1 = \nu_2 = \cdots \nu_k = 1$. Now we let $c_{\bar{x}}^{(\nu_1, \cdots, \nu_k)} = c(x_1, \cdots, x_k)$. The expansion of the equation for the k-dimensional cumulant depends on combinatorial results. Given the numbers (1,2,...k), suppose they are partitioned in a number of ways where n_{gp} represents the number of groups in a

partition p. If g_i^p represents the i-th group of the p-th partition, the k-th order joint cumulant is defined as

$$c(x_1, \cdots x_k) = \sum_p (-1)^{n_{gp}-1} (n_{gp}-1)! \, E\{\prod_{i \varepsilon g_1^p} x_i\} \cdots E\{\prod_{i \varepsilon g_{n_{gp}}^p} x_i\} \tag{1.22}$$

Giannakis mentions that the cumulants are useful measures of joint statistical dependency among a collection of r.v.'s [10]. For second order cumulants the possible partitions of (1,2) are {(1,2)} and {(1),(2)}, so that p=2 and $n_{g1}=1$ and $n_{g2}=2$. As for group membership, $g_1^1=\{x_1,x_2\}$; $g_1^2=\{x_1\}$ and finally, $g_2^2=\{x_2\}$. Therefore,

$$c(x_1,x_2) = E\{x_1x_2\} - E\{x_1\}E\{x_2\}. \tag{1.23}$$

For the case where $x_1=x_2=x$, then in the case of the third order cumulant, i.e. k = 3, the possible partitions of (1,2,3) are { (1, 2, 3) }, {(1),(2,3)}, {(2),(1,3)}, {(3),(1,2)} and {(1),(2),(3)}; so that $n_{g1}=1$, $n_{g2}=n_{g3}=n_{g4}=2$, $n_{g5}=3$. This yields

$$c(x_1,x_2,x_3) = E\{x_1x_2x_3\} + E\{x_1\}E\{x_2x_3\} \tag{1.24}$$

$$+ E\{x_3\}E\{x_1x_2\} + E\{x_2\}E\{x_2x_3\} + 2E\{x_1\}E\{x_2\}E\{x_3\}.$$

For a zero mean random process all terms except for the first disappear. Then for a zero-mean stationary random process, the second, c(m), and third order cumulants, c(k,l), are respectively,

$$c(m) = E\{x(n)x(n+m)\} \tag{1.25}$$

and

$$c(k,l) = E\{x(n)x(n+k)x(n+l)\}. \tag{1.26}$$

Some important properties of the cumulants are detailed in Giannakis [10]. Of particular interest to us is the fact that if collections of random variables are independent of one anther, then the cumulant of their sum will be the sum of their cumulants. If $x_1, \ldots, x_n$ and $y_1, \ldots, y_n$ are independent, then

$$c(x_1+y_1, \cdots, x_n+y_n) = c(x_1, \cdots x_n) + c(y_1, \cdots, y_n) \tag{1.27}$$

The symmetry properties of the third order cumulants are well known [8].

$$R(k,l) = R(l,k) = R(-l,k-l) \tag{1.28}$$

$$= R(k-l,-l) = R(-k,l-k) = R(l-k,-k)$$

This relation partitions the two-dimensional region of support for the two lagged variables into six equivalent wedges. As it turns out we need only know the cumulants in

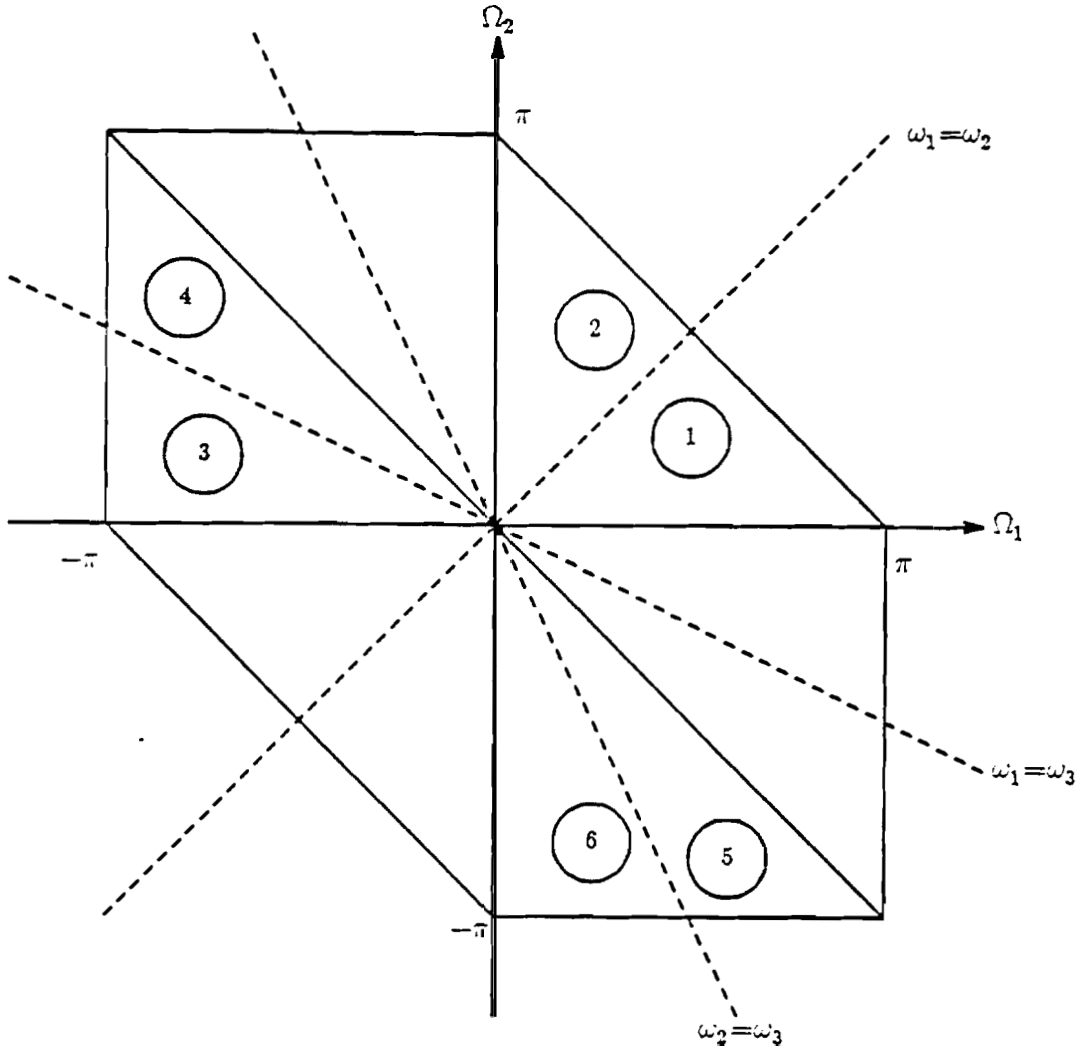

Region 1: $B(\omega_1,\omega_2)$
Region 2: $B(\omega_2,\omega_1)$
Region 3: $B(-\omega_1-\omega_2,\omega_2)$
Region 4: $B(\omega_2,-\omega_1-\omega_2)$
Region 5: $B(\omega_1,-\omega_1-\omega_2)$
Region 6: $B(-\omega_1-\omega_2,\omega_1)$

Figure 1.3 Domains of the Discrete Bispectrum Including Slices Demarcating Critical Sectors

the infinite wedge bounded by the lines k=0, k=l and k,l ≥ 0.

As a consequence of the symmetry property of the cumulants we can show that the bispectrum, $B(\omega_1,\omega_2)$ also observes its own set of equivalencies

$$B(\omega_1,\omega_2) = B(\omega_2,\omega_1) = B(\omega_1,-\omega_1-\omega_2) \tag{1.29}$$

$$= B(-\omega_1-\omega_2,\omega_2) = B(-\omega_2,-\omega_1-\omega_2) = B(-\omega_1-\omega_2,-\omega_2).$$

Then for real time series there is an additional symmetry property

$$B(\omega_1,\omega_2) = B^*(-\omega_1,-\omega_2) \tag{1.30}$$

These symmetry properties create a set of 12 equivalent sectors in the discrete bispectral domain. The frequency domain of the discrete bispectrum is shown in Fig. 1.3. Coupled with the fact that the bispectrum is also doubly periodic, i.e.,

$$B(\omega_1,\omega_2) = B(\omega_1+2\pi,\omega_2+2\pi), \tag{1.31}$$

the bispectrum of real time series is completely described by its values in a triangular region bounded by $\omega_2 \geq 0$, $\omega_1 \geq \omega_2$, and $\omega_1 + \omega_2 \leq \pi$. This triangular region is shown as sector 1 on Fig. 1.3. These sectors are appropriately known as subharmonic sectors where ω_1 and ω_2 add to form a coupled sinusoid at a frequency greater than each separately. Other sectors 3-6 are appropriately called supraharmonic sectors.

1.4 Identification, Higher Order Spectral Analysis and Volterra-Wiener Theory

A distinguishing feature of the linear systems is the fact that the principle of superposition holds. A classical application of higher order spectral analysis is the identification of non-linear systems. The input and output of a non-linear system may be represented in terms of contributions from individual responses of 'linear, quadratic, cubic, etc. subsystems. As first formulated by Volterra in the early part of the twentieth century, the total system response, y(t), may be decomposed into separate excitations of n-th order kernels by the common input(s). In this manner we see that for a single output, y(t), we engender the following Volterra series multiple convolution:

$$y(t) = k_0 + \int_0^\infty k_1(\tau)x(t-\tau)\,dr \tag{1.32}$$

$$+ \int_0^\infty \int_0^\infty k_2(\tau_1,\tau_2)x(t-\tau_1)x(t-\tau_2)\, d\tau_1 d\tau_2$$

$$+ \int_0^\infty \int_0^\infty \int_0^\infty k_3(\tau_1,\tau_2,\tau_3)x(t-\tau_1)x(t-\tau_2)x(t-\tau_3)\, d\tau_1 d\tau_2 d\tau_3 + \cdots$$

where $k_0, k_1(\tau_1), k_2(\tau_1,\tau_2,\tau_3)$ are called the kernels of the system. The first order term is the convolution integral for a linear system [5]. The time domain kernels presented here are the inverse Fourier transforms of the frequency domain Volterra kernels in (1.2) and (1.4). In general for an nth order Volterra expansion we have a series of integrals to represent the output y at time t.

$$y(t) = \sum_{n=0}^{\infty} \left(\int_{-\infty}^{\infty} \cdots \int_{-\infty}^{\infty} k_n(\tau_1,\ldots\tau_n)x(t-\tau_1) \cdots x(t-\tau_n)\, d\tau_1 \cdots d\tau_n \right) \qquad (1.33)$$

Typically, the Volterra series is thought of as a generalization of a Taylor series of a function of multiple arguments. The generalization involves the use of functionals rather than single arguments as in the Taylor series. The Volterra series is considered a functional representation of a system. This functional representation relies on the use of several functions defined over a interval of time usually $-\infty$ to some given time t. The inputs are functions of time, i.e. some $x(t)$ and by analogy to the Taylor series, they replace the powers of multiple variables x_1^m, x_2^n, x_3^k found in the Taylor series expansion. Coefficients of the Taylor series are analogous to the kernels of the Volterra series. Indeed the functional representation of the Volterra series uses integrals to find the individual contributions of each kernel in the series.

Although the Volterra series functional representation is adequate for system description in most cases, i.e. where the functional is analytic, it is not a trivial task to isolate responses of linear, quadratic, cubic, etc. terms to arrive at individual kernels. Kernel calculation is tantamount to system identification and is the goal of research on several fronts [3-5, 9, 11-14]. One of the very first endeavors to exploit the use of higher order spectra in its analysis of system kernels was the work of Leo Tick in the early 1960's [20]. Given a Volterra expansion in the frequency domain for the output $Y(f_m)$

$$Y(\omega_m) = H_L(\omega_m)X(\omega_m) \qquad (1.34)$$

$$+ \sum_k \sum_l H_Q(\omega_k,\omega_l)\, X(\omega_k)\, X(\omega_l)$$

we might use the higher order cross-correlation functions to extract the kernel when

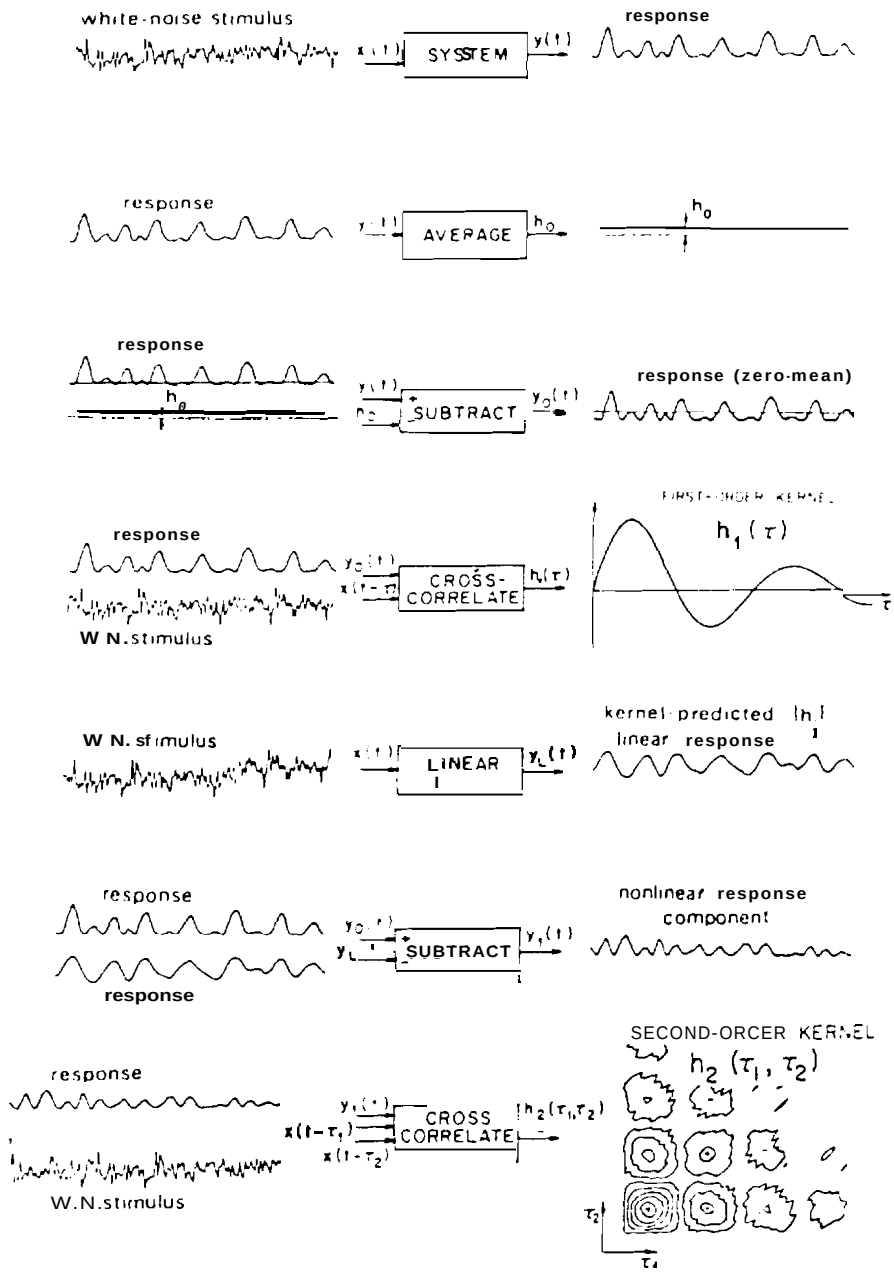

Figure 1.4 Time Domain (Correlative) Scheme for Finding Zeroth, First and Second Order Wiener Kernels from Marmarelis [5]

Gaussian noise is used as an input. Then multiplying (1.36) by $X^*(\omega_m)$ and taking expectations gives

$$E[X^*(\omega_m)Y(m)] = H_L(\omega_m)E[|X(\omega_m)|^2] \tag{1.35}$$

$$+\sum_k\sum_l H_Q(k,l)E[X^*(\omega_m)X(\omega_k)X(\omega_l)]$$

where $k+l=m$. Then multiplying (1.36) by $X^*(\omega_i)X^*(\omega_j)$, after taking expectation the result is:

$$E[X^*(\omega_k)X^*(\omega_l)Y(\omega_m)] = H_L(\omega_m)E[X^*(\omega_k)X^*(\omega_l)X(\omega_m)] \tag{1.36}$$

$$+\sum_k\sum_l H_Q(\omega_k,\omega_l)E[Xs(\omega_i)X^*(\omega_j)X(\omega_k)X(\omega_l)]$$

where $i+j=k+l=m$.

Using the fact that the Gaussian input is a symmetric function and has no odd order moments and the fact that $E[w_1w_2w_3w_4] = E[w_1w_2] + E[w_2w_3] + E[w_3w_4]$ for w_n that is Gaussian distributed, we can then arrive at the linear and quadratic transfer functions under question thusly:

$$H_L(\omega_m) = \frac{E[X^*(\omega_m)Y(\omega_m)]}{E[|X(\omega_m)|^2]} \tag{1.37}$$

$$H_Q(\omega_k,\omega_l) = \frac{E[X^*(\omega_i)X^(\omega_j)Y(\omega_i+\omega_j)]}{2E[|X(\omega_i)|^2]\,E[|X(\omega_j)|^2]}. \tag{1.38}$$

Over a half a century after Volterra, Norbert Wiener was able to synthesize a new set of kernel functions [15]. Under expectation with Gaussian input, each kernel generates a response which is orthogonal to all the other kernels used to represent a given system. The system contains a hierarchy of orthogonal functionals with respect to a Gaussian input. The functional of the zeroth order (average response), $G_0[h_0;x(t)]$, is the constant term h_0. The traditional linear transfer function forms the first order kernel. Then the response functional, $G_1[h_1;x(t)]$, is

$$G_1[h_1;x(t)] = \int_0^\infty h_1(\tau)x(t-\tau)d\tau \tag{1.39}$$

The second order kernel and its functional depend upon the input power spectral density, P, and

$$G_2[h_2;x(t)] = \int_0^{\infty}\int_0^{\infty} h_2(\tau_1,\tau_2)x(t-\tau_1)x(t-\tau_2)d\tau_1 d\tau_2 - P\int_0^{\infty} h_2(\tau_1,\tau_1)d\tau_1. \quad (1.40)$$

Generally, the functional series can be written,

$$y(t) - \sum_{m=0}^{\infty} G_m[h\sum m(\tau_1, \cdots, \tau_m);\ x(t'), t' \le t]. \quad (1.41)$$

The functionals are constructed so that the expected value of the product of any two equals zero. For systems lacking a kernel above the second order one, the Volterra kernels and Wiener kernels are identical. Leo Tick's method also relies on decorrelating responses from linear and quadratic kernels by using a Gaussian input. There *are* formulae to relate Wiener and Volterra kernels for all orders. The key in synthesis of a system representation is to generate stimuli and corresponding kernels that yield a complete set of orthogonal functionals.

The orthogonality condition for the Wiener kernels ensures that we have the best representation of the system function in the mean square error sense at each successive order in identification. The mean square error between the measured system response, $\hat{y}(t)$, and the true system response, $y(t)$, is minimal. This could be termed the completeness property of the Wiener system. The Wiener series also gives the best representation with respect to that Gaussian noise.

Wiener used an expansion in terms of a family of Laguerre functions as orthonormal basis along with a functional representation in terms of Hermite polynomial to characterize his system. His students, Lee and Schetzen (1965) devised the cross-correlation procedure to decouple linear, quadratic, cubic, etc. functional representations. It is analogous to the Gram-Schmidt process for generating an orthogonal vector basis in linear algebra. Now the inner product is correlation under expectation. The scheme is shown in the figure on the following page. We can present the frequency version since that is easier to implement than strictly time domain versions. There is a savings realized in the computational load [5]. Using the frequency domain scheme we can easily see exactly where the cross-bispectrum comes into play. (see Figs. 1.4-1.5)

0. Find the average value h_0 and subtract it from $y(t)$, call this difference $y_O(t)$
1. Compute $Y_O(\omega)$ and $X(\omega)$ via the FFT
2. Form the product $Y(\omega)X^*(\omega)$ which is the cross-spectrum, $\Phi_{xy}(\omega)$
3. Using the spectral density of the while noise input find $h_1(\tau)$ by the product, $(1/P)\phi_{xy}(\tau)$ after taking the FFT of $\Phi_{xy}(\omega)$.

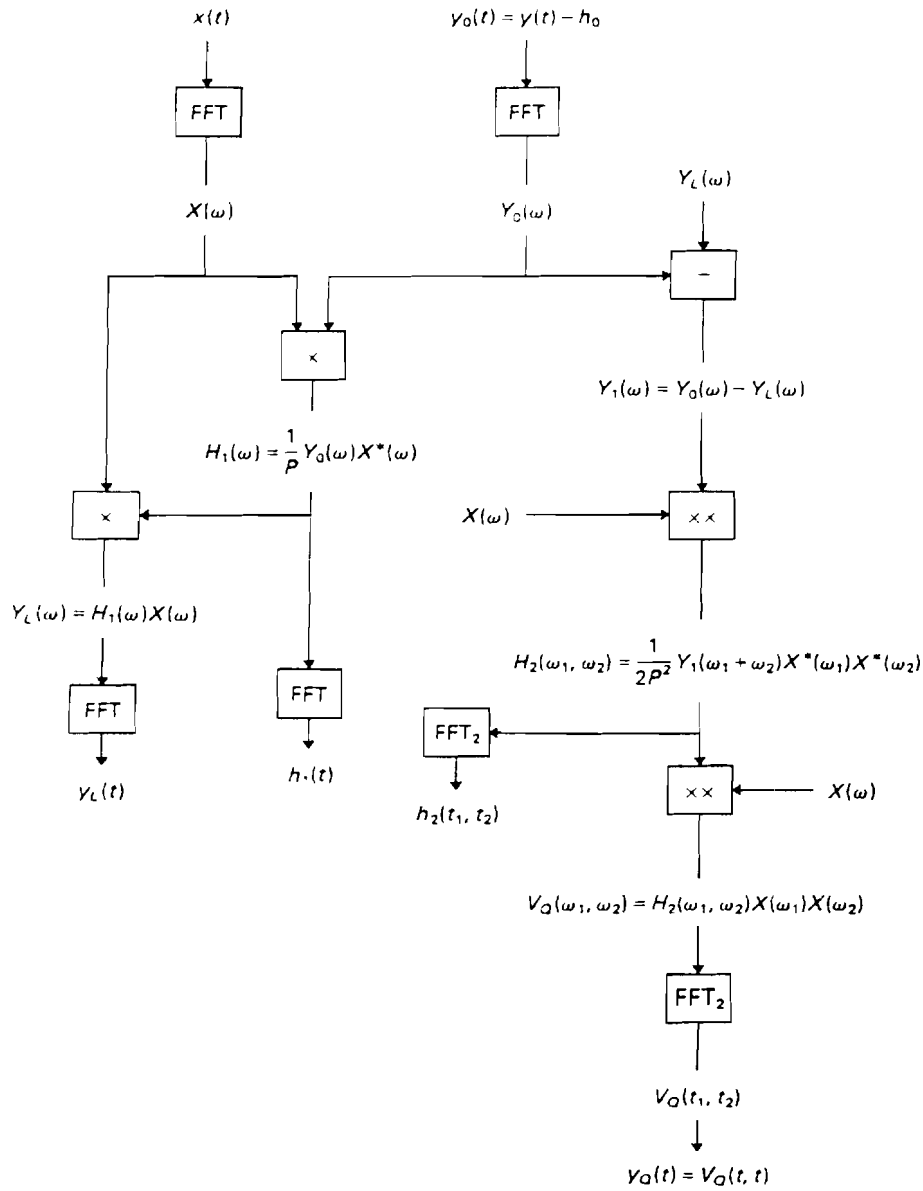

Figure 1.5 Frequency Domain Scheme for Finding Wiener Kernels in the Frequency Domain From Marmarelis [5]

4. Take the transform of $h_1(\tau)$ to find $H_L(\omega)$, the linear transfer function of the system
5. Use $H_L(\omega)$ to find the the linear output $Y_L(\omega)$ by the product $X(\omega)H_L(\omega)$.
6. Subtract the linear response from the total response, $Y(\omega)-Y_L(\omega)=Y_1(\omega)$
7. Cross-correlate $X(\omega)$ with the nonlinear output to get transfer function of quadratic system, namely

$$H_Q(\omega_1,\omega_2) = \frac{1}{2P^2}X(\omega_1)X(\omega_2)Y_1(\omega_1+\omega_2) \tag{1.42}$$

8. Then the residual quadratic response can be formed thusly

$$Y_Q(\omega_1,\omega_2) = H_Q(\omega_1,\omega_2)X(\omega_1)X(\omega_2) \tag{1.43}$$

This formula is actually the cross-bispectrum normalized by the squared spectral density of the input. Other stimuli have been used to generate kernels. True Gaussian white noise is a practical impossibility. Other pseudo-Gaussian white noise signals have been devised to mimic Gaussian noise. Error analysis has been accomplished and detailed in Marmarelis and Marmarelis [5].

1.5 Brief History of Non-Linear Applications of the Bispectrum

Many of the seminal contributions to the early bispectral theory are reviewed by David Brillinger [16]. This is augmented by a general outline of non-linear stochastic system theory and bispectra which appears in the timeline from Table 1.1. Brillinger's interests in higher order spectral analysis arose in part from his professor, John Tukey who coined the terms bi-, tri and poly-spectra and rigorously considered higher moments of time series spectra [17]. Many important early works from Brillinger considered higher order spectra important for understanding deviations from Gaussianity as well as linearity. Glancing at the conventional power spectrum, he mentions that the spectra can broken down into elemental constituent time series through the use of high order spectra. This related directly to the special property of independence of time series and their higher order spectra [18] This was critical for the property of noise immunity. Brillinger, along with Van Ness, was responsible for the key statistical properties of higher order spectra [18, 19]. The ideas of cumulant spectra for non-stationary processes was introduced by Brillinger as well.

Table 1.1 Time Line for Non-Linear Applications of the Bispectrum

Development	Discoverer & Date
Spectral Representation of Higher Order Moments Considered	Tukey **(1958)**
Orthogonal Functional Approach to System Identification	Wiener **(1958)**
Quadratic Cross-Correlation & System Identification	Tick **(1961)**
Quadratic **Non-linearities** Explored	**Hasselman,** et al. **(1963)**
Formal Characterization of Higher Order Spectral Properties	**Brillinger (1965) &** Van Ness **(1966)**
Cross-Correlation Approach to Identifying Wiener Kernels	**Lee & Schetzen (1965)**
Formal Extension of FFT Analysis to **Bispectral** Methods	**Huber,** et al. **(1971)**
Analysis of Physiological Systems Published	Marmarelis **&** Marmarelis **(1978)**
Tests for Gaussianity and Linearity	Subba **Rao &** Gabr **(1980) & Hinich (1982)**
Parametric **Bispectrum** Estimation	**Raghuveer** & **Nikias (1985)**
Shoaling Ocean Waves and Asymmetry	**Elgar &** Guza **(1985)**
Quadratic Contributions to Coherency and Kernel Computation for General Inputs	Kim **&** Powers **(1988)**
Third Order **Cumulant** Matrix & Singular Value Decomposition	Swindlehurst & **Kailath (1989)**

Wiener considered the problem of non-linear system identification by extending the concept of Volterra kernels through the use of orthogonal functionals [15]. In this manner unique representations for coupled linear, quadratic, cubic, etc. systems can be derived that are uncorrelated for certain stimuli, particularly white noise inputs. As discussed above in Section 1.4, higher than second order Volterra kernels are not mutually uncorrelated. Tick discovered important cross-correlation theorems for higher order spectra which lead directly to the identification of quadratic systems' kernels or transfer functions [20].

Hasselman et al. was one of the first investigators to apply the bispectrum to real time series [21]. He applied the autobispectrum to ocean waves. Hasselman et al. related higher order spectral results to fundamental non-linear equations of fluid dynamics and made higher order spectral analysis a practical consideration. Later his work was expanded by Steve Elgar and R. T. Guza at the Scripps Oceanographic Institute [22]. Elgar considered non-linear behavior in water waves at shallower depths than Hasselman et al. He found that stationary segments could be obtained without sacrificing statistical stability. He charted the progression of coupling frequencies with depth. Elgar also looked at exactly how the shapes of waves change with depth and the accompanying a change in biphase of dominant wave frequencies.

The consideration of fluctuations of plasma density associated with energy cascading and turbulence in the edge regions of a tokamak reactor has been a topic of considerable interest [2]. Kim and Powers have extended the kernel method of identification by relaxing the assumption that the input to a composite linear and quadratic system sequence must be Gaussian white noise. Non-Gaussian inputs may also be used in his closed form solution involving the solution of two systems of coupled equations. They also devised a method for calculating the contribution to total coherence of the quadratic portion of a composite system [13].

Much of the work in applying Volterra methods of identification to neural systems as well as a generalized survey of Volterra/Wiener methods have been accomplished by the Marmarelis brothers [5]. The selection of appropriate alternate white noise input sources have been discussed by the authors. These aid in the laboratory synthesis of pseudo-white noise sources from binary digital generators. Different sources of error introduced from the kernel method are also characterized. These authors also consider the characterization of weakly non-linear systems [11]. They authors have devised specialized schemes for each level of identification of the neurons within the retina of the eye.

Subba Rao and Gabr as well as Hinich have devised statistical tests for the hypotheses of Gaussianity and linearity of a time series under study [23, 24]. The test

for Gaussianity considers the null hypothesis:

$$H_0: B(\omega_i, \omega_j) = 0 \text{ for all } \omega_i, \omega_j. \tag{1.44}$$

If the null hypothesis is accepted at given significance level, a, then we may say that the time series under consideration is Gaussian with confidence level 1-a. For the test of Subba Rao and Gabr a restricted region of the bispectrum is selected where the estimates obey a complex normal distribution. A specified grid of samples are selected. A data vector is filled with samples from the grid. The mean vector, $\hat{\eta}$ and covariance matrix, A, are calculated. The complex version of the multivariate Hotellings T^2 test is utilized. Subba Rao's and Gabr's test allows for adjustment of a correlation window. Now frequency points selected beyond a particular separation distance are assumed to be uncorrelated. The longer the data vector, the finer the separation between frequency points. In the case of the Hinich test the independence of samples of the skewnesses (bicoherences) is assumed. For a Gaussian time series the asymptotic distribution of the sum of all data points in domain of bicoherences is said to be chi-squared distributed with 2N degrees of freedom. Here N is the number of points over the entire bispectral domain.

A time series may be linear whether or not the series is considered Gaussian. A second null hypothesis is proposed

$$H_1: bic(\omega_i, \omega_j) \text{ is constant for all } \omega_i, \omega_j \tag{1.45}$$

If this is the case, the time series is said to be linear. The reasoning, behind that test follows. If a linear system, $H(\omega)$, is excited by an i.i.d. noise source:, then the output spectral density for the time series is

$$S_L(\omega) = \frac{\sigma^2}{2\pi} |H(\omega)|^2 \tag{1.46}$$

for all ω. The bispectral density is

$$B_L(\omega) = \frac{\beta^3}{(2\pi)^2} H(\omega_1) H(\omega_2) H^*(\omega_1 + \omega_2) \tag{1.47}$$

Inserting these expressions for the linear system power spectral density and bispectral density into the equation for the bicoherence, the result gives

$$bic(\omega_i, \omega_j) = \frac{\beta^3}{2\pi\sigma^2} \text{ for all i, j} \tag{1.48}$$

Another multivariate Hotellings T^2 is used in the data analysis for Subba Rao. For Hinich's test of linearity the distribution of data points in a non-linear time series' bispectrum is assumed to follow a non-central chi-squared distribution with 2N

degrees of freedom. The non-centrality parameter is determined from the scaled sample mean of the estimated bicoherences. The empirical distribution function of bicoherence estimates is compared to the predicted non-central chi-squared distribution for tests of linearity (see sect. 6.9).

No description of the major discoveries of non-linear applications of by the bispectrum is complete without detailing several of the parametric methods for coupling frequency estimation. In 1985 Raghuveer and Nikias published an autoregressive scheme for estimating coupling frequencies [25]. This publication together with contributions from other researchers in HOS was pivotal in launching the recent surge of interest in this field. Likewise in 1989 Swindlehurst and Kailath developed an eigenstructure approach to the estimation of three wave coupling using the third order cumulant matrix [26].

1.6 List of References

[1] S. Elgar, "Bispectra of Shoaling Ocean Surface Gravity Waves," Workshop on Higher-Order Spectral Analysis, pp. 206-211, Vail, CO, June 1989.

[2] Y.C. Kim, J.M. Beall, E.J. Powers, and R.W. Miksad, "Digital Bispectral Analysis of Self-Excited Fluctuations Spectra," Phys. Fluids, vol. 23, pp. 258-263, Feb. 1980.

[3] E.J. Powers, J.Y. Hong, and Y.C. Kim, "Cross-Sections and Radar Equation for Non-linear Scatterers," IEEE Trans. Aero Elec. Syst., vol. AES-17, pp. 602-605, July 1981.

[4] S.B Kim, E.J. Powers, R.W. Miksad, and F.J. Fischer, "Nonlinear Spectral Decomposition of the Drift Response of Tethered Offshore Structure Subject to Non-Gaussian Irregular Seas," Workshop on Higher-Order Spectral Analysis, pp. 200-205, Vail, CO, June 1989.

[5] P.Z. Marmarelis and V.Z. Marmarelis, Analysis of Physiological Systems, Plenum, New York, NY, 1978.

[6] E.K. Walton and I. Jouny, "Application of Bispectral Techniques to Radar Signature Analysis," Proc. Wkshp. Higher-Order Spec. Anal., pp. 56-61, Vail,CO, June 1989.

[7] T. Bell, "Light that acts like 'natural bits'," IEEE Spectrum, vol. 27, p. 8, Aug. 1990.

[8] C.L. Nikias and M.R. Raghuveer, "Bispectrum Estimation: .A Digital Signal Processing Framework," Proc. IEEE, vol. 75, pp. 869-891, July 1987.

[9] D.R. Brillinger, "The identification of a particular nonlinear time series system," *Biometrika*, vol. 65, pp. 509-525, 1977.

[10] G. B. Giannakis, "Signal Processing Via Higher-Order Statistics," *Ph.D.* Dissertation, University of Southern California, Los Angeles, July 1986.

[11] V.Z. Marmarelis and D. Sheby, "Bispectral Analysis of Weakly Nonlinear Quadratic Systems," in Proc. IEEE 3rd ASSP Workshop on *Spectrum Estimation* and Modeling, pp. 14-16, Boston, MA, Nov. 17-18 1986.

[12] D.R. Brillinger, "The Identification of Polynomial Systems by means of Higher Order Spectra," J. Sound Vibr., vol. 12, pp. 301-313, 1970.

[13] K.I. Kim and E.J. Powers, "A Digital Method of Modeling Quadratically Nonlinear Systems with a General Random Input," IEEE Trans. *Acoust.* Speech Signal Process, vol. ASSP-36, pp. 1758-1769, Nov. 1988.

[14] E.J Powers, C.K. An, S.B. Kim, R.W. Miksad, S.W. Nam, and C.P. Ritz, "Applications of Digital Polyspectral Analysis to Nonlinear Systems Modeling and Nonlinear Wave Phenomena," Workshop on Higher-Order Spectral Analysis, pp. 73-77, Vail,CO, June 1989.

[15] N. Wiener, Non-Linear Problems in Random Theory, MIT Press, Cambridge, MA, 1958.

[16] D.R. Brillinger, "Some History of the Study of Higher-Order Moments and Spectra," Proceedings *Wkshp.* on Higher-Order Spectral *Analysis*, pp. 41-45, Vail,CO, June 1989.

[17] J.W. Tukey, The spectral representation and transformation of higher order *monents* of stationary time series, Reprinted pp. 165-184 in the Collected Works of John W. Tukey, Vol. 1 (ed. D.R. Brillinger)., Wadsworth, Belmont,WA, 1984.

[18] D.R. Brillinger, "An introduction to polyspectra," Ann. Math. Statist., vol. 36, pp. 1351-1374, 1965.

[19] J.W. Van Ness, "Asymptotic normality of bispectral estimates," Ann. Math. Stat., vol. 37, pp. 1257-1272, 1966.

[20] L. Tick, "The Estimation of Transfer Functions of Quadratic Systems," Tech-*nometrics*, vol. 3, pp. 563-577, Nov. 1961.

[21] K. Hasselman, W. Munk, and G. MacDonald, "Bispectra of Ocean Waves," in Time Series Analysis, pp. 125-130, Wiley, New York, NY, 1963.

[22] S. Elgar and R.T. Guza, "Observations of bispectra of shoaling surface gravity waves," J. Fluid Mechanics, vol. 161, pp. 425-448, 1985.

[23] T. Subba Rao and M.M. Gabr, "A test for Linearity of Stationary Time Series," J. Time Series Anal., vol. 1, pp. 145-158, 1980.

[24] M. Hinich, "Testing the Gaussianity and Linearity of a Stationary Time Series," J. Time Series Anal., vol. 3, pp. 169-176, 1982.

[25] M.R. Raghuveer and C.L. Nikias, "Bispectrum Estimation: A Parametric Approach," IEEE Trans. ASSP, vol. ASSP-33, pp. 1213-1220, Oct. 1985.

[26] A.L. Swindlehurst and T. Kailath, "Detection and Estimation Using the Third Moment Matrix," Proc. Int. Conf. ASSP *Soc.*, pp. 2325-2328, Glasgow, Scotland, May 1989.

CHAPTER 2
ALGORITHMS FOR THREE WAVE COUPLING DETECTION AND ESTIMATION

"However it should be emphasized that most of our knowledge of nonlinear wave phenomena (real waves in nature, not mathematical abstractions) has come about as an extension of the linear picture." †

2.1 Introduction

In chapter 2 we provide background material on the bispectrum and model-based measurement of three-wave coupling, particularly the linear autoregressive or AR method of Raghuveer and Nikias [1]. This method starts by estimating the third order cumulants and then solving a set of linear prediction equations based on a single 1-D cumulant slice for the autoregressive coefficients. After parametrizing the system function, the frequency mple product is formed over all the frequencies in the bispectral principle domain. In section 2.4 we show through simulation that the AR method does not provide sharp bispectral peaks at low SNR and instead shows ridges along certain axes. Here it is suggested to use a full 2-D section of the cumulants for nonlinear processes.

Swindlehurst and Kailath use an eigenstructure method [2]. Their mple correlation matrix is built by averaging a signal-mple Kronecker product over several segments of a time series. The singular value decomposition (SVD) of this matrix and the employment of a noise subspace frequency estimator such as the MUSIC (MUltiple SIgnal Classification) algorithm yield coupling frequency estimates [3]. Their method relies on the additive noise being Gaussian. Asymptotically the effects of

† P. Nunez, *The Electric Fields of the Brain.* Oxford, New York, 1981, p. 346

Gaussian noise disappear. Noise effects are minimized. However, the triple Kronecker product method as stated in [2] cannot accommodate white noise with a non-zero third order moment. As bispectral analysis is typically used to study the output of nonlinear systems, it is expected to handle the resulting non-Gaussian noise output.

Although each of these methods provides model-based procedures for detecting three-wave coupling, both ignore the biphase component inherent to the definition of the bispectrum. The biphase measures the temporal dispersion of the third (sum or difference) frequency component relative to the two other members of the sinusoid triad. Temporal dispersion quantifies the relative phase difference among frequencies of a phase-locked sinusoidal triad. Second and higher order Volterra systems with memory have nonlinear phase responses accounting for dispersion. First, here is a review of conventional or nonparametric methods for calculating the bispectrum.

2.2 The FFT-Based Bispectrum -- Direct and Indirect Methods

The indirect method of estimating the bispectrum is described by Brillinger and Rosenblatt & Van Ness and recapitulated by Nikias & Raghuveer [4-6]. This method approximates the third order cumulant sequence and the resulting bispectrum in (1.12) and (1.13), respectfully. For discrete cases with a finite number of points in the series, the procedure to yield an estimate of the third order cumulant sequence, $\hat{R}(k,l)$, for data length N is as follows assuming that { x (1), x (2), ... , x(N)) is our data set:

1. Segment the data into K records of M samples each, i.e. N=KM.
2. Subtract the average of each record.
3. If ($x^{(i)}(k), k = 0, 1, \cdots, M-1$) is the data set in each segment i = 1, 2, ..., K, we obtain an estimate of the third order sequence

$$\hat{r}^{(i)}(k,l) = \frac{1}{M} \sum_{n=s_1}^{s_2} x^{(i)}(n) x^{(i)}(n+k) x^{(i)}(n+l) \qquad (2.1)$$

where

$$i = 1, 2, \cdots, K,$$

$$s_1 = \max(0, -m, -n) \text{ and } s_2 = \min(M-1, M-1-m, M-1-n).$$

In order to form the estimate of the third order cumulant sequence, we must average over all K sections,

$$\hat{R}(k,l) = \frac{1}{K}\sum_{i=1}^{K} r^{(i)}(k,l). \tag{2.2}$$

At this point the bispectrum can be estimated using the discrete Fourier transform for two dimensional data such as a 2-D FFT algorithm over a rectangular region of support with dimensions (2L+1) x (2L+1). Nikias calls this estimate the indirect estimate, $\hat{B}_{IN}(\omega_1,\omega_2)$, or

$$\hat{B}_{IN}(\omega_1,\omega_2) = \sum_{m=-L}^{L}\sum_{n=-L}^{L} \hat{R}(k,l)\, W(k,l)\exp\{-j(\omega_1 m + \omega_2 n)\} \tag{2.3}$$

where W(k,l) is an appropriate window function for smoothing and variance reduction [6]. The properties of these windows and listing of suitable windows appear in the monograph by Subba Rao and Gabr [7]. Naturally, by utilizing the symmetry properties of the bispectrum a good deal of the computational load is reduced.

The 1-D FFT was utilized in the calculation of the bispectrum by Huber et al [8]. Their scheme is considered to be the biperiodogram and is analogous to the use of the periodogram for estimation of the power spectrum. This method has been called the direct method. This method utilizes the segmentation of a record with N data points into K separate records of M points each. The FFT of each record is taken after appropriate windowing by a window w(n)

$$X^{(i)}(\omega) = \sum_{n=0}^{N-1} x^{(i)}(n)w(n)\exp(j\omega n) \tag{2.4}$$

where $X^{(i)}$ is the Fourier transform of the ith record, $x^{(i)}$, of the data sequence, x(n).

For each record the triple product

$$\hat{b}^{(i)}(\omega_1,\omega_2) = X^{(i)}(\omega_1)\, X^{(i)}(Q)\; X^{(i)}(\omega_1+\omega_2) \tag{2.5}$$

is formed. We find the triple products over the region that spans from $0 \le \omega_2 \le \omega_1$ and $0 \le \omega_1 + \omega_2 \le \pi$ radians in accordance with the symmetry relations described above. The triple products are averaged over several records for variance reduction for supposedly stationary sequences to form the direct estimate, $\hat{B}_D(\omega_1,—)$,

$$\hat{B}_D = \frac{1}{K}\sum_{i=1}^{K} \hat{b}^{(i)}(\omega_1,\omega_2). \tag{2.6}$$

This method is known as the direct method since it utilizes the data sequence directly.

Frequency domain smoothing and complex demodulation are other methods that can be utilized for the estimation procedure. Brillinger notes that the expectation of the triple product as calculated by averaging separate biperiodograms does indeed

converge to the Fourier transform of third order cumulant sequence [9] (theorem 4.3).

Huber et al. reiterate the work of Van Ness and mention that the bispectrum is asymptotically normally distributed as well as unbiased for both direct and indirect estimates [8, 10]. For a large number of data records and points per record, the variance of the real portion of the bispectrum equals that of the imaginary portion. The variance of real and imaginary parts of the direct estimator are equal. The variance of each portion is proportional to the power at the frequencies of the sinusoidal triad. The proportionality factor, C, depends on the amount of smoothing, spectral bandwidth, λ, the number of records and the total length of the data record

$$\mathrm{var}\{\mathrm{Re}\hat{B}_{IN}(\omega_1,\omega_2)\} = \mathrm{var}\{\mathrm{Im}\hat{B}_{IN}(\omega_1,\omega_2)\} \approx CP(\omega_1)\,P(\omega_2)\,P(\omega_3) \tag{2.7}$$

where $\omega_3 = \omega_2 + \omega_1$ and $P(\omega_i)$ is the power spectral density at the frequency ω_i. The bicoherence is more often used as a statistical measure of coupling, because it is easier to employ. The bicoherence measures the degree of coupling among a frequency triple. To reiterate, the bicoherence relates what fraction of the total power among a frequency triad is actually involved in coupling. A bicoherence of unity indicates that the all of the sinusoidal power at the three frequencies is involved in coupling.

The statistics of bicoherence are well documented and provide a means of comparing the validity of bispectral measurements. Often, the statistics are described for the magnitude squared bicoherence, $bic^2(\omega_1,\omega_2)$, though both $bic(\omega_1,\omega_2)$, and $bic^2(\omega_1,\omega_2)$ are found throughout the literature. A purely Gaussian process has a true bicoherence of zero for all frequencies in the bispectral domain. The distribution for bicoherence values from a sample of a Gaussian process are asymptotically chi-squared distributed with two degrees of freedom [11]. Hence, its distribution is proportional to an exponential distribution. The expected value of the bicoherence estimator for a Gaussian process is equal to the proportionality constant, C, from the expression for the variance of the bispectral estimator.

For larger expected values of bic^2 the distribution varies. First of all, the bias, $\mathrm{BIAS}[\hat{bic}]$, is

$$\mathrm{BIAS}[\hat{bic}] = \left[\frac{2}{dof}\right](1-bic^2)^2 \tag{2.8}$$

where dof is the degrees of freedom. In (2.8) dof = $2B_eT$ where T is the total record length in time and B_e is the effective bandwidth of one record, $1/T_e$ [12]. The variance, or

$$\mathrm{VAR}[\hat{bic}] = \left[\frac{4(bic)^2}{dof}\right](1-bic^2)^3. \tag{2.9}$$

The distribution of $\hat{bic}^2$ is non-central chi-squared with the degrees of freedom dependent on the taper window used, the number of records used and the total number of data points. The non-central chi-squared distribution can be approximated by an $\alpha\chi^2$ distribution given by

$$f_{\chi^2}\left(\frac{bic^2}{\alpha}\right) = \frac{(bic^2)^{\left(\frac{\nu}{2}-1\right)} e^{-bic^2/2}}{2^{(\nu/2)}\,\Gamma\left(\frac{\nu}{2}\right)}. \tag{2.10}$$

The mean and variance of an alpha chi-squared distribution are $\alpha\nu$ and $2\alpha^2\nu$, respectively. The values of a and v are as follows:

$$a = \frac{E[bic^2]}{\nu} \qquad \nu = \frac{(dof(bic^2))}{2(1-bic^2)^3}. \tag{2.11a-b}$$

There is also a normal approximation to the non-central χ^2-distribution [11].

2.3 Autoregressive Modeling of Three Wave Coupling

The renewed interest in the bispectrum in the 1980's resulted in part from the contributions of Raghuveer and Nikias [1, 6, 13-15]. They developed an autoregressive model using the third order cumulants. Assuming that the system under analysis can be written in the form

$$x(n) = \sum_{i=1}^{p} a_i\, x(n-i) + w(n) \tag{2.12}$$

where p is the order of the system and w(n) is white noise with non-zero third order moment, i.e. $E\{w(n)^3\} = \beta$. The a;, $i = 1, \cdots, p$ are the autoregressive coefficients of the process. Whiteness of the noise is provided by the fact that $E\{w(n)w(n-k)w(n-l)\} = 0$ for all $k,l \neq 0$. Using the fact that x(n) is independent of W(n) we can now multiply the equation above by x(n-k) x(n-l) and take expectations giving

$$R(-k,-l)+\sum_{i=1}^{p} a_i R(i-k,i-l) = \beta\delta(m,n) \tag{2.13}$$

They begin by setting a matrix

$$\mathbf{R} = \begin{bmatrix} R(0,0) & R(1,1) & \cdots & R(p,p) \\ R(-1,-1) & R(0,0) & \cdots & R(p-1,p-1) \\ & & & \\ & & & \\ R(-p,-p) & R(-p+1,-p+1) & \cdots & R(0,0) \end{bmatrix} \tag{2.14}$$

This forms a matrix-based solution by constructing a **Toeplitz** arrangement of the third order cumulants along a diagonal slice in the cumulant domain where

$$\mathbf{Ra} = \beta,$$

$a=[1\ a_1\ a_2\ \cdots\ a_p]^T$ and $\beta=[\beta\ 0\ \cdots\ 0]$. The standard transfer response is found by the following parametrization

$$H(\omega) = \frac{1}{\left[1 + \sum_{i=1} a_i \exp(-j\omega i)\right]}. \tag{2.15}$$

The triple product is formed as shown in (2.16) to form the **biperiodogram** from AR parameters

$$B(\omega_1,\omega_2) = \beta H(\omega_1)H(\omega_2)H^*(\omega_1+\omega_2) \tag{2.16}$$

Now Raghuveer also applies this structure to quadratically phase coupled sinusoids in third order white noise. He claims that the parametrization of the transfer function, $H(\omega)$ above, provides sinusoidal frequency information just as in the second order case. Assuming we allow the poles of our system function to move to the unit circle in the case above, then we approach an extremely narrow band process approximating a sine wave. For quadratically coupled sinusoids, six AR polynomial roots approximate a sinusoidal triple, two roots per term of the sinusoidal triad. This method known as the Third Order Recursion method (TOR) also has a short data version described in [15] which is known as Constrained Third Order Mean (CTOM). Both TOR and CTOM methods have an anti-causal or backwards model as well.

2.4 Shortcomings of the Autoregressive Bispectrum for Three-Wave Coupling

Shortly after Raghuveer's work on the autoregressive bispectrum, Giannakis formalized the ARMA non-minimum phase system identification problem[16, 17]. Giannakis' goal was to calculate the phase character of rational linear time invariant models. As an end result he obtained equations relating second order amplitude sensitive statistics to the phase sensitive statistics of the third order. He: began with the reduced order third order cumulant, $c(m)$, for $k=l=m$ for some linear process $y(n)$ with non-Gaussian noise input, $w(n)$ and impulse response, $h(i)$. Once again the input noise has third order moment, β.

$$R(k,l) = c(m) \equiv E\{y(n)y^2(n+m)\} \tag{2.17}$$

$$= \beta \sum_{i=0}^{\infty} h(i)h^2(i+m)$$

This data is the cumulant information along a diagonal slice in the cumulant domain. If we take the z-transform of $c(m)$, Giannakis showed that

$$C(z) = \beta \sum_{m=-\infty}^{\infty} [\sum_{i=0}^{\infty} h(i)h^2(i+m)]z^{-m} = \gamma_3^v H(z^{-1})H_2(z) \tag{2.18}$$

and

$$H_2(z) = \sum_{m=0}^{\infty} h^2(m)z^{-m} = H(z) * H(z) \tag{2.19}$$

where $*$ stands for complex convolution and $z = \exp(j\omega)$.

Fortunately, we can make use of symmetry relations of the bispectrum to find that the Fourier transform of $c(m)$, $C(\omega)$ is

$$C(\omega) = \frac{1}{2\pi} \int_{-\pi}^{\pi} B(-\omega, \phi)\, d\phi$$

This shows that $C(\omega)$ is a reduced order spectrum called the 1 1/2-D bispectrum. Taking cumulants along the diagonal slice is equivalent to projections in the bispectral domain. This procedure will prove to be the basis or dual of this thesis' contribution of taking cumulant projections to find slice information in the bifrequency domain. Furthermore, Giannakis used this 1 112-D bispectrum to relate phase-sensitive third order statistics to amplitude sensitive second order statistics in this fashion. We can relate input noise power ω^2 to the output spectrum, $S(\omega)$ in this fashion,

$$S(z) = \sigma^2 H(z^{-1}) H(z). \tag{2.20}$$

We can combine (2.20) and (2.18) to yield

$$H_2(z)\, P(z) = \frac{\sigma^2}{\gamma} H(z)\, C(z) \tag{2.21}$$

where P(z) is the power spectral density. It can be seen that the 1 1/2-D spectrum is convenient for identifying the phase character of linear systems. It is obvious that there would be a different form of the bispectral projections for the output of a composite or coupled linear/quadratic system. Still it is important to realize that the 1 1/2-D bispectrum describes only a reduced-order, linearized bispectrum. This does not yield a full 2-D description of the bispectral domain.

Simulations presented by An et al. assessing the performance of AR-based bispectral methods for quadratically phase coupled sinusoids show that an improvement in performance may be obtained when the basic scheme is modified to include more information than the one-dimensional diagonal cumulant slice. [18]. An et al. apply least squares methods to an over-determined set of equations to incorporate additional information from off-diagonal slices. This approach yields better subsequent estimates of the coupling frequencies. The work of An et al. supports the claim that the 1 1/2-D bispectrum does not provide full representation of the bispectrum derived from a nonlinear process.

In low SNR cases, AR estimates of the biperiodogram for three-wave coupling display marked ridge effects as the following shows. In Fig. 2.1 the AR-based bispectra are shown for an 8192 point series consisting of quadratically coupled unit amplitude sinusoids at $f_1 = .34$, $f_2 = .1$, and $f_3 = f_1 + f_2 = .44$ Hz. Initially, no noise is added. Figs. 2.1 and 2.2 show bispectra for a model order of 8 for this noiseless time series with biphases of 0^o and 60^o, respectively. Using the same series, Gaussian noise of unit variance is half-wave rectified and added to the signal component. The signal-to-noise ratio is 4.77 dB. Here the signal power is total power of all 3 members of the sinusoidal triad. The cases with biphases equal to 0^o and 60^o are shown in Figs. 2.3 and 2.4, respectively. The 0^o biphase plot shows an accurate estimate of the coupling frequencies whereas the 60^o biphase case does not indicate the correct frequency. Only when the model order is increased to 12 do both 0^o and 60^o biphase simulations show the correct frequency estimate as shown in Figs. 2.5 and 2.6. However, it is observed that the AR method of calculating discrete bispectra yields three ridges extending from the peak. These ridges are the effect of' the use of the biperiodogram formed from the product of paramemzed transfer functions to display the frequency information. As defined in (2.4)-(2.6), the biperiodogram is a mple

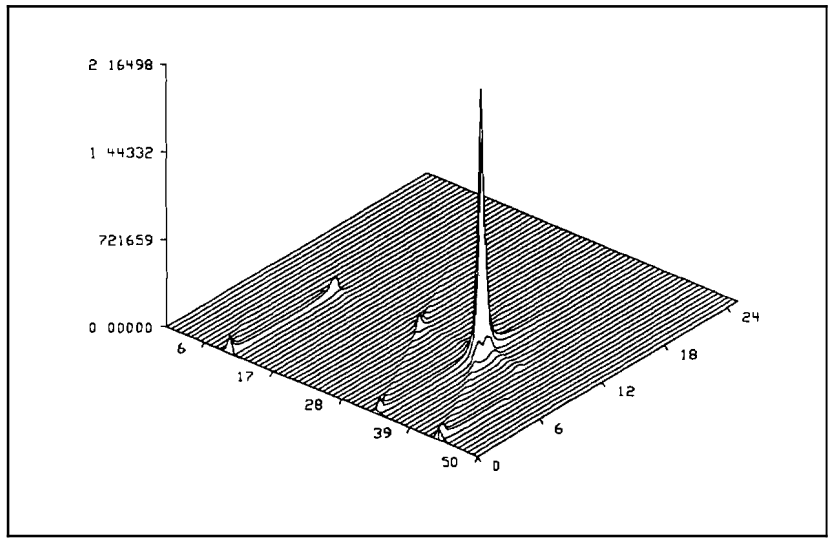

Figure 2.1 **Raghuveer and Nikias AR Modeling of Phase-Coupled Sinusoids: No Added Noise; Order=8; Biphase = 0 degrees**

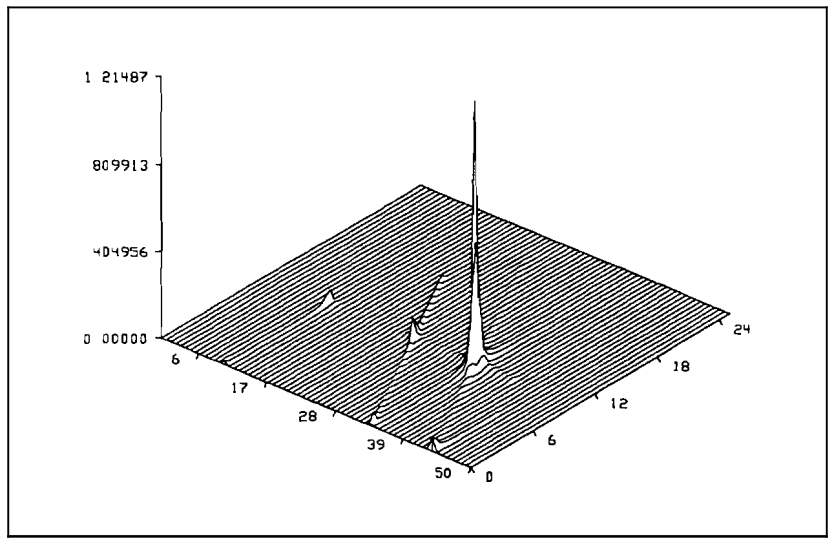

Figure 2.2 **Raghuveer and Nikias AR Modeling of Phase-Coupled Sinusoids: No Added Noise; Order-8; Biphase = 60 degrees**

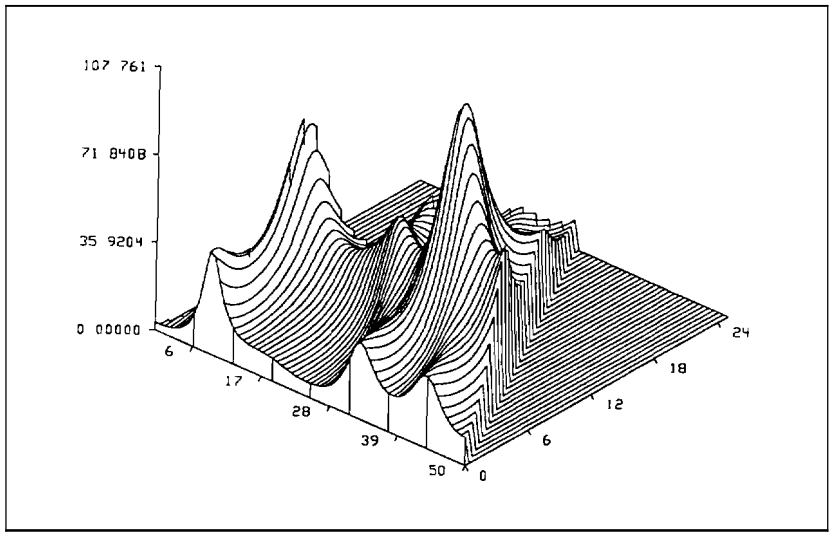

Figure 2.3 Raghuveer and Nikias AR Modeling of Phase-Coupled Sinusoids: Added Exponentially-Distributed Noise, Var=1; Order=8; Biphase = 0 degrees

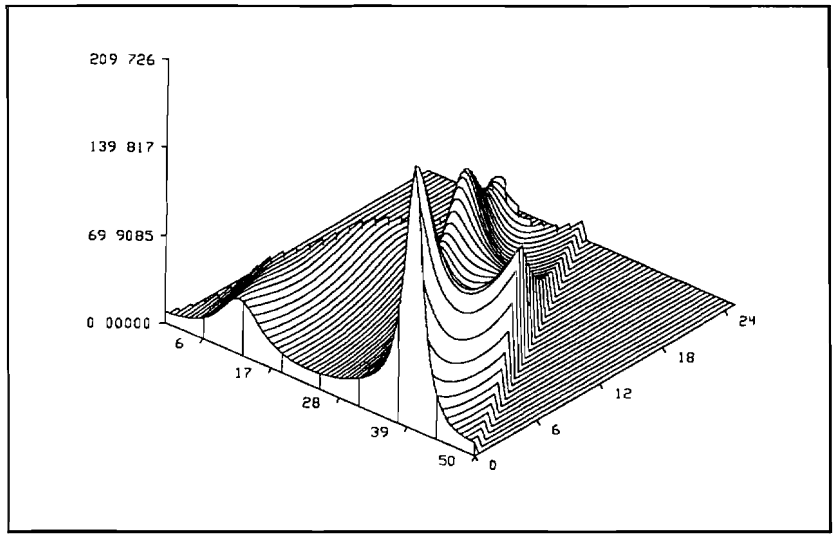

Figure 2.4 Raghuveer and Nikias AR Modeling of Phase-Coupled Sinusoids: Added Exponentially-Distributed Noise; Order=8; Biphase = 60 degrees

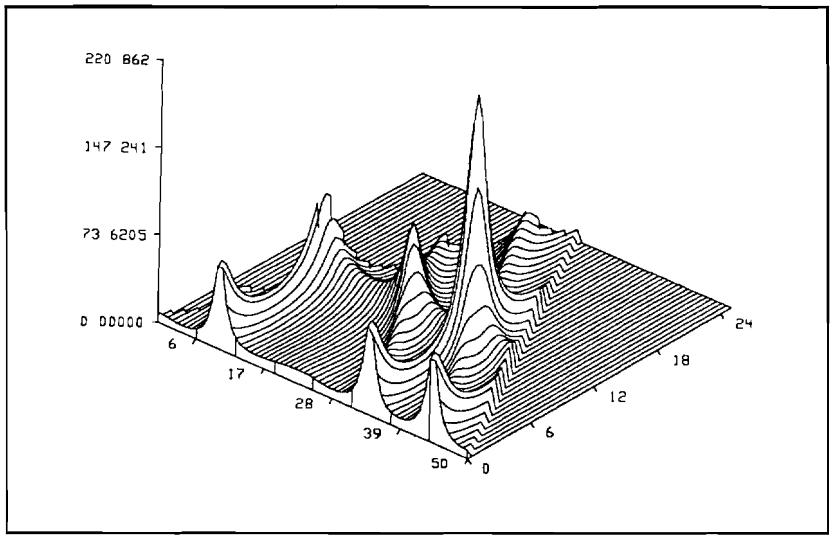

Figure 2.5 Raghuveer and Nikias AR Modeling of Phase-Coupled Sinusoids: Added Exponentially-Distributed Noise, Var=1; Order=12; Biphase = 0 degrees

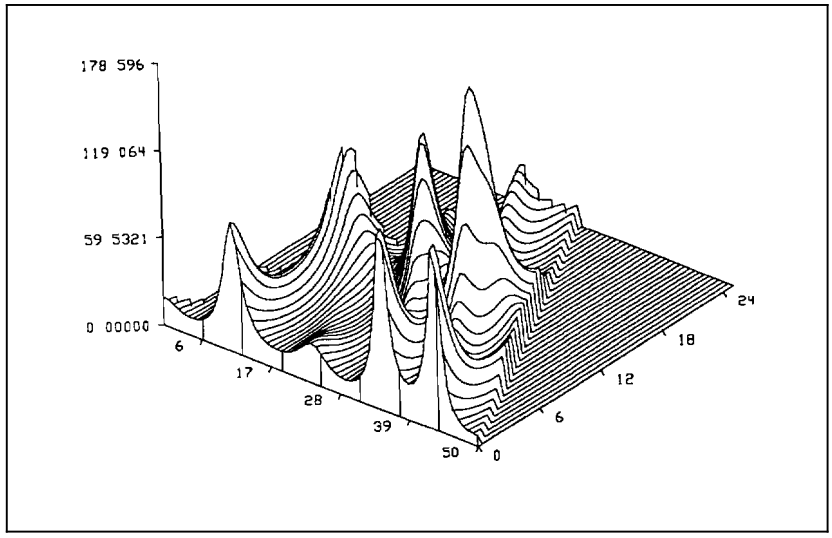

Figure 2.6 Raghuveer and Nikias AR Modeling of Phase-Coupled Sinusoids: Added Exponentially-Distributed Noise; Order=12; Biphase = 60 degrees

product and the first two factors, $H(\omega_1)$ and $H(\omega_2)$ are each functions of only one axis. Accordingly, one ridge runs parallel to the ω_2 axis along the $\omega_1 = 2\pi(.34)$ line. The other ridge runs along the $\omega_2 = 2\pi(.1)$ line (see Figs. 2.5 and 2.6). The diagonal ridge intersects each frequency axis at a frequency value equal to the $\omega_1 + \omega_2 = 2\pi(.44)$. Thus, each ridge presumably corresponds to each of the three constituent transfer functions or factors of the triple product. The point where the ridges coincide gives the peak or point of multiple maximal response.

Also the phase of a sinusoid cannot be accurately represented by an autoregressive model. A 2nd order recursive model of a sinusoid does not contain any starting phase information [19]. Stoica and Nehorai point out that linear prediction can accurately model sinusoids at high signal-to-noise ratios. However, at low SNRs there are severe bias problems that may arise in unconstrained modeling of sinusoids with polynomial roots on the unit circle. In the Raghuveer/Nikias model, the sixth order AR polynomial representing all three coupled sinusoids is a symmetric polynomial. This model is phase neutral [20].

With regard to phase sensitivity for AR models in the case of sinusoidal processes in Gaussian noise, we can show that the same AR coefficients hold for both causal (backward) and anti-causal (forward) prediction cases. We can start with the definition of forward and backward models. Consider a backward prediction AR model of order p+1 for a time series containing a single triad of quadratically phase coupled sinusoids with added Gaussian noise. Using third order cumulants, we have:

$$R(-k,-l) = \sum_{i=1}^{p+1} a_{b,i}\, R(-k+i,-l+i) \tag{2.22}$$

where the $a_{b,i}$ are the backward AR coefficients for a process. Assume that the effects of Gaussian noise are negligible and can be safely ignored. A complimentary forward model of order p+1 could also be constructed where the $a_{f,i}$ are the backward AR coefficients for a process:

$$R(k,l) = \sum_{i=1}^{p+1} a_{f,i}\, R(k-i,l-i). \tag{2.23}$$

As we shall see in chapter 3, the third order cumulant sequence for a single triad of real quadratically phase coupled sinusoids contains three pairs of two dimensional sinusoids. Each pair of terms with the same frequency arguments requires two AR coefficients for a total of 6 AR coefficients. Consider the following backward linear prediction equation relating different points of a single member cosine term of the third order cumulant sequence for quadratically phase coupled sinusoids with an arbitrary phase angle γ and AR coefficients $a_{f,1}$ and $a_{f,2}$:

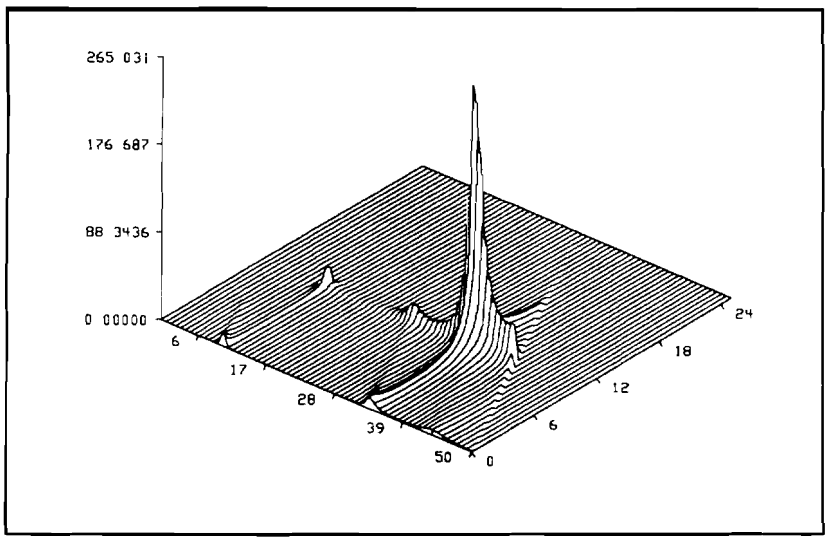

Figure 2.7 Autoregressive Modeling of Phase-Coupled Sinusoids; No Added Noise; Order=6; Symmetric Cumulants; Biphase=30 degrees

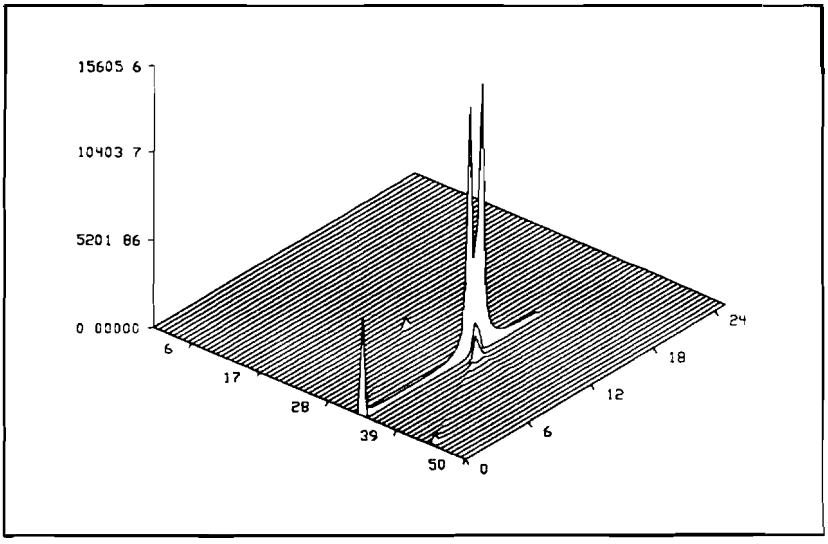

Figure 2.8 Autoregressive Modeling of Phase-Coupled Sinusoids; No Added Noise; Order=6; Skew-Symmetric Cumulants; Biphase=30 degrees

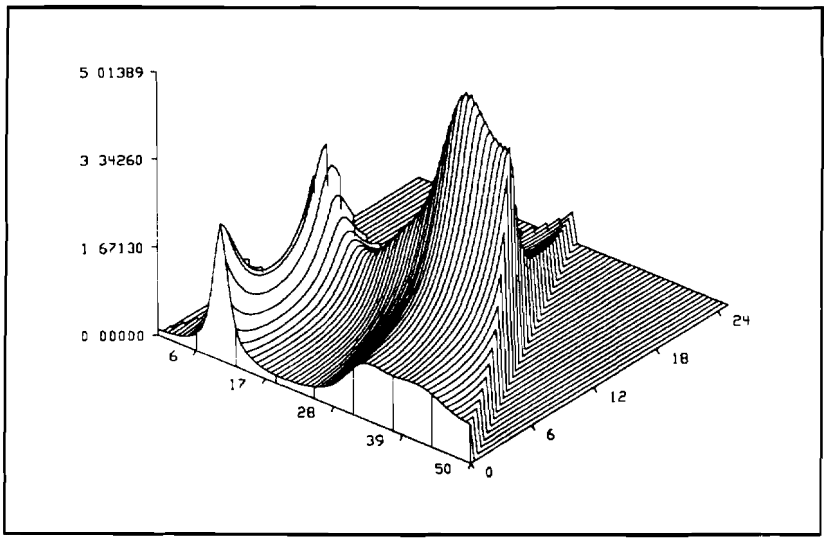

Figure 2.9 Autoregressive Modeling of Phase-Coupled Sinusoids; Added Exponential Noise, Var=1.0; Order=6; Symmetric Cumulants; Biphase=30 degrees

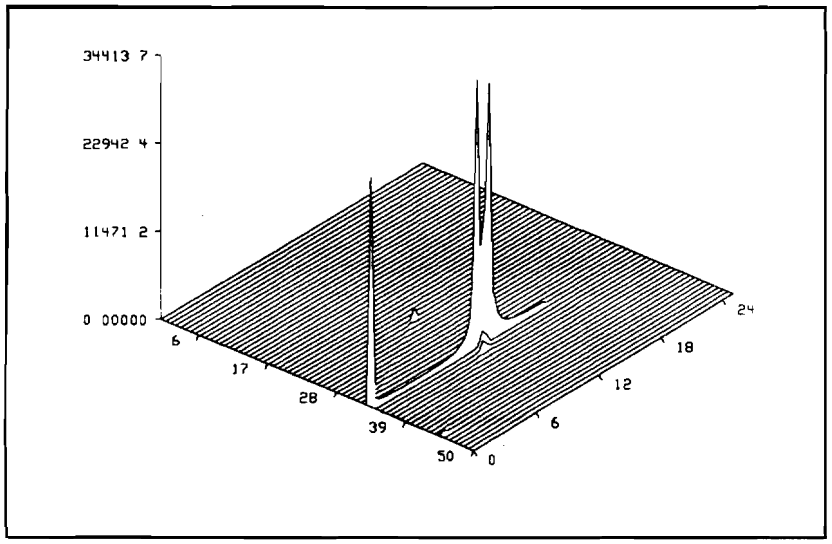

Figure 2.10 Autoregressive Modeling of Phase-Coupled Sinusoids; Added Exponential Noise; Order=6; Skew-Symmetric Cumulants; Biphase=30 degrees

$$\cos(\lambda_1(-k-1) + \lambda_2(-l-1) + \gamma) = a_{b,1}\cos(-\lambda_1 k - \lambda_2 l + \gamma) \tag{2.24}$$

$$+ a_{b,2}\cos(\lambda_1(-k+1) + \lambda_2(-l+1) + \gamma).$$

Using another equation with any choice of starting lags, k' and 1' indexed in a similar fashion, we can solve for $a_{b,1}$ and $a_{b,2}$ and find that

$$a_{b,1} = 2\cos(\lambda_1 + \lambda_2) \tag{2.25}$$

$$a_{b,2} = -1.$$

Likewise in the backward equation for sinusoids

$$\cos(\lambda_1(k+1) + \lambda_2(l+1) + \gamma) = a_{f,1}\cos(\lambda_1 k + \lambda_2 l + \gamma) \tag{2.26}$$

$$+ a_{f,2}\cos(\lambda_1(k-1) + \lambda_2(l-1) + y).$$

Now we see that in fact $a_{f,1} = a_{b,1}$ and $a_{f,2} = a_{b,2}$ so the AR coefficients do not confer any phase sensitivity. Since the forward and backward models are alike in the case of phase-coupled sinusoids, we can write for a (p-tl) x (p-tl) dimensioned cumulant slice matrix for generalized AR coefficients, $a_i = a_{f,i} = a_{b,i}$.

$$\mathbf{R}\,\mathbf{a} = -\mathbf{r}^- \tag{2.27a}$$

$$\mathbf{R}^T\,\mathbf{a} = -\mathbf{r}^+ \tag{2.27b}$$

where $\mathbf{r}^{\pm} = [\mathbf{R}(\pm1,\pm1)\ \mathbf{R}(\pm2,\pm2)\ \cdots\ \mathbf{R}(\pm(p+1),\pm(p+1))]^T$. Also the third order correlation matrix R appears in (2.13). The vector of generalized AK coefficients is $a = [a_1\ a_2\ \cdots\ a_{p+1}]^T$. We have indicated the dimension of matrices and vector by the subscripts in parentheses.

Since both models are equivalent, we might try to construct a composite model combining both forward and backward lagged cumulants. This is the symmetric model employing symmetric cumulants.

$$\tfrac{1}{2}(\mathbf{R} + \mathbf{R}^T)\,\mathbf{a} = 1/2(\mathbf{r}^+ + \mathbf{r}^-) \tag{2.28}$$

In terms of symmetrized cumulants where $\mathbf{R}_{SYM} = \tfrac{1}{2}(\mathbf{R} + \mathbf{R}^T)$ and $\mathbf{r}_{SYM} = \tfrac{1}{2}(\mathbf{r}^+ + \mathbf{r}^-)$:

$$\mathbf{R}_{SYM}\mathbf{a} = \mathbf{r}_{SYM}. \tag{2.29}$$

For any given **k,l** we can write an single constituent equation containing the symmetrized cumulants

$$1/2\{R(k,l) + R(-k,-l)\} = 1/2\sum_{i=1}^{p} a_i\{R(k-i,l-i)+R(-k+i,-l+i)\} \; . \qquad (2.30)$$

or in a more compact rendition,

$$S(k,l) = \sum_{i=1}^{m} a_i \; S(k+i,l+i) \qquad (2.31)$$

where $S(k,l) = \frac{1}{2}(R(k,l)+R(-k,-l))$.

At the same time we can generate a skew-symmetric version of the linear prediction equations regardless of phase relationship expressed by the cumulants

$$1/2(\mathbf{R} - \mathbf{R}^T)\,\mathbf{a}_i = 1/2(\mathbf{r}^+ - \mathbf{r}^-). \qquad (2.32)$$

This forms an equivalent skew- or conjugate symmetric model with the same coefficients as the symmetric model for all biphases in a linear prediction context.

$$\mathbf{R}_{SKW}\mathbf{a} = \mathbf{r}_{SKW} \qquad (2.33)$$

$$1/2\{R(k,l) - R(-k,-l)\} = 1/2\sum_{i=1}^{p} a_i\{R(k-i,l-i)-R(-k+i,-l+i)\} \qquad (2.34)$$

$$A(k,l) = \sum_{i=1}^{m} a_i \; A(k+i,l+i) \qquad (2.35)$$

The following plots illustrate the usefulness of using symmetric and skew-symmetric cumulants for modeling quadratic phase coupling for high signal-to-noise ratio time series. Unit amplitude phase-coupled sinusoids at $\omega_1 = 2\pi(.34)$, $\omega_2 = 2\pi(.1)$ and $\omega_3 = 2\pi(.44)$ without added noise comprise a time series. Symmetric and skew-symmetric cumulant sequences are formed from the cumulants taken from dividing the time series into 64 records of 128 (N = 8192) each. Autoregressive modeling from these cumulant sequence yield satisfactory coupling frequency estimates as can be seen in Figs. 2.7 and 2.8. Once noise is added, however, it can be seen that the coupling frequency estimates based on AR modeling of skew-symmetric cumulants are considerably better than those calculated from the symmetric cumulants. The noise component adversely effects the symmetric cumulants.

A better representation of the sinusoidal information may come from a direct eigenstructure approach. Recently, these models have become commonplace for sinusoidal frequency estimation in both spectral analysis and array processing [3]. The motivation for constructing an eigenstructure model is twofold. First, the eigenstructure approach is model based. The inspiration for the eigenstructure method is that certain eigenvectors of the signal-only correlation matrix span the same vector

subspace as the constituent complex exponential signals. We can view the third order cumulant sequence as composed of sums of complex exponentials.

Second, we would like our eigenstructure model to represent more fully the extent of the 2-D cumulant sequence. i.e. it is desired to expand the region of consideration beyond that of a simple slice or group of slices which is traditionally associated with linear modeling. The Volterra kernel that represents quadratic interactions is truly a function of two time (frequency) variables. Our bispectral estimator could avoid parametrization of the transfer function, $H(\omega)$, along a single cumulant slice. An average of triple products of $H(\omega)'s$ yields a biperiodogram. Brillinger shows that the bi- or tri-periodogram does in fact converge, albeit slowly, to the direct estimate, the 2-D or 3-D Fourier transform, respectively [9]. We would like to bypass the calculation of the linear transfer function and go directly to ascertaining the frequencies of the coupled sinusoids.

Thirdly, and perhaps most importantly, we would like our model to contain information on phase. It is only fitting that the bispectrum contain relative phase information about the sinusoids. The biphase information is a critical component of coupling frequency estimation. In order to discover how an eigenstructure method can be used for biphase estimation, a short overview of eigenanalysis-based spectral estimation via the MUSIC algorithm is required.

2.5 Generalities of the Eigenstructure Method

MUSIC (MUltiple SIgnal Classification) is a very popular spectral analysis technique that requires the estimation of the autocorrelation matrix of a random process assumed to be composed of a known number of complex sinusoidal signals immersed in white noise [3]. The key to improved performance of these methods is the division of information in'the autocorrelation matrix into two vector subspaces, the signal subspace and the orthogonal (or noise) subspace. They also provide high resolution estimates of the sinusoidal frequencies in conventional spectral estimation. The dimensionality of the signal subspace is determined by the number of assumed complex sinusoids immersed in the noise sequence in question. Eigenanalysis allows for removal of extraneous noise contributions for a much higher signal to noise ratio in the ultimate calculation of the frequencies of the embedded sinusoids. The success in subspace approaches for power spectral density estimation have motivated research in applying them to the bispectrum and the investigation of non-linear interactions

among harmonic components of a time series. Giannakis and Swami & Mendel have utilized rank reduction techniques on higher order statistics for robust system identification. [16, 21].

A random process consisting of M unit amplitude, real sinusoids of radian frequency, μ_i , i=1,2...M, of random phase in white noise has a standard autocorrelation function, R(k)

$$R(k) = 1/2\sum_{i=1}^{M} \cos(\mu_i kT) + \rho_i \delta(k) \tag{2.36}$$

where ρ_i is the noise variance and $\delta(k)$ is the Kronecker delta. The (pxl) x (p+1) autocorrelation matrix, where p > 2M, can subsequently be expressed as the sum of corresponding signal and noise autocorrelation matrices:

$$\mathbf{R}_p = \mathbf{S}_p + \mathbf{W}_p. \tag{2.37}$$

The signal matrix can be written in terms of a sum of rank one outer products. The outer products are of the form

$$\mathbf{S}_p = \sum_{i=1}^{M} \frac{P_i}{2} [\mathbf{s}_i \otimes \mathbf{s}_i^H + \mathbf{s}_i^* \otimes \mathbf{s}_i^T] \tag{2.38}$$

where

$$\mathbf{s}_i = [1\ e^{-j\omega_i}\ e^{-j2\omega_i}\ \cdots\ e^{-j(p-1)\omega_i}]^T$$

and P_i is the power in the ith sinusoid. The signal mamx has a completely Vandermonde structure.

Likewise the noise mamx $\mathbf{W}_p = \rho\mathbf{I}$ where ρ is the added white noise. Here $\mathbf{S}_p$ and $\mathbf{W}_p$ are the signal and noise autocorrelation matrices, respectively. The signal matrix will have the eigendecomposition

$$\mathbf{S}_p = \sum_{i=1}^{p+1} \lambda_i [\mathbf{v}_i \otimes \mathbf{v}_i^H] \tag{2.39}$$

where λ_i denotes the ith eigenvalue and $\mathbf{v}_i$, the respective eigenvector and $\lambda_1 \leq \lambda_2 \leq \ldots \lambda_{2M}$. It is clear that of the (p+1) eigenvalues of the signal matrix, $\mathbf{S}^p$, there are M non-zero eigenvalues. The corresponding M eigenvectors known as the principal eigenvectors will span the same subspace as the M real sinusoids comprising the signal portion of the time series. It can be shown that the signal mamx will have exactly 2M non-zero eigenvalues. The eigenvalue/eigenvector decomposition of the of $\mathbf{R}_p$ is

$$\mathbf{R}_p = \sum_{i=1}^{2M} \lambda_i [\mathbf{v}_i \otimes \mathbf{v}_i^H] + \rho_w \sum_{i=1}^{p+1} \mathbf{v}_i \otimes \mathbf{v}_i^H \tag{2.40}$$

The remaining p+1-2M eigenvectors of the signal matrix span the noise subspace. The spectral estimator makes use of the orthogonality between both subspaces. The noise subspace eigenvectors will be orthogonal to any vectors spanning the signal subspace, e.g. the sine waves comprising the signal. This property is exploited by the noise subspace estimator known as the MUSIC algorithm. The frequency estimator is

$$P(f) = \frac{1}{\mathbf{e}^H(\omega)\, \mathbf{N}_v\, \mathbf{e}(\omega)} \tag{2.41}$$

where $\mathbf{e}(f) = [1\ d^m\ \cdots\ e^{j(p+1)\omega n}]^T$ and

$$\mathbf{N}_v = \sum_{i=2M+1}^{p} \mathbf{v}_i \otimes \mathbf{v}_i^H \tag{2.42}$$

constitutes the "noise" or orthogonal complement subspace.

2.6 The Triple Kronecker Product Estimate

Swindlehurst and Kailath exploit the structure of the second order cumulant matrix, i.e. the autocorrelation matrix

$$\mathbf{R}_2 = E\{\mathbf{x} \otimes \mathbf{x}^H\} \tag{2.43}$$

where x is the signal, Es plus Gaussian noise, n vectors [2]. E is an m x d matrix containing the d complex exponential vectors in a Vandermonde form. Then d is the total number of complex exponentials present whether or not every one of them is involved in the coupling. The s vector contains amplitudes and associated phases for the group of sinusoids. They build a third order cumulant matrix from the triple Kronecker product in similar fashion

$$\mathbf{R}_3 = E\{\mathbf{x} \otimes \mathbf{x} \otimes \mathbf{x}^H\} \tag{2.44}$$

If the signal vector x has m elements, then $\mathbf{R}_3$ is an m^2xm dimensioned matrix.

The rank of $\mathbf{R}_3$ is dependent on whether or not phase coupling does occur. For each group of coupled sinusoids, Swindlehurst and Kailath claim that the asymptotic rank of $\mathbf{R}_3$ is equal to 2d' where d' is the number of real sinusoids involved in coupling. They use a singular value decomposition of $\mathbf{R}_3$, i.e. $\mathbf{R}_3 = \mathbf{U}\Sigma\mathbf{V}^H$. They partition U into signal and noise subspaces according to the size of the singular values,

$$\mathbf{U} = [\mathbf{u}_1\ \mathbf{u}_2\ \cdots \mathbf{u}_{m^2}] \tag{2.45}$$

$$= [\mathbf{U}_s \mid \mathbf{U}_n]$$

where $\mathbf{U}_s$ and $\mathbf{U}_n$ represent the signal and noise component singular vectors. The $\mathbf{span}(\mathbf{R}_3) = \mathbf{span}(\mathbf{U}_s)$. We find that the $\mathbf{span}(\mathbf{U}_s)$ is orthogonal to the $\mathbf{span}(\mathbf{U}_n)$. They use an appropriate frequency estimator for the coupling frequency pairs or double frequency terms of the bispectrum, called $\hat{B}_D$.

$$\hat{B}_D(\omega_y, \omega_z) = \frac{1}{\mathbf{e}_{yz}^*\ \mathbf{U}_n \mathbf{U}_n^H\ \mathbf{e}_{yz}} \tag{2.46}$$

where $\mathbf{e}_{yz} = \mathbf{e}(\omega_y) \otimes \mathbf{e}(\omega_z) + \mathbf{e}(\omega_z) \otimes \mathbf{e}(\omega_y)$ and

$$\mathbf{e}(\omega_i) = [1\ e^{j\omega_i}\ e^{j2\omega_i}\ \cdots\ e^{j(m-1)\omega_i}]^T \tag{2.47}$$

Likewise the right singular vectors yield frequencies of single sinusoids involved in coupling in a 1-D formulation using the following estimator.

$$\hat{B}_S(\omega_x) = \frac{1}{\mathbf{e}(\omega_x)^*\ \mathbf{V}_n \mathbf{V}_n^H\ \mathbf{e}(\omega_x)} \tag{2.48}$$

where $\mathbf{V}_n$ are the noise subspace right singular vectors.

2.7 Symmetric and Skew-Symmetric Sequences and Time Reversibility

One of the key conditions that needs to be satisfied in order to do the eigendecomposition of the third order cumulant mamx is that the mamx be Hermitian. Hermitian matrices have real eigenvalues. Also for nonrepetitive eigenvalues, respective eigenvectors are orthogonal. One of the properties lacking in third order spectral analysis is the fact that higher order cumulant sequences lack the symmetry property that characterizes second order statistics, i.e. in general $\mathbf{R(k,l)}$ does not equal $\mathbf{R(-k,-l)}$ or positive lagged sequences do not necessarily equal negative lagged ones. This symmetry property insures that our second order cumulant sequences are always symmetric and therefore can be decomposed spectrally. When positive (forward) statistics do not equal negative (backward) statistics, we say that our series is not time-reversible. The fact that a non-zero bispectrum displays the time reversible character is a direct result of fact that it bears phase information. The third order autocorrelation matrix as it appears in the Nikias and Raghuveer AR formulation is not Hermitian. Here are some further comments about the reversibility of random processes.

A time series (X_t) that is strict sense stationary can be considered to be time reversible (second order) if for every n and every $t_1, t_2, \ldots, t_n$, each collection of random variables

$$\{X(t_1), X(t_2), \cdots X(t_n)\} \text{ and } \{X(-t_1), X(-t_2), \cdots, X(-t_n)\}$$

have the same joint density. Because of stationarity we can state that

$$\{X(m+t_1), X(m+t_2), \cdots X(m+t_n)\} \text{and} \{X(m-t_1), X(m-t_2), \cdots, X(m-t_n)\}$$

have the same density functions. Typically we simply say that the joint density for forward time lags is equal to the joint density for backward time lags. Johnson and Rao mention that all Gaussian signals are time-reversible as the joint amplitude density for a Gaussian signal is dependent only on second order statistics [22]. The autocorrelation function as well as the covariance matrix are symmetric quantities. ARMA processes stimulated by Gaussian noise turn out to be time reversible quantities [23].

For non-time-reversible signals phase information is not present. Simple reversal of the time axis does not reveal any statistical differences that might reveal a phase character to the data. As mentioned before all second order statistics because of their symmetric nature do not reveal phase information. Many spectral analysis algorithms assume that forward and backward prediction errors are equal. Gaussian processes are the only certain cases where such an assumption can be made with any degree of certainty.

We may divide the third order cumulant sequence into two separate portions called the symmetric, $S(k,l)$, and anti-symmetric, $A(k,l)$, cumulants in this fashion

$$S(k,l) = \frac{1}{2}\left[R(k,l) + R(-k,-l)\right] \tag{2.49}$$

$$A(k,l) = \frac{1}{2}\left[R(k,l) - R(-k,-l)\right] \tag{2.50}$$

$$R(k,l) = S(k,l) + A(k,l). \tag{2.51}$$

As a consequence of this division we might differentiate the real and imaginary portions of the bispectrum by their respective cumulant sequences, $S(k,l)$ and $A(k,l)$ [24].

$$\text{Re}\{B(\omega_1,\omega_2)\} = \text{DFT}\{S(k,l)\} \tag{2.52}$$

$$\text{Im}\{B(\omega_1,\omega_2)\} = \text{DFT}\{A(m,n)\} \tag{2.53}$$

There are also cumulative measures of magnitude in the real and imaginary parts of the bispectrum. The skewness, S_{tot}, and asymmetry, A_{tot}, of the time series are

analogous to the total power of second order statistics.

$$S_{tot} = \left[\sum_k \sum_l \mathrm{Re}\{B(\omega_k,\omega_l)\}\right] / \left[\sigma^2\right]^{3/2} \tag{2.54}$$

$$A_{tot} = \left[\sum_k \sum_l \mathrm{Im}\{B(\omega_k,\omega_l)\}\right] / \left[\sigma^2\right]^{3/2} \tag{2.55}$$

where we sum over m and n in entire bispectral domain for each entity. Both quantities **S** and **A** are normalized by the total time series power σ_2. They are analogous to the cumulative measure of power in second order statistics.

With regard to signals, the real and imaginary parts of the bispectrum have special meaning in reference to signal shape. If the bispectrum of a signal has non-zero skewness, it is said to display asymmetry with regard to a horizontal axis. The signal that is represented by the solid line in Fig. 2.11 displays non-zero skewness and is not balanced above and below the **y=0** line. Reciprocal events do not occur above and below this axis of vertical **symmetry/asymmetry.** Conversely, if a signal shows zero skewness and non-zero asymmetry, then the signal is said to show asymmetry with regard to a vertical axis. The dashed signal in that figure is a prime. example of this signal type. **A** vertical line drawn normal to the x-axis at **x=0** is the asymmetric fold-over point for the waveform. Now events that occur below the **y=0** symmetry line also occur above it. The bispectrum could be a useful tool for shape recognition of a signal in a very noisy environment with additive Gaussian noise.

The connection between the real and imaginary parts of the bispectrum and the biphase follows directly. **A** signal with an entirely real bispectrum has a zero biphase throughout for all frequency couplings. By analogy to Fourier theory for deterministic signals, we expect the cumulant series to be an even function of the two arguments. Consider the six term expression for the bispectrum of quadratically coupled sinusoids. With zero biphase, the cumulants are purely symmetric with **R(k,l)=R(−k,l)** and are cosinusoids with zero phase angles. The solid line plot on Fig. 2.11 shows a triad of quadratically coupled sinusoids with zero biphase. The frequency of one of the sinusoids is $\omega = 2\pi(.05)$. The second has $\omega = 2\pi(.1)$. Likewise a non-zero biphase indicates the imaginary portion of the bispectrum is also non-zero. **A** full 90 degrees means **R(m,n) = -R(-m,-n)** and we have a state of full asymmetry. The same frequencies are involved in the couplings for the dashed **line,** but this time the biphase is 90 degrees.

There are several applications where measurements of biphase actually helps characterize system properties. The presence of a non-zero biphase in a triad of

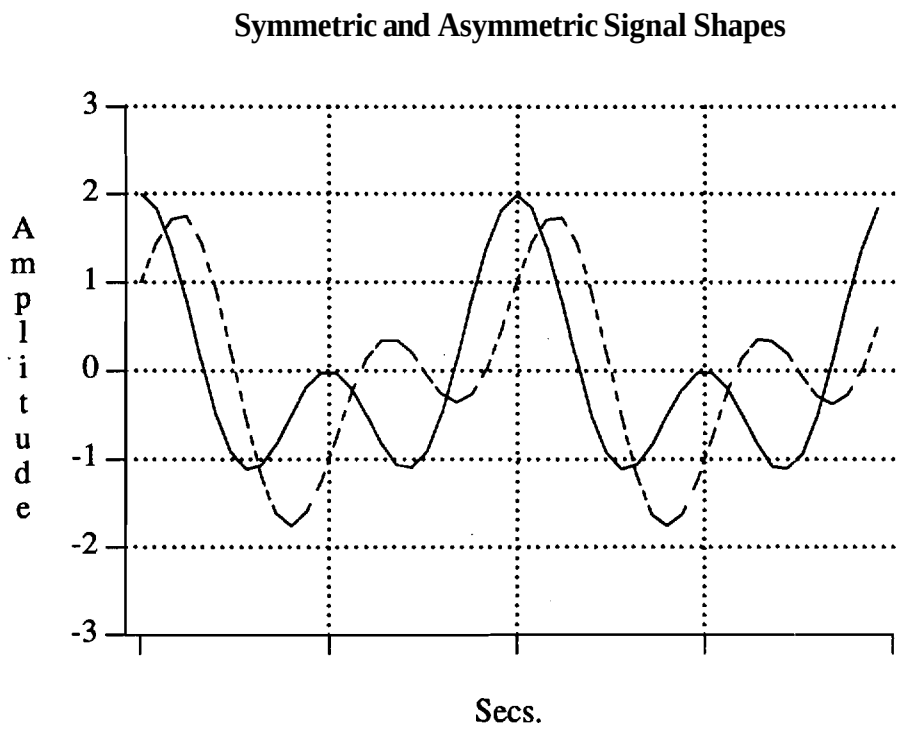

Figure 2.11 Symmetric and asymmetric signal shapes; Solid line: Symmetric Signal, Biphase=0° -- Zero Vertical Asymmetry, Non-Zero Horizontal Skewness; Dotted line: Asymmetric Signal, Biphase=90° -- Non-Zero Vertical Asymmetry, Zero Horizontal Skewness

coupled sinusoids indicates the lack of temporal isotropy. An isotropic medium, for instance, is uniform with regard to change in time direction, $t \rightarrow -t$, or it is called time-reversible. Wave shape is intimately connected with time reversibility. Matsuda and Kuo find that water waves affected by surface winds change their shapes [25]. Waveforms tilted forward and backward by wind exhibit changes in their biphase. They regard changes in temporal asymmetry as related to changes in spatial asymmetry such as changing water depth. Elgar shows that as waves shoal the biphase is a dynamic quantity dependent on both progressions of depth [26].

To illustrate how a non-zero biphase arises, consider the fact that the Volterra kernels have memory along two time lag indices to account for deviations from additive superposition throughout the response interval. If $y(t) = x^2(t-1)$ for instance, then $H_2(f_1, f_2) = e^{-j2\pi(f_1+f_2)}$. We note that a phase factor has been is added to the generated second harmonic from such a transfer response. The phase is proportional to the magnitude of the coupled frequencies input to the system.

2.8 List of References

[1] M.R. Raghuveer and C.L. Nikias, "Bispectrum Estimation for Short Length Data," Proc. *ICASSP-85*, pp. 1352-1355,1985.

[2] A.L. Swindlehurst and T. Kailath, "Detection and Estimation Using the Third Moment Matrix," Proc. Int. Conf. ASSP *Soc.*, pp. 2325-2328, Glasgow, Scotland, May 1989.

[3] R. O. Schmidt, "Mulitple Emitter Location and Signal Parameter Estimation," IEEE Trans. Antennas Propagat, vol. AP-34, pp. 276-280, March 1986.

[4] D.R. Brillinger, "An introduction to polyspectra," Ann. Math. Statist., vol. 36, pp. 1351-1374, 1965.

[5] M. Rosenblatt and J.W. Van Ness, "Estimation of the Bispectrum," Ann. Math. Statist., vol. 36, pp. 1120-1136, 1965.

[6] C.L. Nikias and M.R. Raghuveer, "Bispectrum Estimation: A Digital Signal Processing Framework," Proc. IEEE, vol. 75, pp. 869-891, July 1987.

[7] T. Subba Rao and M. Gabr, An Introduction to Bispectral Analysis and Bilinear Time Series Models: Lecture Notes in Statistics, No. 24, Springer, New York, 1984.

[8] P.J. Huber, B. Kleiner, T. Gasser, and G. Dumermuth, "Statistical Methods for Investigating Phase Relations in Stationary Stochastic Processes," IEEE Trans. Audio Elec., vol. AU-19, pp. 78-86, 1971.

[9] D.R. Brillinger, Time Series, Data Analysis and Theory, Holden-Day, San Francisco, CA, 1981. (expanded edition)

[10] J.W. Van Ness, "Asymptotic normality of bispectral estimates," Ann. Math. Stat., vol. 37, pp. 1257-1272, 1966.

[11] G. Sebert and S. Elgar, "Statistics of Bicoherance and Biphase," Workshop on Higher-Order Spectral Analysis, pp. 223-228, Vail,CO, June 1989.

[12] J.S. Bendat and A.G. Piersol, Random Data: Analysis and Measurement Procedures, Wiley-Interscience, New York, NY, 1971.

[13] M.R. Raghuveer, Bispectrum and Multidimensional Power Spectrum *Estimation Algorithms* Based on Parametric Models with Applicaitions to the Analysis of ECG data, Ph.D. dissertation, Univ. of Connecticut, Storrs, Dec. 1984.

[14] C.L. Nikias, "Higher-Order Spectra in Signal Processing," Workshop on Higher Order Spectral Analysis, vol. Tutorial Session, Vail, CO, June 28-30, 1989.

[15] M.R. Raghuveer and C.L. Nikias, "Bispectrum Estimation: A Parametric Approach," IEEE Trans. ASSP, vol. ASSP-33, pp. 1213-1220, Oct. 1985.

[16] G. B. Giannakis, "Signal Processing Via Higher-Order Statistics," *Ph.D.* Dissertation, University of Southern California, Los Angeles, July 1986.

[17] G.B. Giannakis and J.M. Mendel, "Identification of Nonminimum Phase Systems Using Higher Order Statistics," IEEE Trans ASSP, vol. ASSP-37, pp. 360-377, March 1989.

[18] C.K. An, S.B. Kim, and E.J. Powers, "Optimized Parametric Bispectrum Estimation," Proc. Int. *Conf.* ASSP *Soc.*, pp. 2392-2395, Vail, CO, April 1988.

[19] S. Kay, Modern Spectral Estimation, Prentice-Hall, Englewood Cliffs, NJ, 1988.

[20] P. Stoica and A. Nehorai, "The Poles of Symmetric Linear Prediction Models Lie on the Unit Circle," IEEE Trans. *ASSP*, vol. ASSP-34, pp. 1344-1346, October 1986.

[21] A. Swami and J.M. Mendel, "Cumulant-based approach to the harmonic retrieval and related problems," IEEE Trans. SP, vol. SP-39, pp. 1099-1109, May 1991.

[22] D.H. Johnson and P.S. Rao, "Properties and Generation of Non-Gaussian Time Series," Proc. Int. Conf ASSP *Soc.*, pp. 37-40, New York, NY, April 1987.

[23] G. Weiss, "Time-Reversibility of Linear Stochastic Processes," J. Appl. Prob., vol. 12, pp. 831-836, 1975.

[24] S. Elgar, "Relationships Involving Third Moments and Bispectra of a Harmonic Process," IEEE Trans. *Acoust.* Speech and Signal Proc., vol. ASSP-35, pp. 1725-1726, Dec. 1987.

[25] A. Matsuda and Y. Kuo, "A note on the imaginary part of the bispectrum," Deep-Sea Research, vol. 28A, pp. 213-222,1981.

[26] S. Elgar, "Bispectra of Shoaling Ocean Surface Gravity Waves," Workshop on Higher-Order Spectral Analysis, pp. 206-211, Vail, CO, June 1989.

CHAPTER 3
2-D SKEW-MUSIC: A SINUSOIDAL PARAMETRIZATION FOR THREE-WAVE COUPLING

3.1 Introduction

Since we employ higher order statistics in particular for their phase-sensitive properties, it is therefore appropriate that parametric methods completely utilize all of the phase information provided by the triple correlations. The central concern of this thesis is therefore the development of parametric modeling of three-wave coupling frequencies that includes the key feature of accurate biphase estimation as well as full 2-D representation. In addition we desire to insure that we are truly modeling sinusoids, so our constituent signal correlation matrix is formed from exponential vectors. In this work an eigenstructure approach to estimating triad frequencies and accompanying biphase is taken. These quantities are determined by symmetrizing the phase-sensitive third order cumulants. Phase is extracted as estimable amplitude coefficients of the symmetric and skew-symmetric cumulant sequences.

As a result of cumulant symmetrization, symmetric and skew-symmetric matrices then can be easily utilized for coupling frequency determination through standard subspace decomposition techniques.

3.2 2-D SKEW-MUSIC: Derivation and Properties

Consider the time series $x(n)$ consisting of one triad of quadratically coupled sinusoids in non-Gaussian white noise with non-zero third moment noise $w(n)$. ϕ_1 and ϕ_2 are random variables and uniformly distributed between 0 and 2π. Once again $\gamma(\omega_1, \omega_2)$ is a constant phase offset.

$$x(n) = A\cos[\omega_1 n + \phi_1] + A\cos[\omega_2 n + \phi_2] \tag{3.1}$$

$$+ A\cos[(\omega_1 + \omega_2)n + \phi_1 + \phi_2 + \gamma(\omega_1, \omega_2)] + w(n)$$

Without loss of generality let $\gamma = \gamma(\omega_1, \omega_2)$. The third order cumulant sequence, $R(k,l)$, for $x(n)$ is

$$R(k,l) = \frac{A^3}{4}\{\cos(\omega_1 k + \omega_2 l - \gamma) + \cos(\omega_2 k + \omega_1 l - \gamma) \tag{3.2}$$

$$+ \cos(\omega_1 k - \omega_3 l - \gamma) + \cos(-\omega_3 k + \omega_1 l - \gamma)$$

$$+ \cos(\omega_2 k - \omega_3 l - \gamma) + \cos(-\omega_3 k + \omega_2 l - \gamma)\} + \beta\delta(k,l)$$

where ω_j is the frequency of the jth individual sinusoid. β is the magnitude of the third moment of the non-Gaussian white noise. With zero biphase, the cumulants are purely symmetric with $R(k,l)=R(-k,-l)$ and are cosinusoids with zero phase angles. A biphase of 90 degrees translates into $R(k,l)=-R(-k,-l)$ giving rise to a state of full asymmetry as mentioned in chapter 2.

Consider dividing the third order cumulant sequence into its symmetric, $S(k,l)$, and anti-symmetric, $A(k,l)$, components as

$$S(k,l) = \frac{1}{2}\left[R(k,l) + R(-k,-l)\right] \tag{3.3}$$

$$A(k,l) = \frac{1}{2}\left[R(k,l) - R(-k,-l)\right] \tag{3.4}$$

$$R(k,l) = S(k,l) + A(k,l) \tag{3.5}$$

It is desired to determine the structure of $S(k,l)$ and $A(k,l)$ assuming that the original time series consists of N sets of quadratically coupled sinusoids in white noise. These 6N term cumulant sequences can be viewed as the in-phase and quadrature components of the sequence in (3.2) when generalized for the case of N arbitrary triads. It is assumed here that each triad has distinct coupling frequencies.

$$S(k,l) = \sum_{i=1}^{N} \cos\gamma_i \{ \cos(\omega_{i1}k + \omega_{i2}l) + \ldots + \cos(-\omega_{i3}k - \omega_{i2}l) \} \tag{3.6}$$

$$A(k,l) = \sum_{i=1}^{N} \sin\gamma_i \{ \sin(\omega_{i1}k + \omega_{i2}l) + \cdots + \sin(-\omega_{i3}k + \omega_{i2}l) \} \tag{3.7}$$

The biphases have become amplitude coefficients. Note that we can now build a block matrix which may be expressed as a sum of complex exponential terms. This

matrix is suitable for the application of MUSIC or other signal subspace algorithms. Focusing at this time only on the symmetric cumulant sequence, a. Toeplitz block-Toeplitz matrix, S, is constructed. S is d x d and d = mn. Here m is the block dimension and n is the number of blocks. The blocks are arranged as

$$\mathbf{S} = \begin{bmatrix} \mathbf{S}(0) & \mathbf{S}(1) & \cdots & \mathbf{S}(n-1) \\ \mathbf{S}(-1) & \mathbf{S}(0) & \cdots & \mathbf{S}(n-2) \\ \vdots & \vdots & \ddots & \vdots \\ \mathbf{S}(-n+1) & \mathbf{S}(-n+2) & \cdots & \mathbf{S}(0) \end{bmatrix} \tag{3.8}$$

where each constituent block entry, **S(i),** is a m x m Toeplitz matrix constructed from the symmetric third order cumulants as,

$$\mathbf{S}(i) = \begin{bmatrix} S(i,0) & S(i,1) & \cdots & S(i,m-1) \\ S(i,-1) & S(i,0) & \cdots & S(i,m-2) \\ \vdots & \vdots & \ddots & \vdots \\ S(i,-m+1) & S(i,-m+2) & \cdots & S(i,0) \end{bmatrix}. \tag{3.9}$$

Given the form of the symmetric cumulants in (3.6), S may be decomposed as

$$\mathbf{S} = \mathbf{E}\,\mathbf{P}_\gamma\,\mathbf{E}^{\mathbf{H}} + \beta\,\mathbf{I}. \tag{3.10}$$

Since the cumulants contain N real sinusoidal triads, E has a Vandermonde structure containing 12N complex sinusoidal columns,

$$\mathbf{E} = \left[\, \mathbf{e}(\omega_{11},\omega_{12}) \,\vdots\, \mathbf{e}(-\omega_{11},-\omega_{12}) \,\vdots\, \cdots \,\vdots\, \mathbf{e}(\omega_{N2},-\omega_{N3}) \,\vdots\, \mathbf{e}(-\omega_{N2},\omega_{N3}) \,\right] \tag{3.11}$$

where each block vector, $\mathbf{e}(\omega_{ik},\omega_{ij})$ is the Kronecker product of two complex exponential vectors as

$$\mathbf{e}(\omega_{ik},\omega_{ij}) = \mathbf{e}(\omega_{ik}) \otimes \mathbf{e}(\omega_{ij}) \tag{3.12}$$

where $\otimes$ is the Kronecker product and

$$\mathbf{e}(\omega_{ij}) = \begin{bmatrix} 1 \\ \exp(j\omega_{ij}) \\ \vdots \\ \exp(j\omega_{ij}(m-1)) \end{bmatrix} \tag{3.13}$$

The matrix $\mathbf{P}_\gamma$ in (3.10) is a 12N x 12N diagonal matrix containing the biphase amplitudes, $p_{\gamma,ii} = (\cos\gamma_i)/2$. The first twelve diagonal terms of the $\mathbf{P}_\gamma$ matrix belong to one triad, i.e. they are all equal to $p_{\gamma,ii} = (\cos\gamma_i)/2$, the second twelve diagonal terms belong to the next triad and so forth. (3.8) may be expressed as

$$\mathbf{S} = \sum_{i=1}^{N} p_{\gamma,ii} \left\{ \sum_{j,k} [\mathbf{e}^*(\omega_{ik},\omega_{ij})\, \mathbf{e}^T(\omega_{ik},\omega_{ij}) + \mathbf{e}(\omega_{ik},\omega_{ij})\mathbf{e}^H(\omega_{ik},\omega_{ij})] \right\} + \beta\mathbf{I}. \tag{3.14}$$

Note that S is both symmetric and Toeplitz and the conventional 2-D MUSIC algorithm can now be applied. Since $\mathbf{E}\mathbf{P}_\gamma\mathbf{E}^H$ is not full rank, the dimension of the signal subspace is 12N and the noise subspace is represented by (d-12N) noise eigenvectors. Thus the spectral decomposition of S may be expanded as

$$\mathbf{S} = \sum_{i=1}^{12N} (\lambda_i+\beta)\mathbf{v}_i\mathbf{v}_i^H + \sum_{i=12N+1}^{d} \beta\mathbf{v}_i\mathbf{v}_i^H. \tag{3.15}$$

We can estimate β as the size of the smallest eigenvalue of S. Note that S is not necessarily positive semi-definite as β may be negative depending on the direction of the skewness.

S described by (3.10) is symmetric, but not positive-definite since the noise may be characterized by a negative third order moment. Hence, the smallest eigenvalue may be negative. The signal-only component is composed of the outer products of complex exponential vectors and is thus characterized by all positive eigenvalues. Partitioning the subspaces involves assigning the largest 12N eigenvalues to the signal subspace and the remaining eigenvalues to the noise subspace.

In complementary fashion, we may construct a skew-symmetric block Toeplitz matrix A with the skew-symmetric cumulant sequence, A(k,l), the same way S is constructed from S(k,l) in (3.6). Likewise A can be decomposed as

$$\mathbf{A} = \mathbf{E}\,\mathbf{Q}_\gamma\,\mathbf{E}^*. \tag{3.16}$$

Similar to $\mathbf{C}_\gamma$, $\mathbf{S}_\gamma$ is a 12N x 12N diagonal matrix with diagonal elements of the form

$$q_{\gamma,ii} = \frac{\sin\gamma_i}{2j}. \tag{3.17}$$

The anti-symmetric cumulants, $\mathbf{A}(k,l)$, possess odd symmetry being composed of sine terms so that A is skew-symmetric, i.e. $\mathbf{A}^H = -A$. Similar to (3.14), A may be expressed as

$$\mathbf{A} = \sum_{i=1}^{N} q_{\gamma,ii} \left\{ \sum_{j,k} [\mathbf{e}^*(\omega_{ik},\omega_{ij})\,\mathbf{e}^T(\omega_{ik},\omega_{ij}) - \mathbf{e}(\omega_{ik},\omega_{ij})\mathbf{e}^H(\omega_{ik},\omega_{ij})] \right\}. \tag{3.18}$$

In accordance with the definition of skew-symmetry, the main diagonal $(\mathbf{R}(0,0)-\mathbf{R}(0,0))$ is zero, i.e., it is noise free.

A spectral decomposition of A is possible. The eigenvectors of a skew-symmetric matrix are mutually orthogonal and the corresponding eigenvalues are purely imaginary. The orthogonal subspace for A is characterized by all zero eigenvalues. A suitable partitioning of the subspaces involves associating eigenvectors belonging to the smallest *magnitude* eigenvalues with the orthogonal complement subspace.

Frequency estimates for sinusoidal triads are found by exploiting the orthogonality between constituent signals and noise subspace eigenvectors. A 2-D MUSIC spectrum is constructed as

$$\mathbf{B}_{mus}(\omega_1,\omega_2) = \frac{1}{\mathbf{e}^H(\omega_1,\omega_2)\mathbf{W}\mathbf{e}(\omega_1,\omega_2)} \tag{3.19}$$

where W is constructed from the noise subspace eigenvectors as

$$\mathbf{W} = \sum_{k=12N+1}^{d} \mathbf{v}_k \mathbf{v}_k^H \tag{3.20}$$

The constituent frequencies of coupled frequency triad may be determined by searching $\mathbf{B}_{mus}(\omega_1,\omega_2)$ for peaks over the range of allowable frequency combinations. In the case of a single quadratically coupled triad, there are peaks at (ω_1,ω_2), (ω_2,ω_1), $(\omega_1,-\omega_1-\omega_2)$, etc. in accordance with the symmetry properties of the bispectrum. This redundancy motivate the use of slices of the bispectrum as will be discussed in the next section. Either S or A may be employed to construct $\mathbf{B}_{mus}(\omega_1,\omega_2)$. Typically, if the time series is known to be asymmetric, then A should be used to determine the coupling frequencies and vice versa for the symmetric time series. For a practical implementation the estimates of coupling frequencies may be derived from the matrix whose matrix-2 norm is the largest. Once the frequency estimates are determined, E can be constructed and $\mathbf{P}_\gamma$ subsequently estimated as

$$\mathbf{P}_\gamma = (\mathbf{E}^H\mathbf{E})^{-1}\mathbf{E}^H(\mathbf{S} - \beta\mathbf{I})\mathbf{E}(\mathbf{E}^H\mathbf{E})^{-1}. \quad (3.21)$$

$\mathbf{Q}_\gamma$ may be estimated in a similar fashion by replacing (S − PI) by A in (3.21) to find the amplitudes $p_{\gamma,ii}$ as defined in (3.10-3.14). Since our time series is of finite length, both $\mathbf{P}_\gamma$ and $\mathbf{Q}_\gamma$ are not diagonal though diagonal elements would be used for the biphase estimates. Given the biphase coefficients $p_{\gamma,ii}$ and $q_{\gamma,ii}$, biphases may be determined via a ratio of amplitudes as $\gamma_i = \arctan(q_{\gamma,ii}/p_{\gamma,ii})$. This hybridized MUSIC scheme is referred to as SKEW-MUSIC.

3.3 Simulations of 2-D SKEW-MUSIC

Monte Carlo simulations were conducted to assess the performance of the various algorithms developed in this section. It was desired to test the algorithms herein to check the efficacy of the 2-D SKEW-MUSIC algorithm in estimating quadratic coupling frequencies.

For the Monte Carlo simulations, testing of 2-D SKEW-MUSIC involved synthesizing 8,192 point sequences containing quadratically phase-coupled sinusoids with additive noise generated from an exponential distribution. Each trial was composed of sixty-four 128-point segments. Each segment consists of two unity amplitude sinusoids with random starting phases at frequencies $f_1 = 0.34$ and $f_2 = 0.1$ Hz, respectively and a third sinusoid of the same amplitude phase-locked with a constant phase offset determined by the biphase. The biphases ranged from 0 through 90 degrees in 15 degree increments.

The added exponential noise is adjusted to give signal-to-noise ratios (SNR) of 14.77, 4.77 and 1.76 dB for each complete set of biphase trials. The noise was skewed positively or negatively by changing the polarity of the added noise. A representative trial requires estimating the cumulants for each epoch then averaging the cumulants over all 64 epochs. A 16 x 16 block matrix with a block-Toeplitz structure described in (3.8) and (3.9) is formed for both symmetric and skew-symmetric cumulant sequences. Eigenvector/eigenvalue decompositions are performed for each matrix. Ideally, there are 12 eigenvectors spanning the signal subspace with the remaining 4 eigenvectors spanning the orthogonal .complement or noise subspace. For noise with negative third order moment, the symmetric matrix is no longer positive definite, as this additive noise negatively biases the signal eigenvalues. Values of the 2-D SKEW-MUSIC function defined in (3.19) are computed over the non-redundant

autobispectral triangle, i.e. over (f_1, f_2) satisfying $0 \le f_1 \le 0.5$ Hz., $0 \le f_2 \le 0.25$ Hz and $f_1 + f_2 \ge 0.5$ Hz. Both arguments of the compound exponential frequency kernel in (3.19) were incremented in 0.01 Hz. steps. The frequency estimates are those two frequencies where (3.19) is a maximum. Representative plots of the 2-D SKEW-MUSIC frequency bispectra are displayed in Figs. 3.1 - 3.6 for different biphases using a SNR of 14.77 dB and 20 x20 matrix. In each of these plots the noise used is Gaussian generated from the single precision IMSL subroutine, RRNOR. In Figs. 3.1 & 3.2 a time series of 8192 data points containing a single quadratically phase coupled sinusoid with a biphase of 0^o is analyzed. In Fig. 3.1 the bispectrum generated from the symmetric cumulants is displayed. Fig. 3.2 shows the bispectrum resulting from modeling a symmetric time series with a skew-symmetric cumulant sequence.

Figs. 3.3 and 3.4 show results for a time series containing a triad with a biphase of 30^o. Improvement in the skew-symmetric cumulant results is noted in the case where the biphase has been increased. Satisfactory results for both symmetric and skew-symmetric cumulant sequences are noted in Figs. 3.5 and 3.6 where a biphase of 60^o is used.

The length of the sequence is shortened to 4096 data points as the SNR using Gaussian noise is increased to 24 dB with a 25x25 matrix. Figs. 3.7 and 3.8 show the results for a biphase of 30 degrees using symmetric and skew-symmetric cumulants, respectively. In each case the peaks appear in the correct location of $(f_1, f_2) = (.34, .1)$. The biphase changes to 60^o and we see equally good performance for both symmetric and skew-symmetric cumulant sequences. These peaks are shown in Figs. 3.9 & 3.10. For these low noise cases it is critical to note that the amplitude of the peaks is larger than the high noise cases observed.

Some simulations with non-Gaussian noise show that the algorithms perform very well under particularly low signal-to-noise ratios. White exponential noise (skewness=3/2) noise is added to a single triad of quadratically phase coupled sinusoids so that the SNR=4.77 dB. Two different biphase values, 15^o and 75^o, are employed. Once again symmetric and skew-symmetric cumulant matrices provide estimates depicted in Figs. 3.11-3.14. As can be seen from these simulations poor performance is seen in the case of coupling with low biphase using frequency estimates from the skew-symmetric cumulants. The same is true for the 75^o case using symmetric cumulants.

One hundred Monte Carlo trials were conducted for each biphase, noise level and noise polarity. Sample means for each frequency for an SNR of 4.77 dB are listed in Table 3.1. As the biphase increases from 0^o to 90^o, the accuracy of the estimates derived from the symmetric matrix decreases. Symmetric matrix frequency estimates

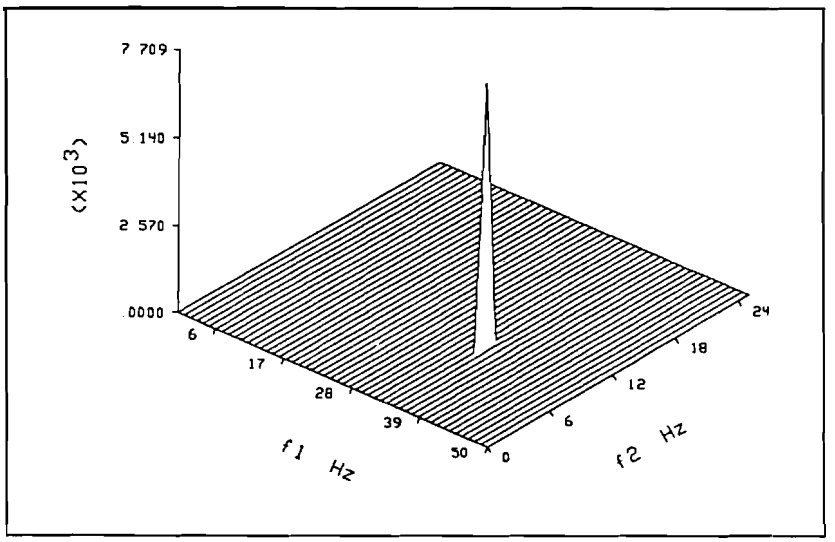

Figure 3.1 2-D SKEW-MUSIC Bispectrum from Symmetric Cumulants; Biphase = 0^o; SNR=14.77 dB; Gaussian Noise; N=8192; Peak at (.34,.1) Hz

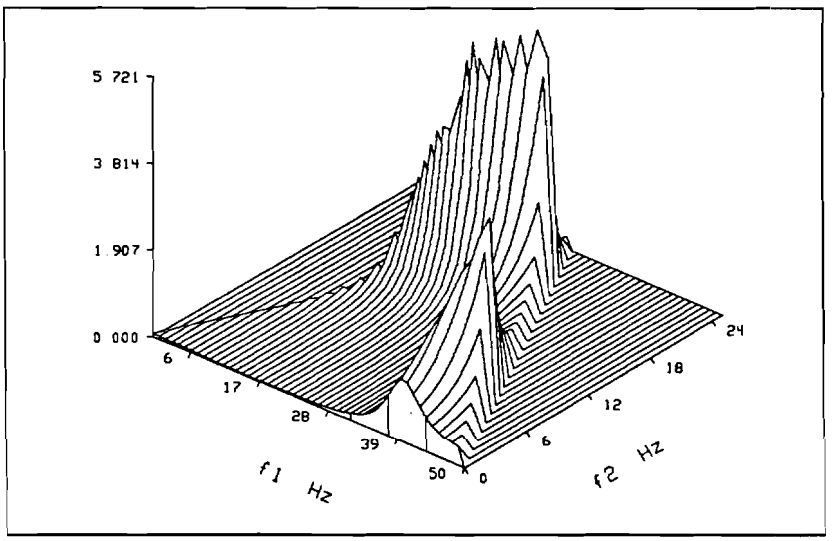

Figure 3.2 2-D SKEW-MUSIC Bispectrum from Skew-Symmetric Cumulants; Biphase = 0^o; SNR=14.77 dB; Gaussian Noise; N=8192; Peak at (.29,.2) Hz

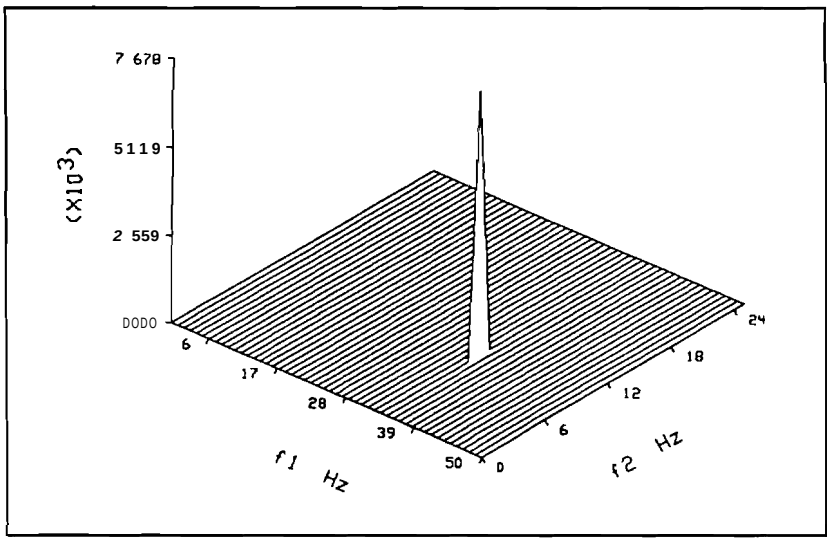

Figure 3.3 2-D SKEW-MUSIC Bispectrum from Symmetric Cumulants; Biphase = 30°; SNR=14.77 dB; Gaussian Noise; N=8192; Peak at (.34,.1) Hz

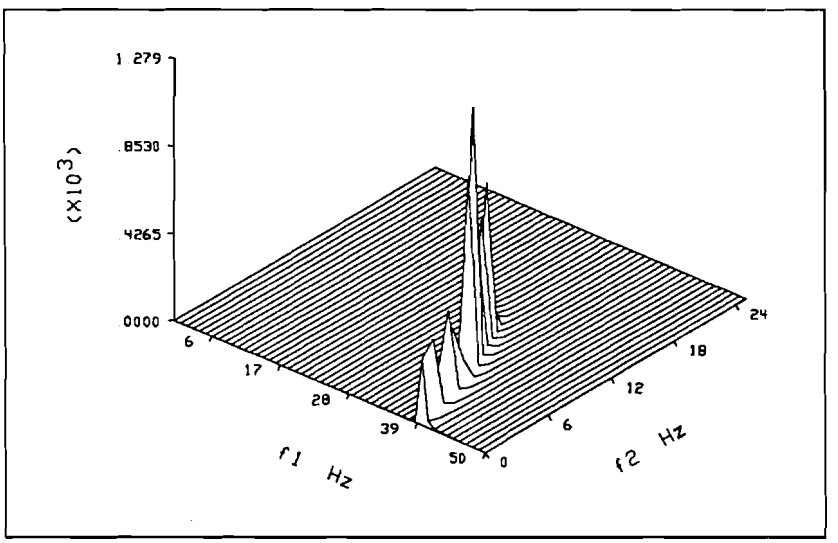

Figure 3.4 2-D SKEW-MUSIC Bispectrum from Skew-Symmetric Cumulants; Biphase = 30°; SNR=14.77 dB; Gaussian Noise; N=8192; Peak at (.36,.08) Hz

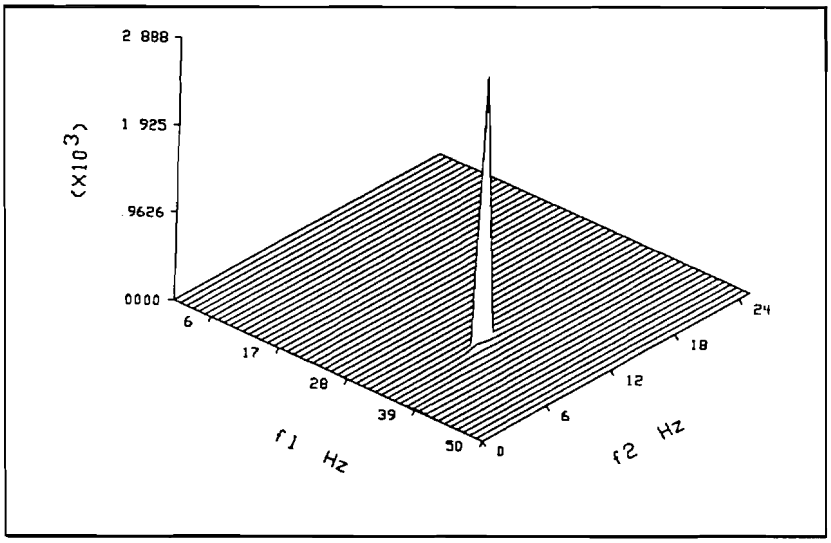

Figure 3.5 2-D SKEW-MUSIC Bispectrum from Symmetric Cumulants; Biphase = 60°; SNR=14.77 dB; Gaussian Noise; N=8192; Peak at (.34,.1) Hz

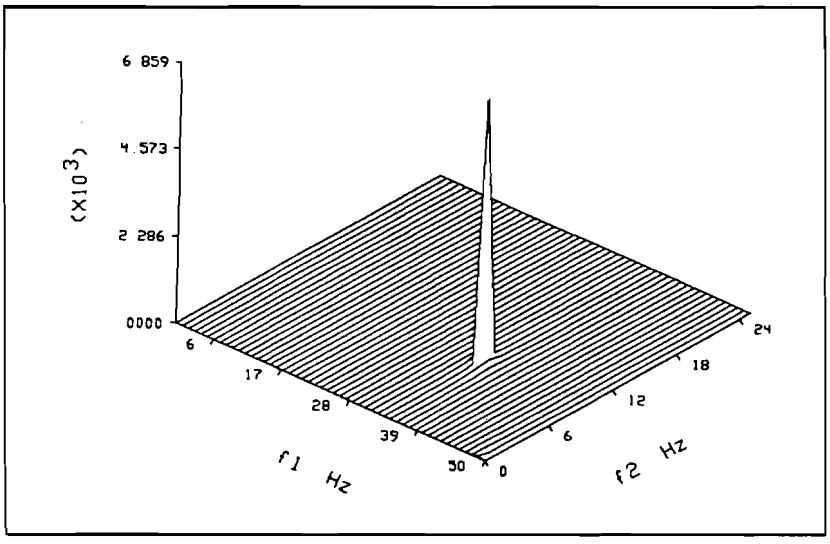

Figure 3.6 2-D SKEW-MUSIC Bispectrum from Skew-Symmetric Cumulants; Biphase = 60°; SNR=14.77 dB; Gaussian Noise; N=8192; Peak at (.34,.1) Hz

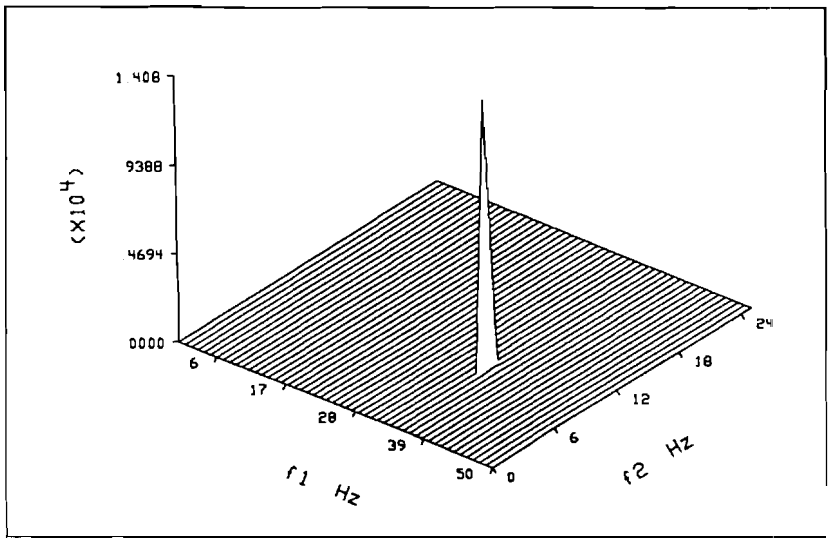

Figure 3.7 2-D SKEW-MUSIC Bispectrum from Symmetric Cumulants; Biphase = 30°; SNR=24 dB; Gaussian Noise; N=4096; Peak at (.34,.1) Hz

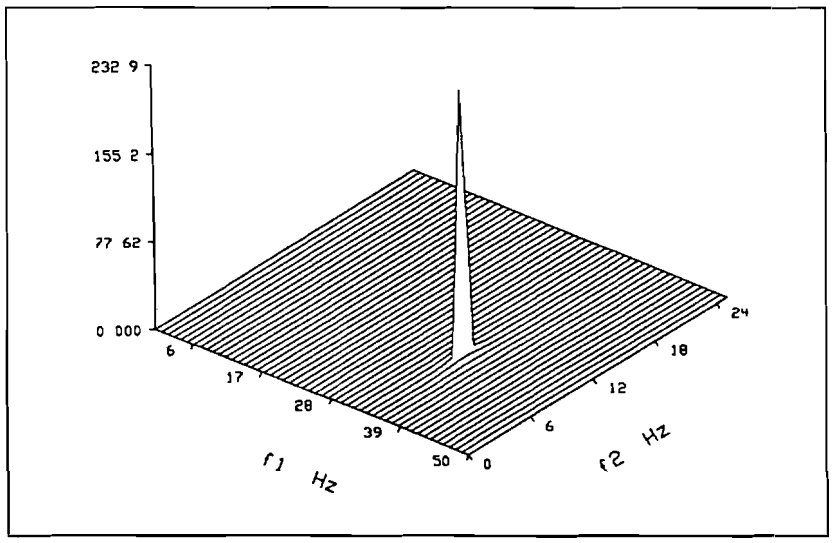

Figure 3.8 2-D SKEW-MUSIC Bispectrum from Skew-Symmetric Cumulants; Biphase = 30°; SNR=24 dB; Gaussian Noise; N=4096; Peak at (.34,.1) Hz

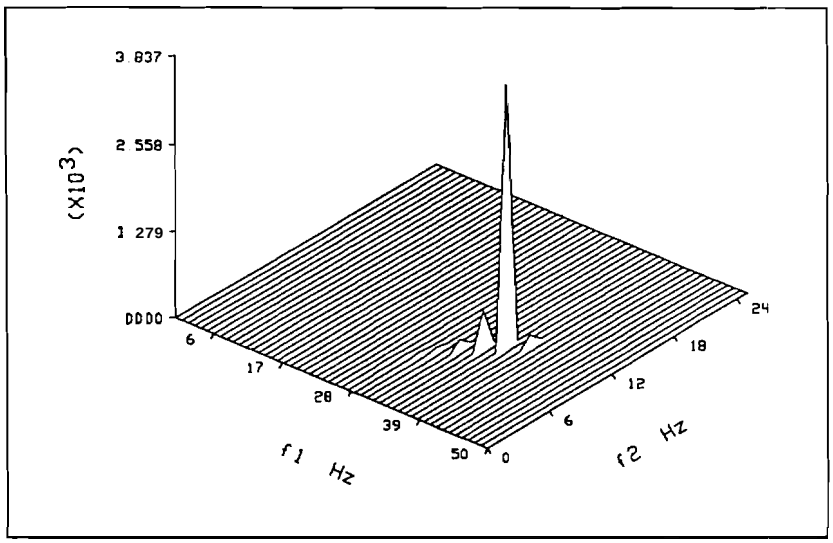

Figure 3.9 2-D SKEW-MUSIC Bispectrum from Symmetric Cumulants; Biphase = 60°; SNR=24 dB; Gaussian Noise; N=4096; Peak at (.34,.11) Hz

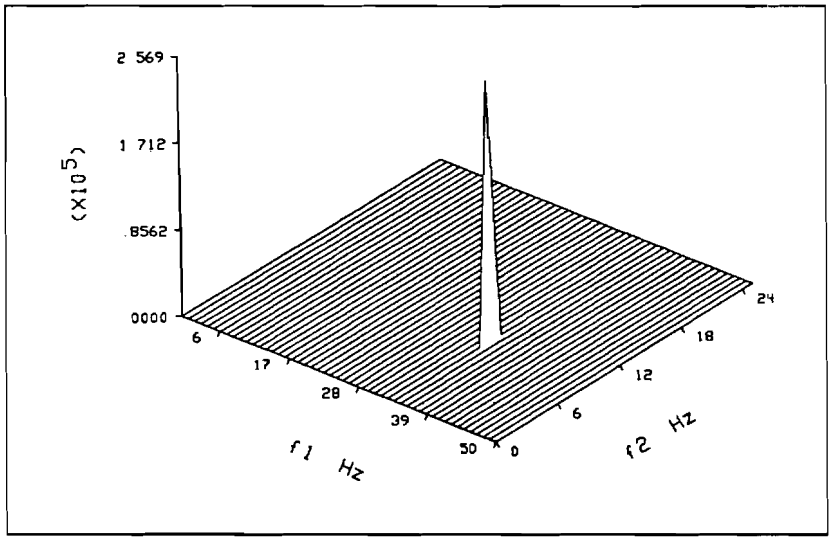

Figure 3.10 2-D SKEW-MUSIC Bispectrum from Skew-Symmetric Cumulants; Biphase = 60°; SNR=24 dB; Gaussian Noise; N=4096 Peak at (.34,.11) Hz

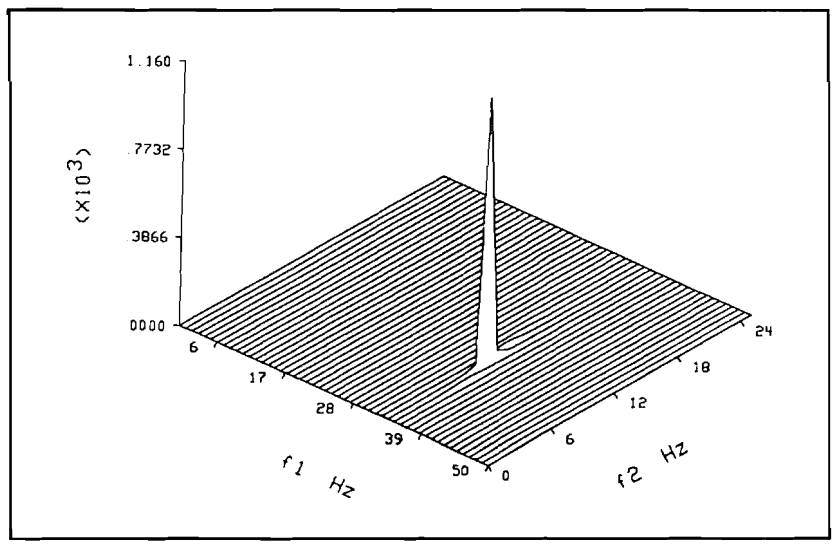

Figure 3.11 2-D SKEW-MUSIC Bispectrum from Symmetric Cumulants; Biphase = 15°; SNR=4.77 dB; Exponentially Distributed Noise; N=8192; Peak at (.34,.1) Hz

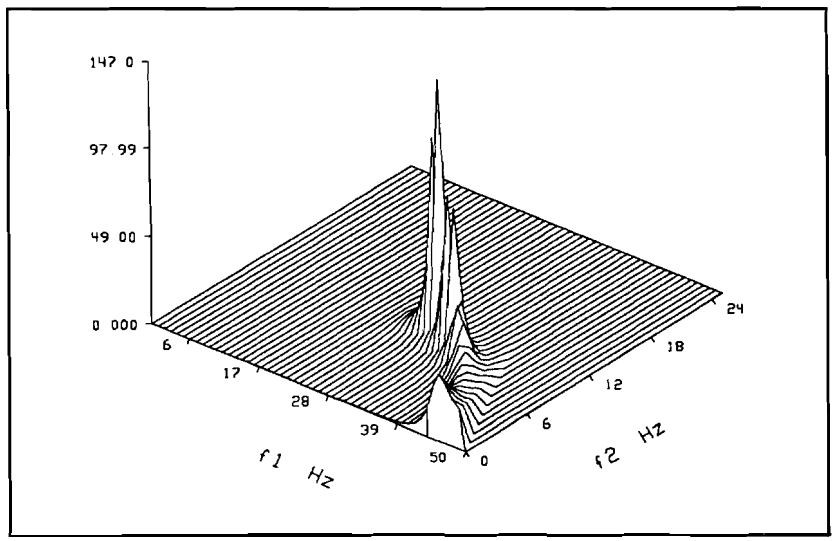

Figure 3.12 2-D SKEW-MUSIC Bispectrum from Skew-Symmetric Cumulants; Biphase = 15°; SNR=4.77 dB; Exponentially Distributed Noise; N=8192; Peak at (.31,.1) Hz

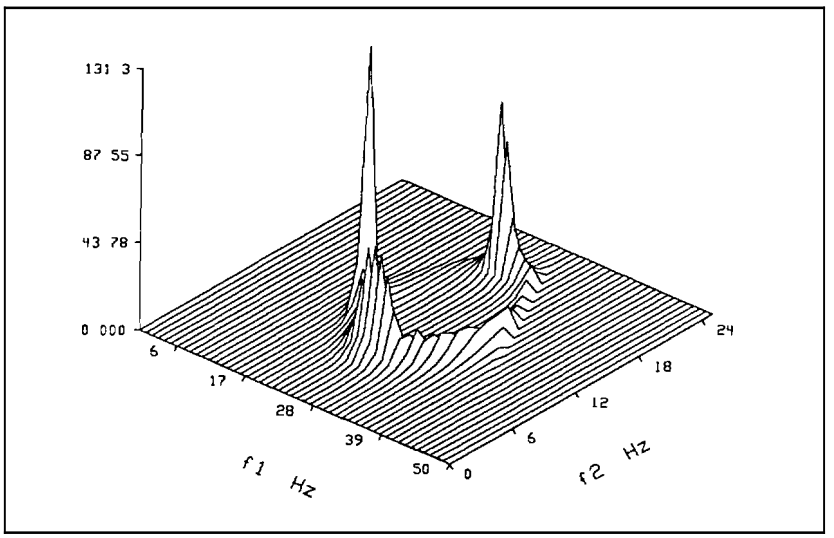

Figure 3.13 2-D SKEW-MUSIC Bispectrum from Symmetric Cumulants; Biphase = 75°; SNR=4.77 dB; Exponentially Distributed Noise; N=8192; Peak at (.18,.12) Hz

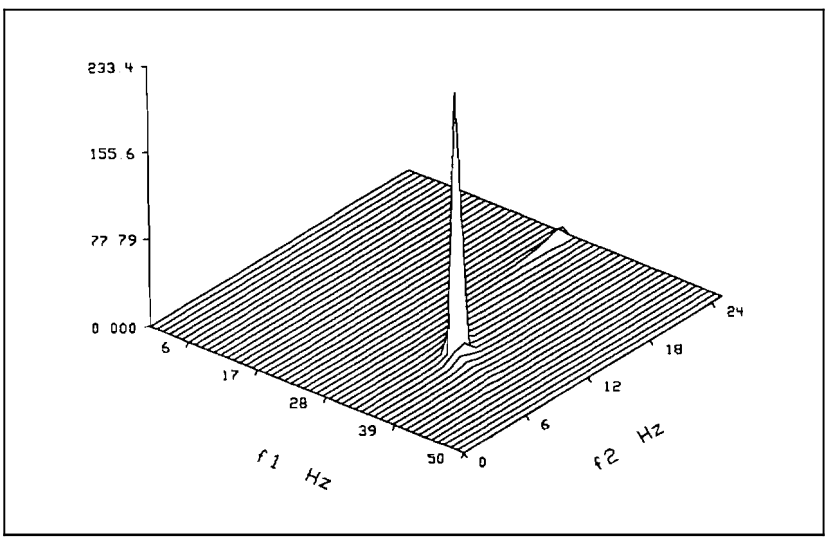

Figure 3.14 2-D SKEW-MUSIC Bispectrum from Skew-Symmetric Cumulants; Biphase = 75°; SNR=4.77 dB; Exponentially Distributed Noise; N=8192; Peak at (.34,.1) Hz

deteriorate maximally for a biphase of 90^o. Conversely, it is expected that the frequency estimates from the skew-symmetric matrix will be more accurate for the large biphase case and poorest in the case where the biphase is close to zero. Interestingly, for this matrix size frequency estimates obtained in the 90^o biphase case with the skew-symmetric matrix exhibit a significant bias. The symmetric matrix frequency estimates do not exhibit a similar bias for a biphase of 0^o. This provided motivation to increase the block size and, hence, the matrix dimension for better accuracy. The computer experiments were rerun employing 20x20 matrices composed of 4 x 5 blocks and a 25 x 25 matrices composed of 5 x 5 blocks. Greatly improved results can be noted in Tables 3.2 and 3.3 for both of these cases.

This algorithm provides the user with an estimate of the central third order moment of the additive noise or the unnormalized skewness. For the exponential distribution, the parameter $1/\lambda$ determines the mean, h, and the central third moment, $2\lambda^3$. To achieve the previously stated SNRs, θ was set equal to either 0.2235, 0.7071 or 1.0. The average of the 4 smallest eigenvalues of the 16 x 16 symmetric cumulant matrix provides an estimate of the third moment. Sample means of the noise skewness were computed for 100 runs using various combinations of biphase in positively and negatively skewed noise. We used the 16 x 16 cumulant matrix for the estimates listed in Table 3.4. It can easily be seen that the accuracy of noise estimates increases for lower SNR. Also there is a noticeable variation of noise estimates for different biphases.

Table 3.5 shows performance of 2-D SKEW-MUSIC as a function of the bicoherence level. The bicoherence level varies from 0.1 to 1.0 by varying the power of uncoupled sinusoids. The power of sinusoids with independent phase at the same frequencies as members of the triad is varied in accordance with the desired level of bicoherence. The biphase for all of these trials was 45^o. 100 trials at each level of bicoherence were performed. Means and standard deviations from f_1 frequency estimates from both symmetric and skew-symmetric cumulant matrices are listed. Interestingly, there is very little trend developed for the bicoherence variation. At this SNR, 21.77 dB, there is little change in performance of the algorithm until the bicoherence is less than 0.1. In fact, there is no clear trend in bias and variance of the estimates for most middle values of coupling fraction. Many more data records to average are required for stable values to be established.

Table 3.1 Table of 2-D SKEW-MUSIC Estimates of Coupling Frequencies from 16 x 16 Symmemc and Skew-Symmemc Mamces;, 100 Trials per Biphase Value

Phase Coupled Sinusoid Frequency Estimate Positively Skewed Noise - SNR = 4.77 dB 16 x16 Matrix Dimension				
Biphase	Matrix Form			
	Symmetric		Skew-Symmetric	
	True f1=0.34 $\hat{f1}$	True f2=0.1 $\hat{f2}$	True f1=0.34 $\hat{f1}$	True f2=0.1 $\hat{f2}$
0°	3363	.1016	2046	1399
15°	.3384	.1008	.2855	.1281
30°	.3368	.0998	.2892	.1264
45°	.3317	.1035	.3021	.1294
60°	.3261	.1030	.2984	.1301
75°	.3237	.1043	.3052	.1347
90°	.2502	,1150	.2936	.1340

Table 3.2 Table of 2-D SKEW-MUSIC Estimates of Coupling Frequencies from 20 x 20 Symmemc and Skew-Syrnrnemc Mamces; 100 Trials per Biphase Value

Phase Coupled Sinusoid Frequency Estimate Positively Skewed Noise - SNR = 4.77 dB 20 x 20 Matrix Dimension				
Biphase	Matrix Form			
	Symmetric		Skew-Symmetric	
	True f1=0.34 $\hat{f1}$	True f2=0.1 $\hat{f2}$	True f1=0.34 $\hat{f1}$	True f2=0.1 $\hat{f2}$
0°	3398	0969	2698	0.1104
15°	.3484	.0930	.3418	.0988
30°	,3457	.0941	.3404	.0972
45°	.3396	.0977	.3409	.0975
60°	.3399	.0957	.3422	.0939
75°	.3378	,1001	.3411	.0965
90°	.2539	,1137	.3455	.0968

Table 3.3 Table of 2-D SKEW-MUSIC Estimates of Coupling Frequencies from 25 x 25 Symmetric and Skew-Symmetric Matrices; 100 Trials per Biphase Value

Phase Coupled Sinusoid Frequency Estimate Positively Skewed Noise - SNR = 4.77 dB 25 x 25 Matrix Dimension				
Biphase	Matrix Form			
	Symmetric		Skew-Symmetric	
	True $f1$=0.34 $\hat{f1}$	True$f2$=0.1 $\hat{f2}$	True $f1$=0.34 $\hat{f1}$	True $f2$=0.1 $\hat{f2}$
0°	.3354	0964	2639	.1024
15°	.3379	.0961	.3255	.0973
30°	.3335	.0961	.3380	.0952
45°	.3381	.0957	.3309	.0951
60°	.3338	.0954	.3318	.1010
75°	.3376	.0970	.3362	.0987
90°	.2508	.1061	.3286	.0968

Table 3.4 Noise Third Order Moment Estimates

Third Moment Noise Estimates Positively & Negatively Skewed Noise						
Biphase	Signal-to-Noise					
	SNR = 14.77 dB		SNR = 4.77 dB		SNR = 1.76 dB	
	True= 0.0223	True= -0.0223	True= 0.7071	True= -0.07071	True= 2.0	True= -2.0
0''	0393	-.0054	.6825	-.6914	1.9061	-1.9796
15°	.0388	-.0060	.6816	-.6921	1.9051	-1.9808
30°	.0367	-.0080	.6789	-.6948	1.9017	-1.9844
45°	.0330	-.0114	.6745	-.6993	1.8958	-1.9909
60°	.0393	-.0160	.6682	-.7059	1.8867	-2.0014
75°	.006	-.0219	.6584	-.7162	1.870	-2.0215
90°	.007	-.0480	.5884	-.7920	1.7583	-2.1490

Table 3.5 Performance of 2-D SKEW-MUSIC Algorithm: Coupling Frequency Estimate Accuracy vs. Bicoherences from 25 x :25 Third Order Cumulant Matrix; 100 Trials per Bicoherence Value Accuracy (Means and Std. Devs.) of f_1 estimate shown; True Value: $f_1 = 0.34$

Coupled Sinusoid Frequency Estimate vs Bic: Symmetric and Skew-Symmetric Cumulant Matrices Exponentially Distributed White Noise - SNR = 21.77 dB 25 x 25 Matrix Dimension;				
Bicoherence	Matrix Type			
	Symmetric		Skew-Symmetric	
	Mean	Std. Devs..	Mean	Std. Devs.
0.02	.3045	1052	3307	1
0.05	.3039	.0933	.3424	.0739
0.1	.3173	.083	.326	.0742
0.2	.3329	.0696	.3327	.0582
0.3	.3255	.0731	.3336	.0607
0.4	.3396	.0666	.3328	.0632
0.5	.3219	.0747	.3257	.0662
0.6	.3264	.0630	.3283	.0664
0.7	.3271	.0658	.3336	.0561
0.8	.3298	.0688	.3354	.0562
0.9	.3319	.0684	.3332	.062
1.0	.3379	.0755	.3366	.06618

CHAPTER 4
THE 1-D BISPECTRUM

4.1 Introduction

Estimation of coupling frequencies can also take place on slices of the bispectrum. Projections in the cumulant domain generate slices in the bispectral domain through the Fourier-slice theorem. Utilizing symmetry relations within the full extent of the bispectral domain, we begin with six 2-D sinusoids which constitute the cumulant sequence for a single phase coupled sinusoid triad. Through projections, certain cumulant components become decoupled. Then through the decoupling process, a single 1-D sinusoid is extracted from the 2-D sinusoids along a slice of the bispectrum. The method based on this principle is presented herein. The techniques of using cumulant projections provide ample contrast to the methods of Raghuveer and Nikias mentioned in chapter 2. We model a slice of the bispectrum whereas they use the cumulants to describe projections of the bispectrum.

The cumulant projections preserve the phase-sensitive statistics. Thus, SKEW-MUSIC can be applied in the 1-D case as well. One of the extensions of SKEW-MUSIC is known as SKEW-ESPRIT. This algorithm exploits the fact that eigenvectors from the symmetric cumulant matrix can be converted to their complementary skew-symmetric form by a simple rotation. A generalized eigenvector (GEV) solution as implemented by the ESPRIT class of algorithms accomplishes this basis rotation. The biphases are directly related to the generalized eigenvalues (GE) as we show below.

One of the keys in the implementation of the ESPRIT algorithm is the reduction of singular and rectangular matrix forms to full rank square forms. The PRO-ESPRIT algorithm of Zoltowski and Stavrinides is explained as well. In the simulations we employ this technique for accurate biphase estimation.

4.2 Motivating the Fourier-Slice Bispectrum

Non-linear system analysis is a computationally intensive enterprise requiring large systems of equations [1-3]. In a system identification context the number of output frequency combinations possible is a geometric function of the number of input frequencies. Authors such as Victor et. al. make use of this fact in their system identification scheme called the sum-of-sinusoids method [4]. Here a group of six or eight sinusoids with virtually random phases is input to a nonlinear system. The output time series of a quadratic system is so rich in frequency diversity that the entire Volterra kernel or quadratic transfer function can be characterized with a limited number of input sinusoids. Sinusoids with incommensurate frequency values can act as an effective substitute for Gaussian noise inputs usually used to characterize composite linear and nonlinear systems. Several occasions warrant only observation of sections of the bispectrum or cross-bispectrum. We may be interested in only couplings involving specific frequency ratios. Self-self couplings are simple frequency doublings such that $\omega_1 = 2\omega_1$. Ratios of frequency couplings are defined by slope lines in the bispectral domain. The slope lines are radial slices defined on a polar region of support.

Access to radial sections of members of a Fourier transform pair is made through the use of the Radon transform. Here projections (summations) are computed in the bicorrelation (cumulant) domain that are orthogonal to a projection axis at an angle 8 with respect to one of the lag axes. The Fourier transform of a given projection yields a slice in the bispectral domain [5, 6]. The orientation of the slice in the complementary domain is specified by the projection axis angle, 8. The advantage of using projections is ultimately a reduction in dimensionality. As the two frequency variables specifying a coupling are related by a simple ratio, our modeling problem becomes a function of one variable only. By taking projections normal to the appropriate axis, simple two dimensional sinusoids are decoupled in the sense that each becomes a function of one frequency argument instead of two [7].

Cumulant projections are not unknown to the higher order spectral analysis community. Alshebeili and Cetin use projections orthogonal to the $\omega_1 = \omega_2$ axis for phase reconstructions [8]. Marmarelis and Marmarelis use projections to gather information about the relative size of the second order Volterra kernel [2]. A slice of the second order kernel is a Volterra filter that selectively pairs input frequencies of particular ratios, i.e., a harmonic Volterra filter. Giannakis and Delopoulos employ cumulant projections to arrive at second order time series statistics by projecting cumulants orthogonal to one of the lag axes [9]. Likewise, Nikias and Bessios use an adaptation

of the biperiodogram to find the bispectrum dong polar rasters [10].

Applying Radon transform theory to the bispectrum, one consideration is to find the form of the projected cumulants in the case of three wave coupling. At first the cumulants are in the form of (3.2). The Radon transform for the discrete form cumulants is an approximation to the derivation discussed in the Appendix as

$$R_\theta(m) = \sum_{k=-K}^{K} \sum_{l=-L}^{L} w_\theta(k,l) R(k,l) \qquad (4.1)$$

where $R_\theta(m)$ is the projected cumulant sequence at an angle of 8 radians with respect to the k-lag axis. Here $w_\theta(k,l)$ is the weighting factor determined by some geometrical considerations based upon a given interpolation rule. For instance, consider a square cell centered around each cumulant value at (k,l). The coefficient $w_\theta(k,l)$ may reflect a weighting based on length of intersection of a projection axis at slope $a = \tan 8$ with a cell centered at (k,l). When $l=\alpha k$, $w_\theta(k,l)$ is a maximum or simply unity. Given that this is a discrete formulation, there will be leakage terms that do not belong to the slice of the bispectrum corresponding to the angle 8. Secondly, an interpolation technique is needed to carefully calculate projections for a discrete system. This involves interpolating from rectangular to polar coordinates. Several candidate schemes are presented in [11]. In addition, transforming to the discrete domain, the bandwidth of the hexagonal bispectral domain is effectively greater or less than n for certain projection angles where n is the bandwidth of the time series. The sampling rate must therefore be increased to include this domain with the maximum $\sqrt{2}\pi$ extent in the Radon transform domain.

In contrast to AR modeling of three-wave coupling as mentioned in chapter 2, our method uses cumulant sequences indexed by one variable only after projections are made which restrict the complementary bispectral region to a one dimensional slice. A one dimensional parametrization of the cumulants as in [12] limits the representation in the bispectral domain to a single dimension. This method attempts to utilize a one dimensional representation of nonlinear processes in order to generate a full 2-D bispectral representation. The AR modeling method is founded on the reduced dimension bispectral techniques known as the 1 1/2-D bispectrum discussed in chapter 2. This procedure is used in representing linear processes and as we have seen may not adequately describe the complete two dimensional bispectrum. A full 2-D extent of the cumulants may be required for satisfactory description of nonlinear processes unless the projections are made restricting the bifrequency domain to a slice.

4.3 The ESPRIT algorithm: The Generalized Eigenvalue Approach

The ESPRIT algorithm devised by Roy and Kailath has been used in spectral analysis and direction-of-amval (DOA) [13, 14]. One method of dealing with singular forms of the ESPRIT matrix pencil is the PRO-ESPRIT algorithm devised by Zoltowski and Stavrinides and our explanation of this algorithm follows their derivation for the general case when dealing with singular and rectangular matrix pencils [14]. We must now build the ESPRIT matrix pencil from the block data matrices X and Y where we have D sources impinging on 2M sensors. M sensors belong to the X array. Each of the M remaining sensors belonging to the Y array is displaced by a specified distance and direction from its complement in the X array. We assume that we are observing the noiseless case and that the received data matrices for N snapshots resulting in data X and Y which have N columns.

$$\mathbf{X} = [\mathbf{x}(1), \mathbf{x}(2), \cdots, \mathbf{x}(N)] \tag{4.2}$$

$$\mathbf{Y} = [\mathbf{y}(1), \mathbf{y}(2), \cdots, \mathbf{y}(N)] \tag{4.3}$$

where $\mathbf{x}(i)$ and $\mathbf{y}(i)$ are the ith snapshot vectors each of length M belonging to X and Y, respectively. With D wavefronts arriving at the sensors we can rewrite (4.2) and (4.3) as

$$\mathbf{X} = \sum_{i=1}^{D} \mathbf{a}_i \mathbf{s}_i^T = \mathbf{AS} \tag{4.4}$$

$$\mathbf{Y} = \sum_{i=1}^{D} \Phi_{ii} \mathbf{a}_i \mathbf{s}_i^T = \mathbf{A\Phi S}. \tag{4.5}$$

A contains D DOA vectors, $\mathbf{a}(\omega_i)$. The displacement or scaling factor, Φ_{ii}, that creates the phase difference between arriving wavefronts in the X and the Y data matrices is

$$\Phi_{ii} = \exp(j\frac{2\pi}{\lambda}\vec{d} \cdot \vec{u}). \tag{4.6}$$

We note that Φ is a unitary diagonal matrix. The basis of the ESPRIT algorithm is that we might combine (4.4) and (4.5)

$$\mathbf{Y} - \lambda\mathbf{X} = \sum_{j=1}^{D} (\Phi_{jj} - \lambda)\, \mathbf{a}_j \mathbf{s}_j^T. \tag{4.7}$$

Solving for the set of generalized eigenvalues, $\{\Phi_{11}, \cdots, \Phi_{DD}\}$, of this matrix pencil yields bearing angle estimates contained in Φ_{ii}.

In developing PRO-ESPRIT, Zoltowski and Stavrinides mention that in an array processing context the data matrices X and Y have some evident redundancies [14]. They mention, "1) X and Y have the same D-dimensional column space, range{A} which is typically referred to in the literature as the 'signal subspace...' In addition to this, however, we also note that each matrix has the same row space, range{S^T}, a D-dimensional subspace of N-dimensional space. This space spanned by the D (complex) time series vectors, s_i, i = 1, . . . ,D. ...we will here refer to it as the 'source subspace'[14]." Exploiting these redundancies, our goal is to reduce the singular MxN data matrix pencil "to an 'equivalent' square DxD matrix pencil having the same D nonzero generalized eigenvalues as the original matrix pencil [14]." We accomplish this at the core rotations level by simultaneous subspace rotations First, examine the singular value decomposition of the data matrices, X and Y. Here

$$\frac{1}{\sqrt{N}}\mathbf{X} = \sum_{i=1}^{D} \sigma_{x_i}\mathbf{u}_{x_i} \otimes \mathbf{v}_{x_i} = \mathbf{U}_x^D \boldsymbol{\Sigma}_x^D \mathbf{V}_x^{DH} \tag{4.8}$$

$$\frac{1}{\sqrt{N}}\mathbf{Y} = \sum_{i=1}^{D} \sigma_{y_i}\mathbf{u}_{y_i} \otimes \mathbf{v}_{y_i} = \mathbf{U}_y^D \boldsymbol{\Sigma}_x^D \mathbf{V}_y^{DH} \tag{4.9}$$

where the superscript D belonging to a matrix refers to the rank of the respective matrix. We include left ($\mathbf{U}_x^D$) and right ($\mathbf{V}_x^D$) singular vectors that are associated with nonzero GEs. We can write the resultant matrix pencil as

$$\frac{1}{\sqrt{N}}(\mathbf{Y} - \lambda\mathbf{X}) = \mathbf{U}_y^D \boldsymbol{\Sigma}_y^D \mathbf{V}_y^{DH} - \lambda\mathbf{U}_x^D \boldsymbol{\Sigma}_x^D \mathbf{V}_x^{DH} \tag{4.10}$$

$$= \mathbf{U}_x^D \mathbf{Q}_u \boldsymbol{\Sigma}_y^D \mathbf{Q}_v^H \mathbf{V}_x^{DH} - \lambda\mathbf{U}_x^D \boldsymbol{\Sigma}_x^D \mathbf{V}_x^{DH}$$

$$= \mathbf{U}_x^D \{ \mathbf{Q}_u \boldsymbol{\Sigma}_y^D \mathbf{Q}_v^H - \lambda\boldsymbol{\Sigma}_x^D \} \mathbf{V}_x^{DH}$$

where the unitary matrix Q, is the invariant subspace rotation matrix relating the left singular vectors of X to those of Y as

$$\mathbf{Q}_u = \mathbf{U}_x^{DH}\mathbf{U}_y^D \qquad \mathbf{Q}_v = \mathbf{V}_x^{DH}\mathbf{V}_y^D \tag{4.11a-b}$$

Here an analogous rotation matrix, $\mathbf{Q}_v$, exists for the right singular vectors of X and Y. Zoltowski and Stavrinides mention that GEVs of the DxD core rotations matrix pencil, $\{\mathbf{Q}_u\boldsymbol{\Sigma}_y^D\mathbf{Q}_v, \boldsymbol{\Sigma}_x^D\}$ are the D nonzero GEVs of the MxN singular pencil $\{(1/\sqrt{N})\mathbf{Y}_D, (1/\sqrt{N})\mathbf{X}_D\}$.

The goal of the PRO-ESPRIT scheme is to convert singular or rectangular forms to a reduced square core rotations matrices to find the DOAs. In our case we shall find that the PRO-ESPRIT algorithm is used to find the biphases by constructing a matrix

pencil from symmetric and skew-symmetric projected cumulants and finding the generalized eigenvalues. Later in chapter 5 we can use the PRO-ESPRIT algorithm to find **biphases** for a 2-D matrix form, the third order cumulant matrix of Swindlehurst and **Kailath [15].**

4.4 Symmetric and Skew-Symmetric Subspaces- A Rotational **Invariance** Approach

Consider the decomposition of the approximate projected cumulants, $R_\theta(m)$, into symmetric and skew-symmetric portions, $S_\theta(m)$ and $A_\theta(m)$, below. The Radon transform preserves phase. Following Appendix A.1 and section 4.1, in the case of a single triad the projection angle θ is equal to $\tan(\omega_2/\omega_1)$ we have

$$S_\theta(m) = 1/2(R_\theta(m) + R_\theta(-m)) = \cos(\gamma)\cos(\omega m) + \beta\delta(m) \tag{4.12}$$

$$A_\theta(m) = 1/2(R_\theta(m) - R_\theta(-m)) = \sin(\gamma)\sin(\omega m) \tag{4.13}$$

where the polar frequency $\omega = \omega_1\cos\theta + \omega_2\sin\theta$. Here we observe the one dimensional version of symmetrization. Once again the biphase angle θ has been extracted as the trigonometric coefficients of the sinusoidal cumulants. Instead of one triad assume that there are a total of k sinusoidal triads that fall along a particular slice of the **bispectrum** at a radial angle of θ radians. Symmetric and skew-symmetric projected cumulants may be expressed as

$$S_\theta(m) = \sum_{i=1}^{k} \cos\gamma_i\,(\cos\omega_i m) + \beta\delta(m) \tag{4.14}$$

$$A_\theta(m) = \sum_{i=1}^{k} \sin\gamma_i\,(\sin\omega_i m). \tag{4.15}$$

Suppose each sequence is now written in vector form where the projected cumulant's lag indexes the elements as $\mathbf{s}_\theta = [S_\theta(0)\ S_\theta(1)\ \cdots\ S_\theta(p-1)]^T$ and $\mathbf{a}_\theta = [A_\theta(0)\ A_\theta(1)\ \cdots\ A_\theta(p-1)]^T$. After converting the sinusoids to their equivalent complex exponential form, the two respective vectors may be **expressed** as

$$\mathbf{s}_\theta = \mathbf{E}\,\mathbf{p}'_\gamma + \beta\delta(m) \tag{4.16}$$

$$\mathbf{a}_\theta = \mathbf{E}\,\mathbf{J}\,\mathbf{q}'_\gamma \tag{4.17}$$

where the amplitude coefficient vectors are given by

$$\mathbf{p'}_{\gamma} = [\cos\gamma_1 \cos\gamma_1 \cdots \cos\gamma_k \cos\gamma_k]^T \tag{4.18}$$

and

$$\mathbf{q'}_{\gamma} = [\sin\gamma_1 \sin\gamma_1 \cdots \sin\gamma_k \sin\gamma_k]^T \tag{4.19}$$

The reduced dimension 2k x 2k Vandermonde matrix, E, is composed of individual complex exponential columns as

$$\mathbf{E} = [\,\mathbf{e}(\omega_1) \vdots \mathbf{e}(\omega_{-1}) \vdots \mathbf{e}(\omega_2) \vdots \mathbf{e}(\omega_{-2}) \vdots \cdots \vdots \mathbf{e}(\omega_k) \vdots \mathbf{e}(\omega_{-k})\,] \tag{4.20}$$

where the 2k x 1 element vector of complex exponentials, $\mathbf{e}(\omega_i)$, is defined as

$$\mathbf{e}(\omega_i) = \frac{1}{2}[1 \;\; \exp(j\,\omega_i) \;\; \exp(j\,2\,\omega_i) \;\; \cdots \;\; \exp(j\,(2k-1)\,\omega_k)]^T \tag{4.21}$$

and $\mathbf{e}(\omega_{-i}) = \mathbf{e}^*(\omega_i)$. The 2k x 2k diagonal matrix, J, which contains the rotational constants or phase shifts, is defined as

$$\mathbf{J} = \text{diag}\,\{j, -j, j, \cdots j, j, -j,\}. \tag{4.22}$$

J is the 90 degree phase shift matrix which effectively shifts complex exponentials by positive or negative $\pi/2$ radians in accordance with the sign of the respective column in E. In this case J converts complementary column pairs of E from cosine functions to sine functions.

This construction is used to form the Toeplitz symmetric and skew-symmetric projected cumulant matrices, $\mathbf{S}_\theta$ and $\mathbf{A}_\theta$, respectively. The projected third order cumulant matrix filled with symmetric cumulants, $\mathbf{S}_\theta$ is both symmetric and Toeplitz and written as

$$\mathbf{S}_\theta = \begin{bmatrix} S_\theta(0) & S_\theta(1) & \cdots & S_\theta(n) \\ S_\theta(-1) & S_\theta(0) & \cdots & S_\theta(n-1) \\ \cdot & \cdot & \cdot & \cdot \\ \cdot & \cdot & \cdot & \cdot \\ \cdot & \cdot & \cdot & \cdot \\ S_\theta(-n) & S_\theta(-n+1) & \cdots & S_\theta(0) \end{bmatrix} \tag{4.23}$$

As stated earlier for the 2-D cumulant case, it is possible to decompose $\mathbf{S}_\theta$

$$\mathbf{S}_\theta = \mathbf{E}\,\mathbf{P'}_{\gamma}\,\mathbf{E}^H + \beta\mathbf{I} \tag{4.24}$$

where $\mathbf{P'}_{\gamma} = \text{diag}\{\mathbf{p'}\}$ is a 2k x 2k dimensioned matrix. Likewise $\mathbf{A}_\theta$ may be expressed as

$$\mathbf{A}_\theta = \mathbf{E}\,\mathbf{Q}'_\gamma\,\mathbf{J}\,\mathbf{E}^H \tag{4.25}$$

and analogous to the preceding equation, $\mathbf{Q}'_\gamma = \mathbf{diag}\{\ q'\ \}$.

Note that S and A are both of full rank equal to $\rho=2k$. The range space for each matrix is the same. The only difference between the two is that the eigenvectors representing the constituent bases are rotated from S to A. The rotation is exploited in forming the matrix pencil

$$S - \kappa A = \mathbf{E}\,(\,\mathbf{P}'_\gamma - \kappa\,\mathbf{S}_\gamma\mathbf{J}\,)\,\mathbf{E}^H. \tag{4.26}$$

The rank decreases by one, i.e. $\rho = 2k - 1$, when κ satisfies,

$$\{p_{\gamma,ii}\} = j^{2i+1}\kappa\,\{q_{\gamma,ii}\}. \tag{4.27}$$

In this case

$$j^{2i+1}\kappa = \frac{\{p_{\gamma,ii}\}}{\{q_{\gamma,ii}\}} = \cot\gamma_k \tag{4.28}$$

where $\{p_{\gamma,ii}\}$ and $\{q_{\gamma,ii}\}$ are the ith diagonal elements of $\mathbf{P}_\gamma$ and $\mathbf{Q}_\gamma$, respectively. Here $k = \frac{i+1}{2}$ or $k=\frac{1}{2}$ depending on the position of the biphase argument γ_j in $\mathbf{P}_\gamma$ or $\mathbf{A}_\gamma$. Furthermore, the biphases, γ_i, $1 \le i \le k$, are obtainable since the elements of the $\mathbf{\Phi}$ matrix are known, through

$$\mathrm{arccot}[\ \kappa\ \{j^{2i+1}\}\ ] = \gamma_j. \tag{4.29}$$

Thus, κ is a generalized eigenvalue (GE) of the matrix pencil (S, A). Working with this matrix pencil the biphases are found without the knowledge of the constituent frequencies. Each GE.is the ratio of corresponding symmetric and skew-symmetric biphase gain factors multiplied by the corresponding phase shift factor $\pm j$. Therefore simply knowing the GEs enables one to find all the biphases of quadratically coupled sinusoids lying along a particular projection angle. Knowledge of the coupling frequencies is not required.

4.5 Simulations of 1-D SKEW-MUSIC

Simulations demonstrating the efficacy of the Fourier-Slice bispectrum extensions to SKEW-MUSIC are presented next. For the purpose of generating cumulant projections, cumulants were estimated over a hexagonal grid whose maximum extent

is ± 30 cumulant lags along any lag axis. In this context, projections are taken normal to the 45^{o} axis and provide information about the $f_1 = f_2$ frequency axis of the bispectrum. For these simulations each trial consists of a sinusoid triad where $f_1 = f_2 = .05$ Hz and $f_3 = 0.1$ Hz with varying biphases.

As in the case of 2-D SKEW-MUSIC the noise from an exponential distribution necessary to generate a SNR of 4.77 dB was used. The noise was white. The reduced order bispectrum has a spacing or sampling rate for a given slice dependent on the size of the bispectral hexagon bandwidth relative to the maximal $\sqrt{2}\pi$ bandwidth of the polar raster. Suitable full coverage of the cumulant domain yields cumulant projections as illustrated in Figs. 4.1 - 4.8 for biphases of 15^{o}, 45^{o}, 60^{o} and 75^{o}, respectively. Note that the changing biphase is evident in the relative sizes of the symmetric and skew-symmetric cumulants provided in the graphs. Also as the symmetric projected cumulants begin to decrease in amplitude, the noise peak becomes more prominent. These estimates were taken from the eigenvectors belonging to the noise subspace of the 6 x 6 matrices filled according to (4.21)-(4.23). For the slice selected there is one real sinusoid so that the appropriate signal subspace dimension is two. The plots indicating coupling frequencies for the two lower biphase cases were generated using symmetric cumulants. The skew-symmetric cumulants were used to generate the frequency plot of the higher biphase case.

Monte Carlo simulations of the biphase estimation algorithms, 1-D SKEW-MUSIC and SKEW-ESPRIT, were run. In each case the biphases of a coupled pair of sinusoids along the $f_1 = f_2$ main diagonal of the bispectral domain were checked. Four different biphase are used in this simulation set: 15^{o}, 45^{o}, 60^{o}, and 75^{o}. The noise level was enough for a 4.77 dB SNR. 100 trials were run at each biphase value. The bicoherence level is 1.0. We fill two 10x10 matrices from the projected symmetric and skew-symmetric sequences.

Assume that we only have a single real sinusoid that is isolated by the procedure of taking cumulant projections at a 45 degree angle. Using this information we reduce this singular matrix to a 2x2 core rotations level matrix pencil with the procedure of PRO-ESPRIT applied with rotation matrices Q_u and Q_v. The eigenvalues of the core rotations matrix pencil yield the biphases as described earlier. The results of these simulations for the 1-D SKEW-ESPRIT algorithm are shown in Table 4.1. Likewise the 1-D SKEW-MUSIC algorithm is tested for biphase estimation as well. Starting with the 10 x 10 matrices described above, biphases are found using a 1-D version of (3.21). For this simulation knowledge of the coupling frequencies are needed. The coupling frequencies as described above are placed in the algorithm

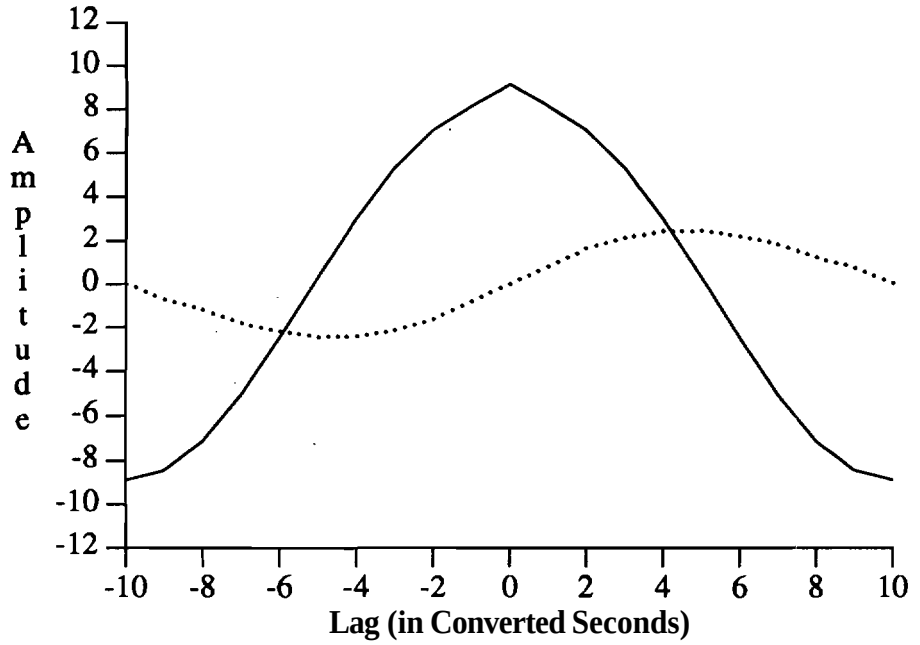

Figure 4.1 **Projected Cumulants for Biphase of 15° (Along $f_1=f_2$ Axis)**

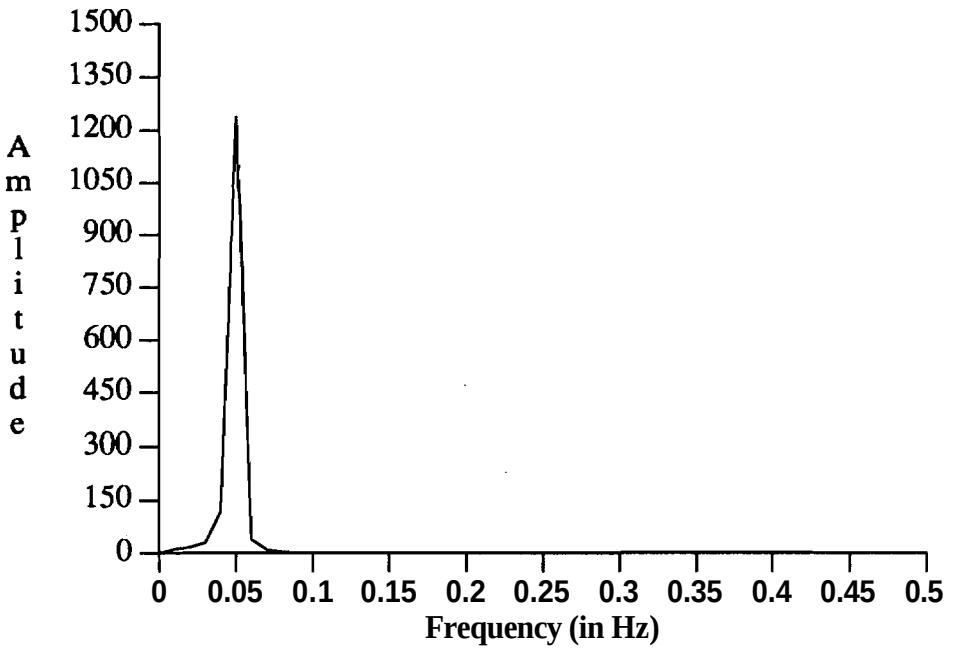

Figure 4.2 **MUSIC spectrum from Projected Cumulants for Biphase of 15°**

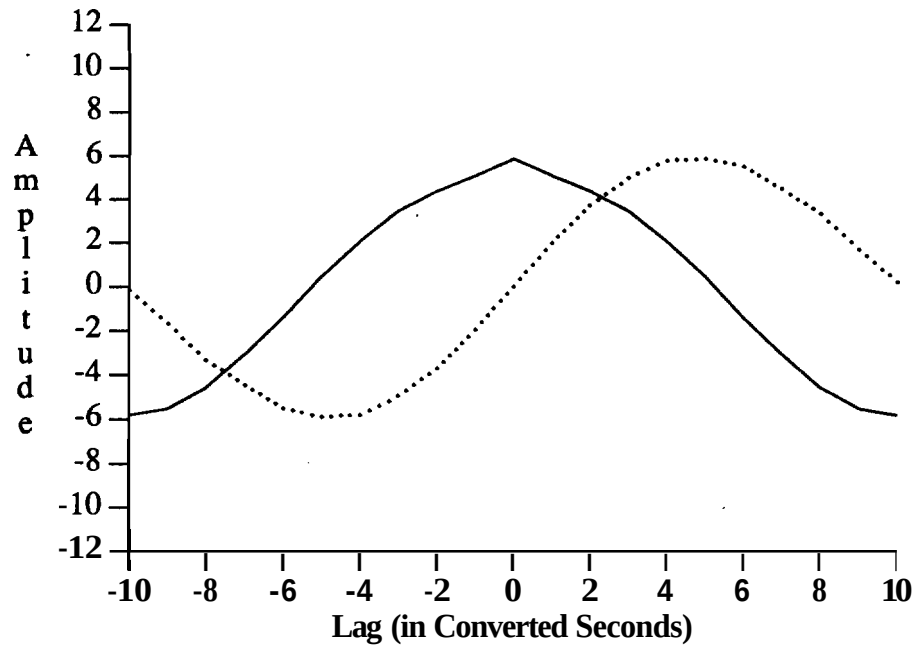

Figure 4.3 Projected Cumulants for Biphase of 45°

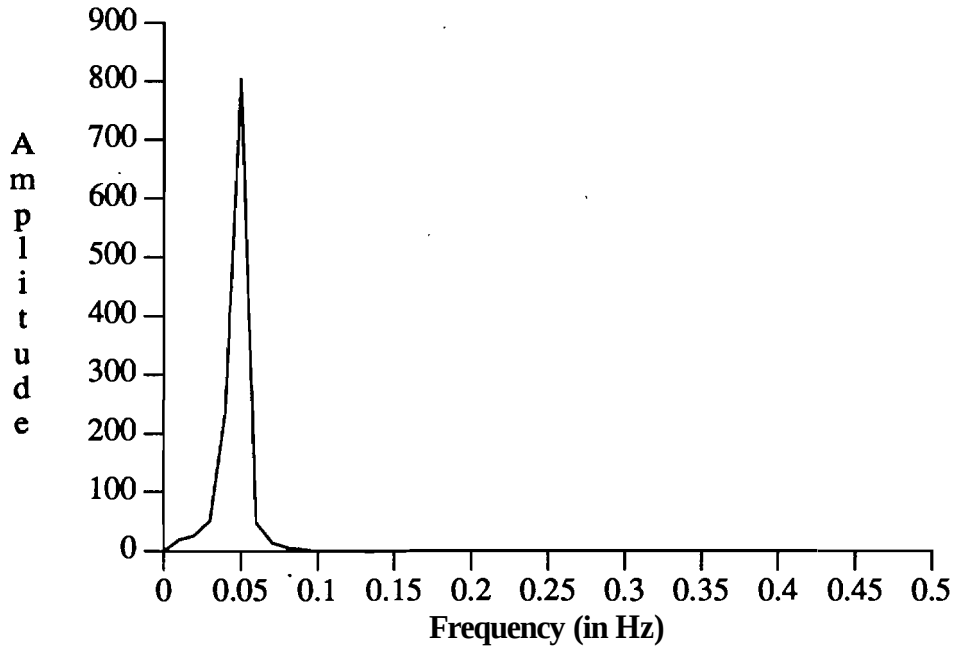

Figure 4.4 MUSIC spectrum from Projected Cumulants for Biphase of 45°

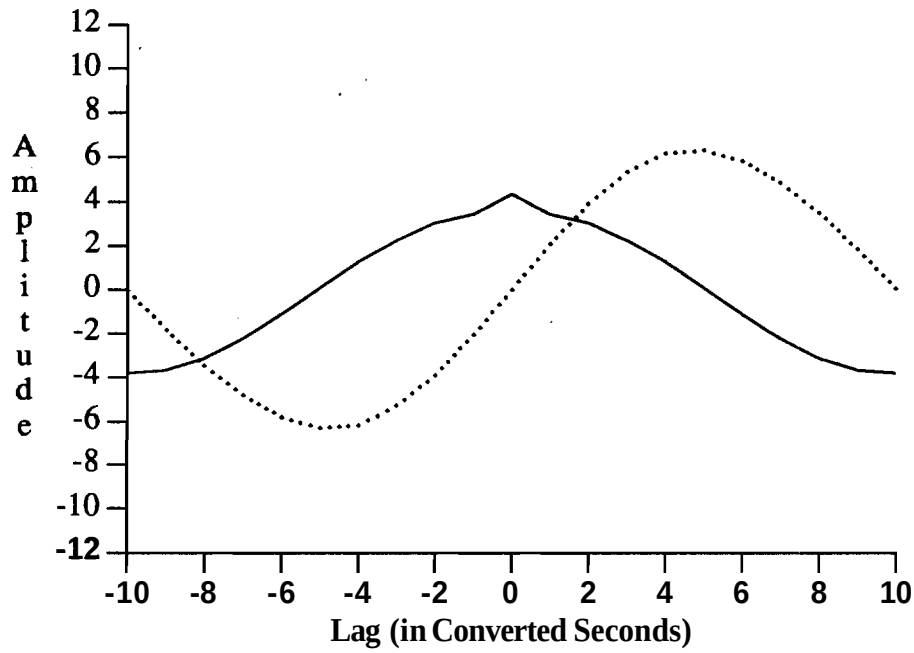

Figure 4.5 **Projected Cumulants for Biphase of 60°**

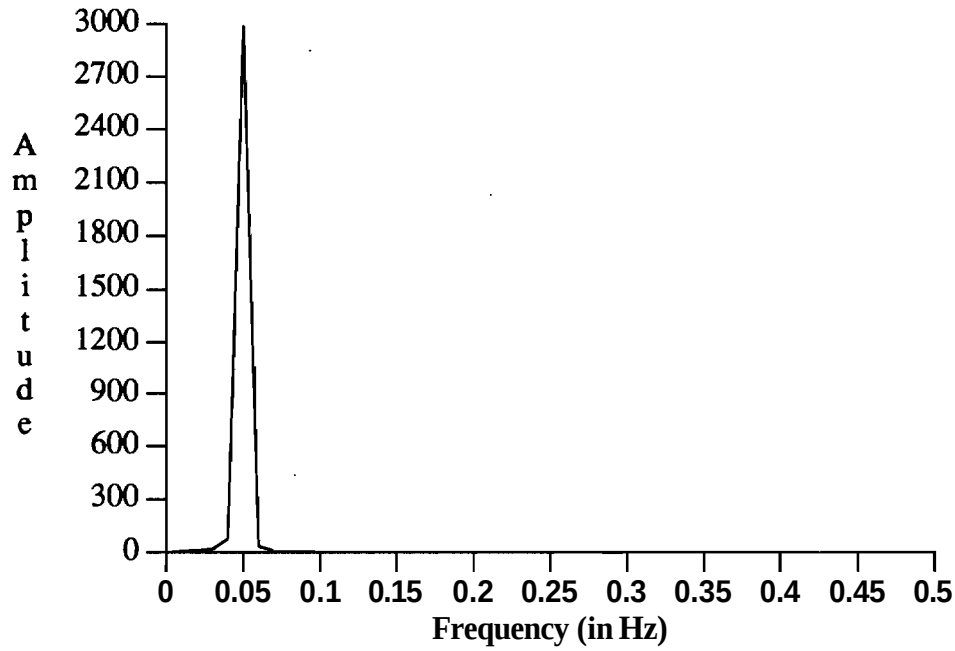

Figure 4.6 **MUSIC spectrum from Projected Cumulants for Biphase of 60°**

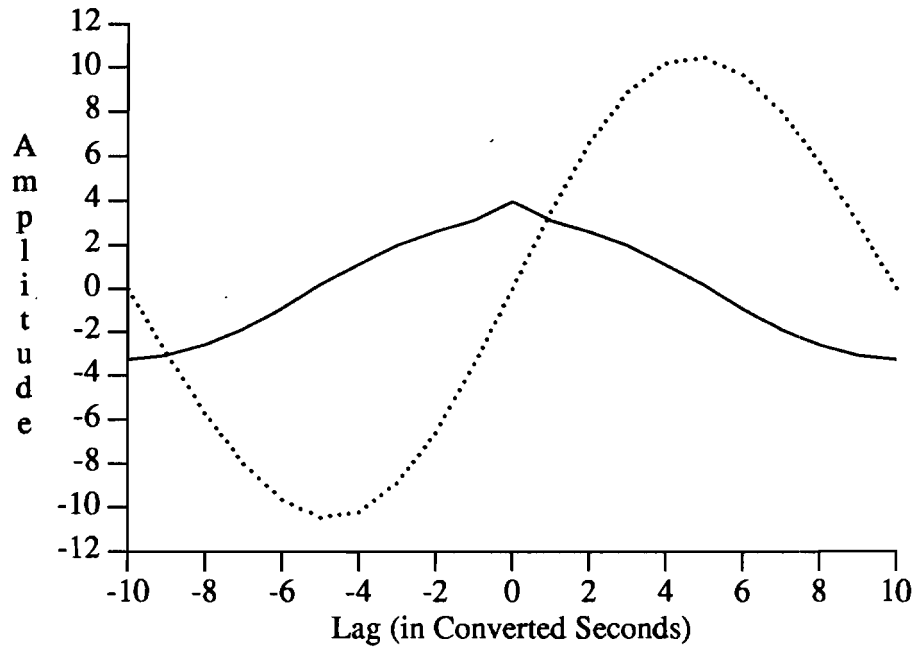

Figure 4.7 Projected Cumulants for Biphase of 75°

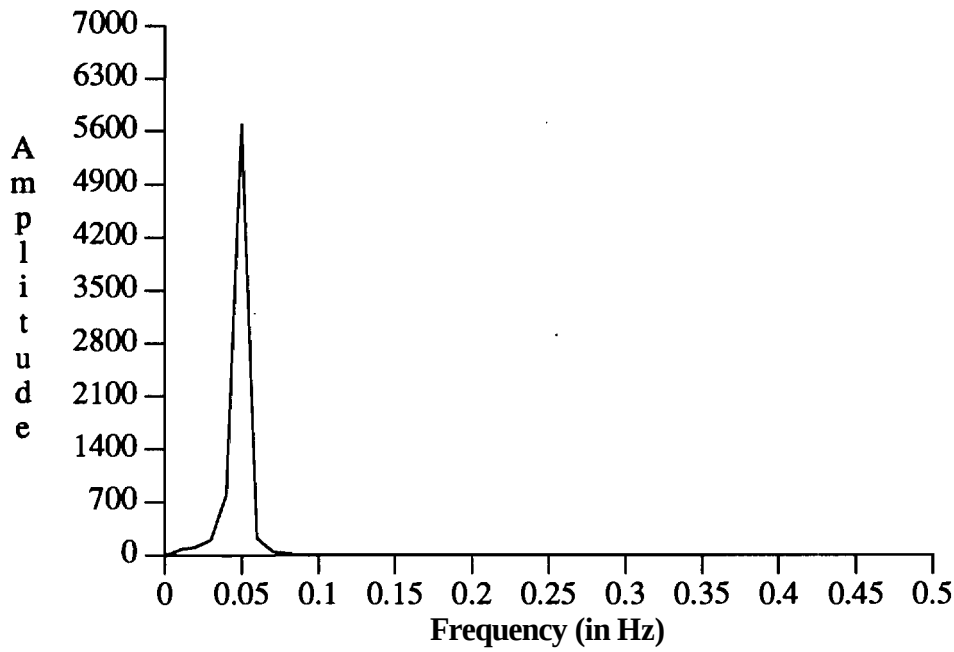

Figure 4.8 MUSIC spectrum from Projected Cumulants for Biphase of 75°

Table 4.1 **Biphase Estimates Using SKEW-MUSIC and SKEW-ESPRIT Using Fourier-Slice Bispectrum along f1=f2 Projection Axis**

Biphase Estimates Using Fourier-Slice Bispectrum Positively Skewed Noise - SNR = 4.77 dB				
Biphase	Algorithm			
	SKEW-MUSIC		SKEW-ESPRIT	
	$\hat{\gamma}$	sdev($\hat{\gamma}$)	$\hat{\gamma}$	sdev($\hat{\gamma}$)
15°	15.9347	1.4414	15.1	1.093
45°	46.569	1.222	45.04	1.065
60°	61.1859	1.2832	59.18	1.101
75°	75.1635	1.2976	74.46	1.15

4.6 List of References

[1] K.I. Kim and E.J. Powers, "A Digital Method of Modeling Quadratically Nonlinear Systems with a General Random Input," IEEE Trans. Acoust. Speech Signal Process, vol. ASSP-36, pp. 1758-1769, Nov. 1988.

[2] P.Z. Marmarelis and V.Z. Marmarelis, Analysis of Physiological Systems, Plenum, New York, NY, 1978.

[3] M. Schetzen, The Volterra and Wiener Series of Nonlinear Systems, Wiley, New York, NY, 1980.

[4] J.D. Victor and B.W. Knight, "Nonlinear Analysis with an Arbitrary Stimulus Ensemble," Quart. App. Math., vol. 37, pp. 113-136, July 1979.

[5] G. Beylkin, "Discrete Radon Transform," IEEE Trans. Acoust. Speech Signal Proc., vol. ASSP-35, pp. 162-172, Feb. 1987.

[6] D. E. Dudgeon and R. M. Mersereau, Multidimensional Digital Signal Processing, Prentice-Hall, Englewood Cliffs, NJ, 1984.

[7] D.L. Sherman and M.D. Zoltowski, "Decoupling Higher Order Cumulant Sequences Resulting Three-Wave Coupling Processes," Proc. 5th ASSP Wkshp. on SEM, pp. 227-231, Rochester, NY, Oct. 1990.

[8] S. ALshebeili and A.E. Cetin, "A Phase Reconstruction Alogorithm from Bispectrum," IEEE Trans. Geosci. Remote Sensing, vol. GEO-28, pp. 166-170, May 1990.

[9] G. Giannakis and A. Delopoulos, "Nonparametric Estimation of Autocorrelation and Spectra Using Cumulants and Polyspectra," Proc. *SPIE*, vol. 1348, pp. 503-517, July 1990.

[10] A.G. Bessios and C.L. Nikias, "FFT-based bispectrum computation on polar rasters," IEEE Trans. SP, vol. SP-39, pp. 2525-2539, Nov. 1991.

[11] N. Srinivasa, Applications of LP Modelling and Filtering in Radon Space, Ph.D. Dissertation, Indian Institute of Science, Bangalore, August 1988.

[12] M.R. Raghuveer and C.L. Nikias, "Bispectrum Estimation: A Parametric Approach," IEEE Trans. ASSP, vol. ASSP-33, pp. 1213-1220, Oct. 1985.

[13] R. Roy, A. Paulraj, and T. Kailath, "ESPRIT - A Subspace Rotation Approach to Estimation of Parameters of Cisoids in Noise," IEEE Trans. ASSP, vol. ASSP-34, pp. 1340-1342, October 1986.

[14] M. Zoltowski and D. Stavrinides, "Sensor Array Signal Processing Via a Procrustes Rotations Based Eigenanalysis of the ESPRIT Data Pencil," IEEE Trans. ASSP, vol. 37, pp. 832-861, June 1989.

[15] A.L. Swindlehurst and T. Kailath, "Detection and Estimation Using the Third Moment Matrix," Proc. Int. Conf. ASSP *Soc.*, pp. 2325-2328, Glasgow, Scotland, May 1989.

CHAPTER 5
BIPHASE ESTIMATION AND THE TRIPLE KRONECKER PRODUCT MATRIX

5.1 Introduction

In this section we generalize the third order moment matrix method of Swindlehurst and Kailath for biphase estimation [1]. Starting at the signal level with the use of the triple Kronecker product, we are able to redefine the third order Kronecker product matrix in terms of forward and backward signal vectors. Matrices consisting of symmetric and skew-symmetric cumulants can be be built from the forward and backward third order Kronecker product matrices. Either of these rectangular matrices can be used for coupling frequency determination. Reduction of the rectangular matrix pencil of symmetric and skew-symmetric matrices to an equivalent square form allows the biphases to once again be estimated from the GEs.

5.2 Derivation

The algorithm of Swindlehurst and Kailath utilizes the triple Kronecker product of signal vectors to form a triple correlation matrix $\mathbf{R_3}$. A novel feature of this method is that it is formed directly from the actual signal vectors instead of starting with the cumulants. A conventional rendering of the triple Kronecker product matrix has been mentioned in chapter 2. To reiterate we see that

$$\mathbf{R_3} = E\{\mathbf{x} \otimes \mathbf{x} \otimes \mathbf{x}^H\} \tag{5.1}$$

where

$$\mathbf{x} = [x(n)\ x(n+1)\ \cdots\ x(n+m-1)]^T \tag{5.2}$$

is the data vector. We can decompose the matrix in (53) as an m^2 x m block matrix

$$\mathbf{R_3} = \begin{bmatrix} \mathbf{R_3}(0) \\ \mathbf{R_3}(1) \\ \vdots \\ \mathbf{R_3}(m-1) \end{bmatrix}. \tag{5.3}$$

Consequently, each m x m block $\mathbf{R_3}(i)$ is built from the cumulants as

$$\mathbf{R_3}(i) = \begin{bmatrix} R(i,0) & R(i,1) & \cdots & R(i,m-1) \\ R(i-1,-1) & R(i-1,0) & \cdots & R(i-1,m-2) \\ & & \vdots & \\ R(i-m+1,-m+1) & R(i-m+1,-m+2) & \cdots & R(i-m+1,0) \end{bmatrix} \tag{5.4}$$

The use of the singular value decomposition (SVD) of $\mathbf{R_3}$ together with the appropriate signal subspace algorithm generates estimates of the coupling frequencies from a nonlinear process. This method also utilizes the full 2-D cumulant domain when estimating frequencies involved in quadratic phase coupling. Unfortunately, this algorithm also assumes that constituent sinusoidal triads all have zero biphase. It would be advantageous to adapt this method to insure that the biphases can be estimated along with coupling frequencies.

Additionally, $\mathbf{R_3}$ is a rectangular m^2 x m matrix. The third order moment term, R(0,0), does not lie along the main diagonal as in the SKEW-MUSIC symrnemc mamx described in chapter 3. Since the additive white noise in the Swindlehurst and Kailath formulation is Gaussian, asymptotically this component does not augment the R(0,0) term. For non-Gaussian additive white noise the R(0,0) term would also contain a noise component which would perturb the SVD. We seek to eliminate the R(0,0) term while insuring that we can estimate the biphases of constituent coupled sinusoids from our time series. In this fashion the methods of SKEW-MUSIC and SKEW-ESPRIT can be generalized for rectangular matrices. Ultimately, a method such as PRO-ESPRIT is applied to the singular form $\mathbf{R_3}$ in the estimation of the biphases [2].

First, however, let us estimate biphases and coupling frequencies in the case considered by the Swindlehurst and Kailath, that of quadratrically phase coupled sinusoids with added Gaussian noise. The vector $\mathbf{x}$ is composed of a signal, Es, plus an added Gaussian noise component vector, n, so that $\mathbf{x} = Es + n$. Assuming that the

time series **x(t)** contains only phase-coupled sinusoids and Gaussian noise, E is a matrix of complex exponential columns. Here d is the number of sinusoids in the time series irrespective of quadratic phase coupling. The general structure of E is like that of (4.20)-(4.21). However, this time there are 2d columns each of length m. Each sinusoid has an amplitude and phase as well. These are contained in the s vector also of length 2d

$$\mathbf{s} = [\, A_1 e^{j\phi(\omega_1)} \; A_1 e^{-j\phi(\omega_1)} \; \cdots \; A_d e^{j\phi(\omega_d)} \; A_d e^{-j\phi(\omega_d)} \,]^T \tag{5.5}$$

Following [1] in the case of quadratically phase coupled sinusoids in Gaussian noise the expectation in (5.1) becomes

$$\mathbf{R_3} = E\{(\mathbf{Es} + \mathbf{n}) \otimes (\mathbf{Es} + \mathbf{n}) \otimes (\mathbf{Es} + \mathbf{n})^H\} \tag{5.6}$$

$$= E\{\mathbf{Es} \otimes \mathbf{Es} \otimes \mathbf{s}^* \mathbf{E}^*\}$$

$$= \sum_{i=1}^{d} \sum_{k=1}^{d} \sum_{1=1}^{d} A_i A_k A_l [\mathbf{e}(\omega_i) \otimes \mathbf{e}(\omega_j) \otimes \mathbf{e}^H(\omega_l)] \, E\{e^{j(\phi(\omega_i) + \phi(\omega_k) - \phi(\omega_l)}\}$$

When there is quadratic phase coupling present for real **x(t),** the terms under the expectation become the biphase angle, namely $e^{j\gamma}$. If there are N triads in the time series **x(t),** each having a biphase γ_i, the triple Kronecker product representation, $\mathbf{R_3}$ can be written in complex exponential form including biphases of component complex exponential vectors using the conventions of [1] as

$$\begin{aligned} \mathbf{R_3} = \sum_{i=1}^{N} A_{i1} A_{i2} A_{i3} \{ & e^{j\gamma_i} \mathbf{e}_{112} \mathbf{e}^H(\omega_{i3}) + e^{-j\gamma_i} \mathbf{e}_{11\bar{2}} \mathbf{e}^T(\omega_{i3}) \\ & + e^{j\gamma_i} \mathbf{e}_{13\bar{1}} \mathbf{e}^H(\omega_{i2}) + e^{-j\gamma_i} \mathbf{e}_{11\bar{3}} \mathbf{e}^T(\omega_{i2}) \\ & + e^{j\gamma_i} \mathbf{e}_{13\bar{2}} \mathbf{e}^H(\omega_{i1}) + e^{-j\gamma_i} \mathbf{e}_{12\bar{3}} \mathbf{e}^T(\omega_{i1}) \}. \end{aligned} \tag{5.7}$$

In this context $\mathbf{e}(\omega_{ik})=[1 \; \exp(j\omega_{ik}) \; . \; . \; . \; \exp(j(m-1)\omega_{ik})]^T$ and the compound complex exponential vector formed from the sum of double Kronecker products is

$$\mathbf{e}_{ikl} = \mathbf{e}(\omega_{ik}) \otimes \mathbf{e}(\omega_{il}) + \mathbf{e}(\omega_{il}) \otimes \mathbf{e}(\omega_{ik}) \tag{5.8}$$

for general $\mathbf{e}(\omega_{ik})$ and $\mathbf{e}(\omega_{il})$, and k, l=1, 2, 3 refers to the member number of the ith triad. Also a bar over one (or both) of the subscripts for $\mathbf{e}_{xy}$ in (5.7) indicates that the conjugate has been taken of one (or both) of the constituent vectors. If it is desired to make third order cumulant matrices filled with symmetric or skew-symmetric cumulants, forward and backward vectors, $\mathbf{x_F}$ and $\mathbf{x_B}$, need to be defined

$$\mathbf{x}_F = [x(n)\ x(n+1)\ x(n+2)\ \cdots\ x(n+m-1)]^T \tag{5.9}$$

$$\mathbf{x}_B = [x(n)\ x(n-1)\ x(n-2)\ \cdots\ x(n-m+1)]^T \tag{5.10}$$

We can write $\mathbf{R}_{3FFF}$ and $\mathbf{R}_{3BBB}$ as

$$\mathbf{R}_{3FFF} = E\{\mathbf{x}_F \otimes \mathbf{x}_F \otimes \mathbf{x}_F^H\} \qquad \mathbf{R}_{3BBB} = E\{\mathbf{x}_B \otimes \mathbf{x}_B \otimes \mathbf{x}_B^H\} \tag{5.11a-b}$$

$\mathbf{R}_{3FFF}$ has the form of (5.3)-(5.4) whereas $\mathbf{R}_{3BBB}$ can be written as

$$\begin{aligned}\mathbf{R}_{3BBB} = \sum_{i=1}^{N} A_{i1}A_{i2}A_{i3}\{ & e^{j\gamma_i}\mathbf{e}_{i\bar{1}\bar{2}}\mathbf{e}^T(\omega_{i3}) + e^{-j\gamma_i}\mathbf{e}_{i12}\mathbf{e}^H(\omega_{i3}) \\ & + e^{j\gamma_i}\mathbf{e}_{i\bar{3}\bar{1}}\mathbf{e}^T(\omega_{i2}) + e^{-j\gamma_i}\mathbf{e}_{i\bar{1}\bar{3}}\mathbf{e}^H(\omega_{i2}) \\ & + e^{j\gamma_i}\mathbf{e}_{i\bar{3}\bar{2}}\mathbf{e}^T(\omega_{i1}) + e^{-j\gamma_i}\mathbf{e}_{i\bar{2}\bar{3}}\mathbf{e}^H(\omega_{i1})\}\end{aligned} \tag{5.12}$$

Changes in directionality from forward to backward vectors only conjugate frequency terms and leave resulting biphase factors with the same sign. We can then write the symmetric, $\mathbf{S}_3$, and skew-symmetric, $\mathbf{A}_3$, matrices using forward-backward triple Kronecker products

$$\mathbf{S}_3 = 1/2[\ \mathbf{R}_{3FFF} + \mathbf{R}_{3BBB}\ ] \qquad \mathbf{A}_3 = 1/2[\ \mathbf{R}_{3FFF} - \mathbf{R}_{3BBB}\ ]. \tag{5.13a-b}$$

The general formulation of $\mathbf{S}_3$ for multiple triads specifically involves the product of left and right complex exponential Vandermonde mamces as

$$\mathbf{S}_3 = \mathbf{E}_L \mathbf{P} \mathbf{E}_R^H. \tag{5.14}$$

Assuming that there are N distinctive sets of phase-coupled sinusoids, $\mathbf{E}_L$ is a m^2 x D mamx containing columns of the compound complex exponential vectors, $\mathbf{e}_{12}$, $\mathbf{e}_{\bar{1}\bar{2}}$, etc. and. D = 6N. $\mathbf{E}_R$ contains the simple complex exponential vectors of the form $\mathbf{e}(\omega_3)\ \bar{\mathbf{e}}(\omega_3)$, etc. This mamx is m x D. Finally, P, is a D x D diagonal mamx with terms of the form $A_1A_2A_3\cos\gamma_i$.

In a complementary rendition, $\mathbf{A}_3$ can be written as

$$A3 = \mathbf{E}_L \mathbf{Q} \mathbf{J} \mathbf{E}_R^H. \tag{5.15}$$

As before, $\mathbf{Q}$ contains terms such as $A_1A_2A_3\sin\gamma$ along its diagonal. $\mathbf{J}$ is a unitary mamx with alternating phase shifts of ±90 degrees. Singular value decompositions of either $\mathbf{S}_3$ or $\mathbf{A}_3$ can be accomplished for coupling frequency estimation using the appropriate estimator as outlined in [1].

To estimate the biphases we again exploit the property of common row and column spaces by first writing a rectangular mamx pencil $\{\mathbf{S}_3, \mathbf{A}_3\}$,

$$\mathbf{S}_3 - \kappa\mathbf{A}_3 = \mathbf{E}_L\,(\mathbf{P} - \kappa\mathbf{Q}\mathbf{J})\mathbf{E}_R^H \tag{5.16}$$

As before when $\kappa_j^{2i+1} = \cot\gamma_i$, the rank of the matrix pencil decreases by one from D to D–1. The set $\{\cot\gamma_1, \cot\gamma_2, \cdots, \cot\gamma_N\}$ are the GEs of the rectangular matrix pencil $\{\mathbf{S}_3, \mathbf{A}_3\}$. To estimate the GEs and hence the biphases, we must reduce the rectangular pencil to an "equivalent" DxD square pencil $\{\mathbf{S}_{3D}, \mathbf{A}_{3D}\}$ having the same nonzero GEs as (5.16). Once again the techniques of PRO-ESPRIT give us the appropriate square pencil based upon the non-zero singular values and corresponding left and right singular vectors of both $\mathbf{S}_3$ and $\mathbf{A}_3$ [1]. This method of finding coupling frequencies and respective biphases will be termed SKEW-PRO-ESPRIT.

In the case of additive white non-Gaussian noise it is desired to eliminate the R(0,0) term from the third order cumulant matrix. To prevent the term R(0,0) from occurring anywhere in (5.13) we need to eliminate all triple correlations with terms having identical time lags, i.e., terms such as E{x(i)x(i)x(i)} cannot appear. This condition can be prevented by the use of mixed forward-backward Kronecker products and time-delay signal vectors. The appropriate alternate definitions of triple Kronecker product matrices are given below. Recall that the time series x(t) is real-valued,

$$\mathbf{R}_{3FFB-} = E\{\mathbf{x}_F \otimes \mathbf{x}_F \otimes \mathbf{x}_{B-}^T\} \qquad \mathbf{R}_{3BBF+} = E\{\mathbf{x}_B \otimes \mathbf{x}_B \otimes \mathbf{x}_{F+}^T\} \tag{5.17a-b}$$

where the time-shift signal vector, $\mathbf{x}_{F+} = [x(n+1)\ x(n+2)\ \cdots\ x(n+m)]^T$ and $\mathbf{x}_{B-} = [x(n-1)\ x(n-2)\ \ldots\ x(n-m)]^T$. Consequently, we can construct matrices filled with symmetric and skew-symmetric cumulants from $\mathbf{R}_{3FFB-}$ and $\mathbf{R}_{3BBF+}$ as

$$\mathbf{S}_{3'} = 1/2[\mathbf{R}_{3FFB-} + \mathbf{R}_{3BBF+}] \qquad \mathbf{A}_{3'} = 1/2[\mathbf{R}_{3FFB-} - \mathbf{R}_{3BBF+}]. \tag{5.18a-b}$$

At this juncture SKEW-PRO-ESPRIT can be performed to find coupling frequencies and biphases in the manner described earlier. As we will see in the simulations section, the modified Swindlehurst and Kailath method allows for accurate biphase estimation in either Gaussian or non-Gaussian distributed noise.

5.3 Comparing the Structure of the 2-D SKEW-MUSIC Matrix and the Triple Kronecker Product Matrix

Examining the structure of the matrix used in 2-D SKEW MUSIC we notice that it does feature Kronecker products of the compound exponential vectors, that is the double Kronecker product generated from the Kronecker product of exponential

vectors. Restating (3.14) from chapter III, we see that the S matrix used for 2-D SKEW MUSIC is written as

$$\mathbf{S} = \sum_{i=1}^{N} p_{\gamma,ii} \left\{ \sum_{j,k} [\mathbf{e}^*(\omega_{ik},\omega_{ij})\, \mathbf{e}^T(\omega_{ik},\omega_{ij}) + \mathbf{e}(\omega_{ik},\omega_{ij})\mathbf{e}^H(\omega_{ik},\omega_{ij})] \right\} + \beta \mathbf{I} \quad (5.19)$$

where $\mathbf{e}_{ik}$ is an exponential vector

$$\mathbf{e}_{ik} = [\, 1 \;\; \exp(\omega_{ik}) \;\; \exp(2\omega_{ik}) \;\; \cdots \;\; \exp(m\omega_{ik}) \,]^T$$

and $\mathbf{e}(\omega_{ik},\omega_{ij}) = \mathbf{e}_{ik} \otimes \mathbf{e}_{ij}$ which is a 2nd order Kronecker product. The coefficient $p_{\gamma,ii} = \dfrac{(\cos\gamma_i)}{2}$ contains biphases. Likewise **A** can be decomposed as

$$\mathbf{A} = \sum_{i=1}^{N} q_{\gamma,ii} \left\{ \sum_{j,k} [\mathbf{e}^*(\omega_{ik},\omega_{ij})\, \mathbf{e}^T(\omega_{ik},\omega_{ij}) - \mathbf{e}(\omega_{ik},\omega_{ij})\mathbf{e}^H(\omega_{ik},\omega_{ij})] \right\} \quad (5.20)$$

Here again we indicate that the coefficient $q_{\gamma,ii} = (\sin\gamma_i)/2j$ contains biphases. In each case we can write the matrices in terms of simple Kronecker products:

$$S = \sum_{i=1}^{N} p_{\gamma,ii} \sum_{j,k} \{ [\mathbf{e}_{ij} \otimes \mathbf{e}_{ik}]^* \otimes [\mathbf{e}_{ij} \otimes \mathbf{e}_{ik}]^T + [\mathbf{e}_{ij} \otimes \mathbf{e}_{ik}] \otimes [\mathbf{e}_{ij} \otimes \mathbf{e}_{ik}]^H \} \quad (5.21)$$

In much the same fashion **A** also has a clear Kronecker product rendition:

$$\mathbf{A} = \sum_{i=1}^{N} q_{\gamma,ii} \sum_{j,k} \{ [\mathbf{e}_{ij} \otimes \mathbf{e}_{ik}]^* \otimes [\mathbf{e}_{ij} \otimes \mathbf{e}_{ik}]^T - [\mathbf{e}_{ij} \otimes \mathbf{e}_{ik}] \otimes [\mathbf{e}_{ij} \otimes \mathbf{e}_{ik}]^H \} \quad (5.22)$$

The matrices from 2D SKEW-MUSIC can in fact be constructed from sums of 4th order Kronecker products of exponential vectors. Third order cumulant terms corresponding to product terms comprise the matrix entries. The only difference between the matrices is the coefficients of Kronecker products.

The third order cumulant matrix of Swindlehurst and Kailath does not have $\mathbf{R}(0,0)$ diagonal terms. Being a rectangular matrix $\mathbf{S}_3$ and $\mathbf{A}_3$, the noise terms cannot be isolated nor can either of these matrices be termed symmetric or skew-symmetric. The 2D SKEW-MUSIC matrices, S and **A**, are normal matrices with noise third order moment contributions lying along the main diagonal. The symmetric or skew-symmetric structure is once again evident when we glance at the structures of the matrix decompositions in (3.10) and (3.11). The structure of the matrices for 2-D

SKEW-MUSIC could also used for biphase determination in much the same manner described in this chapter or earlier in chapter 3.

There have been several algorithms using higher order statistics for array processing and harmonic retrieval applications using 4th order statistics[3, 4]. Though our matrix has a 4th order structure, we do not fill the matrix with 4th order statistics as those harmonic retrieval algorithms require. Our 4th order products are generated from purely exponential vectors. The other algorithms begin with products of signal vectors. Likewise the cumulants in the 2-D SKEW MUSIC matrices are indexed by only two time lag indices, not three as would be the case for fourth order cumulants. It would be interesting to compare the structure of our matrix with that generated from a true 4th order signal Kronecker product for three-wave coupled sinusoids.

5.4 Simulations

The standard Swindlehurst and Kailath third order cumulant matrix technique is tested initially [1]. This method features unsymmetrized cumulants. In their simulations these authors did not vary the biphase, but used a reference biphase of zero degrees. We performed simulations with a variety of phase shifts among the sinusoidal components in Figs. 5.1 - 5.6 and found that the algorithm performed well for nonzero biphase arguments. Figs. 5.5 and 5.6 are especially interesting as they show that the algorithm gives satisfactory results for the imaginary biphase of 90^{o}.

Also Swindlehurst and Kailath used a block data procedure to build their third order cumulants matrix. We first calculate the cumulants separately within records that are 128 data points long. After 32 (N=4096) such segments we average the cumulants and load our matrix as outlined in (5.1)-(5.5). The algorithm was tested with both Gaussian and non-Gaussian (exponentially distributed noise). In all simulations in this section a 16x10 matrix was used and the left singular vectors belonging to the six largest singular values were used in these runs. The compound Kronecker product frequency kernel and bispectral estimator in (2.46) were used to find the location in the bispectral domain where coupling occurs.

Monte Carlo simulations of the method outlined in [1] were run over a range of bicoherence levels in the same manner as in Table 3.6. The bicoherence values span from 0.02 to 1.0. The number of data points used in these simulations is 4096. In Table 5.1 the results of those simulations are reported for both Gaussian and exponentially distributed noise. The results for both noise distributions are similar. In fact, for

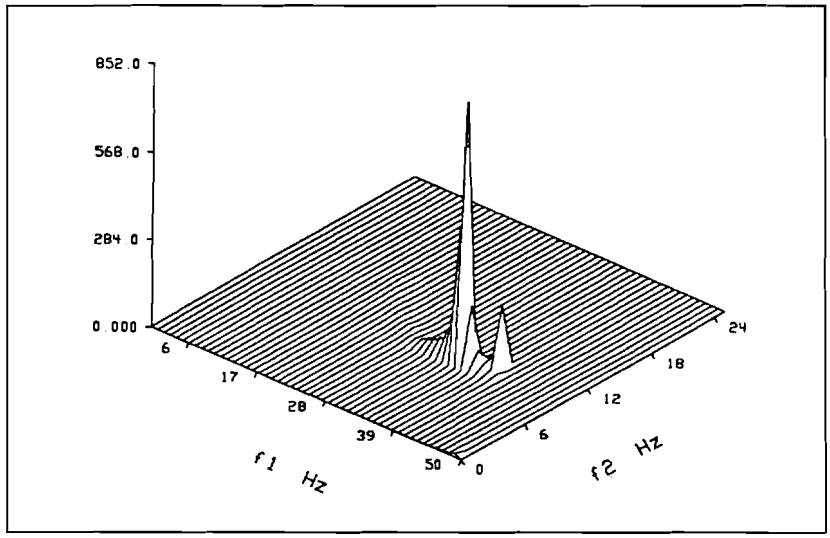

Figure 5.1 Standard Swindlehurst and Kailath algorithm; Biphase = 0°; SNR = 4.77 dB; Gaussian Noise; N=4096; Peak at (.35,.1) Hz

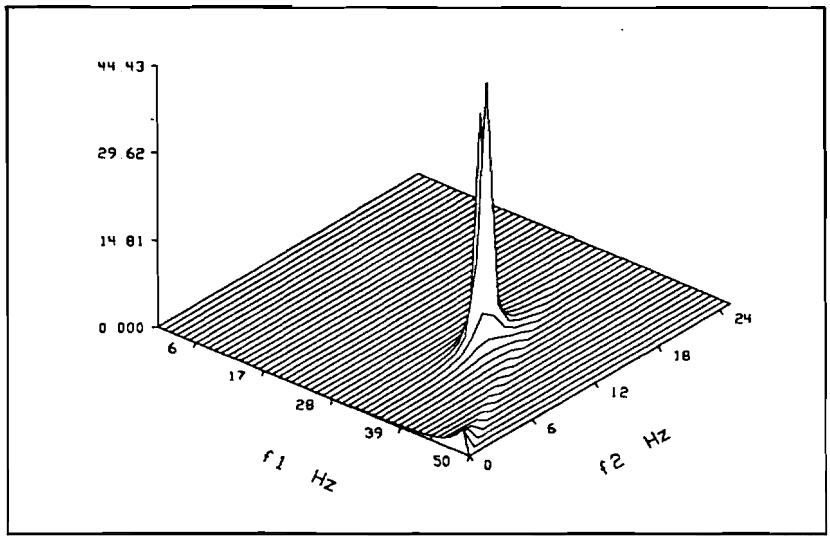

Figure 5.2 Standard Swindlehurst and Kailath algorithm; Biphase = 0°; SNR = 4.77 dB; Exponentially Distributed Noise; N=4096; Peak at (.34,.12) Hz

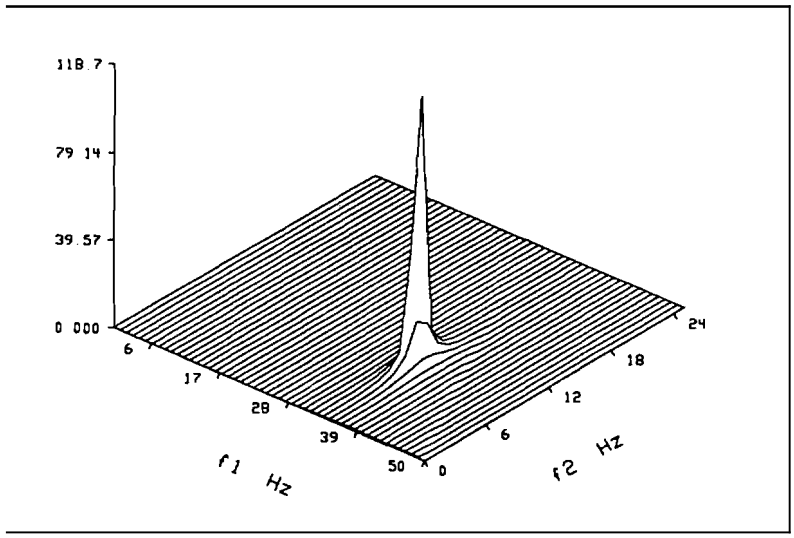

Figure 5.3 Standard Swindlehurst and Kailath algorithm; Biphase = 30°; SNR = 4.77 dB; Gaussian Noise; N=4096; Peak at (.34,.1) Hz

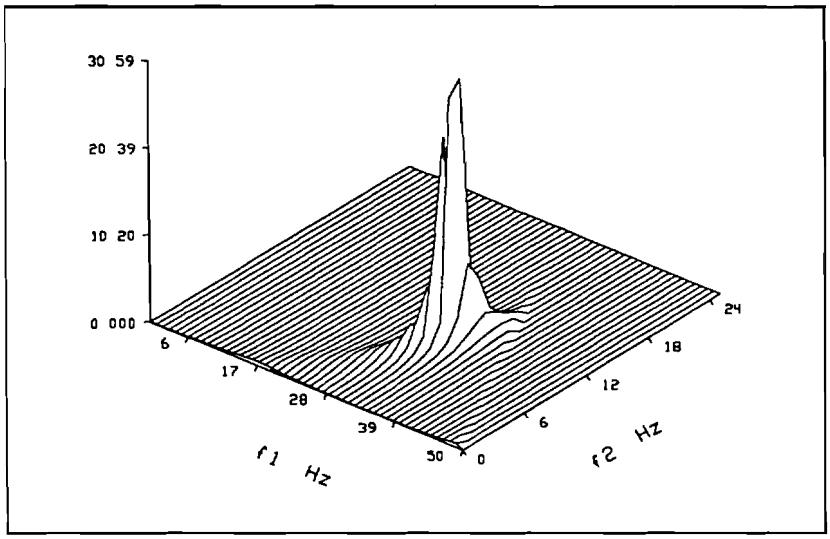

Figure 5.4 Standard Swindlehurst and Kailath algorithm; Biphase = 30°; SNR = 4.77 dB; Exponentially Distributed Noise; N=4096; Peak at (.33,.11) Hz

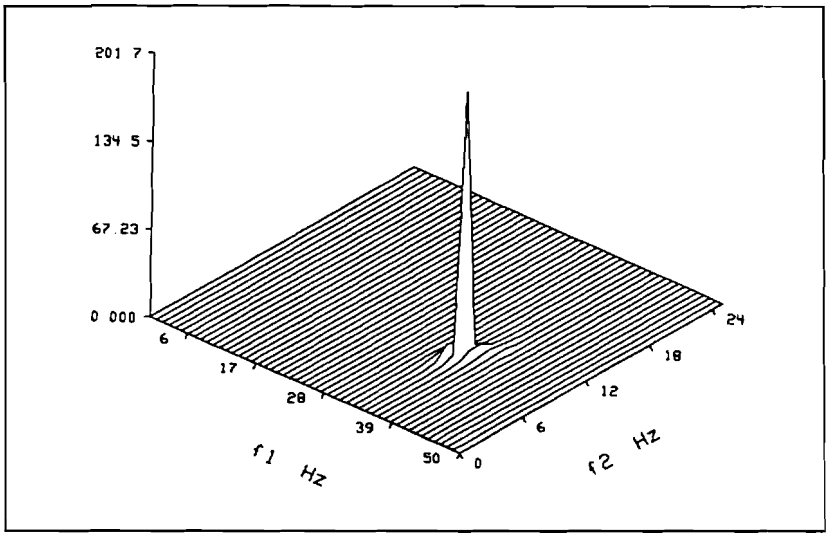

Figure 5.5 Standard Swindlehurst and Kailath algorithm; Biphase = 90°; SNR = 4.77 dB; Gaussian Noise; N=4096; Peak at (.35,.1) Hz

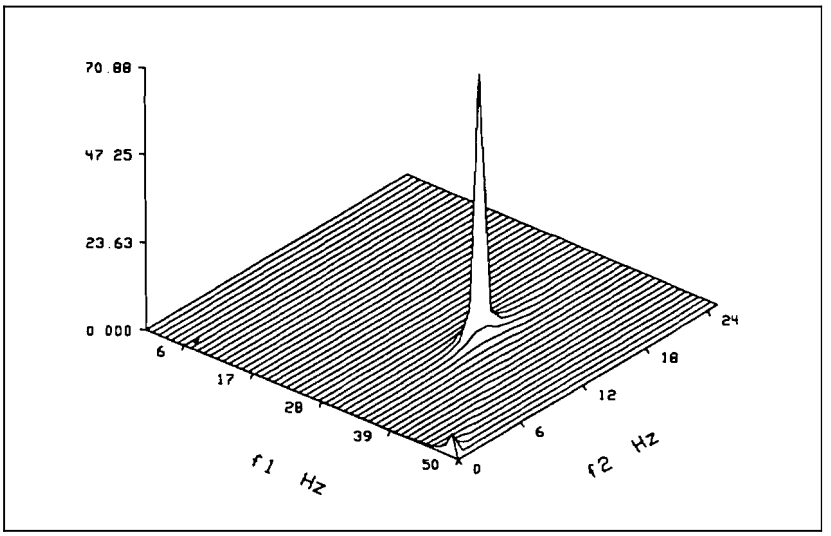

Figure 5.6 Standard Swindlehurst and Kailath algorithm; Biphase = 90°; SNR = 4.77 dB; Exponentially Distributed Noise; N=4096; Peak at (.33,.13) Hz

several bicoherence values the non-Gaussian noise does remarkably well and exceeds performance levels for Gaussian noise. This occurs in spite of the fact that this algorithm is especially designed to handle only added noise that is Gaussian-distributed. It is believed that over such short data lengths the Gaussian character of the added noise is irrevelant. Asymptotic effects do not come into play with only 32 segments of length 128.

Unlike the case of 2D SKEW-MUSIC as presented in chapter 2, there is clear trend line due to the fact that the bicoherence or fraction of power in coupled sinusoids is lowered. Obviously the effects of the bicoherence are marked and improvement is noted as the bicoherence increases. The variance decreases by almost 66% in moving from the lowest bicoherence to unity. What is remarkable is the fact that the Swindlehurst and Kailath algorithm performs so much better that the 2D SKEW-MUSIC algorithm in these tests. Examining the standard deviation at a bicoherence of 0.1, it is noted that the best performance using 2D SKEW-MUSIC and non-Gaussian additive noise was 0.0838 In the third order cumulants matrix method the standard deviation had a value of 0.048. Using the third order cumulant matrix provided a 42% improvement in standard deviation. This difference less pronounced at a bicoherence level of 1.O. Here performance was almost 31% better for the triple Kronecker product method. Lower bias also characterized the triple Kronecker product method at all levels of bicoherence.

Moving on to the modified Swindlehust algorithm, Monte Carlo simulations were run to determine the accuracy of biphase estimation through the division of the cumulants into.symmetric and skew-symmetric portions. The cumulants were formed from 8192 data point long segments containing a single triad of phase coupled sinusoids. Separate sessions of 100 trials each were run with biphases of 15^o, 45^o and 60^o. Noise levels were maintained at 4.77 dB for all sessions.

Symmetric and skew-symmetric cumulants were placed in the 16 x 10 $\mathbf{S}_3$ and $\mathbf{A}_3$ matrices, respectively as in (5.18a-b). As part of the modification to the classical third order cumulant mamx method, the R(0,0) term was deleted as described above. The matrix pencil, $\{ \mathbf{S}_3, \mathbf{A}_3 \}$, forms the starting point for SKEW-PRO-ESPRIT, the rendition of the PRO-ESPRIT algorithm for biphase determination directly from the third order cumulant sequence. Separate singular value decompostions are performed for each matrix. $\mathbf{Q}_u$ and $\mathbf{Q}_v$ are formed from the left and right singular vectors corresponding to the 6 largest singular values of the each matrix. Thus applying $\mathbf{Q}_u$ and $\mathbf{Q}_v$ reduced the matrix pencil, $\{ \mathbf{S}_3, \mathbf{A}_3 \}$, to the the required core rotations square matrix pencil as in (4.10). This 6 x 6 matrix pencil yield 6 GEs. These GEs are subsequently averaged. The inverse tan function yields the biphases.

As can be seen from Tables 5.2 and 5.3 accurate biphase estimates are possible using the PRO-ESPRIT algorithm on 2-D cumulant data. Both exponentially and Gaussian distributed noises are added to create SNRs of 11.76, 4.77 and 1.76 dB in separate trial sessions. The data length is 8192 points with 64 segments of 128 points used throughout. Naturally, as the noise power is increased the variance of the estimates increases. Gaussian noise seems to generate higher biphase variances than does the exponentially distrbuted added noise. Exponential noise has higher bias values when the SNR is low at 1.77 dB; otherwise non-Gaussian noise does not cause results to deteriorate at all. This may be a fortunate result of removing the noise bearing term, $R(0,0)$, from $\mathbf{A}_3$.

In Figures 5.7-5.12 plots of coupling frequency estimates are shown for several combinations of biphase, noise, and cumulant type using the matrices from SKEW-PRO-ESPRIT. Accurate estimates of the true coupling frequencies, $f_1 = .34$ and $f_2 = .1$, are noted. The only exceptions among this collection are for the symmetric cumulant matrix, $\mathbf{S}_3$, for both Gaussian and non-Gaussian noise.

Table 5.1 **Performance of Standard Swindlehurst and Kailath Algorithm: Coupling Frequency Estimate Accuracy vs. Bicoherences from 16 x 10 Third Order Cumulant Matrix; 100 Trials per Bicoherence Value Accuracy (Means and Variances) of f_1 estimate shown; True Value: f_1 =0.34**

Coupled Sinusoid Frequency Estimate vs Bic: Gaussian & Exponentially Distributed White Noise - SNR = 21.76 dB 16 x 10 Matrix Dimension;				
Bicoherence	Noise Distribution			
	Gaussian		Exponential	
	Mean	Std.Dev.	Mean	Std.Dev.
0.02	.3643	.096	.3521	.0924
0.05	.3512	.0859	.3543	.0663
0.1	.3411	.0523	.3451	.048
0.2	.339	.0519	.3335	.0522
0.3	.3427	.0409	.3428	.0404
0.4	.3437	.0393	.3402	.0382
0.5	.3415	.0378	.3408	.0375
0.6	.3389	.0381	.3382	.038
0.7	.3404	.0364	.3408	.0375
0.8	.3413	.0367	.3402	.0349
0.9	.3428	.0379	.3403	.0348
1.0	.3398	.0355	.34	.037

Table 5.2 Biphase Estimates Using Modified Third Order Cumulant Matrix; Gaussian Noise-- N=8192; Varying Both Biphase and SNR

Biphase Estimates Using Modified Third Order Cumulant Matrix Gaussian Noise -- N=8192						
True Biphase	Signal-to-Noise Ratio					
	SNR = 11.77 dB		SNR = 4.77 dB		SNR = 1.76 dB	
	Mean	Std.Dev.	Mean	Std.Dev.	Mean	Std.Dev.
15°	15.0992	.5248	15.0641	1.7962	15.2673	1.7043
45°	45.0659	.4929	45.1117	1.0992	45.0714	1.6191
60°	60.0480	.4822	60.0466	1.0738	59.9196	1.5733

Table 5.3 Biphase Estimates Using Modified Third Order Cumulant Matrix; Exponentially Distributed Noise-- N=8192; Varying Both Biphase and SNR

Biphase Estimates Using Modified Third Order Cumulant Matrix Exponentially Distributed Noise -- N=8192						
True Biphase	Signal-to-Noise Ratio					
	SNR = 11.77 dB		SNR = 4.77 dB		SNR = 1.76 dB	
	Mean	Std.Dev.	Mean	Std.Dev.	Mean	Std.Dev.
15°	14.9680	.5140	14.6393	.9821	13.9205	1.3027
45°	44.9401	.4681	44.0284	.9786	42.0101	1.3742
60°	59.9330	.4542	58.7489	.9962	56.2813	1.4568

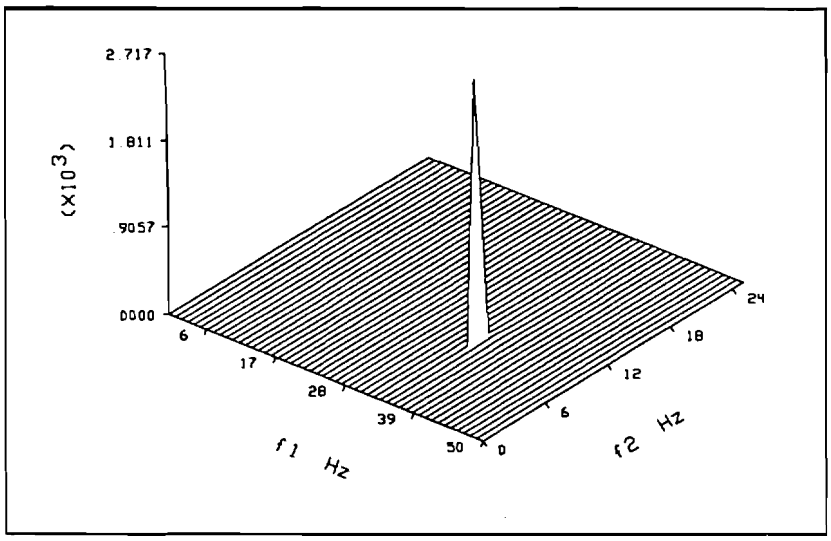

Figure 5.7 SKEW-PRO-ESPRIT adaptation of Standard Swindlehurst and Kailath algorithm; Symmetric Cumualants; Biphase = 0°; SNR = 4.77 dB; Gaussian Noise; N=4096; Peak at (.34,.1) Hz

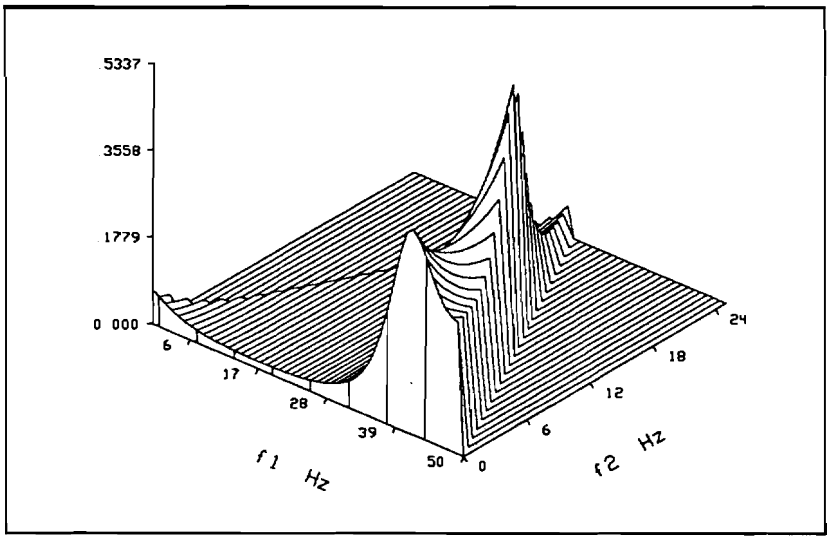

Figure 5.8 SKEW-PRO-ESPRIT adaptation of Standard Swindlehurst and Kailath algorithm; Skew-Symmetric Cumulants; Biphase = 0°; SNR = 4.77 dB; Gaussian Noise; N=4096; Peak at (.37,.13) Hz

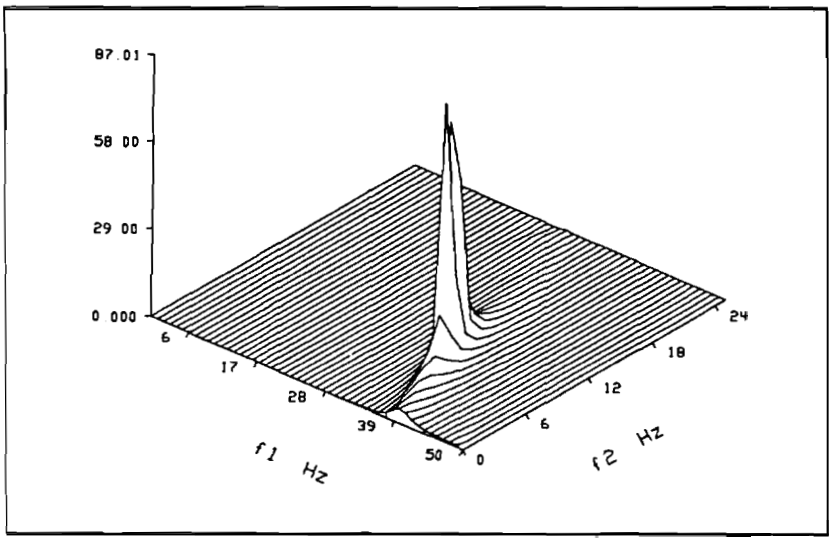

Figure 5.9 SKEW-PRO-ESPRIT adaptation of Swindlehurst and Kailath algorithm; Symmetric Cumualants; Biphase = 60°; SNR = 4.77 dB; Gaussian Noise; N=4096; Peak at (.35,.08) Hz

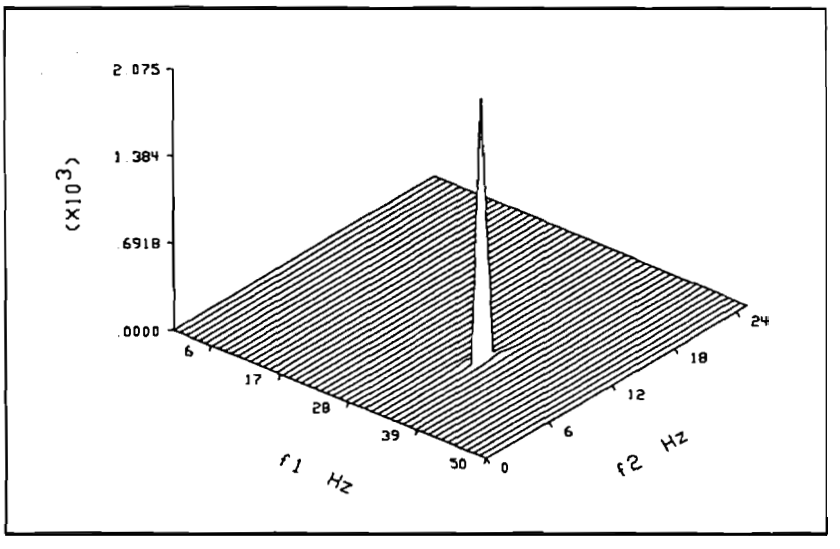

Figure 5.10 SKEW-PRO-ESPRIT adaptation of Standard Swindlehurst and Kailath algorithm; Skew-Symmetric Cumulants; Biphase = 60°; SNR = 4.77 dB; Gaussian Noise; N=4096; Peak at (.34,.1) Hz

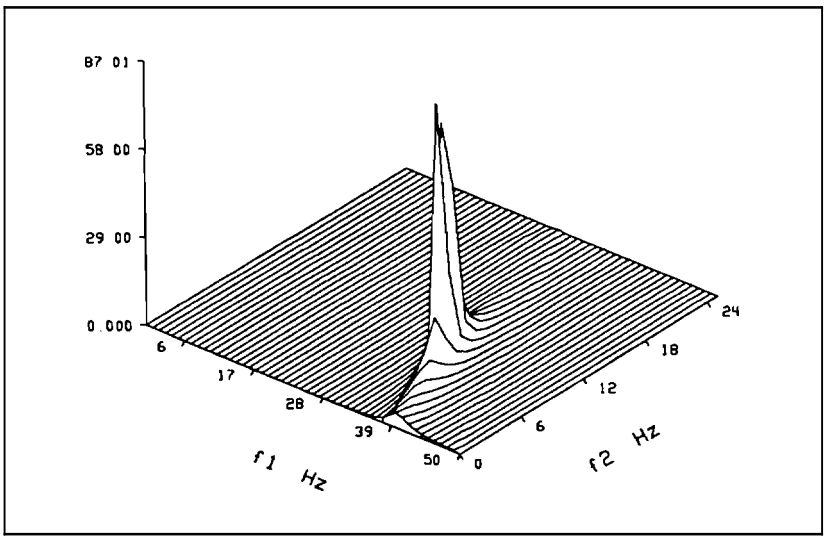

Figure 5.11 SKEW-PRO-ESPRIT adaptation of Swindlehurst and Kailath algorithm; Symmetric Cumualants; Biphase = 60°; SNR = 4.77 dB; Exponentially Distributed Noise; N=4096; Peak at (.35,.08) Hz

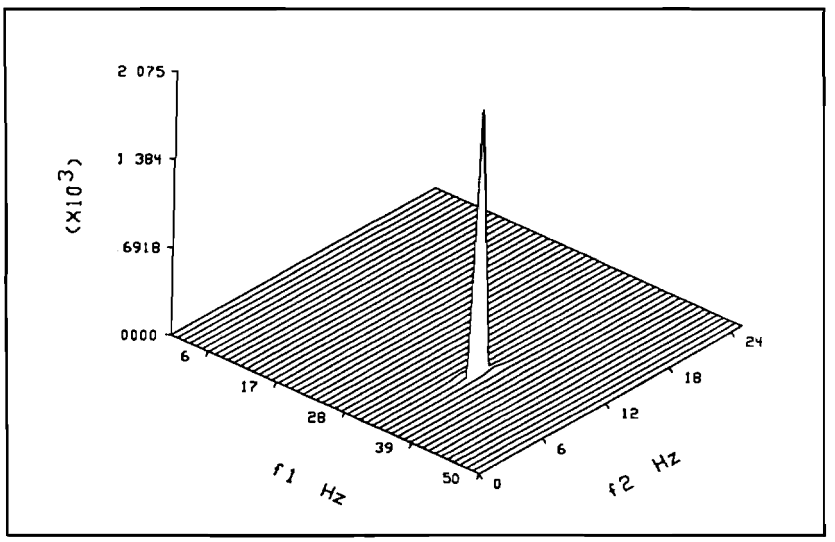

Figure 5.12 SKEW-PRO-ESPRIT adaptation of Standard Swindlehurst and Kailath algorithm; Skew-Symmetric Cumulants; Biphase = 60°; SNR = 4.77 dB; Exponentially Distributed Noise; N=4096; Peak at (.34,.1) Hz

5.5 List of References

[1] A.L. Swindlehurst and T. Kailath, "Detection and Estimation Using the Third Moment Matrix," Proc. *Int.* Conf. ASSP *Soc.*, pp. 2325-2328, Glasgow, Scotland, May 1989.

[2] M. Zoltowski and D. Stavrinides, "Sensor Array Signal Processing Via a Procrustes Rotations Based Eigenanalysis of the ESPRIT Data Pencil," *IEEE* Trans. ASSP, vol. 37, pp. 832-861, June 1989.

[3] A. Swami and J.M. Mendel, "Cumulant-based approach to the harmonic retrieval and related problems," *IEEE Trans. SP*, vol. SP-39, pp. 1099-1109, May 1991.

[4] B. Porat and B. Friedlander, "Direction Finding Algorithms Based on High-Order Statistics," *IEEE* Trans. SP, vol. SP-39, pp. 2016-2024, Sept. 1991.

CHAPTER 6
THE EEG AND THREE-WAVE COUPLING

"In fact, the EEG researcher should remain especially wary of mathematics in search of an application. (One should not ask what EEG can do for mathematics, but rather what mathematics can do for EEG)" †

6.1 Introduction

The time series used for testing the algorithms developed in chapters 3, 4 and 5 is the electroencephalogram or the EEG. Typically the EEG is recorded off the scalp of the human head and reflects the underlying activity of neurons of the cerebral cortex. Disc electrodes about 1 cm. wide are placed over an area of the brain and they record the surnmated activity of neurons lying directly underneath the scalp placement area. To a lesser extent other cells distant from the conducting electrode also influence the signal measured. These neurons have their distant effects felt through the conducting medium. Cardiac electrical effects and circulatory blood flow as well as other contaminants, such as the electrooculogram (EOG) and other muscular artifacts, also influence the final EEG output signal recorded.

The EEG actually measures three kinds of cerebral function. The first is paroxysmal activity which is characterized by spikes and sharp waves. K complexes and vertex transients in sleep are other examples of paroxysmal activity. Spiky paroxysmal activity is not well suited to spectral analysis since the energy is spread over the entire spectrum. Evoked activity such as the sensory event-related potential in response to exogenous stimuli is typically time limited and is analyzed in the time domain.

† *P.* Nunez, *The Electric Fields of the Brain,* Oxford, New York, 1981, p. 214

The non-paroxysmal background EEG activity occurs spontaneously in the awake adult human. The processes recorded off the scalp are called EEG rhythms and are studied by the use of the power spectrum or spectral density. Using the power spectrum, the primary unit of analysis is the frequency band. Different rhythms such as alpha or beta rhythm occupy specific frequency ranges. All spectral parameters are defined within bandwidths. These include power in a band, peak frequency, peak intensity, peak half power bandwidth among others.

The use of the bispectrum as a means of understanding EEG background activity challenges the notions of observing EEG within the band window. The question of interrelationships among frequency bands forces the researcher to perhaps look outside of this window for the total view of EEG activity. Is activity in higher frequency bands independent or simply harmonics of lower frequency components? Correlated high frequency activity enables the scientist to narrow his/her field of view as these oscillations yield no new information. Can the special property of Gaussian noise immunity aid the EEG researcher to uncover new details about the rhythms? Evidence is cited from a number of sources in this chapter to help promote using the bispectrum, in general, and the high resolution parametric bispectrum, in particular, for EEG analysis.

6.2 Spectral Considerations and Problem Statement

The Electroencephalogram or EEG is a time series recovered typically from the scalp which reflects underlying brain activity. The EEG is the spatial average of the synchronized or coherent activity of neurons belonging to the cerebral cortex. Strong or salient coherencies among large groups of neurons create pronounced rhythms in the EEG spectrum. Voltage ranges are between $\pm 50\ \mu V$ for most references on the upper portion of the head. Frequency ranges of interest for the EEG range from 0 to about 100 Hz. The typical frequency range of interest for the normal waking adult is between 0 to about 40 Hz. The frequency range for EEG is divided into bands as shown in Table 6.1.

Predominant activity occurs in the alpha band between 8 and 13 Hz. The alpha band is the most pronounced. It also displays the most dynamic activity that can be easily traced to the presence or absence of direct sensory stimulation. When there is no direct sensory stimulation of any variety, most importantly the lack of visual stimulation, the alpha wave appears most prominently in the EEG record as very nearly

Table 6.1 Major Divisions of the EEG Spectrum to 23 Hz

EEG Bands and their Spectral Regions	
Delta	1-3 Hz
Theta	4-7 Hz
Alpha	8-13 Hz
Beta I	13-18 Hz
Beta II	18-23 Hz

sinusoidal in shape. The alpha rhythm is said to dominate as the single most noticeable feature of the EEG spectrum. Shortly after sensory stimulation commences, the alpha wave disappears into the background leaving higher frequency phenomena in the normal waking adult to prevail. Opening the eyes in total darkness causes the alpha rhythm to fade only partially. It then reappears momentarily.

The process of the fading alpha rhythm when sensory stimulation occurs is usually referred to as alpha blocking or alpha desynchronization. Typically, it occurs bilaterally. The frequency is said to vary by as much as 1 Hz. in normal subjects. It can rise to about 2 Hz faster than its stable rhythm immediately after eye closure -- this is called the squeak phenomenon. Most subjects concentrate their mean alpha rhythm between 9-10 Hz. There are usually small differences in mean frequency between the hemispheres of the brain with only the largest concentration of alpha power occurring in the right hemisphere. This degree of alpha power variation is dependent on type of responding pattern that a subject exhibits. Most typical is the responsive or R type alpha. There are certain responders who display P or persistent type alpha activity that diminishes only temporarily during the open eyes condition. There is the M or minimal response for subjects who show little or no predominant alpha signal. Their EEG records are much flatter than either P or R type subjects. In fact, except for peaks in the beta region, their EEG spectra have no distinctive features during waking.

Alpha tends to occur mainly in the posterior portion of the head. On the International 10-20 scheme for electrode source positions this would tend to be strongly in the electrodes of the occipital and parietal lobes, i.e. the O1, O2, P3 and P4 electrodes. The generalized positioning of all major electrodes on the human head is shown in Fig. 6.1. Interestingly, beta concentration appears more pronounced on

frontal or central (C3 or C4) positions. Beta is normal, waking rhythm of the adult human. It does not respond to sensory input. It can appear to be more pronounced during periods where the organism is carefully attending or "highly alert and focusing his attention on a target [1]."

The alpha rhythm derived from occipital origins exhibits a characteristic "waxing and waning." Some authors mention that the visual record of the alpha rhythm indicates that it is both amplitude and phase modulated [3]. A glance at a sample 1 second interval of EEG recorded from the 0 1 electrode shows that that there is indeed a portion that is amplitude modulated. This section of data is shown in Fig. 6.2. The phase modulation is more apparent from data taken near the end of the segment. In the power spectrum (Fig. 6.3) for this short section of data, it is clear that a peak in the neighborhood of 10.5-11 Hz dominates. It is difficult to decide if much smaller "sidebands" are seen in the delta region and in the beta-11 bands.

Another section of data taken from a more anterior derivation (P3) recorded simultanwusly shows an entirely different harmonic structure. Now components in the beta-I1 band and the delta bands are more pronounced and a wider bandwidth is noticeable at this scaling. The alpha wave is reduced in strength. The beta-II band could easily be thought of as a harmonic of the alpha wave. These are shown in Figs. 6.4 and 6.5.

In these short term series, we paid strict attention to peaks while ignoring accompanying noise by reviewing candidate EEG segments and choosing distinctively noise-free segments. We should now turn to a long duration (32 second) segment of EEG data from two subjects' P3 electrode derivations. A generalized model for the spectrum of spontaneous EEG activity was presented by Dumermuth and Molinari [4]. This model is composed of three spectral portions: 1.) a flat, white noise portion; 2.) a pink noise portion that begins with a peak near the low end of the delta frequency band with a characteristic decreasing slope and DC intercept; 3.) the colored noise portion which comprises power in specific peaks, namely the alpha and beta peaks. A sample spectrum containing these three components is shown in Figure 6.6. The white noise portion is considered to be an artifact as it can be ongoing noise generated from extra-cortical or exogenous sources. It can also represent instrumental noise. In the cases of paroxysmal activity it may represent epileptiform spikes of short duration. The pink noise portion has a cortical origin and is thought of as an "underlying, unstructured EEG component which is a natural feature of empirical data and often called amorphous or arhythmic activity" [4].

The remaining part of the spectrum is the peaks at the alpha and beta band. The nature of these peaks and their interrelationship is of key interest to the EEG

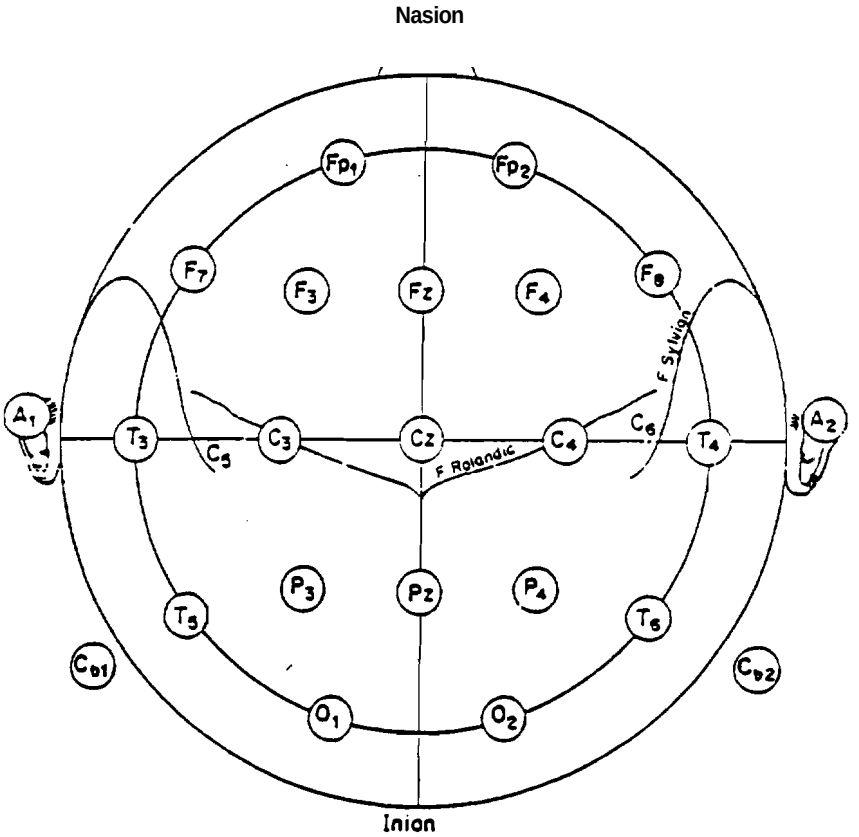

Figure 6.1 The International 10-20 system for positioning of electrodes [2]

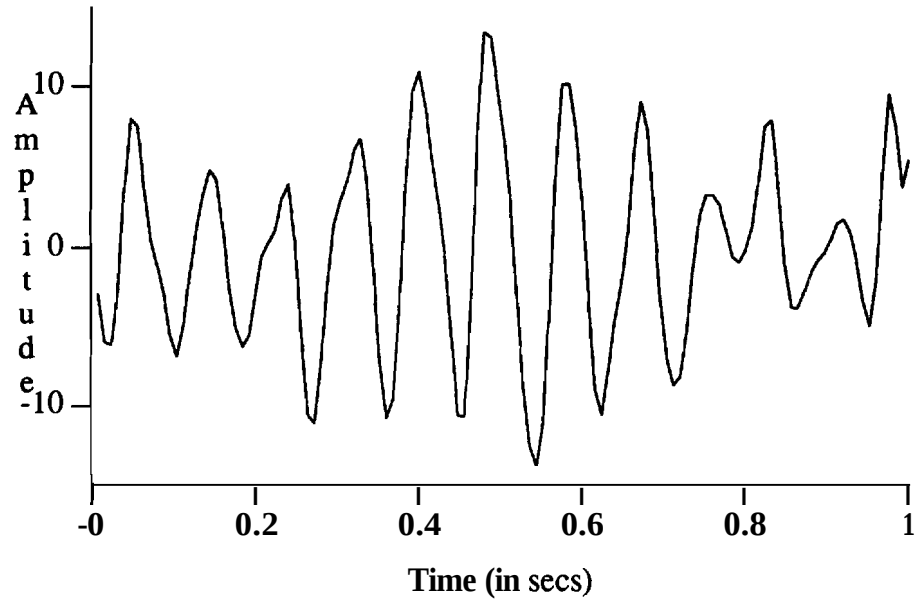

Figure 6.2 **Segment of EEG Time Series Data from S1 O1 electrode;** 1 sec.

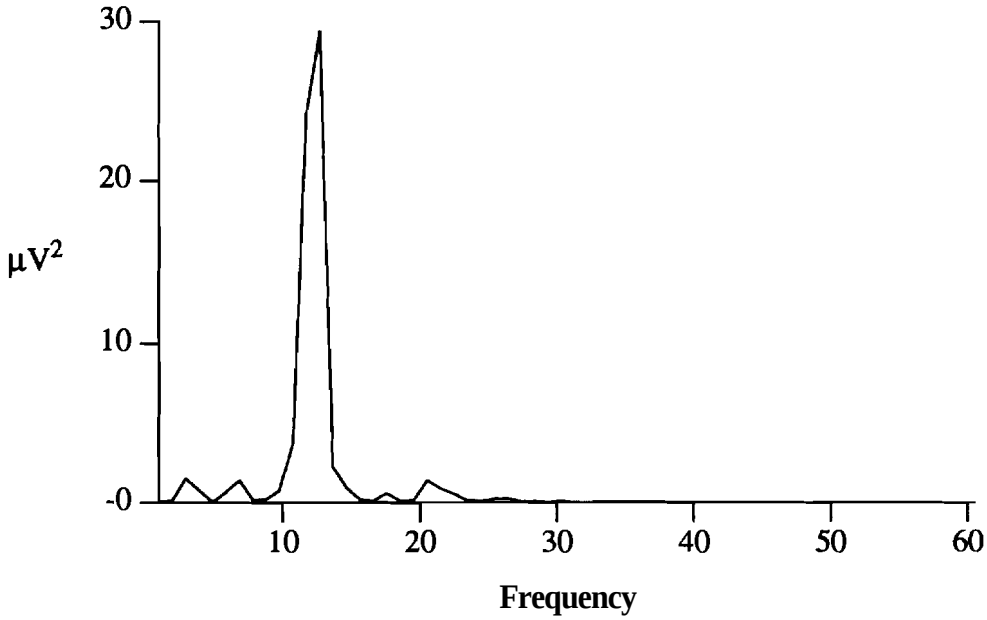

Figure 6.3 **Power Spectral Density from 0 1 Time Series Data**

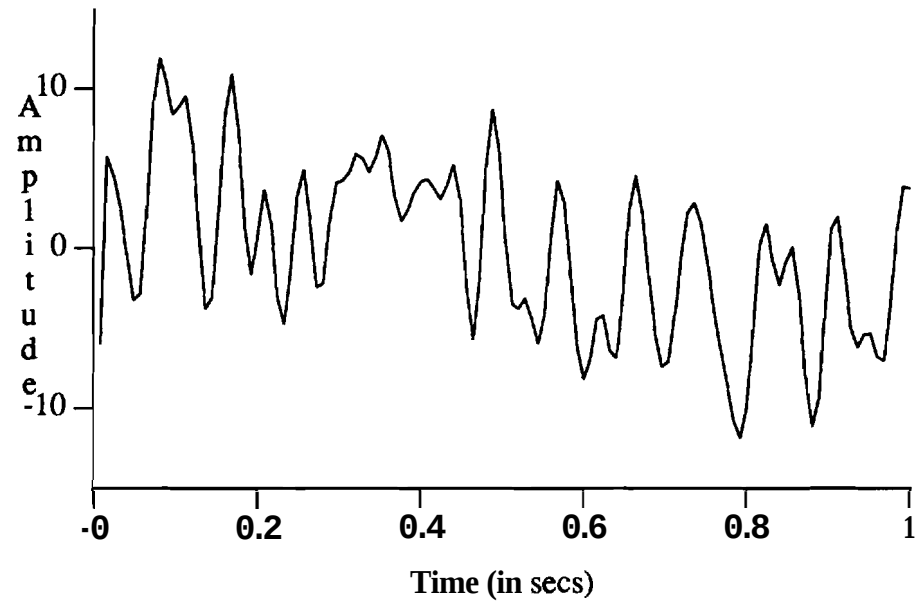

Figure 6.4 **Segment of EEG Time Series Data from S1 P3 electrode; 1 sec.**

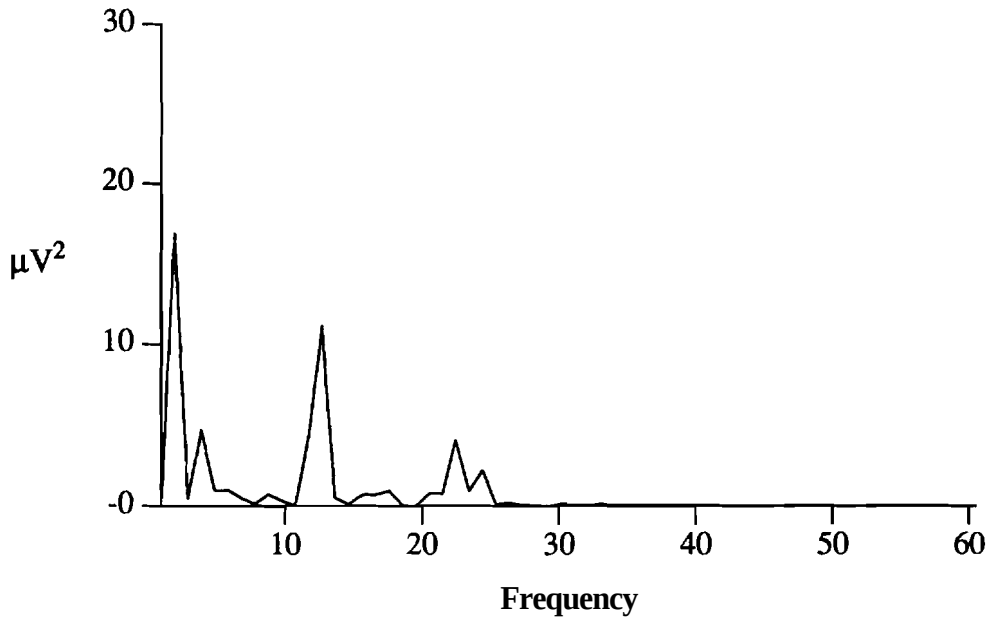

Figure 6.5 **Power Spectral Density from P3 Time Series Data**

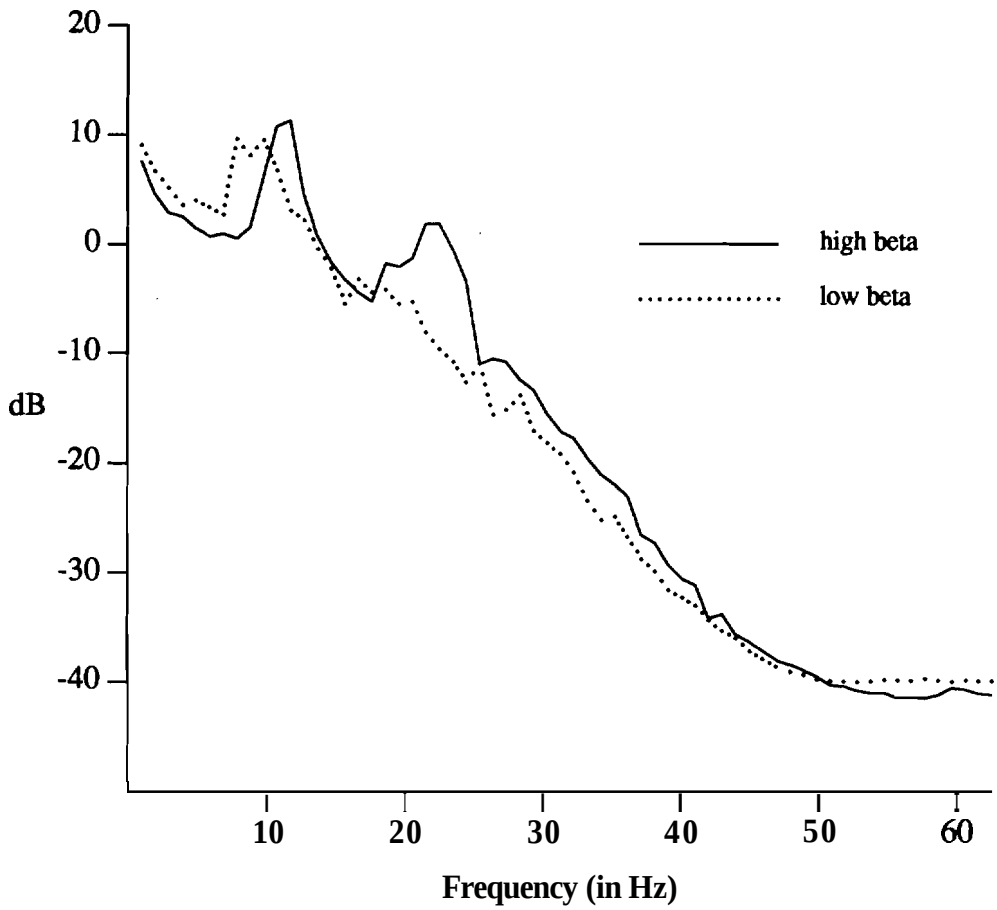

Figure 6.6 Long Term EEG Spectrum from Ss 1 & 3: Containing Critical EEG Spectral Constituents: 1.) White Noise "Floor"; 2.) Pink Noise: 1/f Type Noise Sloping Contour; 3.) Peaks Which Are Colored or Narrowband Phenomenon

researcher. Questions about their harmonic character immediately become apparent. The prominent peak at beta-II is approximately twice the frequency of the corresponding alpha peak.

The nature of the noise is critical to understanding the peaks themselves Suppose the white and pink noises are Gaussian and the signal as represented by the spectral peaks is non-Gaussian. Bispectral analysis is one to aid in enhancing the peaks. Once the noise components have been removed the peaks themselves remain. The question about the nature of the peaks still persists. If the peaks are simply narrowband Gaussian noise as considered by Dick and Vaughn, the bispectrum should not detect their presence [5]. If, on the other hand, the peaks alone represent the only non-Gaussian portion of the spectrum, bispectral analysis should isolate the peaks if they happen to be quadratically phase-coupled.

Isolating the peaks from the various noise components is performed in several studies. Naturally, the slope and intercept of the pink noise spectrum can be calculated and this portion of the spectrum simply subtracted out to reveal the peaks, if the beta peak is not submerged in noise [4]. Other studies have focused on enhancing the EEG spectrum by extracting the white noise component to isolate key peaks. Yarman-Vural, Onaral and Cetin [6] assume that the raw spontaneous EEG signal, $y(n)$, can be represented by an embedded signal $x(n)$ contaminated by additive white noise $w(n)$ as $y(n) = x(n) + w(n)$. It is assumed that the additive white originates from a number of non-cortical sources. The actual EEG signal $x(n)$ can be modeled as an AR process. Raw EEG measurements may be represented by the ARMA model Yarman-Vural et al. develop a procedure whereby they enhance the measured EEG time series by inverse filtering using the MA model [6]. The additive white noise component is removed leaving EEG peaks at alpha and beta locations that are more pronounced.

6.3 Bispectral Studies

The landmark study of the EEG and the bispectrum was the work of Huber et al. [7, 8]. Not only was this study an effective application of the bispectrum to natural signals, but [7] laid out the statistics and formal algorithmic details of the biperidogram for the signal processing community in 1971. As evidence supporting the use of the bispectrum, they pointed out the following: 1.) the assumption of stationarity was obviated for long records; 2.) the Gaussianity assumption is also violated for records

exceeding four seconds in length; 3.) there was commonly phase-locking found in paroxysmal and non-paroxysmal EEG samples. They suspected that there might be important phase relations among different components.

Huber et al. averaged data corresponding to 80 seconds of EEG [7]. They found peaks in the bispectral frequency ranges corresponding to second and third harmonics of the alpha band. This indicates that the predominant activity was sighted between alpha and its 20 Hz component in beta-II as well among alpha, beta-II and the 30-Hz component in beta-III. These studies focus on deviations from Gaussianity. Significant peaks and their confidence intervals are measured with respect to the central χ^2-distribution. P-values as low as 10^{-16} reflected slim probabilities of respective peaks originating from a Gaussian time series.

Ning and Bronzino have conducted studies dealing with the study of EEG in the hippocampus during various vigilance states as well as sleep states[9]. During REM (rapid eye movement) sleep there is increased theta-theta coupling for harmonic alpha components. They are able to differentiate different states by summing all bispectral values in a manner akin to constructing the third order moment of the process. Their summation is thought to be an index for deviation from Gaussianity. It does not, however, take into consideration relative power values of individual time series.

Another Ning and Bronzino study focused on the cross-bispectrum from two different regions of the hippocampus of the adult rat [10]. There are once again indications of significant theta region coupling to alpha frequencies during generation of the alpha.

A key study by Barnett et al. studied the bispectrum in human adults in both waking and sleeping [11]. In a fully alert state, the most significant bifrequency peaks were found at approximately (10 Hz, 10 Hz). About one half of total of eight subjects had high alpha activity. It was primarily these subjects which had the significant bispectral values. These authors do not describe how they arrive at the measure of significance in their observations. The authors consider the fact that a large proportion of the beta activity can considered harmonically dependent on alpha amounts. There were particularly strong bispectral patterns revealed during sleep.

Whitton et al. look at the hereditary influences on the bispectrum [12]. Since there is a strong genetic basis to alpha wave parameters, these authors decided to test if this hypothesis could be extended to alpha harmonics. Using the bispectral test of collinearity, they discovered that monozygotic twins exhibited a highly coincident bispectrum.

6.4 Alpha-Beta Interrelations in the EEG

Evidence about the harmonic nature of the beta response comes from the work of Shirninke [13]. Eye opening diminished both alpha and beta responses while closure increased the amplitude of both. It was proposed that beta could be both the second and third harmonic of the alpha rhythms. Beta may underly the alpha activity which becomes synchronized to the beta. Regardless, alpha and beta were thought to originate from the same source.

Gaarder and Speck explained that a certain percentage of the population have coupled alpha and beta reactions [14]. Both peaks seem to dominate. One peak was always twice the frequency of the first. Alpha was said to occur whenever every other beta cycle was suppressed. Desynchronization was said to occur when the individual was involved in some cognitive task.

True indication of the correlations between alpha and beta came in the study by Johnson et al. [15]. These scientists tested both waking and sleeping subjects to check band power interrelationships. Among awake adults exhibiting high alpha only beta band power shows significant ($p < .01$) correlation. Dumermuth and Molinari present several examples of EEG with harmonic beta components [16]. These are listed in the Table 6.2

Table 6.2 Activities with Harmonic Beta Components; Adapted from [16].

Activities with Harmonic Beta Components
Mu Rhythm
Frontal Theta or Alpha Activity
14+6/sec positive spikes
Psychomotor variant
Photic Driving
Monophasic Sleep Spindles in Babies
Spiky, i.e. monophasic alpha rhythm

They also classify several forms of beta activity in clinical and normal controls. The divisions include narrow, broadband and harmonic forms of beta activity. Most common however is the mixed beta. Often independent and harmonic generators of

beta activity superimpose and the bispectrum is needed to separate the components.

The mu rhythm also known as the 'rhythme rolandique en arceau' appears in some adults [17]. It has a distinctive (9 ± 2 Hz) and stable characteristic shape which insures very strong second harmonic response. The reactivity of the mu rhythm is discussed in the work by Pfurtscheller and Aranibar on cerebral ischemia [18]. The simultaneous reactivity of power in both alpha and beta bands can be monitored by the "event related desynchronization' procedure useful in clinical practices. Average power in several epochs of EEG background activity prior to and after motor activation or sensory stimulation is often used to detect a variety of clinical conditions. An asymmetrical desynchronization is often useful in detecting ipsilateral ischemic attacks.

Studies of lateral asymmetry have shown that the beta-I1 band has particularly low interhemispheric coherence. Only in the frontal lobe does this rhythm exhibit significant coherence between hemispheres. At the same time frontal alpha shows the same level of significant bilateral correlations [19]. There have been several studies where the beta wave has been determined to be influenced by cognitive factors, whereas the alpha rhythm is generally thought to be chiefly influenced by generalized sensory inputs arousal and concomitant attention levels. The landmark study by Ray and Cole [20] was successful in determining that alpha and beta power levels have separate determinants that interact in the appropriate experimental contexts. Alpha wave power discriminates cognitive tasks dependent on external environmental involvement called the intake/rejection factor. EEG beta rhythm responses can differentiate types of cognitive tasks, i.e. verbal and mathematical task by asymmetry of response. Since alpha and beta interact there is some simultaneous increase in both alpha and beta along the cognitive (analytic/spatial) dimension. Davidson et al. also look at the correlation between alpha and beta powers in a study of lateralization of spectral powers in psychometrically-matched cognitive processing [21]. They challenged the conventional view that alpha and beta powers should be reciprocally related. Beta band processing was also shown to exhibit positive correlation with alpha band power for a variety of tasks and electrode references.

Photic flicker or photic driving creates interesting EEG frequency patterns. Photic flicker has its own special pattern or shape like paroxysmal activity yet is typically analyzed completely in the spectral domain as non-paroxysmal activity. Typically, an electronic stroboscope delivering short duration flashes from 1 to 100 per second. A frequency following response that is occipital in origin with a characteristic shape emerges in response to the flashes. The main component of the response is a positive-wave response with a latency of 70-90 ms in reaction to isolated flashes. As

the flash frequency is increased, individual discharges merge to form a spiky rhythm that lacks a sinusoidal character, but has higher harmonics present. The rhythm increases through the subjects' natural alpha rhythm frequency and then decreases. Amplitude decreases as well. The harmonic content of the flicker response increases as one moves away from the occipital regions along with a less pronounced amplitude. Subharmonics dominate in parietal and temporal areas whereas in the anterior supraharmonics are commonplace [17].

Mundy-Castle's studies point to definite associations between alpha and beta frequencies in light of the photic evoked response that can be created containing alpha and its second and thud harmonics [22]. A strong reaction was observed between beta and the second and/or thud harmonic of the stimulation frequency. It was also pointed out there were more occasions of following in the beta region. Those subjects with high (>10.3 Hz) mean alpha frequency had much more following by the second and third harmonic components of the this rhythm. Observations showed that it might be better to look at the harmonic components of the driving response which depend to a degree upon the functional state of the brain and the stimulus intensity [23]. These harmonics seem to be one of the main indicators of level of excitation of cortical neurons. Those subjects with high beta activity or who have a tendency for high frequency alpha activity are much more likely to exhibit this higher harmonic response.

Nunez describes some of the reasons why beta wave scalp recordings are so lacking in power [24]. Interestingly, some believe that the scalp, cerebrospinal fluid (CSF) and skull act as a low pass filter to eliminate high frequency portions of the EEG spectrum. It has been shown that beta activity up to 30 Hz actually is the dominant rhythm in recordings from the depth recordings from the frontal lobe [24]. Immediately it might be seen that the scalp and skull selectively attenuate beta frequencies. However, there is no evidence from physiology and physics that would dictate that intervening brain tissue and CSF would act as a low pass filter. Using pairs of sinusoidal subdural current sources over a range of frequencies, Nunez explains that the tissue does not act as a low pass filter. The most likely explanation for the attenuation of the beta frequency components is that the signal is not spatially coherent over large surface areas. This would indicate that that the comparatively large surface area of the disc electrode would fail to capture coherent signal energy in the beta region. The content of EEG at higher frequencies has been shown to be dependent on location as well. Nunez and his colleagues have shown that there is a 4:1 amplitude ratio for cortex-to-scalp recordings in the beta frequency range for central derivations. That ratio is only 2:1 for frontal locations. Outside of the beta frequency range (15 to 25 Hz) that ratio is much closer to unity at all recording sites.

6.5 Coupling and Synchronization I: Loss of Phase Information in Narrowband Gaussian Models of Alpha Rhythms

Several schemes have appeared modeling the alpha through complex demodulation which involves heterodyning the alpha band to base band and then low pass filtering. Ultimately, capturing the alpha band energy in the envelope requires removing phase information in the alpha band. Likewise, the beta band is not considered at all as the focus remains on the portion of the frequency band transferred to baseband.

A dominant model .for the alpha wave has been the narrowband Gaussian noise model for the EEG which was proposed by Dick and Vaughn [5]. The model for the alpha rhythm in this scenario includes an envelope which is Rayleigh-distributed and a uniformly distributed phase. The experimental scheme involves constructing an analog circuit device for the complex demodulation of the alpha wave which was accomplished on an analog computer. The authors compared the alpha wave amplitude distribution to the normalized Gaussian density function. Likewise, after complex demodulation, they compared the distribution of envelope amplitudes to the Rayleigh distribution. The power spectrum of narrowband Gaussian noise was compared to standardized alpha spectra to discover similarities as well. The authors discovered that the power spectra do not match accurately, because of the existence of band components outside of the alpha band, particularly at higher frequencies. They admitted that the filtering operation involved in the complex demodulation process results in a loss of information.

One review of the different methods of extraction of instantaneous envelope and phase was the work of Ktonas and Papp [25]. They use the complex demodulation technique to study.the a-spindles occurring during sleep which are believed to be triggered by subcortical thalamic centers. The a-spindles have an average frequency of about 14 Hz. They occur in short 1-2 second bursts and have an frequency deviation average of about 2 Hz which is discovered through zero crossing techniques.

A classic study testing the ideas of aniplitude modulation and coupling for EEG alpha wave modeling was the study of Okyere et al. [3]. Here phase is actually considered part of the model to account for some of the frequency modulation of the alpha rhythm. A fluctuation in central frequency is noteworthy as Dick and Vaughan mention that this frequency is always changing thus making complex demodulation a difficult procedure to implement [3]. The waxing and waning of the alpha rhythms was thought to be highly correlated with the measure of average cerebral metabolism as revealed in the quantity of blood flow through the brain. This study tested the

relationship between modulation parameters of the alpha wave and the regional cerebral blood flow (rCBF). A composite amplitude and frequency modulation signal model is suggested.

$$f(t) = A_c[1 + k_b m_1(t)] \cos \left[2\pi f_c t + 2\pi k_f \int_0^t m_2(t)\, dt \right] \qquad (6.1)$$

where A_c is a constant, f_c is the frequency of the unmodulated carrier wave, k_f is the frequency modulation index. Also note that k_m is the amplitude modulation index. The modulating signals for the AM and FM processes, are $m_1(t)$ and $m_2(t)$, respectively. Schemes for the measurement of the amplitude and the frequency modulation indices were devised. Amplitude modulation index showed significant correlation with rCBF. The authors speculate that the driving mechanisms for the amplitude modulation might be related to neural activity in the cerebral cortex.

6.6 Coupling and Synchronization II: Augmenting the Oscillatory Model of Alpha Generation

We have seen that the idea of three-wave coupling involves the synchronization of harmonically related components. The higher order spectrum looks at frequency components that are phase locked to sub- or supra-harmonics. Interestingly, it is often noted that coupled oscillations among various neural units on a broad-based network level create strong rhythms or peaks in the spectral record. What do the two versions of couplings have in common? Does the physiological coupling refer only to coupling at the single given frequency? Does the physiology point to multiple frequency couplings? A glance at the literature gives many tentative answers.

The theories of coupled oscillators account for much of the wavelike properties of the EEG. It is important to realize that the EEG is a spatial average of the underlying activity of as many as 100 million neurons that are "shadowed" by an electrode. As the sensor or EEG electrode is primarily integrative, the widespread temporal and spatial character of the EEG is due to coordinated activity of large groups of neurons. Much of the cortical rhythmicity is actually said to reside in salient coherencies. Couplings for the neurophysiologist refer to interactions among several neurons. Strong rhythms are said to be generated when groups of neurons all oscillate at the same frequency. Steriade et al. consider coupling from two points of view. The first is the tuning characteristic of individual neurons. They also postulate that properties of

large groups of neurons acting in unified, holistic fashion are responsible for the rhythms [26]: "Synchronization is a state in which two or more oscillators display the same frequency because of some forms of co-interaction. There is no necessity in deciding between two parts of the alternative, whether the intrinsic properties of single neurons are essential for the genesis of brain waves with different frequencies or whether such rhythms basically emerge from synaptic interactions in large neuronal pools. Both these factors should be eclectically considered. [26]"

The very idea of coupling in time and frequency has a strong physiological basis as MacVicar and Dudek report on actual pyramidal cells in the rat hippocampus which exhibit coupling in their response[27]. Electrotonic couplings from interconnected neurons are indicated by the presence of fast pre-potentials (FPPs) in neighboring neurons. These FPPs provide definitive evidence of neuronal synchronization. These authors reason that the electrotonic coupled networks are reverberating circuits that could sustain strong coordinated rhythms.

Models such as these prove to be even' more complicated when oscillations of several groups of cells are synchronized by outside pacemakers. These pacemakers convey a dominant frequency that is thalamic in origin to groups of single cells. As Steriade et al. [26] mention, "In the intact brain, however, the intrinsic properties of single cells are subject to controlling influences from synchronizing pacemakers or driving forces within given neuronal'networks that unite single cells. Indeed, the notion of EEG synchronization supposes the coactivation of a large number of neurons, the summed synaptic events of which become sufficiently large to be recorded with gross electrodes within the brain or over the scalp. The role of synaptic networks in the genesis of various EEG rhythms is emphasized by frequency differences between various oscillations..." [26].

The thalamocortical feedback network theory was proposed in a classic study by Lopes da Silva et al. in 1974 and updated in several recent studies [1, 26, 28, 29]. A general review of the model and the means with which it generates time dependencies in the EEG is reviewed in Nunez [24]. The thalamocortical model is used to build the oscillatory alpha rhythm from component neurons through basically two different types of neurons, the thalamocortical relay cells (TRC) and the interneurons (IN). The inhibitory or negative feedback model depends on a strength of couplings between TRC and IN neurons. If either coupling coefficient is very large, it indicates that there is strong input or feedback of TRC neurons to IN neurons and vice versa.

Nunez discusses several reasons why this model should be expanded to include multiple frequencies of oscillation. The preferred frequency of oscillation is dependent on the rise time and duration of the inhibitory post-synaptic potentials (IPSPs),

excitatory (EPSPs) and feedback gains. For instance, pyramidal cells in the cerebral cortex are thought to have much shorter PSPs than discussed in the Lopes da Silva model. These will produce higher frequency oscillations.

The model also assumes that the potentials are derived from a fairly large population of neurons. Nunez discusses the fact that the space average theory focuses only on macroelectrode potentials which provide a linearized version of underlying processes. Actually more detailed approaches may be required for some brain processes. Obviating the space average approach involves looking at smaller units of analysis wherein the linearity assumption is no longer an assumption. To recover information on harmonic beta will require a different level of analysis.

6.7 Key Studies of Gaussianity of the EEG

A key component in the study of the relationship of coupling among neural units and the statistical properties of the EEG was the work of Rafael Elul from 1969 [30]. Elul looked upon the EEG as being the random fluctuations of largely asynchronous neurons. At times slow wave and large amplitude activity would occur that was indicative of coordination among those neural elements. He called this synchronous activity coupling. When large groups of neurons acted synchronously, the EEG features would better reflect underlying activity on a cellular level. Complete asynchrony of activity of the EEG generators was assumed to reflect underlying Gaussianity. Synchronous activity established nonlinearities. The nonlinear relationships among generators caused a change in the amplitude distribution function of the generators. The EEG was not merely noise, but actually contained a fixed signal portion evident during non-Gaussian episodes.

Elul's ideas about recruitment of interactions among neurons manifest in the EEG were tested in a cognitive task study. During a mental task when more couplings were hypothesized to occur, the time series was said to become non-Gaussian. He tested this hypothesis by having subjects perform a mathematical computation while their EEG was recorded. The short segments of the EEG that were tested were several 4 second segments. The chi-squared goodness of fit test was applied to each segment. During baseline activity, 64 percent of the segments passed the test of Gaussianity, i.e., the null hypothesis was accepted. Under testing of the subjects during performance of a mathematical problem, only 32 percent of the short segments proved to be Gaussian.

A follow-up study to the work of Elul was McEwen and Anderson's exhaustive study of EEG during different levels of anesthesia [31]. In an attempt to provide real time monitoring of anesthetic level during surgery these authors chose varying lengths of EEG data recorded while under the influence of two type of general anesthetic as well as during baseline activity. They employed the one sample Kolmogorov-Smirnov (K-S) test for Gaussianity and the two-sample K-S test for wide-sense stationarity. They mention that the K-S test is truly the more powerful test when compared to the χ^2 goodness-of-fit test. To eliminate the influence of sample dependencies among the data points, they chose to use a variety of length-compensated sampling rates. They reasoned that shorter sampling interval time series turns out to have greater correlation among the data samples. Certainly for the Gaussianity hypothesis to be satisfied, the EEG should be sampled at a rate only slightly higher than the Nyquist rate. The significant difference in K-S test results was revealed in that many more data segments of length 4 seconds or shorter were deemed Gaussian than in the Elul study. They found varying degrees of Gaussianity and stationarity through all the electrode derivations. For instance, on average only about 8 percent of the data segments 32 seconds in length or longer turned out to be Gaussian. For any given length of data, stationarity is more likely to be satisfied than Gaussianity. Interestingly, they discovered that a 32-second long section of data is perhaps the best compromise balancing tradeoffs for stationarity and transient reduction.

6.8 The Hinich Tests for Gaussianity and Linearity

The χ^2-Goodness of fit test used by Elul and the Kolmogorov-Smirnov test used by McEwen and Anderson rely on the assumption of independent data samples for all the tests [30, 31].

As described in chapter 1, Hinich has derived tests for Gaussianity and linearity based on the statistics of the biperiodogram and its corresponding bicoherence. These tests are described in detail in [32]. The test for Gaussianity relies upon the sampled distribution of a properly scaled bicoherence estimator $X_{m,n}$ where

$$X_{m,n} = (N/M^2)^{1/2}[P_{xx}(m)P_{xx}(n)P_{xx}(m+n)]^{-1/2}\hat{B}_x(m.n). \qquad (6.2)$$

Here N is the total data record length, M is the block or segment length. (Data and segment length are related to the degrees of freedom (dof) for untapered records as related in chapter 2 for the bias and variance of the bicoherence estimator. Recall that dof $= 2B_eT$. In this context, $T = N\Delta T$ and $B_e = 1/(M\Delta T)$. AT is the sampling interval.)

Since $X_{m,n}$ is distributed as complex normal random variable with unit variance and non-zero mean, $2|X_{m,n}|$, is chi-squared with 2 degrees of freedom and non-centrality parameter

$$\lambda_{m,n} = 2N/M^2 \frac{|B_x(m,n)|^2}{P_x(m)P_x(n)P_x(m+n)}. \tag{6.3}$$

It is assumed that the $X_{m,n}$ are independent random variables. It turns out that the statistic

$$G = 2 \sum_{(m,n)\varepsilon L} |X_{m,n}|^2 \tag{6.4}$$

is distributed as $\chi^2_{2P}(\lambda)$. Here L represents domain of bispectral data points. P is the total number of points in L.

The Hinich test for Gaussianity poses the following null hypothesis using the asymptotic variance-covariance matrix for the bispectral estimates: When the time series $x(n)$ is Gaussian, $B(\omega_1, \omega_2) = 0$. We reject the null hypothesis at level of significance α, if $\hat{G} > t_\alpha$, where $a = Pr(\chi^{2P}_2(0) > t_\alpha)$.

The test for linearity relies on the fact that in general the sample distribution of of $2|X_{m,n}|^2$ is approximately $\chi^2_2(\lambda_{m,n})$ where $\lambda_{m,n}$ is given by (6.3). As mentioned in chapter 2 the test for linearity relies on the fact that asymptotically the bicoherence is constant across all bifrequencies for linear processes. The Hinich test of linearity involves a robust nonparametric test of dispersion. The sample distribution of $2|X_{m,n}|^2$ is compared to the estimated distribution of $\chi^2_2(\hat{\lambda})$ where $\hat{\lambda}$ is a consistent estimator of λ. Let R be the sample interquartile range of $2|X_{m,n}|^2$ for all the bicoherences in the non-redundant sample bispectral domain. The hypothesis of linearity is rejected when R is significantly larger or smaller than the interquartile range of $\chi^2_2(\hat{\lambda})$. In practice the estimate $\hat{\lambda}$ is the mean of the quantities $2|X_{m,n}|^2$ for all m and n.

6.9 Justification for Parametric Modeling of Alpha Coupling

With the statistics of the bispectrum well understood through the work of Hinich in higher order spectra, there is the question of why we would need to do parametric modeling of EEG wave coupling. Is there any information that we would gain by the use of model-based estimation of three-wave coupling? We need to consider the various reasons to warrant the use of modeling techniques described herein.

These parametric techniques are considered to be high resolution procedures for second order statistics. They should be able to resolve closely spaced peaks in a highly accurate fashion. The problems of leakage and extensive windowing of finite length sequences would be eliminated. The resolution issue is a critical one since the leakage issue is exaggerated in two-dimensions for the biperiodogram estimator. Since the bispectral estimator has a high variance in the first place, the leakage effects only compound the highly fluctuating results. The resolution effects are even an obstacle for the autoregressive estimator. As detailed in chapter 2, the autoregressive bispectral estimator has difficulty producing sharp peaks in the presence of significant amounts of added noise. For low SNR cases the eigenstructure based procedures provide more well defined peaks.

More importantly however to active researchers in EEG and new-science are the phenomenological concerns. There are fundamental structural reasons necessitating sinusoidal modeling. Both the alpha and beta rhythms are truly wide-band processes. Compare the bandwidth of alpha wave to total bandwidth of the relevant portions of the EEG spectrum. Nunez mentions that the peak power histogram of the alpha rhythm gives one the opportunity to define a total of three distinct alpha frequencies within the range of 8.5 to 13 Hz [24]. First of all, there is the lowest frequency making a contribution to the total power. The peak frequency exhibits the most power. There is also the highest peak within the bandwidth. All of these are identifiable components of EEG analysis within a single band using low resolution spectral measures! The alpha rhythm cannot necessarily be considered a narrow band process. For all subjects in non-paroxysmal EEG studies, the EEG alpha rhythm is not stationary, but tends to fluctuate over the course of most studies[24].

Several studies point to multiple generators for alpha frequencies. Walter et al. point to the fact that there are two independent generators functioning in the same frequency band. They also suggest that there were wider than usual sidebands of the alpha wave at 2 to 5 Hz separation from the main frequency [33].

Although it is possible that many sidebands of alpha and beta waves are phase-locked, it is not likely considering certain bandwidth consideration. A key study in understanding spectral bandwidth of EEG is the work of Wennberg and Zetterberg [34]. They define and classify key spectral parameters of the EEG and detail the relationships among frequency bands. Although it is possible that many frequencies may be involved in coupling, it is likely that coupling involves narrow frequency ranges within the alpha and beta band. Critical evidence was presented by these authors focusing on which portions of the alpha and beta bands are actually involved in coupling. Beta is assumed to be a supraharmonic as delta is considered to be a

subharmonic of the theta wave.

Additional evidence can stem from different types of alpha responses that are exhibited by human subjects. P-type alpha responders show persistent alpha presence even during the eyes open condition. In these cases we have to include those that show a double-peaked alpha. Double-peaked alpha subjects display one peak belong 9.0-9.5 Hz and one peak above this boundary. 'During the eyes open condition the upper peak disappears while the lower peak remains. We can see in certain subjects that the alpha-alpha coupling remains during the eyes open condition often with the lower peak. It remains to be seen which of the two peaks remain coupled to high frequency beta-11 rhythms. Inouye et al. discuss the notion of endogenous and exogenous generators or sources of the alpha rhythms [35]. Posterior (parietal and occipital) sources exhibit strong endogenous components with high frequency (> 9.5 Hz) alpha rhythms. On the other hand, anterior derivation provide alpha activity from low frequency exogenous generators from 8 to 9.5 Hz. Since we are examining primarily posterior electrode sites, it may turn out that high frequency alpha components are the critical spectral regions of coupling with the beta-II band.

More evidence comes from the comments made by Gasser et al. in their study of EEG parameter stability [36]. They mention that bandwidth is totally reliant on the degree of synchronization or coupling among the neurons. A narrow bandwidth typically means more synchronization among elements. It is therefore reasonable to believe that sustainable coupling among individual frequencies would require even tighter restrictions on bandwidth. In the case of self-self coupling an alpha bandwidth of σ_α when translated to a frequency band one octave higher becomes $\sigma_\beta = 2\sigma_\alpha$. We know from Wennberg and Zetterberg [34] that alpha and beta bandwidths do not observe this relation. It is reasonable to assume that only a narrow portion of the alpha band is actually involved in coupling.

As we shall see one of the most important reasons for applying sinusoidal parametrization to EEG three-wave coupling is the form of cumulants. Since our methods are correlation-based, the form of these time domain entities is critical in our assessment. The projected cumulants for the EEG segments. as seen in the next chapter, are taken normal to the 45^o main diagonal of the cumulant domain. They are sinusoidal in shape. As Barnett et al. mention the most prominent peak occurs in the alpha-alpha coupling region near the (10, 10) Hz bifrequency point [11]. In chapter 4 and in the Appendix we saw that the projected cumulants for a three-wave coupling process are 1-D sinusoids. This exciting fact alone ensures that sinusoidal modeling of EEG three-wave coupling offers interesting research possibilities.

6.10 List of References

[1] F. Lopes da Silva, "Neural mechanisms underlying brain waves: from neural membranes to networks," Electroencephal. clin. Neurophysiol., vol. 79, pp. 81-93, 1991.

[2] H.H. Jasper, "Report of the Committee on Apparatus - Recommendations to Manufacturers," Electroencephal. clin. Neurophysiol., vol. 10, p. 378, 1958.

[3] J.G. Okyere, P.Y. Ktonas, and J.S. Meyers, "Quantification of the Alpha EEG Modulation and Its Relation- to Cerebral Blood Flow," IEEE Trans. Biomed. Eng., vol. BME-33, pp. 690-696, July 1986.

[4] G. Dumermuth and L. Molinari, "Spectral Analysis of EEG Background Activity," (in EEG Handbook: Methods of Analysis of Brain Electrical and Magnetic Signals), vol. 1, pp. 85-130, Elsevier Science, Dublin, Ireland, 1987.

[5] D.E. Dick and A.O. Vaughn, "Mathematical Description and Computer Detection of Alpha Waves," Mathematical Biosciences, vol. 7, pp. 81-95, 1970.

[6] F. Yarman-Vural, B. Onaral, and E. Cetin, "Enhanced Parametric Estimation of Electroencephalograms Under Acceleration Stress," Proc. IEEE Eng. in Med. Biol., vol. 2, pp. 837-839, Philadelphia, PA, Nov. 1990.

[7] P.J. Huber, B. Kleiner, T. Gasser, and G. Dumermuth, "Statistical Methods for Investigating Phase Relations in Stationary Stochastic Processes," IEEE Trans. Audio Elec., vol. AU-19, pp. 78-86, 1971.

[8] G. Dumermuth, P.J. Huber, B. Kleiner, and T. Gasser, "Analysis of the Interrelations between Frequency Bands of the EEG by Means of the Bispectrum: A Preliminary Study," Electroenceph. clin. Neurophysiol., vol. 31, pp. 137-148, 1971.

[9] T. Ning and J.D. Bronzino, "Autoregressive and Bispectral Analysis Techniques: EEG Applications," IEEE Eng. in Med. and Bio., vol. 9, pp. 47-50, March 1990.

[10] T. Ning and J.D. Bronzino, "Cross-Bispectra of the Rat During REM Sleep," Proc. IEEE Eng. in Med. Biol. *Conf.*, pp. 447-448, Orlando, FL, Nov. 1991.

[11] T.P. Barnett, L.C. Johnson, P. Naitoh, N. Hicks, and C. Nute, "Bispectrum Analysis of the Electroencephalogram during Waking and Sleeping," Science, vol. 172, pp. 401-403, 1971.

[12] J.L. Whitton, S.M. Elgie, H. Kugel, and H. Moldofsky, "Genetic Dependence of the Electroencephalogram Bispectrum," Electroencephal. clin. Neurophysiol., vol. 60, pp. 293-298, 1985.

[13] G.A. Shiminke, "Alpha and Beta Waves in the Human Electroencephalogram," Pavlov J Higher *Nerv* Activ, vol. 11, p. 256, 1961.

[14] K. Gaarder and L.B. Speck, "The Quasi-Harmonic Relations of Alpha and Beta Peaks in the Power Spectrum," Brain Research, vol. 4, p. 110, 1967.

[15] L. Johnson, A. Lubin, P. Naitoh, N. Hicks, and M. Austin, "Spectral Analysis of the EEG of Dominant and Non-Dominant Alpha Subjects during Waking and Sleeping," Electroencephal. clin. Neuropsych., vol. 26, pp. 361-370, 1969.

[16] G. Dumermuth, T. Gasser, A. Hecker, M. Herdan, and B. Lange, "Exploration of EEG Components in the Beta Frequency Range," (In: Quantitative Analytic Studies in Epilepsy, by P. Kellaway & I. Petersen), pp. 533-558, Raven, New York, 1976.

[17] L.G. Kiloh, A.J. Comas, and J.W. Osselton, Clinical *Electroencephalography*, (3rd. Ed.), Appleton-Centure Crofts, New York, 1972.

[18] G. Pfurtscheller and A. Aranibar, "Event-related cortical desynchronization detected by power measurements of scalp EEG," Electroencephul. clin. Neurophysiol., vol. 46, pp. 138-146, 1977.

[19] D.M. Tucker, D.L. Roth, and T.B. Bair, "Functional Connections Among Cortical Regions: Topography of EEG Coherence," Electroenceph. clin. Neurophysiol., vol. 63, pp. 242-250, 1986.

[20] W.J. Ray and H.W. Cole, "EEG Alpha Activity Reflects Attentional Demands, and Beta Activity Reflects Emotional and Cognitive Processes," Science, vol. 228, pp. 750-752, May 1985.

[21] R.J. Davidson, J.P. Chapman, L.J. Chapman, and J.B. Henriques, "Asymmetrical Brain Electrical Activity Discriminates Between Psychomemcally-Matched Verbal and Spatial Cognitive Tasks," Psychophysiology, vol. 27, pp. 528-543, Sept. 1990.

[22] A.C. Mundy-Castle, "An analysis of central responses to photic stimulation in normal adults," Electroencephal. clin. Neurophysiol., vol. 5, p. 1, 1953.

[23] N.M. Danilova, "Electroencephalographic responses to flickering light in the alpha-rhythm frequency range," Pavlov *J.* Higher *Nerv.* Activ., vol. 2, p. 8, 1961.

[24] P. Nunez, The Electric Fields of the *Brain*, Oxford, New York, 1981.

[25] P.Y. Ktonas and N. Papp, "Instaneous Envelope and Phase Extraction from Real Signals: Theory, Implementation, and An Application to EEG Analysis," Signal Processing, vol. 2, pp. 373-385, 1980.

[26] M. Steriade, P. Gloor, R.R. Llinar, F.H. Lopes da Silva, and M.-M. Mesulam, "Basic Mechanisms of cerebral rhythmic activities," Electroencephul. clin. Neurophysiol., vol. 76, pp. 481-508, 1990.

[27] B.A. MacVicar and F.E. Dudek, "Electrotonic Coupling Between Pyramidal Cells: A Direct Demonstration in Rat Hippocampal Slices," Science, vol. 213, pp. 782-785, Aug. 14, 1981.

[28] F.H. Lopes da Silva, A. Hoeks, H. Smits, and L.H. Zetterberg, "Model of Brain Rhythmic Activity: The Alpha Rhythm of the Thalamus," Kybernetik, vol. 15, pp. 27-37, 1974.

[29] A. van Rotterdam, F.H. Lopes da Silva, J. Van Den Ende, M.A. Viergever, and A.J. Hermans, "A Model of Spatial-Temporal Characteristics of the Alpha Rhythm," Bull. Math. Biol., vol. 44, pp. 283-305, 1982.

[30] R. Elul, "Gaussian Behavior of the Electroencephalogram: Changes During Performance of Mental Tasks," Science, vol. 164, pp. 328-331, 1969.

[31] J.A. McEwen and G.B. Anderson, "Modeling the Stationarity and Gaussianity of Spontaneous Electroencephalographic Activity," IEEE Trans. Biomed. *Eng.*, vol. BME-22, pp. 361-369, 1975.

[32] M. Hinich, "Testing the Gaussianity and Linearity of a Stationary Time Series," J. Time Series Anal., vol. 3, pp. 169-176, 1982.

[33] D.O. Walter, J.M. Rhodes, D. Brown, and W.R. Adey, "Comprehensive spectral analysis of human EEG generators," Electroencephal. clin. Neurophysiol., vol. 20, p. 224, 1966.

[34] A. Wennberg and L.H. Zetterberg, "Application of computer-based model for EEG analysis," Electroencephal. clin. Neurophysiol., vol. 31, p. 457, 1971.

[35] T. Inouye, K. Shinosaki, A. Yagasaki, and A. Shimizu, "Spatial Distribution of Generators of Alpha Activity," Electroenceph. clin. Neurophysiol., vol. 63, pp. 353-360,1986.

[36] T. Gasser, P. Baecher, and H. Steinberge, "Test-Retest Reliability of the Spectral Parameters of the EEG," Electroenceph. clin Neurophysiol., vol. 85, pp. 312-319,1985.

CHAPTER 7
EEG SIMULATIONS

"The final objective in a signal processing scenario is to process a finite set of data (either single-sensor or multiple sensor) and extract important information which is "hidden" in the data. This is usually achieved by combining the development of mathematical formulations which reach a certain level of estimation performance with their algorithmic implementation (either in software or hardware) and their application to real data." †

7.1 Introduction

Different algorithms introduced in this thesis and in other scholarly works are tested with electroencephalographic (EEG) data for the detection and estimation of three-wave coupling. At first, conventional methods including the biperiodogram and the Hinich tests for Gaussianity and Linearity are used to furnish a description of the data. These methods are then used to establish criteria for the selection of candidate time series for testing with parametric algorithms. Three eigenstructure methods are used for testing the EEG data. They are the 2-D SKEW-MUSIC method described in chapter 3, the standard Swindlehurst and Kailath method introduced in [1] and the SKEW-PRO-ESPRIT method discussed in chapter 5. We chose not to make any definitive claims of accuracy rankings of these methods. Our goal is only to establish that the all methods are likely to provide coupling frequency estimates that are localized within appropriate sectors of the bispectrum using a low model order. 1-D methods are also shown to provide reasonable estimates of frequency interactions as well. The right singular vectors belonging to symmetric and skew-symmetric third

† C.L. Nikias & M.R. Raghuveer, Bispectral Estimation: A Digital Signal Processing Framework, *Proc.* IEEE, vol. 75, July 1987, p. 869

order cumulant matrices give individual coupling frequency estimates. The 1-D MUSIC bispectra from cumulant projections are also examined for biphase estimation.

We desire to apply each method to EEG time series displaying predominantly alpha-alpha coupling. In the non-redundant sector of the bispectrum this is the frequency support region of $8 \le f_1 \le 13$ Hz and $8 \le f_2 \le f_1$ Hz. We can anticipate the need for low model order based on the fact that substantial power is concentrated in the alpha band. Also the proportion of alpha power actually involved in coupling is relatively strong in this region. This is indicated by the skewness at each point in the bispectrum [2].

7.2 Materials and Methods

Seven subjects participated in an experiment to establish appropriate features for detection of lateral asymmetry during cognitive tasks in a previous study at Purdue University [3]. The tasks used to generate lateral asymmetries were letter completion, multiplication (mathematical), 3-D object rotation, number visualization and baseline. Each task was completed under two separate states of eye closure in the original study, eyes open and eyes closed. The time series selected for bispectral processing belonged only to EEG generated during baseline and eyes closed conditions. We wished to maximize the appearance of alpha wave coupling around the 10 Hz - 10 Hz region without necessarily producing pronounced alpha band power asymmetries.

For each subject the EEG was recorded during five nonconsecutive 10 second segments. All occurred within a 3 minute time interval. The EEG was recorded during this period from electrode sites, C3, C4, P3, P4,O1 and 0 2 according to the International 10-20 electrode location system [4]. One eyeblink (EOG) channel was also recorded simultaneously. Each 10 second data sequence was sampled at 250 Hz after passing through a linear phase filter with low pass cutoff of 100 Hz and high pass cutoff of 0.1 Hz from a Grass 7P511J amplifiers. In an earlier study, [5], the time delay associated with the Grass amplifiers was verified. These amplifiers have a constant time delay of 2.7 msec over the frequency band of interest. After the data was sampled, the five separate segments of data were combined to form a 50 second data set. Artifact rejection was accomplished by examining the EOG channel for $V_\Delta > 50\mu V$ over a 10 msec window. If that threshold was exceeded, the corresponding EEG channel data segments were rejected. Preprocessing of data also included low pass

filtering by FIR filter, decimation-in-time by a factor of 2 and trend removal to yield thirty-two seconds of data. Each one second block length of 125 pts was augmented with zeros to make total block length equal 128 points The cumulants as well as periodograms and biperiodograms were calculated from 32 blocks of data (N=4096). Periodogram data was tapered with a 10% taper window. The subjects were divided into a high and low alpha groups. This division was based on the height of the average parietal alpha spectral peak. There were 4 members of the high alpha group and 3 in the low group.

7.3 Qualifying the Data for Inclusion in the Test Data Sample Set

Before testing the data sets available, a set of criteria was adopted to select candidate sets for the application of the variety of eigenstructure and autoregressive algorithms. Skewnesses and their statistics were also calculated according to [2]. These included the estimated significance of each peak based upon the estimated parent noncentral χ^2 distribution. Statistics of Gaussianity and linearity were calculated for all seven subjects and are presented in Tables 6.1-6.3. Examining the statistics for Gaussianity we find all of the EEG time series are highly non-Gaussian with a high degree of variability in the Z-scores for all the electrode sites. Part of the reason for this stems from the fact that our estimator or χ^2 statistic does not approximate a consistent one. The equation $M^C = N$ relates data segment length, M, to total data length, N. Consistency is approached when $c \geq 2$. Our data segment length was chosen to balance competing desires to achieve high resolution while adhering to the stationarity guidelines provided by McEwen and Anderson [6].

The interquartile range data reveal that the empirical distribution closely matches the estimate of the parent noncentral χ^2 distribution. Only when moving to the interdecile data (Table 7.3) does the quantile match between sample distribution and estimated parent begin to deviate slightly. It would appear that the tails of the empirical distribution are slightly truncated. Actual statements of linearity would have to be made by closer examination of individual time series data. Table 7.4 shows the large variation in the estimated noncentrality parameter.

For examining individual peaks and their skewness, it was decided to divide the relevant section of the EEG bispectral domain into coupling regions based on their antecedent bands in the power spectrum. The EEG hyperbands are illustrated in Fig.

Table 7.1 Z-Scores for Level of Gaussianity based on Hinich Test: Based on Normal Approximation to χ^2; dof = 2048

EEG Time Series Z-Scores for Level of Gaussianity N=4096; (128x32); 7 Subjects		
Derivation	Mean	St. D.
Central	12.42	5.99
Parietal	12.322	4.61
Occipital	10.42	6.36

7.1. This grid becomes our chief unit of analysis. It serves to first determine the area in the EEG bispectrum with the most significant peaks. Later it provides a convenient map for describing accuracy of 2-D bispectral peak placement.

For all electrode derivation and all 7 subjects, the alpha-alpha coupling region has by far the largest average number of significant peaks ($p < .01$). For the P3 site the average number of peaks at or above this level is 1.14, i.e. greater than unity. For the P4 electrode it is over 2, namely 2.43. The alpha-alpha sector has 22 bifrequency points in it. The entire bispectral domain has 1024 individual points. So the alpha-alpha hyperband represents just over 2% of the total number of points. There were two other occasions when different regions had a greater average number of significant peaks than the alpha self-coupling region. The alpha-beta-I sector had more peaks in the P3 derivation. The theta-beta II hyperband had more peaks in the 0 1 derivation. Both of these sectors are larger in area than the alpha-alpha sector.

Since the few significant nonlinearities are concentrated within one sector, we expect that we need low model order to faithfully capture the coupling frequency information. To insure that there are few competitor peaks in the bispectrum the following procedure was followed in selecting candidate time series for testing: After the biperiodogram and associated statistics for each time series were run, the largest 10 bispectral peaks were isolated. These 10 peaks were inspected to check for member peaks in the alpha-alpha coupling region as well as the theta-theta coupling region. If there were peaks present in those regions, their skewnesses were checked to see if they were significant ($p < .01$). If all other peaks among the top ten were not significant, that EEG time series was declared a candidate to be tested. Out of the 14 possible time series at each of three bilateral derivations, 10 parietal, 8 occipital and 6 central time series met these criteria.

Table **7.2** Interquartile Ranges for Level of Linearity based on Hinich Test: Based On Estimates for Noncentrality Parameter, Bilateral Electrode Derivations

EEG Time Series Interquartile Ranges N=4096; (128x32); 7 Subjects		
Derivation	Mean	St. D.
Central	**0.508**	**0.0222**
Parietal	**0.505**	**0.025**
Occipital	**0.51**	**0.0251**

Table **7.3** Interdecile Ranges for Level of Linearity based on Hinich Test: Based On Estimates for Noncentrality Parameter; Bilateral Electrode Derivations

EEG Time Series Interdecile Ranges N=4096; (128x32); 7 Subjects		
Derivation	Mean	St. D.
Central	**0.816**	**0.0187**
Parietal	**0.816**	**0.0268**
Occipital	**0.8207**	**0.259**

Table **7.4** Estimates of Noncentrality Parameter: Hinich Test for Nonlinearity

EEG Time Series Noncentrality Parameter Estimates N=4096; (128x32); 7 Subjects		
Derivation	Mean	St. D.
Central	**0.784**	**0.377**
Parietal	**0.898**	**0.5055**
Occipital	**0.859**	**0.5793**

The chosen parietal bispectral peaks had 5 biphases above 45 degrees and 5 below. The average biphase was 43.355 degrees. The occipital was also evenly divided with an average biphase of 36.168 degrees. The central electrode had 5 biphases greater than 45 degrees and 1 less than 45 degrees for an average biphase of 62.33'. The occipital and central derivations all belonged to the high alpha group. There were two parietal derivations in the low alpha group.

7.4 Algorithm Specifications

After selecting the time series, the algorithms selected for testing are: 1.) 2-D SKEW-MUSIC; 2.) the classical triple Kronecker product method of Swindlehurst and Kailath [1]; 3.) the method which includes adaptations to the triple Kronecker product method for symmetric and skew-symmetric cumulants and removal of the R(0,0) term from the matrix (SKEW-PRO-ESPRIT); 4.) the autoregressive approach of Raghuveer and Nikias [7]. The 2-D SKEW-MUSIC equations, (3.8)-(3.10) and (3.16)-(3.18), represent the symmetric and skew-symmetric cumulant matrices, respectively. For this method matrix dimensions of 25 x 25and 30 x 30 were chosen. Signal subspace dimensions of 6, 12, 18 and 24 were used when applicable. The smallest dimension represents peaks along the main diagonal of the bispectrum. These are self couplings and represent a phase-locked $f_1 = f_2$ dyad. The largest dimension is used for 2 sets of triads assuming that $f_1 \neq f_2$ for each triad. Coupling frequencies were estimated using (3.19) with noise eigenvectors from both symmetric and skew-symmetric matrices.

For the triple Kronecker matrix techniques, (5.3) was utilized with matrix dimensions of 16 x 10, 25 x 10 and 36 x 15. Here signal subspace dimensions of 6, 8, 10 and 12 were candidate sizes. Using SKEW-PRO-ESPRIT both (5.18a) and (5.18b) were used and filled with symmetric and skew-symmetric cumulants, respectively. The dimensions of the SKEW-PRO-ESPRIT matrices used were the same as the triple Kronecker product matrices. For both methods the SVD of all matrices was taken. The left singular values furnished 2-D bifrequency estimates using (2.46). Also in the case of 1-D frequency estimates, the right singular vectors of both the symmetric and skew-symmetric cumulant matrices are utilized. Only 16 x 10 and 25 x 10 matrix dimensions are used for this estimation procedure. Single coupling frequencies are estimated using (2.48).

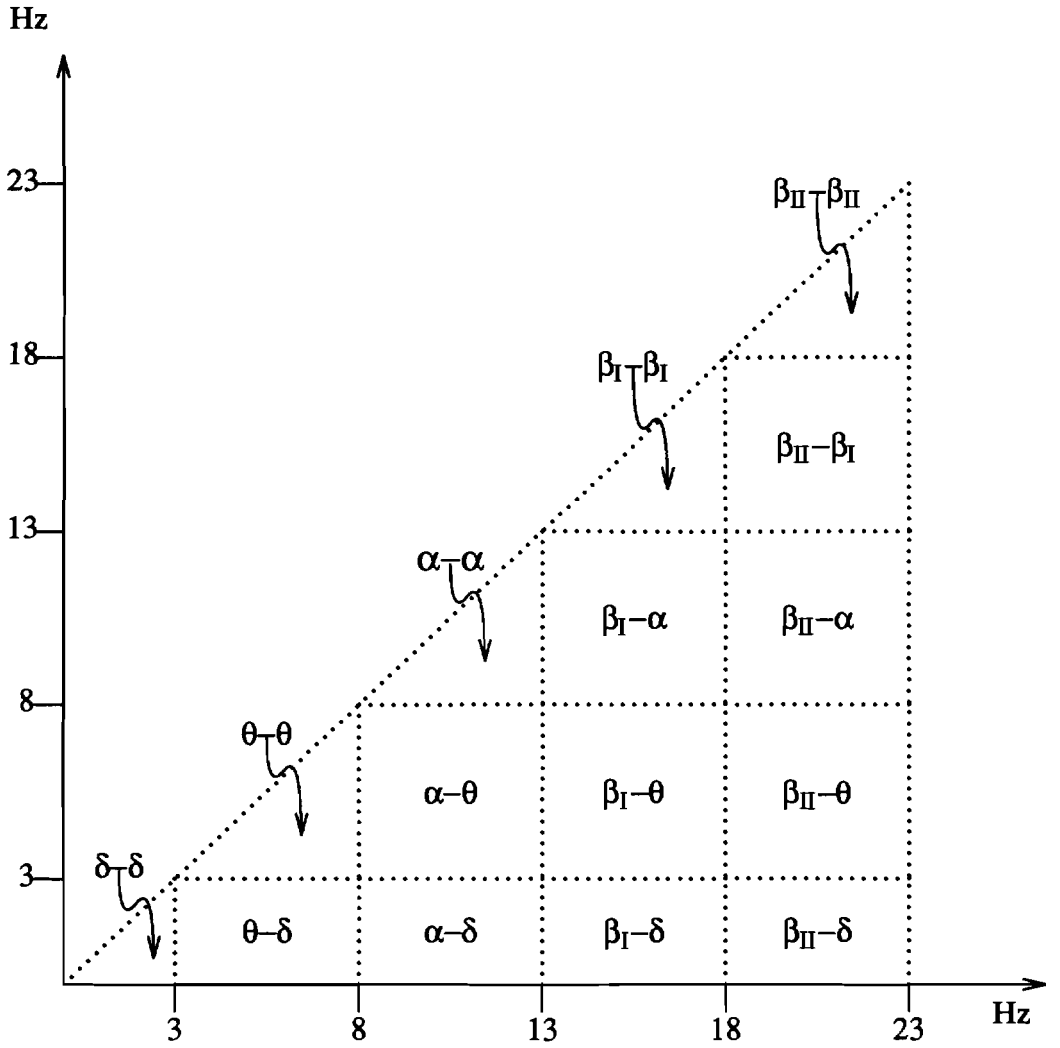

Figure 7.1 EEG Band-Band Coupling Regions or Hyperbands

Finally, the AR method is used for coupling frequency estimation with (2.14)-(2.16). These equations are used with symmetric, skew-symmetric and unsymmetrized cumulants. Square matrices with AR model orders of 4, 6, 8, 10 and 12 were employed.

Frequency resolution for the parametric methods was maintained at the same $f_\Delta = 0.98$ Hz as used for the standard biperiodogram. Once bifrequency estimates have been generated, the estimates were sorted according to magnitude. If the largest peak on the 2-D hyperband grid fell within the same hyperband as the selected biperiodogram peak value, then a hit was recorded. The number of hits are counted for each matrix size and signal subspace dimension. A hit rate is computed by dividing the number of hits for a given derivation, matrix dimension, model order and cumulant type by the number of sample time series at that derivation. Those matrix sizes possessing the greatest number of hits are shown in the Appendix in convenient bar graph hit rate profiles.

A hit rate profile is also computed for the 1-D SKEW-PRO-ESPRIT coupling frequency estimates. For each 1-D bispectrum constructed from the right singular vectors, a hit was registered when the two largest peaks appeared in the appropriate bands corresponding to the biperiodogram peak. Only self couplings were reported. A hit rate was computed for these as well.

We also tested the 1-D SKEW-MUSIC and SKEW-ESPRIT algorithms for coupling frequency and biphase accuracy. Projected cumulants were made for all 42 time series belonging to the subjects. The projections were made along a 45^o projection axis. A rectangular window of length 21 was used. This supplied 10 forward and 10 backward lags each plus a zero lag term. For each projected cumulant lag value, twenty one 2-D cumulants were summed.

To arrive at frequency estimates 10 x 10 matrices were constructed according to (4.23)-(4.24) and (4.25). Eigenvector/eigenvalue decompositions were done for both symmetric and skew-symmetric projected cumulant matrices. Signal subspace dimensions of 2 and 4 were utilized for frequency estimates. These dimensions were utilized under the assumption that only one or two decoupled sinusoids would appear along the central bispectral slice typically in the alpha-alpha or theta-theta coupling frequency scenarios.

For biphase estimation the same matrices were utilized. The implementation of the SKEW-PRO-ESPRIT entailed reducing each of the matrices down to 2 x 2 or 4 x 4 core rotations level matrices as in (4.10). The generalized eigenvalues of the reduced order matrices contain the biphases as in (4.29).

7.5 Results

Some sample 3-D plots for bifrequency estimation are shown in Figs. 7.2-7.13. In Fig. 7.1 the biperiodogram for a P4 derivation is shown. Several estimates for three different parametric methods are shown in accompanying plots. In the 2-D SKEW-MUSIC estimate the model order of 18 insures that we have two main diagonal peaks that correspond to the biperiodogram peak exactly. Model order 8 in the triple Kronecker product method also corresponds to two main diagonal peaks. Low model order is achieved for the skew-symmetric cumulants in the case of SKEW-PRO-ESPRIT.

Viewing the second set of bispectral plots (Figs. 7.6-7.9), we note there are several delta-alpha peaks that are located near the DC axis of the biperiodogram. Subject 7's P3 derivation is used for this series of bispectra. These competitor peaks do not have as large a bicoherence value as the main alpha-alpha peaks do. Each of the three eigenstructure methods provides accurate estimates of coupling frequencies with low model order. Only in the case of 2-D SKEW-MUSIC does the signal subspace require a full complement of eigenvectors for two self coupling peaks. As can be seen on that plot there are two peaks visible along the main diagonal.

In Figs. 7.10-7.11 we see the bispectra for another parietal time series. A large model order (24) in a 30 x 30 2-D SKEW-MUSIC matrix with skew-symmetric cumulants provides an exact estimate of the coupling frequency along the main bispectral diagonal. Fig. 7.12 shows a large central (C3) biperiodogram peak along with much delta band diffuse coupling. A distinctive triple Kronecker peak in Fig. 7.13 models that peak closely. This time a model order of 12 is used.

Turning now to the hit rate profiles in the Appendix (Fig. A.1-A.12) we see a variety of performance levels. For the parietal sites, 2-D SKEW-MUSIC has its best performance at a model order of 18 with an average hit rate above 0.5. Though symmetric and skew-symmetric biphases are evenly represented, the most hits are generated with the skew-symmetric cumulants. Symmetric cumulant hits increase to their peak at model order 12 and then decrease again. It is important to realize that 2-D SKEW-MUSIC has fewer distinct model orders to model the coupling frequencies. Many of its middle value model orders may indicate better performance than individual model orders of other methods.

The AR method shows a lower average hit rate profile for parietals. Perhaps the AR method is more model order specific and less redundant. The best performance is seen for a model order of 6 or one triad. That preferred order selection is also seen for the SKEW-PRO-ESPRIT. Here symmetric and skew-symmetric cumulants are

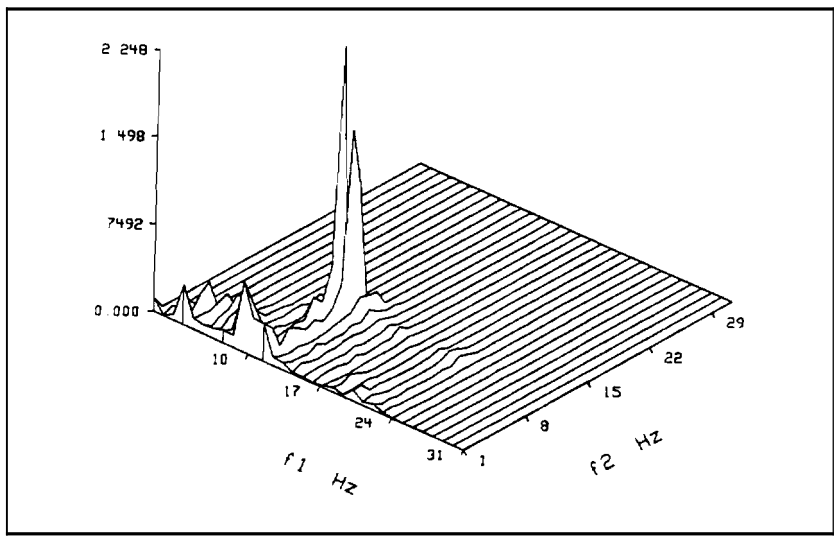

Figure 7.2 **Biperiodogram: S1; P4 Derivation; Peak at** (10.74,10.74) **Hz**

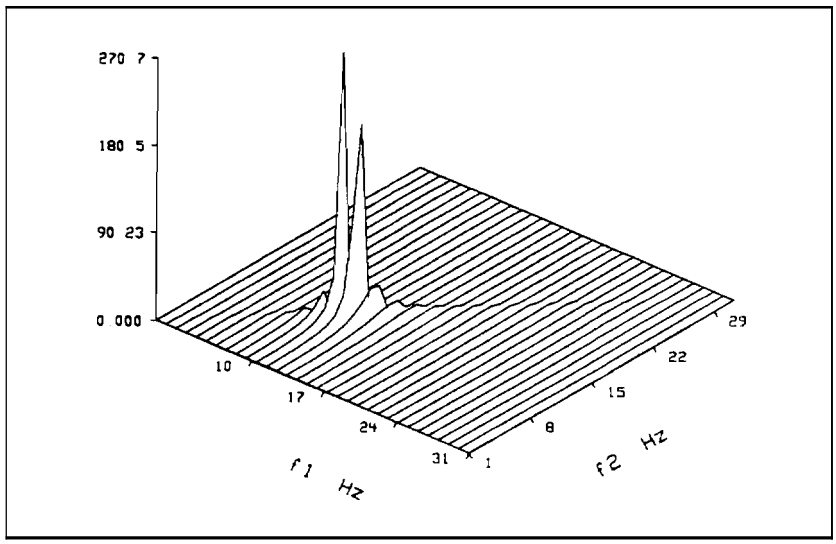

Figure 7.3 **2-D SKEW-MUSIC: S1; P4 Derivation; 30 x 30 mamx, Skew-Symmetric Cums, Signal Subspace Dim: 18; Peak at** (10.74,10.74) **Hz**

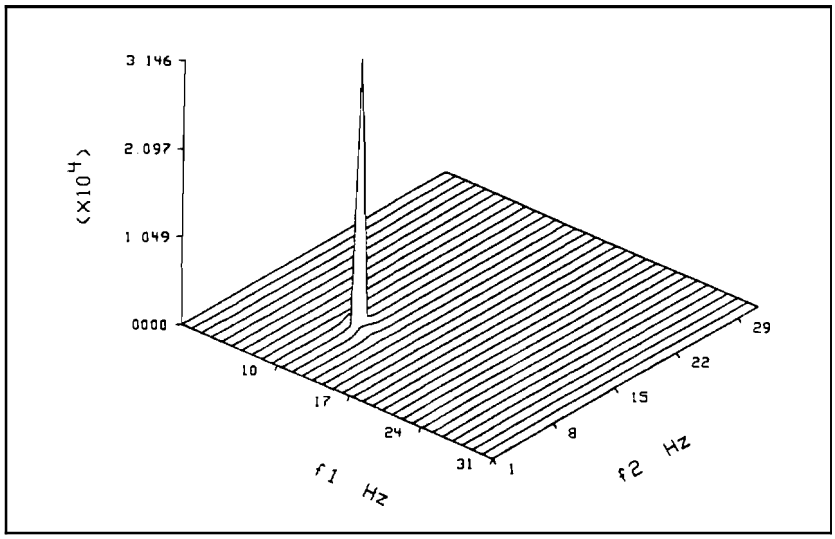

Figure 7.4 S&K Triple Kron. Method: S1; P4 Derivation; 25 x 10 mamx, Signal Subspace Dim: 8; Peak at (9.77,10.74) Hz

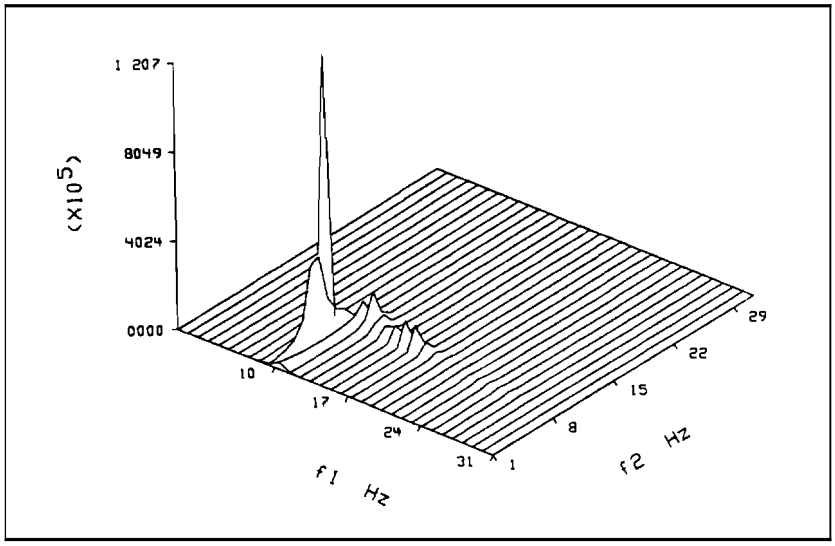

Figure 7.5 SKEW-PRO-ESPRIT: S1; P4 Derivation; 16 x 10 mamx, Skew-Symmemc Cums, Signal Subspace Dim: 6; Peak at (8.79,8.79) Hz

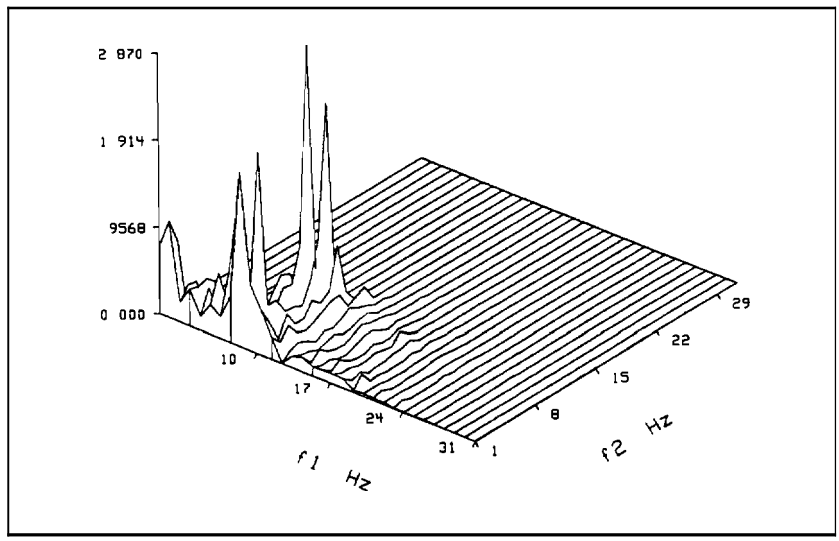

Figure 7.6 Biperiodogram: S7; P3 Derivation; Peak at (8.79,8.79) Hz

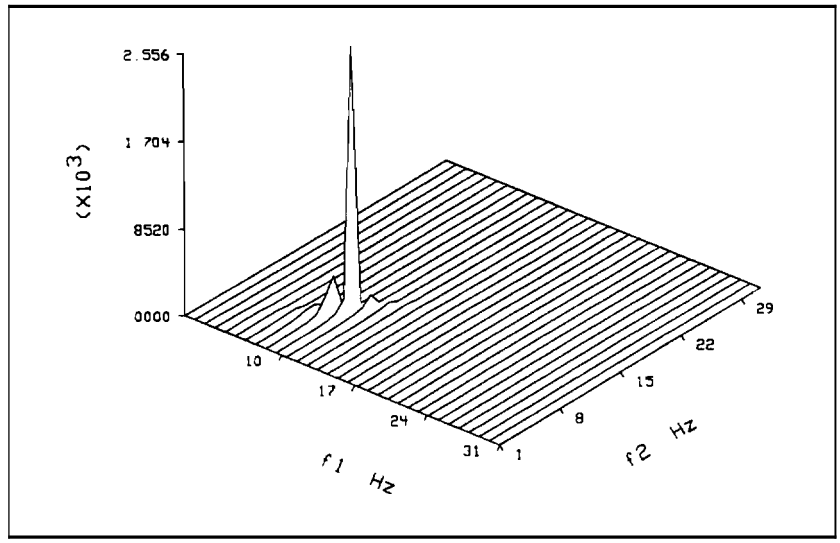

Figure 7.7 2-D SKEW-MUSIC: S7; P3 Derivation; 25 x 25 matrix, Skew-Symmetric Cums, Signal Subspace Dim: 12; Peak at (9.77,9.77) Hz

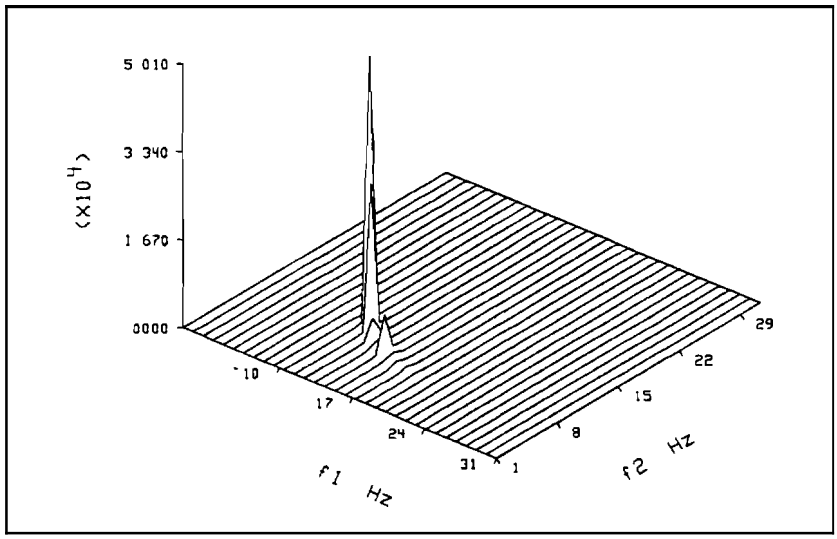

Figure 7.8 S&K Triple Kron. Method: S7; P3 Derivation; 25 x 10 matrix, Signal Subspace Dim: 8; Peak at (10.74,10.74) Hz

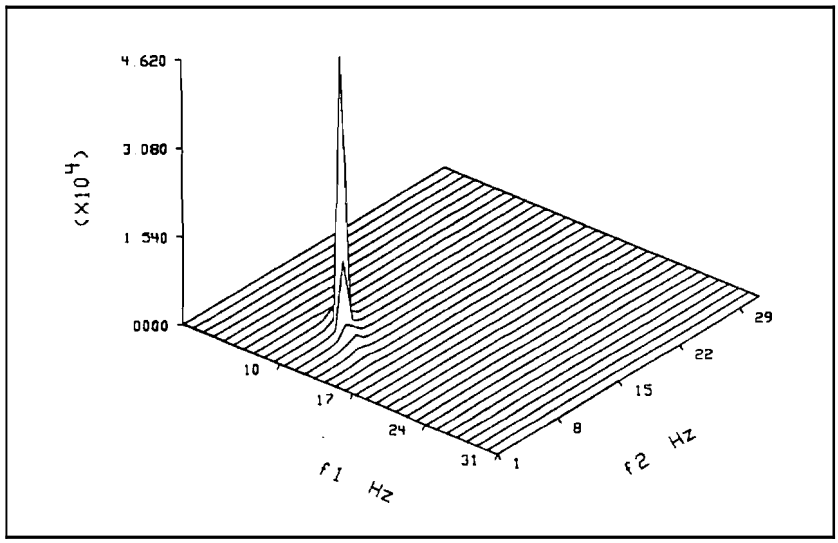

Figure 7.9 SKEW-PRO-ESPRIT: S7; P3 Derivation; 16 x 10 mamx, Skew-Symmemc Cums, Signal Subspace Dim: 6; Peak at (8.79,9.76) Hz

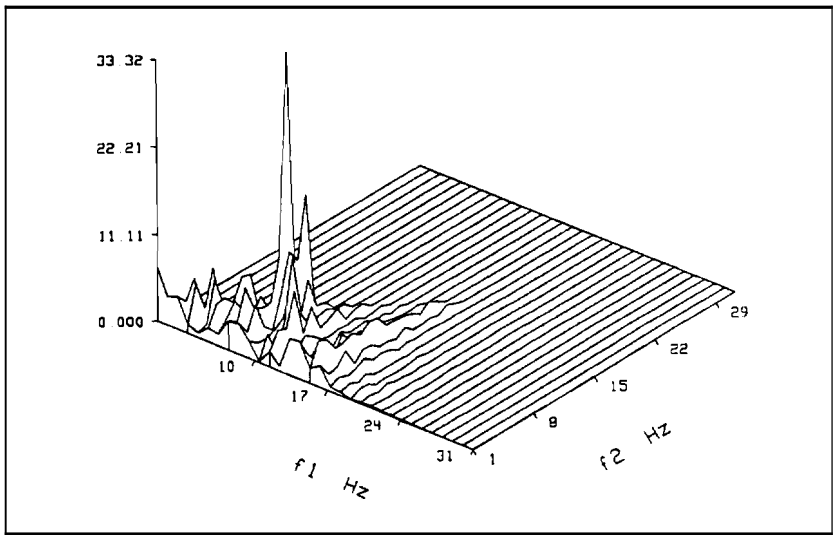

Figure 7.10 Biperiodogram: S6; P4 Derivation; Peak at (7.81,7.81) Hz

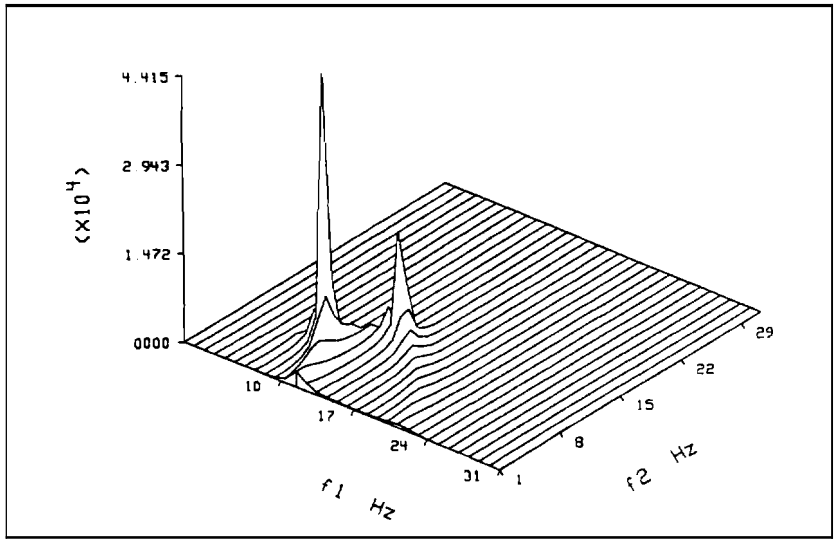

Figure 7.11 2-D SKEW-MUSIC: *S6;* P4 Derivation; 30 x 30 matrix, Skew-Symmetric Cums, Signal Subspace Dim: 24; Peak at (7.81,7.81) Hz

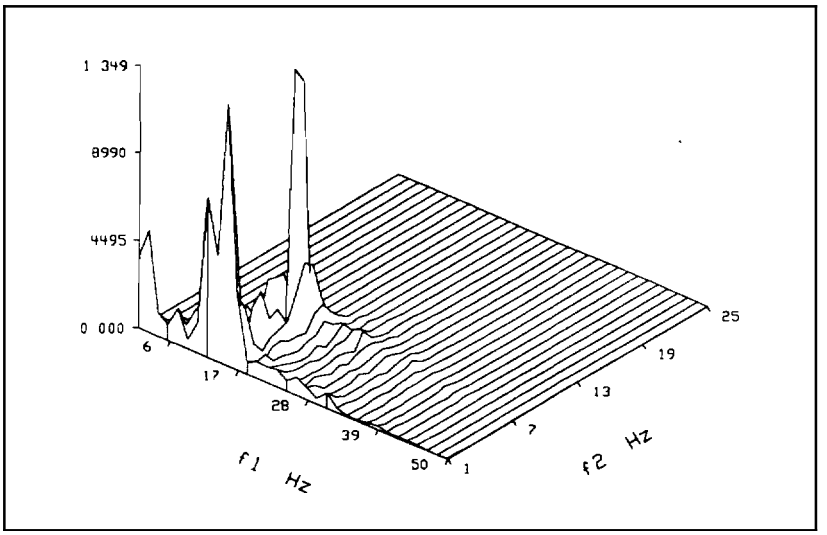

Figure 7.12 Biperiodogram: S7; 0 2 Derivation; Peak at (9.77,8.79) Hz

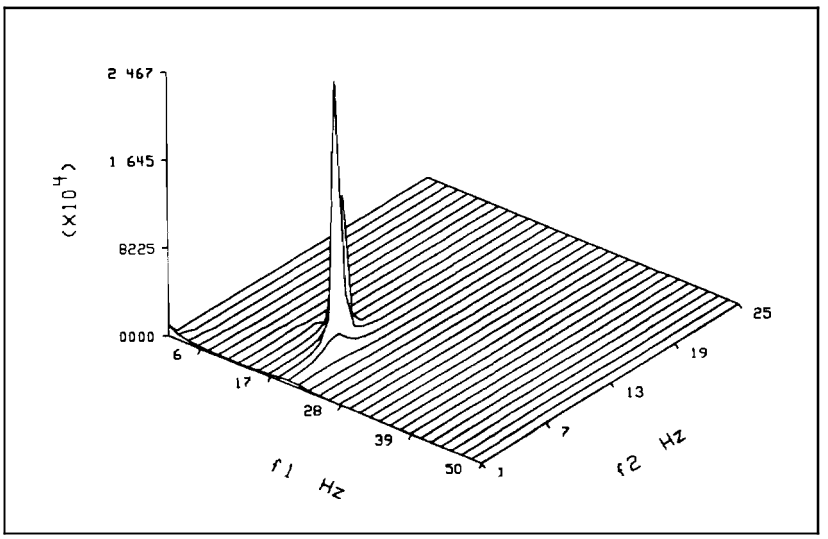

Figure 7.13 SKEW-PRO-ESPRIT: S7; 0 2 Derivation; 16 x 10 matrix, Symrnemc Cums, Signal Subspace Dim: 6; Peak at (7.81,11.72) Hz

evenly represented in the different model orders.

For the central derivations the hit rates are low for all four methods. Only in the case of the triple Kronecker product method are hit rates sizable. Once again the preferred model order is 8. Also all the symmetrizable methods show best hit rates for the skew-symmetric cumulants.

All modeling schemes show their best results for the occipital recording sites. Several model orders provide hit rate probabilities well above 50%. It is particularly interesting to note that here, higher model orders are favored for 2-D SKEW-MUSIC and SKEW-PRO-ESPRIT. 2-D SKEW-MUSIC still has best hit rate results for the skew-symmetric cumulants. Clearly the occipital sites deliver the best AR results. The triple Kronecker product favors signal subspaces of dimension 8 while recording its best hit rates for other model orders.

The 1-D coupling frequency estimates from the right singular vectors have representative hit rate profiles in the Appendix (A.13-A.15) as well. In these cases the hit rates from both 16 x 10 and 25 x10 size matrices were averaged together. For all derivations the model with largest hit rates was model order 8. Two representative 1–D coupling frequency plots are shown from two subjects, Ss 1 & 7, in Fig. 7.14 and 7.15. The model order 6 provides us with enough information to judge that alpha=alpha self coupling is present in the bispectral domain.

The remaining eight figures in this chapter (Figs. 7.16-7.23) depict results from the 1-D SKEW-MUSIC and SKEW-ESPRIT algorithms. Plots of the symmetric and skew-symmetric cumulants for each derivation are given. The projections closely resemble single 1-D sinusoids. Along with each set of cumulant projections is the measured biphase from the 1-D SKEW-ESPRIT matrix pencil. The FFI' biphase is the biphase derived from the biperiodogram. This cited FFI' biphase may belong to either the peak on the slice with the largest bispectral magnitude or the largest bicoherence. This same convention applies for 1-D frequency information below.

Below each correlation-domain plot is the frequency information from 1-D SKEW-MUSIC. The same signal subspace dimension used to generate biphase information also generates the SKEW-MUSIC frequency information. Tables in the Appendix (Tables A.l-A.2) list all 42 EEG time series and their deviations from biperiodogram generated frequency estimates. A table with average deviations for all electrode sites appears below. Slightly better performance is noted for the signal subspace dimension of 4. Table A.3 in the Appendix shows 22 of the closest 42 biphase estimates from 1-D SKEW-ESPRIT. Each of these estimates are within $\pm 15^{o}$ of their respective conventional biperiodogram estimate. In Table 7.6 the summary statistics for these estimates are listed according to derivation.

Table **7.5** Summary Statistics for 1-D SKEW-MUSIC EEG Coupling Frequency Estimates

Statistics for 1-D SKEW-MUSIC Coupling Frequency Deviations from FFT Estimates: EEG Data				
Site	Model Order			
	2		4	
	Mean	St.D.	Mean	St.D
Parietal	**1.61**	**1.822**	**1.67**	**2.147**
Central	**1.05**	.892	**.77**	.783
Occipital	**1.12**	**2.023**	**.84**	**1.79**

Table **7.6** Summary Statistics 1-D SKEW-ESPRIT EEG Biphase Estimates

Statistics for 1-D SKEW-ESPRIT Biphase Deviations from FFT Estimates: EEG Data from **22** "Closest" Derivations		
Site	Statistics	
	Mean	St.D.
Parietal (N=9)	**4.49**	**3.0615**
Central (N=7)	**5.193**	**3.3709**
Occipital (N=6)	**6.148**	**3.83**

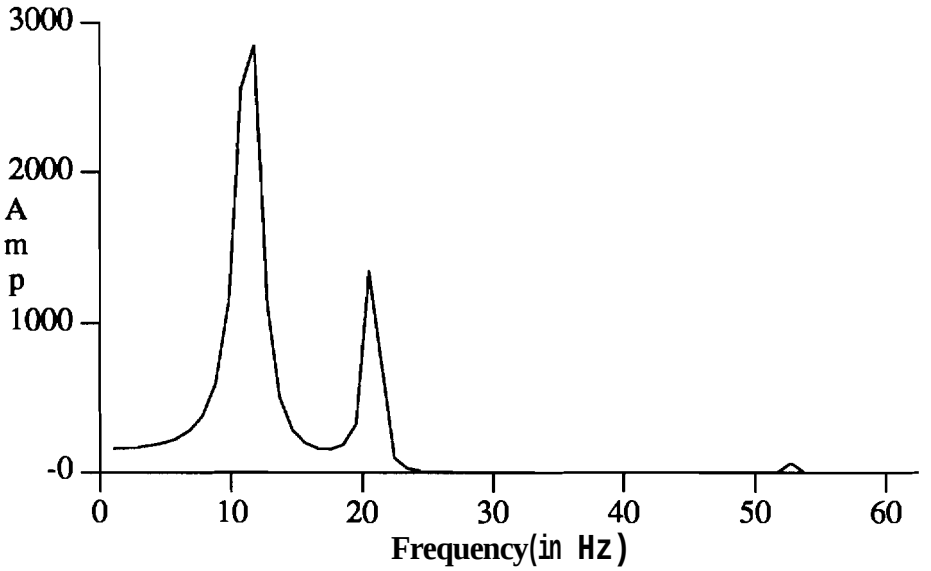

Figure 7.14 1-D Coupling Frequency Estimates: S1 P3 Derivation; 16 x 10 matrix using Symmetric Cumulants; Signal Subspace Dim: 6

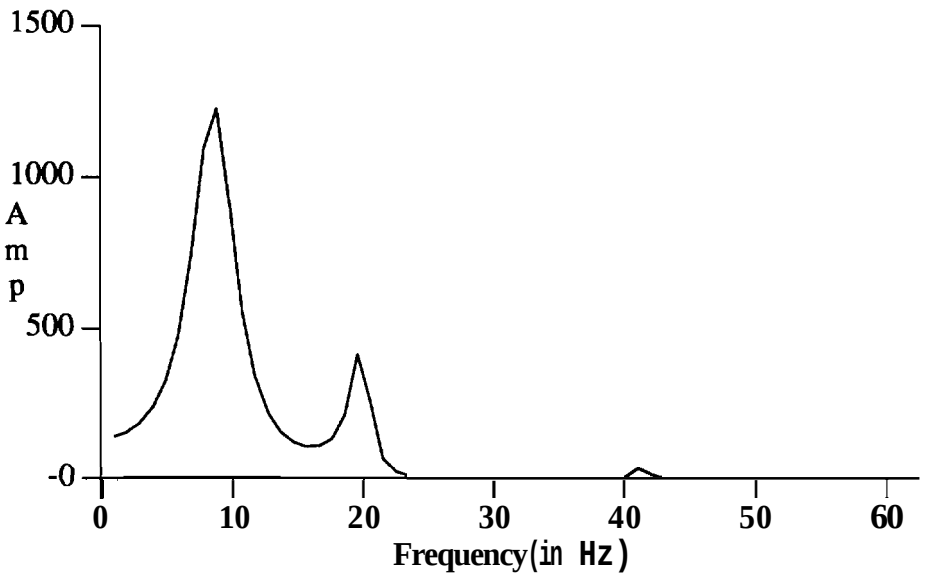

Figure 7.15 1-D Coupling Frequency Estimates: S7 P4 Derivation; 16 x 10 matrix using Symmetric Cumulants; Signal Subspace Dim: 6

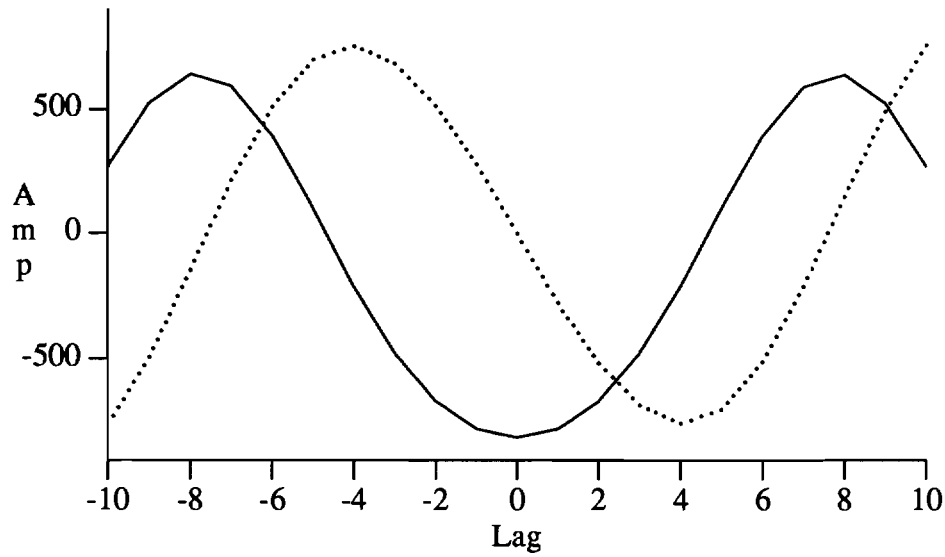

Figure 7.16 Projected Cumulants from S6: C3 Derivation; Solid: Symmetric; Dotted: Skew-Symmemc; ESPRIT Biphase: 50.06; FFT Biphase: 59.73

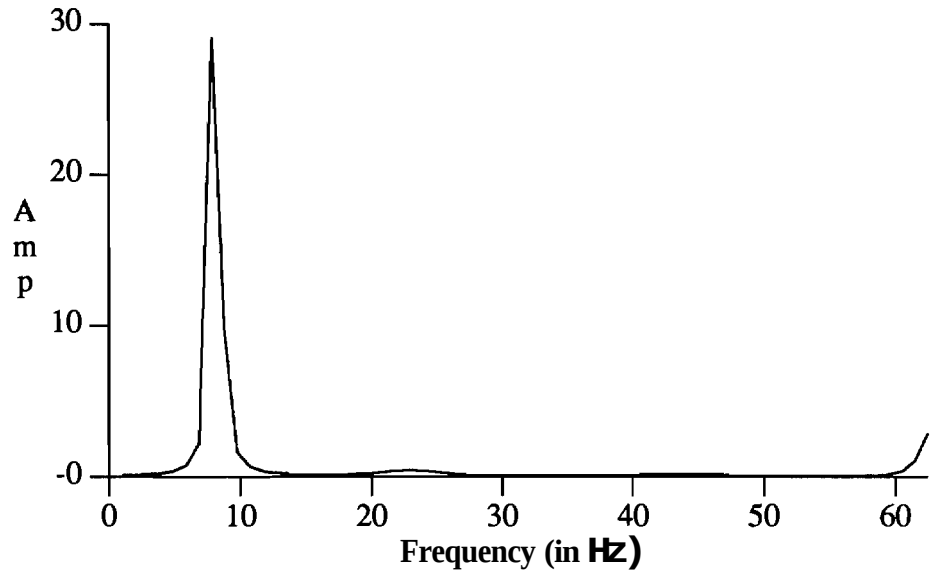

Figure 7.17 1-D SKEW-MUSIC Bispectrum from S6: C3 Derivation from Skew-Symmemc Projected Cumulants; Signal Subspace: 2; SKEW-MUSIC Peak Freq.: 7.81 Hz; FFT Peak: 7.81 Hz

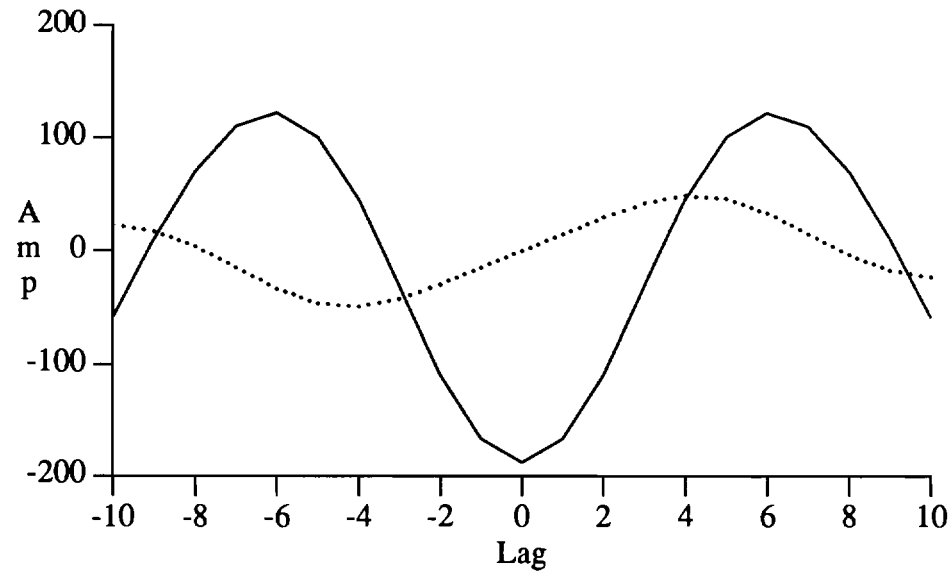

Figure 7.18 Projected Cumulants from S7: 0 2 Derivation; Solid: Symmetric; Dotted: Skew-Symmetric; ESPRIT Biphase: 22.02; FFT Biphase: 23.28

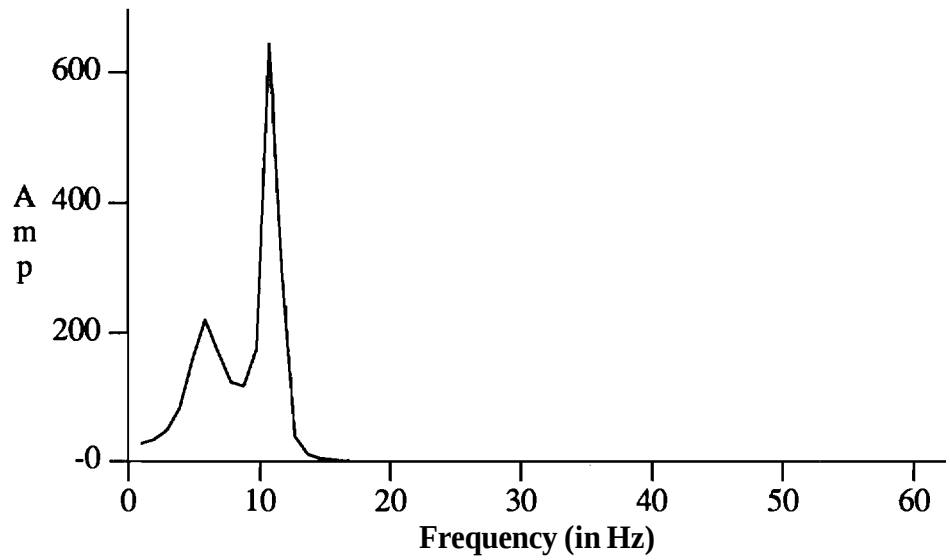

Figure 7.19 1-D SKEW-MUSIC Bispectrum from S7: 0 2 Derivation from Symmetric Projected Cumulants; Signal Subspace: 2; SKEW-MUSIC Peak Freq.: 10.74 Hz; FFT Peak: 9.77 Hz

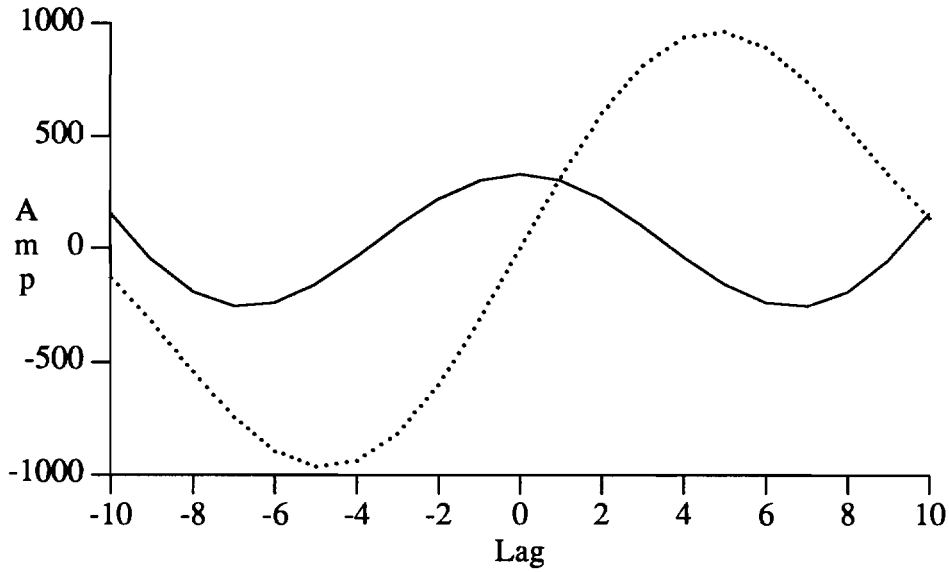

Figure 7.20 Projected Cumulants from S3: P3 Derivation; Solid: Symmetric; Dotted: Skew-Symmetric; ESPRIT Biphase: 71.04; FFT Biphase: 66.57

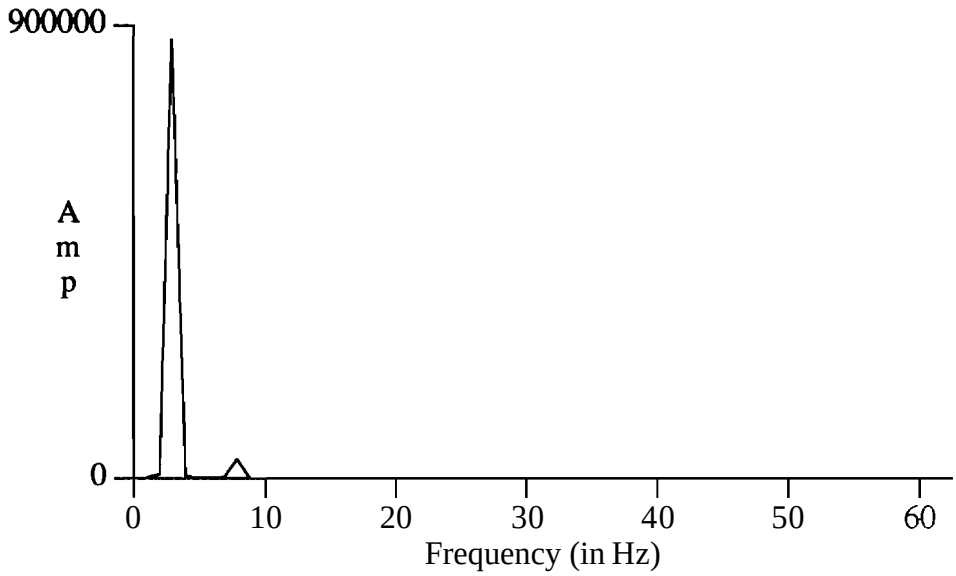

Figure 7.21 1-D SKEW-MUSIC Bispectrum from S3: P3 Derivation from Skew-Symmetric Projected Cumulants; Signal Subspace: 4; SKEW-MUSIC Peak Freq.: 2.93 Hz; FFT Peak: 4.88 Hz

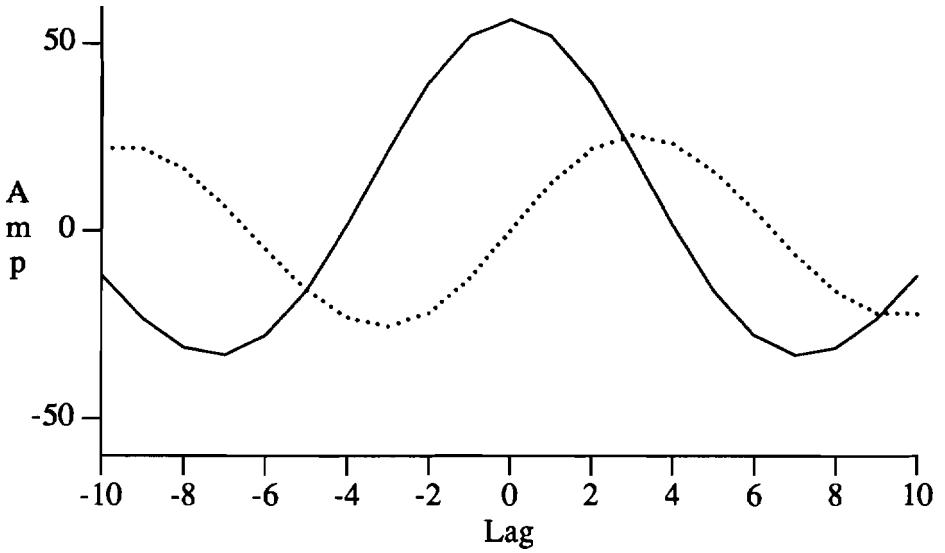

Figure 7.22 **Projected Cumulants from S4: C4 Derivation; Solid: Symmetric; Dotted: Skew-Symmetric; ESPRIT Biphase: 23.82; FFT Biphase: 23.4**

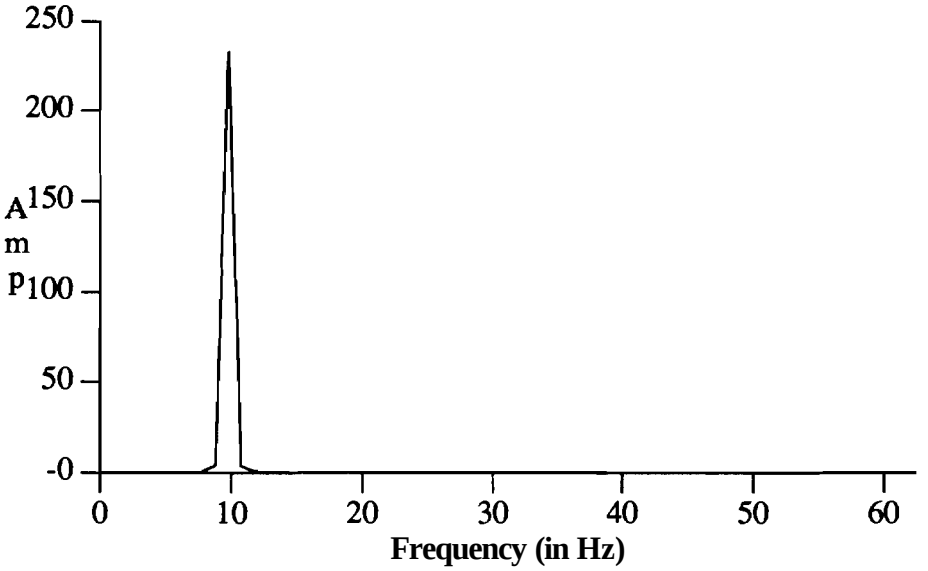

Figure 7.23 **1-D SKEW-MUSIC Bispectrum from S4: C4 Derivation from Symmetric Projected Cumulants; Signal Subspace: 2; SKEW-MUSIC Peak Freq.: 9.77 Hz; FFT Peak: 8.79 Hz**

7.6 List of References

[1] A.L. Swindlehurst and T. Kailath, "Detection and Estimation Using the Third Moment Matrix," Proc. Int. Conf. ASSP *Soc.*, pp. 2325-2328, Glasgow, Scotland, May 1989.

[2] M. Hinich, "Testing the Gaussianity and Linearity of a Stationary Time Series," J. Time Series Anal., vol. 3, pp. 169-176, 1982.

[3] Z. Keirn, Alternative Modes of Communication Between Man and Machine, MSEE Dissertation, Purdue University, West Lafayette, IN, Dec. 1988.

[4] H.H. Jasper, "Report of the Committee on Apparatus - Recommendations to Manufacturers," Electroencephal. clin. Neurophysiol., vol. 10, p. 378, 1958.

[5] M.P. Plonski, Biocybernetic Measures of Workload, PhD Dissertation, Purdue University, West Lafayette, IN, Dec. 1987.

[6] J.A. McEwen and G.B. Anderson, "Modeling the Stationarity and Gaussianity of Spontaneous Electroencephalographic Activity," IEEE Trans. Biomed. Eng., vol. BME-22, pp. 361-369, 1975.

[7] M.R. Raghuveer and C.L. Nikias, "Bispectrum Estimation: A Parametric Approach," IEEE Trans. ASSP, vol. ASSP-33, pp. 1213-1220, Oct. 1985.

CHAPTER 8
DISCUSSION

8.1 EEG Signal Processing Issues and Insights

Simulations using EEG time series from on-going, background activity have shown that each of four parametric algorithms can be used for satisfactory representation of three-wave coupling. This coupling belongs to a non-Gaussian but generally linear time series. Since it is linear, the couplings are few and restricted in extent over the bifrequency domain. Pronounced peaks localized to a 10 Hz self coupling region can be fairly readily captured with low model orders.

Proof of the economy in representation comes from a number of EEG simulations. Extending the idea of the band to quadratic systems, we note that the major concentration of spectral power in the EEG alpha band is accompanied in the bispectrum by the greatest number of peaks with high skewness in the alpha-alpha hyperband. All of the algorithms have a great probability of placing bispectral maxima in this region which covers just over 2% of the entire grid. Model orders ranging from 1 self-coupled dyad to 2 full triads uncovered peaks in this region of nonlinearities. Some of the algorithms were shown to have a certain degree of redundancy as several models belonging to the same scheme placed peaks in the alpha-alpha region.

These methods work well with short data lengths as well. The original work by Huber et al. [1] used EEG data segments that were 80 seconds in length. This is more than double the length used in this study! These methods, particularly the triple Kronecker product approaches, are sensitive enough to display sharp coupling frequency peaks. At the same time it is assumed that alpha-alpha coupling is a stable process which is active during the entire time that alpha synchronization takes place. Given that the EEG is not considered particularly stationary, the fact that these methods work with short data lengths is an extra dividend. Previous studies of EEG spectral parameter stationarity [2, 3] point to the fact that the alpha wave is a spectral "island" of stability in an otherwise stormy sea of waves. However, because of coupling, a good deal of beta band power will have appreciable inter-trial constancy.

Since this alpha self-coupling is so readily detected with these parametric methods, the alpha coupling must be a stable phenomenon which is not so easily averaged out.

The alpha rhythm may be comprised of many components. An extremely narrowband of the alpha rhythm is coupled with beta frequencies. Yet as the alpha band is particularly wide (see sect. **6.8** and **[4]),** another portion is definitely linear and uncoupled with other frequency bands. It may be worthwhile to talk about more than one alpha rhythm. Low resolution methods such as conventional **FFT-based** techniques and the autoregressive procedure may mask these attributes of the alpha rhythm.

Though earlier we noted the deficiencies of the autoregressive model, it does perform quite well in simulations. As a linear "approximation" to three-wave coupling, it reveals coupling in a few select circumstances. Its hit rate profile for the occipital derivations is quite high. Perhaps for well-defined situations where less **computation**ally intensive algorithms are required, narrowband AR modeling may suffice.

The high **performance** of the AR algorithm in the occipital regions is noteworthy in another respect. Typically, occipital derivations are not known for high concentrations of beta band frequencies. Their frequency content is typically purely sinusoidal with some low frequency modulation. This would be revealed in closely spaced alpha sidebands. This envelope is extracted in complex demodulation and narrowband Gaussian noise contexts. Our studies reveal quite a sizable proportion of coupling with second harmonic frequencies. Perhaps our methods work so proficiently for occipital sites, because there is so much less interference from uncorrelated beta frequency power. The greatest quantity of uncoupled beta is to be found in more anterior electrode locations.

When the 2-D methods are augmented with certain 1-D analogs, more model order information can be verified. These 1-D methods spotlight the rhythms belonging only to the power spectrum and those with dual membership in both the PSD and bispectrum. The use of the Swindlehurst and **Kailath SVD** formulation often shows two peaks corresponding to alpha and beta-I1 waves. Dyadic coupling between alpha and beta-II is the major feature of the EEG bispectrum. These are the key sinusoids involved in coupling.

Likewise 1-D SKEW-MUSIC is a convenient method to filter the bispectrum to highlight specific harmonic relations. Domain restrictions help to capture weak alpha-alpha coupling for those subjects without prominent bispectral features. 1-D SKEW-MUSIC is much like a microscope. Though it narrows the field of vision, it brings to light many obscured bispectral attributes. One of the key issues discussed in the Dumermuth et al. articles **[5]** and section **6.8** was the extremely narrow bands

involved in quadratic phase coupling. Taking narrow slices of the bispectrum provides an instrument for inspecting the fine details used by the brain for synchronous activity across frequency ranges. All of these eigenstructure methods furnish low model order responses.

Achieving high resolution, we can begin to examine the phase relationships between alpha and beta waves. Phase is more easily visualized as the delay between 1-D signals so it is natural to view the dispersive component of the EEG signals by examining cumulant projections. Several cases of EEG time series provided ample evidence that 1-D SKEW-ESPRIT can accurately estimate the phase difference between alpha and beta-11.

At the end of section 6.8 we discussed the fact that the cumulant projections provided the best reason for utilizing eigenstructure approaches for EEG quadratic phase coupling. In our brief survey of projected cumulants in chapter VII, all of the projected cumulants had a distinctively sinusoidal character. In fact simply measuring the peaks of symmetric and skew-symmetric projected cumulants and forming their ratio, would yield accurate biphases. Here 1-D methods uncover necessary information about cumulant form that lend support for the use of sinusoidal parametrization.

8.2 Conclusions and Future Research Suggestions

This study developed new tools for the investigation of harmonic phenomena in stochastic systems. As phase is a signature trait of nonlinear interactions, it was critical that these tools provided accommodations for phase measurements. Phase sensitivity is also a distinguishing characteristic of the bispectrum. Autoregressive approaches to bispectral modeling lacked phase measurement facilities. Nonlinear interactions require a 2-D representation as inter-frequency modulations are generated from different frequencies beating together to form new harmonics.

A sinusoidal parametrization best represents modulation processes. Phase can be easily integrated in an eigenstructure-based scheme. Two-dimensional methods were created to be higher order forms of the MUSIC algorithm [6]. Third and fourth order Kronecker product matrices were formed from symmetrized cumulants. Phases were decoupled during symmetrization which provided a basis for their estimation as amplitude coefficients of the sinusoidal 2-D cumulant sequence. Multidimensional versions of the ESPRIT algorithm allowed the user to estimate these dispersion relations without accompanying frequency information. This approach relied on the

Procrustes rotation [7] to furnish reduced dimension full rank square matrix pencils. The generalized eigenvalues containing the biphases were estimated from the core rotations level matrices.

One-dimensional versions of the eigenvector methods supplied new information about the form of the cumulants and coupling frequencies over a restricted domain or slice of the bispectrum. In cases where specific harmonic relations need to be understood, the 1-D SKEW-MUSIC algorithm provides these details [8, 9].

All of these algorithms were tested with EEG data exhibiting strong alpha wave coupling. Parametric methods are useful in cases with restricted coupling domains so that low model orders may be used. Testing EEG time series showed that the alpha self coupling domain provides highly significant coupling peaks in the bispectrum. Coupling frequencies and biphases may be extracted from I-D methods. These I-D methods provide the rationale for sinusoidal modeling of EEG coupling [10, 11].

Future research may include faster algorithms for computation of the cumulants. Schemes may be provided to speed up the calculation of the cumulant projections. Algorithms need to be devised for identification of systems along a bispectral slice. The concept of quadratic and Volterra filtering is dealt with in this thesis. For weakly nonlinear systems adaptive Volterra filtering within a frequency slice may be all that is needed for improved system identification performance. Multichannel algorithms might also be devised.

In the brain wave realm extensive new studies could look at phase coupling from cerebral surface or depth recordings. These methods could also be applied to thalamocortical relays to check if coupling originates within pacemakers that drive or extinguish the alpha rhythm. Experiments could be performed at this juncture to vary the spectral beta power independently of alpha. The object would be to discover if inter-band coupling deteriorates under those conditions. Also it would be interesting to see if the classical Lopes da Silva oscillatory model of the alpha rhythm could be altered ever so slightly to incorporate higher harmonics [12].

8.3 List of References

[1] P.J. Huber, B. Kleiner, T. Gasser, and G. Dumermuth, "Statistical Methods for Investigating Phase Relations in Stationary Stochastic Processes," IEEE Trans. Audio Elec., vol. AU-19, pp. 78-86, 1971.

[2] T. Gasser, P. Baecher, and H. Steinberge, "Test-Retest Reliability of the Spectral Parameters of the EEG," Electroenceph. clin Neurophysiol., vol. 85, pp. 312-319, 1985.

[3] B.S. Oken and K.H. Chiappa, "Short-term variability in EEG frequency analysis," Electroencephal. clin. Neurophysiol., vol. 69, pp. 191-198, 1988.

[4] A. Wennberg and L.H. Zetterberg, "Application of computer-based model for EEG analysis," Electroencephal. clin. Neurophysiol., vol. 31, p. 457, 1971.

[5] G. Dumermuth, P.J. Huber, B. Kleiner, and T. Gasser, "Analysis of the Interrelations between Frequency Bands of the EEG by Means of the Bispectrum: A Preliminary Study," Electroenceph. clin. Neurophysiol., vol. 31, pp. 137-148, 1971.

[6] D.L. Sherman and M.D. Zoltowski, "Eigenstructure-Based Bispectrum Estimation," Proc. 26th Annual Allerton Conf., Champaign-Urbana, IL, Sept 1988.

[7] M. Zoltowski and D. Stavrinides, "Sensor Array Signal Processing Via a Procrustes Rotations Based Eigenanalysis of the ESPRIT Data Pencil," IEEE Trans. ASSP, vol. 37, pp. 832-861, June 1989.

[8] D.L. Sherman and M.D. Zoltowski, "Frequency and Biphase Estimation of Quadratically Coupled Sinusoids Using Cumulant Projections," Proc. ICASSP-90, pp. 2373-2376, Albuquerque, NM, April 1990.

[9] D.L. Sherman and M.D. Zoltowski, "Decoupling Higher Order Cumulant Sequences Resulting Three-Wave Coupling Processes," Proc. 5th ASSP Wkshp. on SEM, pp. 227-231, Rochester, NY, Oct. 1990.

[10] D.L. Sherman and M.D. Zoltowski, "Application of Eigenstructure Based Bispectrum Estimation: EEG Wave Coupling in Cognitive Tasks," Workshop on Higher-Order Spectral Analysis, pp. 135-140, Vail, CO, June 1989.

[11] D.L. Sherman and M.D. Zoltowski, "Decomposing the Alpha Rhythms: Comparative Performance Evaluation of Parametric Bispectral Alogorithms for EEG," Proc. 6th SSAP Statistical Signal and Array Processing *Wkshp*., pp. 522-525, Victoria, BC, CA, October 1992.

[12] F.H. Lopes da Silva, A. Hoeks, H. Smits, and L.H. Zetterberg, "Model of Brain Rhythmic Activity: The Alpha Rhythm of the Thalamus," Kybernetik, vol. 15, pp. 27-37, 1974.

Appendix A: The Form of Projected Cumulants for Quadratically Phase Coupled Sinusoids

Here we show the form projected cumulants of a time series containing quadratically phase coupled sinusoids plus noise. Consider an arbitrary continuous third order cumulant series, $C(\tau,\nu)$, for a single triad of quadratically phase coupled sinusoids in non-Gaussian and its 2-D Fourier transform, $B(\omega_1,\omega_2)$. It is desired to isolate the projected cumulants corresponding to a radial slice of the 2-D bispectrum $B(\omega\cos\theta,\omega\sin\theta)$ at angle θ with respect to the τ axis. In this context ω is the radial frequency. Assume a bispectral peak for the triad lies along this 1-D radial slice at $B_\theta(\omega) = B(\omega\cos\theta,\omega\sin\theta)$. To compute the Radon transform, the cumulants are parametrized so that the axes are rotated by 0, i.e., new axes $\hat{\tau}$ and $\hat{\nu}$ through the unitary transformations

$$\hat{\tau} = \tau\cos\theta + \nu\sin\theta \tag{A1}$$

$$\hat{\nu} = -\tau\sin\theta + \nu\cos\theta \tag{A2}$$

Taking the Radon transform involves substituting the inverse of the parametrization above to our cumulant function and then forming the projections, $C_\theta(\hat{\tau})$, along lines normal to the new axis, $\hat{\tau}$, i.e., parallel to $\hat{\nu}$. The expression for the triad of quadratically coupled sinusoids in third order white noise is parametrized by using the inverse unitary transformation. The cosine terms are expressed in terms of their constituent complex exponential factors and terms in $\hat{\tau}$ and $\hat{\nu}$ are collected together for each real sinusoid as 2-D sinusoids are easily factored. The subsequent integration yields the following set of projected cumulants for the case of a single quadratically coupled sinusoidal triad:

$$\begin{aligned} C_\theta(\hat{\tau}) = {} & \cos[(\omega_1\cos\theta + \omega_2\sin\theta)\hat{\tau} - \gamma]\,\delta(\omega_1\sin\theta - y\cos\theta) \\ & + \cos[(\omega_2\cos\theta + \omega_1\sin\theta)\hat{\tau} - \gamma]\,\delta(\omega_2\sin\theta - \omega_1\cos\theta) \\ & + \cos[(\omega_3\cos\theta - \omega_2\sin\theta)\hat{\tau} - \gamma]\,\delta(\omega_3\sin\theta + \omega_2\cos\theta) \\ & + \cos[(\omega_2\cos\theta - \omega_3\sin\theta)\hat{\tau} - \gamma]\,\delta(\omega_2\sin\theta + \omega_3\cos\theta) \\ & + \cos[(\omega_3\cos\theta - \omega_1\sin\theta)\hat{\tau} - \gamma]\,\delta(\omega_3\sin\theta + \omega_1\cos 0) \\ & + \cos[(\omega_1\cos\theta - \omega_1\sin\theta)\hat{\tau} - \gamma]\,\delta(\omega_1\sin\theta + \omega_3\cos 0) + \beta\,\delta(\hat{\tau}) \end{aligned} \tag{A3}$$

The presence of a Kronecker delta function multiplying each term in the projected cumulants indicates that there is a reduction from six terms to one term per

triad on certain slices after taking projections. For the slice within the non-redundant sector of the autobispectrum, that is, between $0 \leq \theta$ I $\pi/4$, we pick the projection axis angle θ to satisfy $\omega_1 \sin e - \omega_2 \cos\theta = 0$ so that $\delta(\omega_1 \sin e - \omega_2 \cos\theta) = 1$. The last five sinusoidal terms of (A3) vanish leaving only

$$C_\theta(\hat{\tau}) = \cos[\omega\,\hat{\tau} - \gamma] + \beta\delta(\hat{\tau}) \quad \text{for} 0 \leq \theta \leq \pi/4 \tag{A4}$$

where $\omega = \omega_1 \cos\theta + \omega_2 \sin\theta$ is the equivalent radial frequency. In this context we have shown projected cumulants for a time series with a single triad of sinusoids reduce to one 1-D sinusoid from six 2-D sinusoids. This is for projections normal to an angle θ for a peak at $S_\theta(\omega)$.

Appendix B: Simulation Results

Table A.l EEG Coupling Frequency Estimates: 1-D SKEW-MUSIC: Ss: 1-3

EEG COWLING FREQUENCY ESTIMATES 1-D SKEW-MUSIC: Subjects: 1-3					
S#	Electrode	Model Order			
		2		4	
		SYM/SKW	Deviation	SYM/SKW	Deviation
1	P3	SKW	0.0	BOTH	0.0
1	P4	BOTH	.976	BOTH	.976
1	C3	SYM	.976	SYM	0.0
1	C4	SYM	.976	SYM	.976
1	0 1	SYM	0.0	SKW	0.0
1	0 2	SYM	0.0	SKW	0.0
2	P3	SYM	1.96	SYM	0.976
2	P4	SYM	5.86	SYM	5.86
2	C3	SYM	.976	SYM	0.0
2	C4	SYM	.976	SYM	.976
2	0 1	SYM	0.0	SKW	0.0
2	0 2	SYM	0.0	SKW	0.0
3	P3	SKW	0.0	BOTH	1.96
3	P4	BOTH	.976	BOTH	.976
3	C3	SYM	.976	SYM	0.0
3	C4	SYM	.976	SYM	.976
3	0 1	SYM	0.0	SKW	0.0
3	0 2	SYM	0.0	SKW	0.0

Table A.2 EEG Coupling Frequency Estimates: 1-D SKEW-MUSIC: Ss: 4-7

EEG COUPLING FREQUENCY ESTIMATES 1-D SKEW-MUSIC: Subjects: 4-7					
S#	Electrode	Model Order			
		2		4	
		SYM/SKW	Deviation	SYM/SKW	Deviation
4	P3	SYW	1.96	SYM	0.976
4	P4	SKW	4.887	SKW	6.836
4	C3	SYM	1.96	SYM	0.976
4	c 4	SYM	.976	SYM	.976
4	0 1	SYM	1.95	SYM	0.976
4	0 2	SYM	7.815	SYM	6.839
5	P3	SKW	0.0	SKW	0.0
5	P4	SKW	2.93	SKW	2.93
5	C3	SYM	0.0	SKW	0.0
5	C4	SYM	2.93	SYM	2.93
5	0 1	SYM	0.976	SYM	0.976
5	0 2	SKW	0.976	SKW	0.976
6	P3	SYM	0.976	SYM	0.0
6	P4	SYM	.976	SYM	.976
6	C3	SKW	0.0	SYM	0.976
6	C4	SKW	0.0	SYM	.976
6	0 1	BOTH	0.976	SKW	0.0
6	0 2	SYM	0.976	SKW	0.0
7	P3	SYM	0.0	SYM	1.956
7	P4	SYM	.976	SYM	.976
7	C3	SYM	1.956	SYM	0.0
7	C4	SYM	1.956	SYM	.976
7	0 1	SYM	0.976	SKW	0.976
7	0 2	SYM	0.976	SKW	0.976

Table A.3 Low Error Estimates of Biphases for EEG data from 1-D SKEW-ESPRIT

EEG Biphase Estimates Using 1-D SKEW-ESPRIT					
Subject	Electrode	Order	FFT-Estimate	SKEW-ESPRIT Estimate	Deviation
1	P3	2	66.244	60.117	6.127
1	P4	2	82.82	80.717	2.103
1	C3	2	38.935	45.434	-6.499
1	C4	4	5.369	4.066	1.303
2	O1	2	24.911	29.266	-4.355
2	C3	4	46.716	41.686	5.03
3	P3	4	66.57	71.04	-4.47
3	P4	2	73.782	61.968	11.815
3	O2	2	41.347	34.348	6.999
4	P4	4	72.377	68.509	3.868
4	C3	2	.147	1.092	-0.945
4	C4	2	23.402	23.823	0.421
4	O2	4	73.979	67.302	6.667
6	P3	4	4.307	6.393	-2.632
6	P4	2	14.639	18.01	-3.371
6	C3	2	59.729	50.058	9.671
6	O1	2	74.624	61.813	12.811
6	O2	2	58.846	51.246	7.6
7	P3	4	19.335	17.645	1.69
7	P4	4	20.069	24.423	-4.354
7	C3	2	61.987	53.294	8.693
7	O2	4	23.282	22.025	1.257

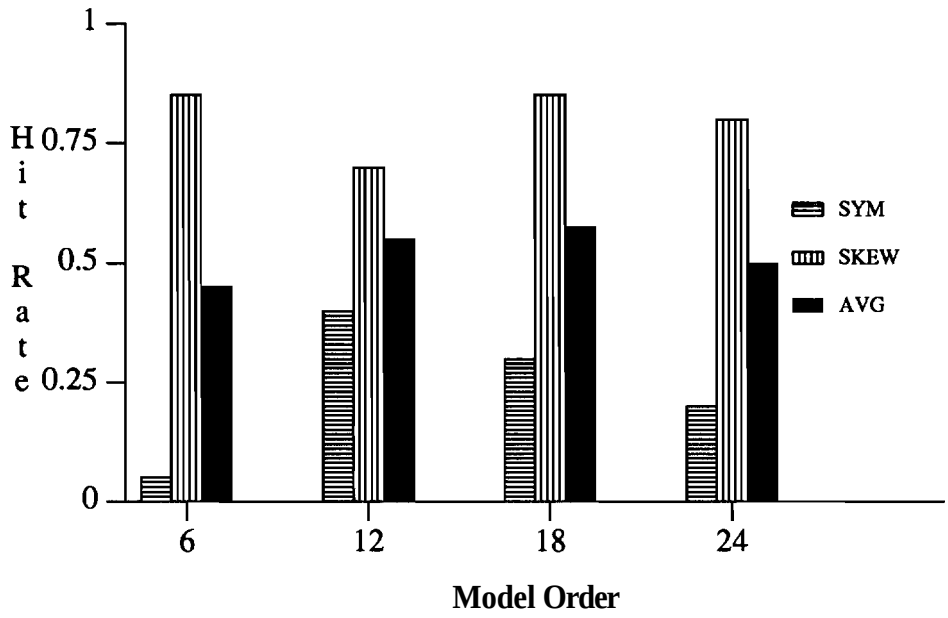

Figure A.1 Parietal Hit Rate Profile for 2-D SKEW MUSIC: 30x30 Mamx Dimension

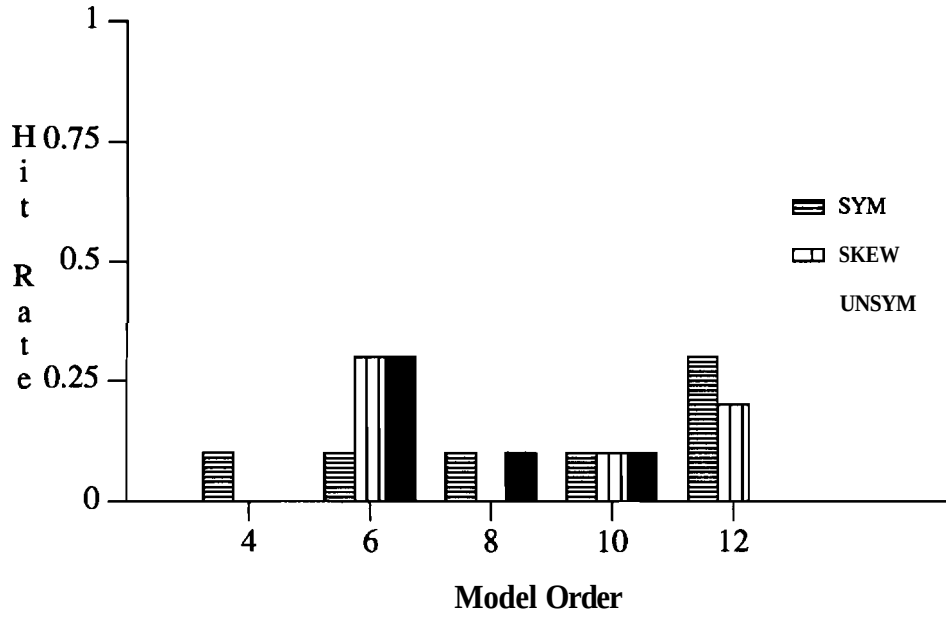

Figure A.2 Parietal Hit Rate Profile: Autoregressive Method

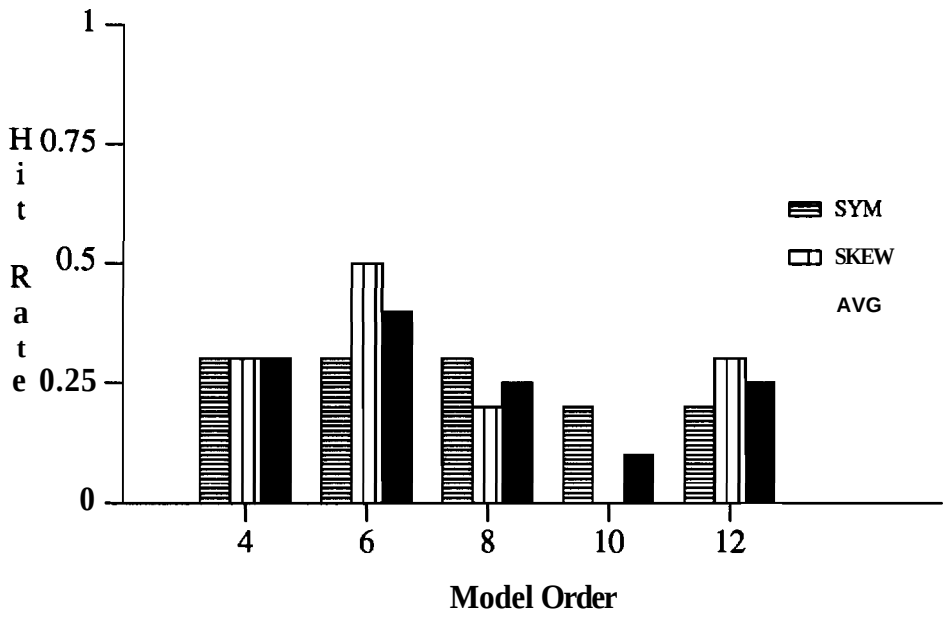

Figure A.3 **Parietal Hit Rate Profile: SKEW-PRO-ESPRIT: 36x15 Matrix Dimension**

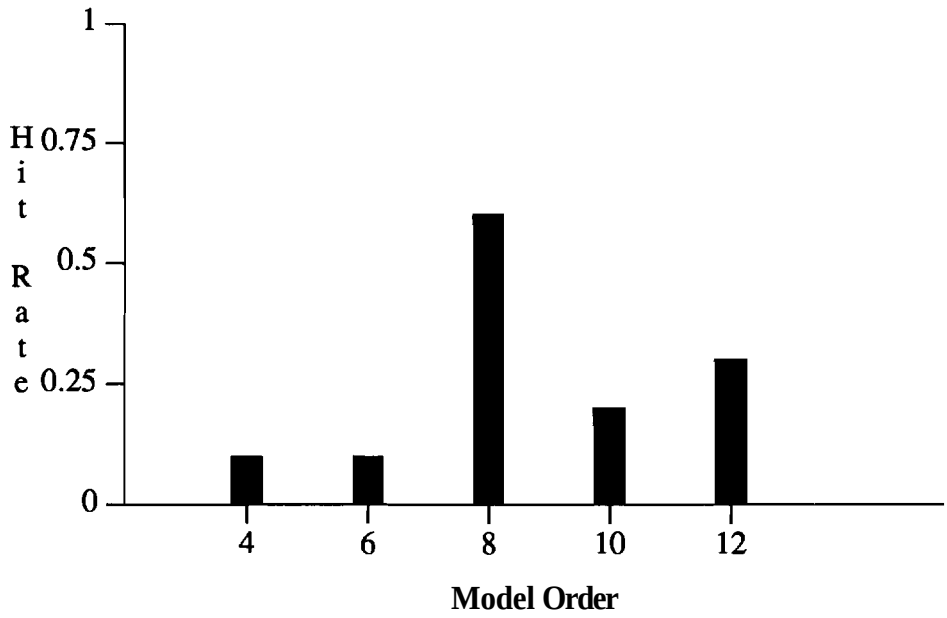

Figure A.4 **Parietal Hit Rate Profile for Triple Kronecker Product Method: 36x15 Matrix Dimension**

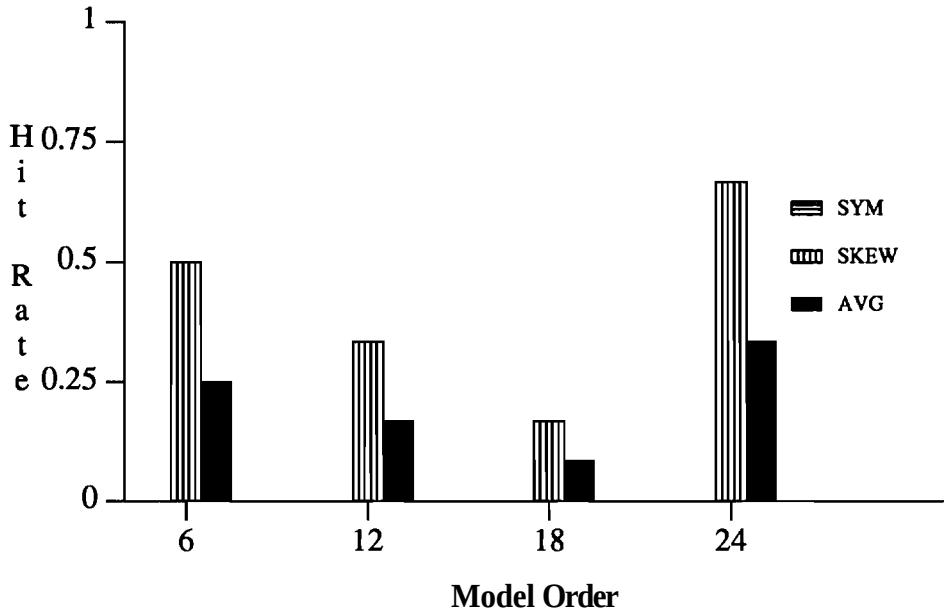

Figure A.5 Central Hit Rate Profile for 2-D SKEW MUSIC: 30x30 Matrix Dimension

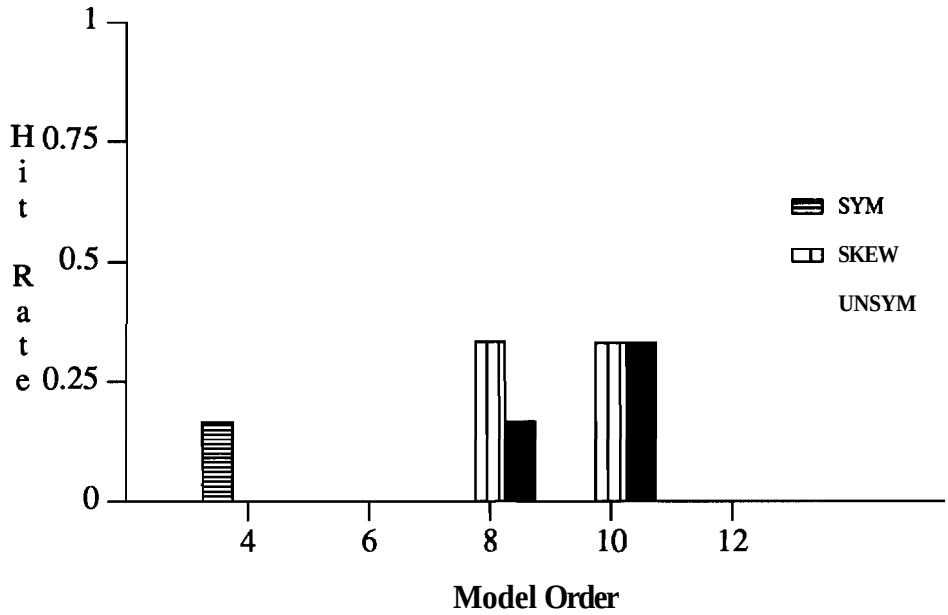

Figure A.6 Central Hit Rate Profile: Autoregressive Method

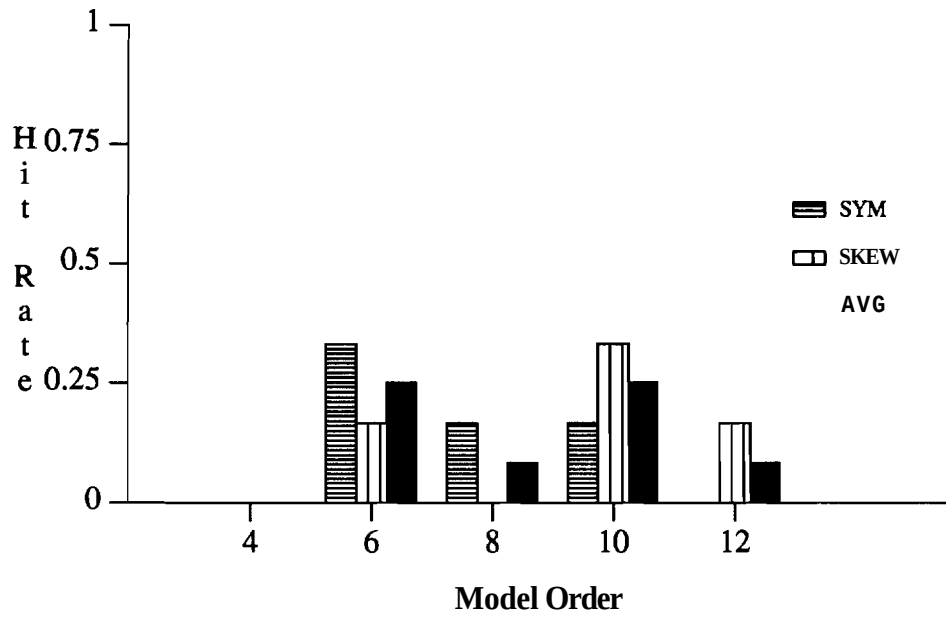

Figure A.7 Central Hit Rate Profile: SKEW-PRO-ESPRIT: 16x10 Matrix Dimension

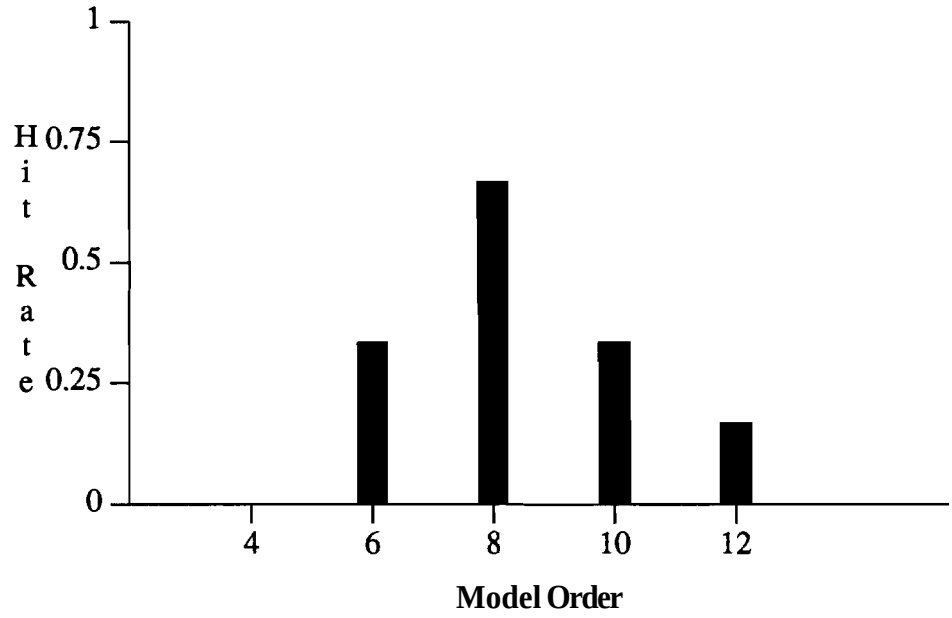

Figure A.8 Central Hit Rate Profile for Triple Kronecker Product Method: 25x10 Matrix Dimension

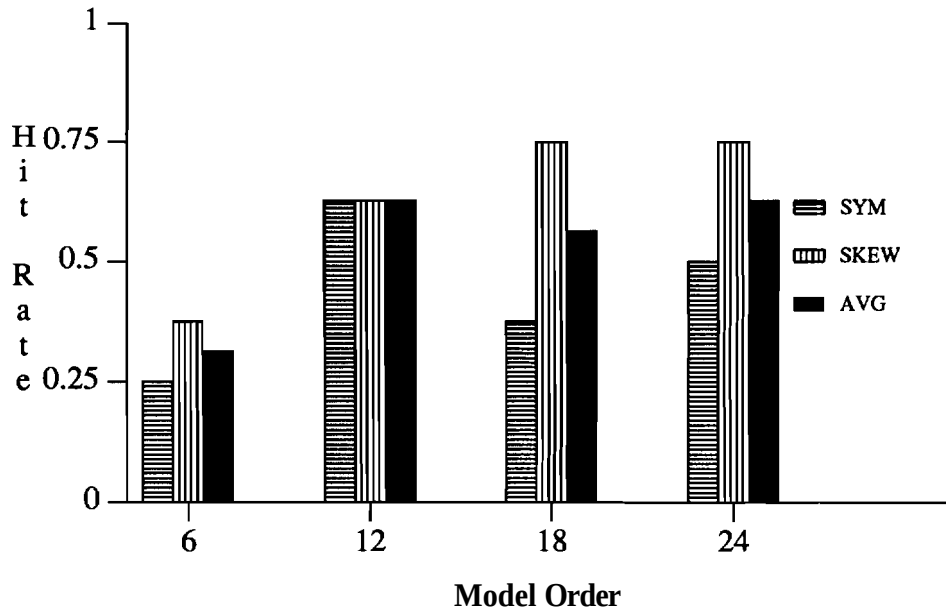

Figure A.9 Occipital Hit Rate Profile for 2-D SKEW MUSIC: 30x30 Mamx Dimension

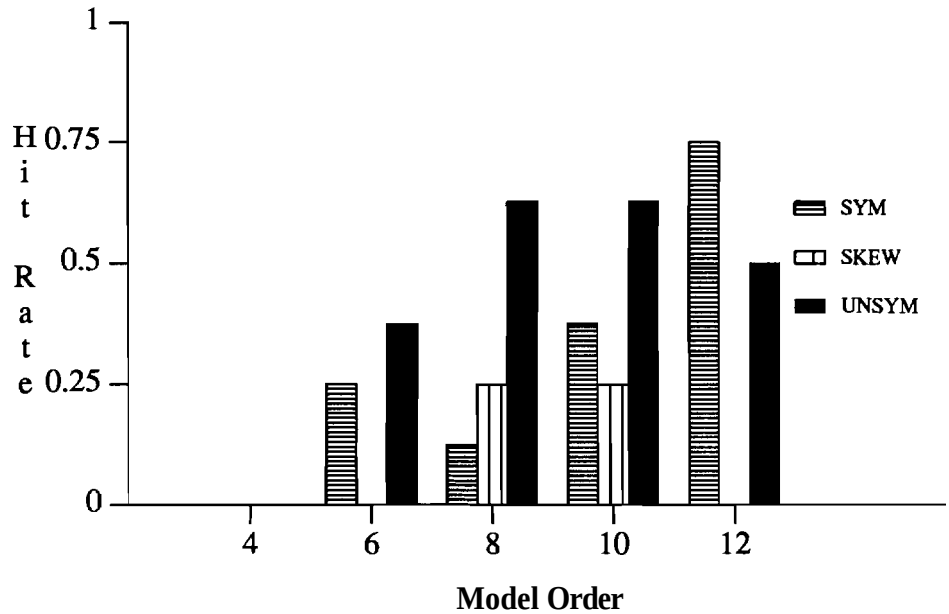

Figure A.10 Occipital Hit Rate Profile: Autoregressive Method

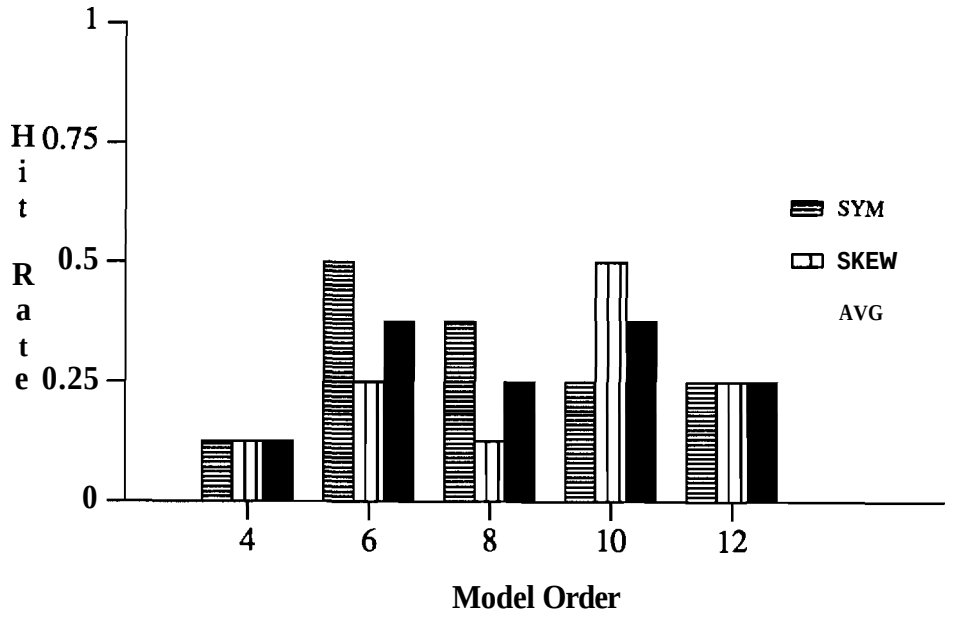

Figure A.11 Occipital Hit Rate Profile: SKEW-PRO-ESPRIT: 16x10 Matrix Dimension

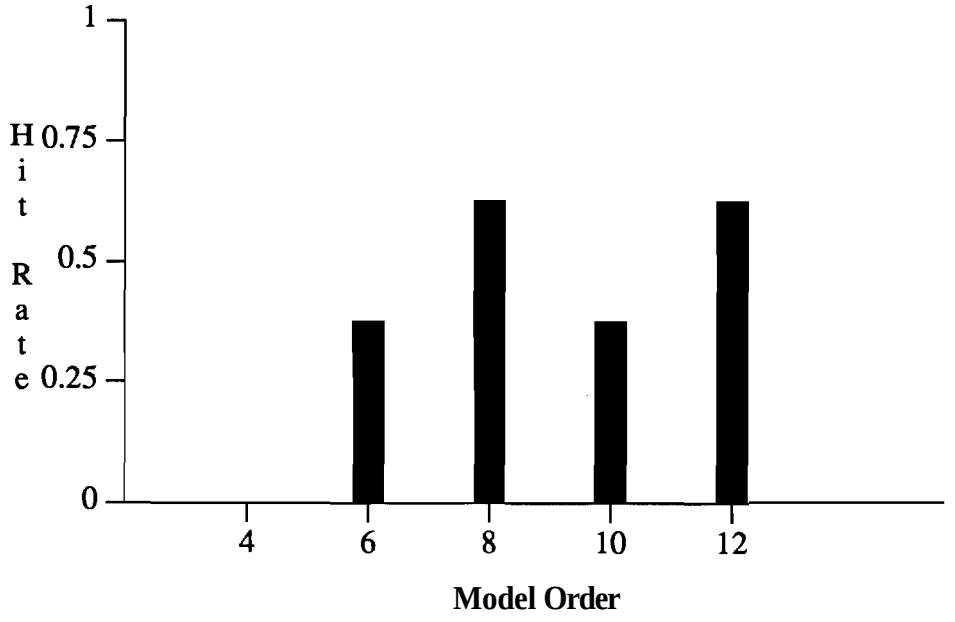

Figure A.12 Occipital Hit Rate Profile for Triple Kronecker Product Method: 36x15 Matrix Dimension

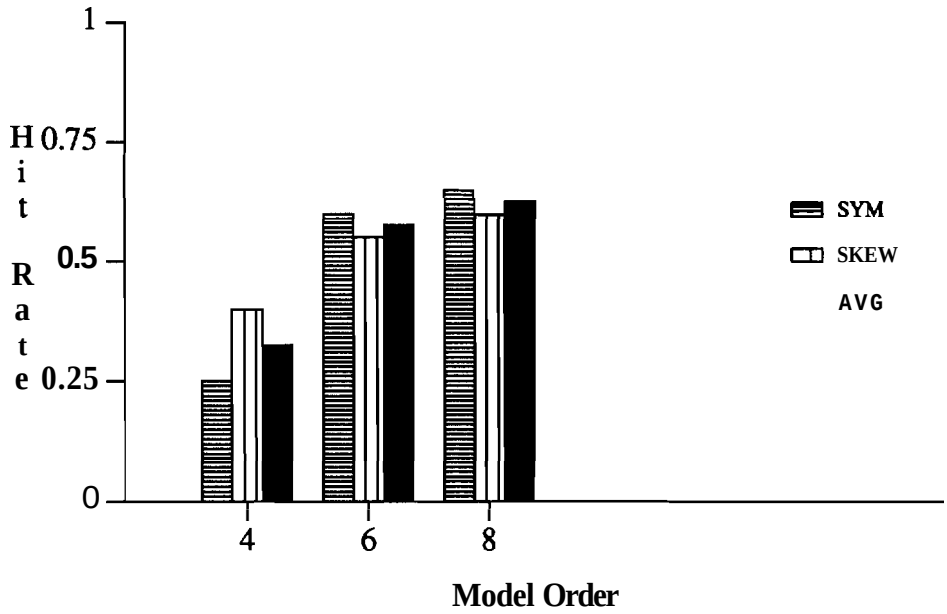

Figure A.13 Parietal Hit Rate Profile: Results from SKEW-PRO-ESPRIT Right Singular Vectors: 16x10 and 25x10 Matrix Dimensions

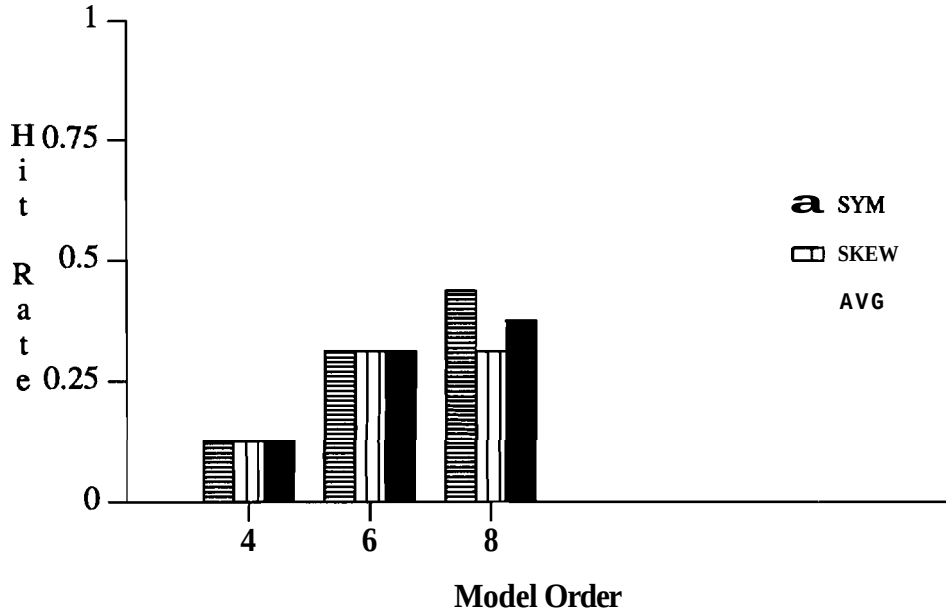

Figure A.14 Central Hit Rate Profile: Results from SKEW-PRO-ESPRIT Right Singular Vectors: 16x10 and 25x10 Matrix Dimensions

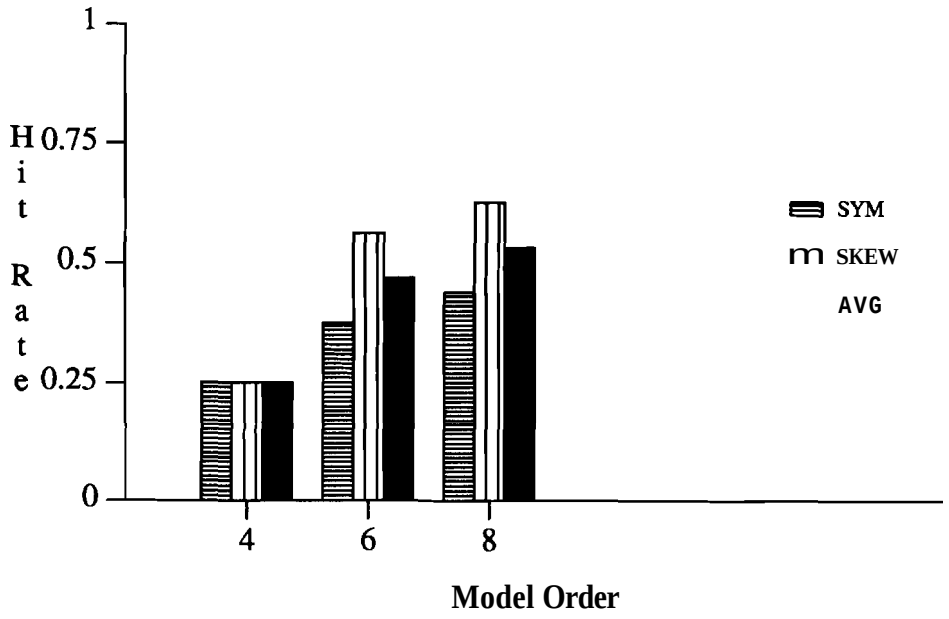

Figure A.15 Occipital Hit Rate Profile: Results from SKEW-PRO-ESPRIT Right Singular Vectors: 16x10 and 25x10 Matrix Dimensions